



**PREDICTING FATIGUE LIFE OF WELDED
JOINTS UNDER VARIABLE AMPLITUDE
LOADING SPECTRA**

A thesis submitted for the degree of
Doctor of Philosophy by:

Xu Liu

Department of Mechanical and Aerospace Engineering
Brunel University London
London
United Kingdom

To my family

献给我挚爱的家人

Acknowledgement

This research project was sponsored by Brunel University London and TWI Ltd, and carried out in Fatigue Integrity Management (FIM) section at TWI Ltd. TWI is one of the world's foremost independent research and technology organisations for welding and joining. It is a membership-based not-for-profit organisation that provides a technical consultancy service across several industry sectors. The project was funded through TWI's Core Research Programme.

I would like to thank my family - my parents, my wife, and my son. Their unconditionally support is the foundation of every step I move forward, the source of my encouragement to tackle the problems I have ever met in my life. Without their tremendous understanding and encouragement in the past few years, it would be impossible for me to complete my study.

I also would like to express my deep and sincere gratitude to my academic supervisor, Dr. Bin Wang and industrial supervisor, Dr. Yanhui Zhang, for providing me invaluable guidance throughout my study. Their dynamic, vision, sincerity and motivation have deeply inspired me.

My colleagues and technicians in the FIM section also provided me with great help during my PhD study. They are always very patient with me to deal with the questions and problems since I joined TWI. Special thanks go to Professor Xiang Zhang and Dr. Niall Smyth who also offered great help to me. Finally, my appreciation also goes out to my friends for their encouragement and support all through my studies.

Abstract

This study aims to improve the understanding of fatigue damage in welded joints under variable amplitude (VA) loading spectra and provide recommendations for future revision of fatigue design standard BS 7608 with respect to the guidance on the assessment of fatigue damage under VA loading.

Fatigue tests and analyses were conducted in the present study, aiming to address concerns about the fatigue performance of welded joints under VA loading. Welded joints with transverse fillet welded attachments, manufactured using S355 steel plates with three thicknesses, were tested under cycling down (CD) loading sequences with various constant maximum stresses under either uniaxial or bending loading. In addition to as-welded joints, life-improved welded joints treated by ultrasonic impact treatment (UIT), were also fabricated, and tested. Test results suggest that the CD sequence with a high maximum stress can significantly degrade the fatigue performance of welded joints, with the Miner's sum D being only of around 0.5 at fatigue failure. However, the severity of such a loading sequence decreases when the maximum stress is below a certain level, with a D value much higher than unity when fatigue failure occurs. Besides, the D value is also found to be dependent on the plate thickness proportionally. UIT can improve the fatigue life of the welded joints under VA loading, and the extent of the improvement depends on the maximum stress applied under CD loading sequence.

Residual stresses at the weld toes of several specimens with different thicknesses were measured using either the X-ray diffraction or the Centre-hole drilling method in both as-welded and fatigue-tested conditions. Measurement results show the magnitudes of the residual stress in the as-welded specimens are in proportion to the plate thickness. Residual stress relaxation occurs in both tensile and compressive loading conditions. The residual stress decreases significantly within the first two loading cycles and then becomes almost constant – only minor reductions were seen in further loading cycles.

The effect of the applied mean stress on the fatigue performance of welded joints was investigated by considering the actual maximum stress, which is the combination of the applied maximum stress and the residual stress, and new mean stress correction models were developed

accordingly on the basis of the conventional correction models. In addition to the mean stress effect, the models developed also can consider the effect of different VA loading sequences through a newly introduced factor. Experimental data obtained from the present study and reported in the published literature were adopted for validation. Results show that the proposed new models can more accurately predict the fatigue life of welded joints under given VA loading spectra, with the Miner's sum D at fatigue failures mainly being in the range between 0.5 and 1.5.

The fatigue crack growth (FCG) under VA loading was also studied. A new sequence factor which can take into account the effect of a VA loading sequence was introduced by considering the local residual mean stress as the primary mechanism for the interaction between stresses in a VA loading sequence. FCG predicted by the new model shows a good agreement with the experimental data. Fatigue lives can also be predicted reasonably well using the model developed, with the values of D at fatigue failures ranging between 1 and 2.

Declaration

This PhD study is, to the best of my knowledge, original and has been carried out without collaboration. The author's contribution to the research performed, and that of others is given below.

To perform the research, the author participated in the training in strain gauging, centre-hole drilling residual stress measurement as well as preparation, set up and conducting fatigue testing. The author performed all the experimental works mentioned in the thesis at the TWI fatigue laboratory under the supervision of technicians. The X-ray diffraction measurement was performed at Coventry University by the author under the direction of Dr Niall Smyth and Professor Xiang Zhang.

Some parts of the work have been published in the following papers:

1. Xu L, Yanhui Z, Bin W. Fatigue performance of welded joints under variable amplitude loading spectra. Proceedings of ASME 2019 Pressure Vessels & Piping Conference 2019. San Antonio, Texas, USA, 2019. Paper No. PVP2019-93073.
2. Xu L, Yanhui Z, Bin W. Effect of mean stress on fatigue life of welded joints under variable amplitude loading spectra. Proceedings of the 15th International Conference on Engineering Structural Integrity Assessment and the 2019 International Symposium on Structural Integrity, Brian Tomkins, Shan-Tung Tu, Peter EJ Flewitt, and John K Sharples. Cambridge, UK, 2019.

Nomenclature and Definitions

Nomenclature	Definition	Units
a	Crack depth	mm
a_c	Final crack depth	mm
a_i	Initial crack depth	mm
A	Material constant in cyclic crack growth relationship	-
ACPD	Alternating current potential drop (a crack depth measurement method)	-
b	Shape factor of a loading spectrum in Gassner distribution	-
b'	The thickness and bending exponent	-
Block	The stress history between successive applications of the peak stress in the spectrum	-
Block length N_L	Total number of cycles in a variable amplitude loading block	cycles
c	Half of crack length	mm
C	Material constant for S-N curve	-
CA	Constant amplitude	-
CD	Cycling down from a constant maximum stress	-

CD sequence	A loading sequence with all stresses cycling down from a constant maximum stress	-
CHD	Centre-hole drilling (a residual stress measurement method)	-
CM	Cycling about a constant mean stress	-
CM sequence	A loading sequence with all stresses cycling about a constant mean stress	-
CU	Cycling up from a constant minimum stress	-
CU sequence	A loading sequence with all stresses cycling up from a constant minimum stress	-
D	D represents fatigue damage according to the linear damage accumulation rule. It is expressed as $D = \sum_1^k \frac{n_i}{N_i}$, where n_i is the number of cycles at applied stress range $\Delta\sigma_i$ and N_i is the corresponding number of cycles to failure under constant amplitude loading at stress range $\Delta\sigma_i$. k is the number of stress range levels	-
D_m	Fatigue damage estimated after mean stress correction	-
D_{ms}	Fatigue damage estimated using the model developed in the present study where both the mean stress and VA loading sequence effects are considered	-
E	Young's modulus	GPa
FCG	Fatigue crack growth	-
FCGR da/dN	Fatigue crack growth rate	mm/cycle
HSS	Hot spot stress	MPa

k_p	Stress concentration factor	-
K'	Material constant	-
K_b	Bending factor	-
L	A best fit parameter	-
m	The slope of S-N curve	-
M_k	Stress intensity magnification factor	-
n_i	The number of cycles of the i th stress range in a spectrum	cycles
n'	Material constant	-
N_E	Exceedence corresponding to a particular P_i	cycles
N_{\max}	Aimed block length	cycles
P_i	Relative stress range in a spectrum ($=\Delta\sigma_i/\Delta\sigma_{\max}$)	-
R	Stress ratio ($=\sigma_{\min}/\sigma_{\max}$)	-
R_{eff}	Effective stress ratio ($=(\sigma_{\min} + RS)/(\sigma_{\max} + RS)$)	-
Relative fatigue damage D_{ri}	The ratio of the fatigue damage at a particular stress level $\Delta\sigma_i$ against that at the maximum stress range $\Delta\sigma_{\max}$	-
R_{Pi}	Overload ratio	-
RS	Residual stress	MPa

S-N curve	The relation between applied stress range and fatigue life in cycles to failure under constant amplitude loading	-
SIF ΔK	Stress intensity factor	$N/mm^{3/2}$
SMYS	Specified minimum yield stress	MPa
Spectrum	A representation of stress range(s) distribution with time or number of cycles	-
Stress histogram	Table or plot showing number of cycles at each stress range level	-
T	Plate thickness	mm
UIT	Ultrasonic impact treatment	-
VA	Variable amplitude	-
XRD	X-ray diffraction (a residual stress measurement method)	-
Y	Stress intensity correction factor	-
Z	Specimen length	mm
Z_a	Attachment height	mm
Z_w	Width of attachment and welds	mm
Z_t	Weld width	mm
σ_f	Fracture stress	MPa

σ_m	Mean stress	MPa
σ_{max}	Maximum stress in a loading cycle	MPa
σ_{min}	Minimum stress in a loading cycle	MPa
$\sigma_{max,L}$	Maximum local stress in a loading cycle	MPa
$\sigma_{min,L}$	Minimum local stress in a loading cycle	MPa
$\sigma_{m,L}$	Local residual mean stress	MPa
σ_p	Material parameter, such as σ_{UTS} and σ_{tf} etc.	MPa
$\sigma_{R,m}$	The mean stress of the equivalent stress range $\Delta\sigma_R$	MPa
σ_{tf}	True fracture stress	MPa
σ_{UTS}	Ultimate tensile strength	MPa
σ_y	Yield stress	MPa
Ω	Degree of bending ($=\Delta\sigma_b/(\Delta\sigma_b + \Delta\sigma_m)$)	-
ΔK_{eff}	Effective stress intensity factor	$N/mm^{3/2}$
$\Delta\sigma$	Stress range	MPa
$\Delta\sigma_b$	Bending stress range	MPa
$\Delta\sigma_{CA, equ}$	Equivalent (constant amplitude) stress range - the CA stress range which, according to Miner's rule, is equivalent in terms of fatigue damage to the VA loading spectrum	MPa

$\Delta\sigma_{FL}$	Fatigue limit	MPa
$\Delta\sigma_{FL,R=-1}$	Fatigue limit under fully reversed loading, i.e., $R = -1$	MPa
$\Delta\sigma_L$	Local stress range	MPa
$\Delta\sigma_i$	The i th stress range in a loading spectrum	MPa
$\Delta\sigma_{max}$	Maximum stress range in a loading spectrum	MPa
$\Delta\sigma_{OL}$	Overload	MPa
$\Delta\sigma_R$	Equivalent stress range with the stress ratio at which the S-N curve is produced	MPa
$\Delta\sigma_{R=-1}$	Equivalent stress range, which is fully reversed, i.e., $R = -1$	MPa
$\Delta\sigma_{UL}$	Underload	MPa
$\Delta\varepsilon_L$	Local strain range	-

Contents

Acknowledgement	I
Abstract.....	II
Declaration.....	IV
Nomenclature and Definitions.....	V
Contents.....	XI
List of Tables.....	XVIII
List of Figures	XX
1. Chapter 1 Introduction.....	1
1.1 Research background	1
1.2 Research aim, objective and approach	2
1.3 Structure of the thesis.....	5
2. Chapter 2 Literature review	7
2.1 Introduction	7
2.2 Fatigue damage	7
2.3 Fatigue of welded joints	8
2.4 S-N curve.....	10
2.5 Variable amplitude loading spectrum	12
2.6 Cumulative damage under variable amplitude loading.....	14
2.6.1 Cumulative damage rule.....	14
2.6.1.1 Overview.....	14
2.6.1.2 Linear cumulative damage rule.....	14
2.6.2 The fatigue damage of variable amplitude loading	15
2.6.3 Fatigue design under variable amplitude loading.....	18
2.7 Residual stress in welded joints	19
2.7.1 Formation of residual stress in welded joints	19
2.7.2 Effect of residual stresses	22
2.7.3 Residual stress relaxation	24
2.7.4 Residual stress measurement methods	25

2.8 Mean stress correction.....	25
2.9 Effect of plate thickness on the fatigue life of welded joints	27
2.10 Fatigue life improvement	29
2.10.1 Overview of fatigue life improvement techniques	29
2.10.2 Ultrasonic impact treatment	30
2.10.3 Fatigue design for life improved welded joints	30
2.11 Linear elastic fracture mechanics	31
2.12 Crack tip plasticity	34
2.13 Fatigue crack growth under variable amplitude loading	35
2.13.1 Effect of overload on crack growth	35
2.13.1.1 Single overload	35
2.13.1.2 Periodical overloads.....	36
2.13.2 Effect of underload on crack growth	37
2.13.3 Effect of other variable amplitude loading sequences.....	38
2.14 Mechanisms for load interaction under variable amplitude loading	38
2.14.1 Fatigue crack growth rate retardation due to overload	38
2.14.2 Effective stress intensity factor.....	40
2.14.3 Fatigue crack growth rate acceleration due to underload	41
2.15 Non-linear cumulative rule and prediction models for metal under VA loading.....	42
2.15.1 Category	42
2.15.2. Damage curve models.....	42
2.15.3. Life curve modification models	44
2.15.4 Continuum damage mechanics models.....	45
2.15.5 Energy based method	46
2.16 Fatigue life under variable amplitude multiaxial loading	46
2.17 Summary of the background and literature review	48
3. Chapter 3 Fatigue testing under variable amplitude loading spectra	50
3.1 Introduction	50
3.2 Test specimens	50
3.2.1 As-welded specimens	50

3.2.2 Ultrasonic impact treated specimens	53
3.3 Fatigue tests.....	54
3.3.1 Constant amplitude S-N curves for the as-welded specimens.....	54
3.3.2 Variable amplitude loading spectra	55
3.3.2.1 Spectrum I.....	55
3.3.2.2 Spectrum II.....	57
3.3.3 Loading sequences.....	58
3.3.4 Loading modes	58
3.3.5 Arrangement of strain gauges.....	60
3.3.6 Fatigue crack growth monitoring	61
3.3.7 Fatigue testing	62
3.3.7.1 As-welded specimens.....	62
3.3.7.2 Ultrasonic impact treated specimens	64
3.4 Results for as-welded specimens and discussion	65
3.4.1 Fatigue lives and Miner's sum.....	65
3.4.2 Effect of the maximum stress in cycling down loading sequence.....	66
3.4.3 Effect of the minimum stress in cycling up loading sequence	68
3.4.4 Effect of type of loading sequence	70
3.4.5 Effect of plate thickness	72
3.4.6 Effect of type of welds.....	73
3.4.7 Comparison of fatigue lives between experiments and predictions based on BS 7608	73
3.4.8 Post-test examination.....	74
3.5 Results for ultrasonic impact treated specimens and discussion.....	75
3.5.1 Fatigue lives and Miner's sum.....	75
3.5.2 Failure locations of the ultrasonic impact treated specimens	78
3.5.3 Comparison of fracture surfaces between as-welded and ultrasonic impact treated specimens	79
3.6 Conclusions	80
4. Chapter 4 Residual stress measurements	82

4.1 Introduction	82
4.2 Residual stress measurements on the as-welded specimens using the X-ray diffraction method.....	82
4.2.1 Specimen	83
4.2.2 Locations of measurement.....	83
4.2.3 Measurement facilities.....	83
4.2.4 Measurement results	84
4.3 Residual stress measurements on the as-welded specimens using the Centre-hole drilling method	87
4.3.1 Specimen	87
4.3.2 Measurement conditions.....	87
4.3.3 Locations of measurement.....	88
4.3.4 Measurement facilities.....	88
4.3.5 Measurement results	89
4.3.5.1 Initial residual stress	90
4.3.5.2 Residual stress relaxation.....	90
4.4 Residual stress measurements on the ultrasonic impact treated specimens using the X-ray diffraction method.....	91
4.4.1 Specimen	91
4.4.2 Locations of measurement.....	92
4.4.3 Measurement facilities.....	93
4.4.4 Measurement results	93
4.5 Discussion	95
4.5.1 The magnitude of residual stress in as-welded welds.....	95
4.5.2 Effect of residual stress on the fatigue life of welded joints under variable amplitude loading	96
4.5.3 Stress ratio correction advised in IIW	97
4.6 Conclusions	98
5. Chapter 5 Development of analytical models to predict the fatigue life of welded joints under variable amplitude loading spectra.....	100
5.1 Introduction	100

5.2 Development of analytical models	100
5.2.1 Conventional mean stress correction models	100
5.2.2 Development on the conventional mean stress correction models.....	102
5.2.3 Variable amplitude loading sequence factor	103
5.3 Data collection and input parameters	104
5.3.1 Input parameters for the present study	104
5.3.1.1 S-N curve	104
5.3.1.2 Residual stress.....	105
5.3.1.3 Reference maximum stress	107
5.3.2 Input parameters for Study I.....	107
5.3.2.1 S-N curve	107
5.3.2.2 Loading sequence.....	107
5.3.2.3 Residual stress.....	108
5.3.2.4 Reference maximum stress	108
5.3.3 Input parameters for Study II.....	108
5.3.3.1 S-N curve	108
5.3.3.2 Loading sequence.....	109
5.3.3.3 Residual stress and reference maximum stress	109
5.3.4 Input parameters for Study III	109
5.3.4.1 S-N curve	109
5.3.4.2 Loading sequence.....	110
5.3.4.3 Residual stress and reference maximum stress	110
5.4 Comparison of fatigue lives between experiments and predictions under cycling down loading sequences.....	110
5.5 Comparison of fatigue lives between experiments and predictions under cycling up loading sequences.....	112
5.5.1 Fatigue lives predicted based on BS 7608.....	112
5.5.2 Sequence factor for cycling up loading sequence	113
5.5.3 Fatigue life prediction based on analytical models developed in the present study	119

5.6 Comparison of fatigue lives between experiments and predictions under constant mean stress sequences.....	120
5.6.1 Fatigue life predicted based on BS 7608.....	120
5.6.2 Sequence factor for constant mean loading sequence.....	120
5.6.3 Fatigue life predicted based on analytical models developed.....	122
5.7 Conclusions.....	122
6. Chapter 6 Fracture Mechanics Analysis.....	124
6.1 Introduction.....	124
6.2 Fatigue crack growth data under variable amplitude loading sequences.....	124
6.3 Fracture Mechanics approach.....	125
6.4 Input parameters.....	127
6.4.1 Parameters for the present study.....	127
6.4.2 Parameters for Study I.....	128
6.4.3 Parameters for Study IV.....	128
6.5 Matlab code for the calculation.....	129
6.6 Predictions based on BS 7910.....	129
6.6.1 Fatigue crack growth predictions under cycling down loading sequences.....	129
6.6.2 Fatigue crack growth predictions under cycling up loading sequences.....	130
6.7 Development of the analytical model.....	131
6.7.1 Effective stress intensity factor.....	131
6.7.2 Estimation of parameter U	132
6.7.3 Estimation of sequence factor.....	133
6.7.3.1 Local residual mean stress mechanism.....	133
6.7.3.2 Estimation of parameter H	133
6.7.3.3 Calculation of local stress.....	135
6.7.3.4 Estimation of parameter L	136
6.8 Model validation.....	138
6.8.1 Validation under cycling down loading sequences.....	138
6.8.2 Validation under cycling up loading sequences.....	140
6.9 Prediction of the fatigue endurance.....	141

6.10 Conclusions	143
Chapter 7 Conclusions, recommendations, and future works	145
7.1 Conclusions of the research.....	145
7.1.1 Fatigue behaviour of both ultrasonic impact treated and as-welded specimens under variable amplitude loading spectra	145
7.1.2 Residual stress measurements	146
7.1.3 Development of the mean stress correction model to predict the fatigue life under variable amplitude loading spectra	147
7.1.4 Fracture Mechanics analysis.....	148
7.2 Fatigue design recommendations for welded joints under variable amplitude loading spectra.....	149
7.3 Recommendations for future works	150
Reference.....	152
Appendix A Geometry measurement on welds	167
Appendix B The sketch of the rigs.....	168
Appendix C Fracture surface.....	169
Appendix D Residual stress measurement location and results	174
Appendix E Details on welded joints geometries and variable amplitude loading sequences in the literature	176
Appendix F Matlab code.....	183

List of Tables

<i>Table 2.1 The primary benefits of the widely used improvement techniques.</i>	29
<i>Table 2.2 Improvement in fatigue strength due to weld toe peening suggested in BS 7608.</i>	31
<i>Table 3.1 Material properties of S355 structure steel.</i>	51
<i>Table 3.2 Dimensions of the test specimens (in mm).</i>	52
<i>Table 3.3 Stress histograms of VA Spectrum I and II.</i>	57
<i>Table 3.4 Specimen ID for the tests performed under axial loading.</i>	63
<i>Table 3.5 Specimen ID for the tests performed under bending loading.</i>	64
<i>Table 3.6 Specimen ID for the tests performed under axial loading.</i>	65
<i>Table 3.7 Specimen ID for the tests performed under bending loading.</i>	65
<i>Table 3.8 Results of the specimens tested under axial loading.</i>	66
<i>Table 3.9 Results of the specimens tested under bending loading (cycling down for the top welds and cycling up for the bottom welds).</i>	66
<i>Table 3.10 Results of UIT specimens tested under axial loading.</i>	76
<i>Table 3.11 Results of UIT specimens tested under bending mode.</i>	77
<i>Table 3.12 Comparison between the fatigue life of as-welded and UIT specimen.</i>	78
<i>Table 4.1 Details on residual stress measurements.</i>	82
<i>Table 4.2 Specimen ID for the residual stress measurements using the CHD method.</i>	87
<i>Table 4.3 Residual stress (RS) measurement results.</i>	89
<i>Table 4.4 Residual stress measurements on UIT specimens using the XRD method.</i>	92
<i>Table 5.1 Residual stress for CD loading sequences.</i>	106
<i>Table 5.2 Residual stress for CU loading sequences.</i>	106
<i>Table 5.3 The overload ratio and the corresponding average D_m value after mean stress correction.</i>	117

Table 5.4 Parameters in the correlation between RPi and the average Dm value obtained after mean stress correction. 118

Table 6.1 Fatigue crack growth data extracted for the welded joints tested under VA loading sequences. 126

Table 6.2 Comparison of the experimental fatigue lives and those predicted using either best-fitted or average value of parameter L 137

Table 6.3 Comparison of fatigue endurance between experimental data and prediction based on the fracture mechanics model developed in the present study..... 143

List of Figures

<i>Figure 1.1 Schematic showing three cycling down VA loading sequences with different constant maximum stresses.....</i>	<i>1</i>
<i>Figure 2.1 Typical mean and design (mean-2SD) S-N curve for steel welded joints.....</i>	<i>11</i>
<i>Figure 2.2 Typical variable amplitude loading histories in service [40]:(a) pressure variation in a pipeline; (b)pressure variation in the condensation chamber of a reactor; (c) acceleration in the gravity of a transport plane.</i>	<i>13</i>
<i>Figure 2.3 Illustration of rain flow counting method.</i>	<i>13</i>
<i>Figure 2.4 Schematic illustration showing the three sequences used in the VA tests [5] : (a) cycling down from a constant maximum stress; (b) cycling at a constant mean stress and (c) cycling up from a constant minimum stress.</i>	<i>16</i>
<i>Figure 2.5 An example of wideband loading history [6].....</i>	<i>17</i>
<i>Figure 2.6 Formation of residual stress in welds: (a) before welding and (b) after welding [28].</i>	<i>20</i>
<i>Figure 2.7 Typical residual stress distributions due to a butt weld between two plates: (a) longitudinal and (b) transverse [6].....</i>	<i>20</i>
<i>Figure 2.8 Transverse residual distribution in T welded joints: (a) sketch of T welded joints; (b) transfers residual stress profile..</i>	<i>21</i>
<i>Figure 2.9 Superposition of applied stress and residual stress of tensile yield magnitude.....</i>	<i>22</i>
<i>Figure 2.10 Mean stress correction methods.</i>	<i>27</i>
<i>Figure 2.11 Simple Paris law crack growth relationship.....</i>	<i>32</i>
<i>Figure 2.12 Fatigue crack growth under VA loading sequence: (a) CU loading sequence. (b) change in FCGR after an overload. (c) change in crack size after an overload. (d) CD loading sequence. (e) change in FCGR after an underload. (f) change in crack size after an underload.</i>	<i>36</i>
<i>Figure 2.13 Various variable amplitude loading sequences.</i>	<i>39</i>
<i>Figure 2.14 Comparison between linear and non-linear cumulative damage rule under a high-low VA loading sequence.</i>	<i>43</i>

<i>Figure 3.1 Fatigue test specimens: (a) the fabrication process and (b) sketch of the welded specimen (not to scale).</i>	51
<i>Figure 3.2 Typical engineering and true stress-strain curve for S355 structural steel [175].</i>	52
<i>Figure 3.3 Ultrasonic Impact Treatment (UIT) on welded joints: (a) the Stressonic® NOMAD portable Ultrasonic Peening Equipment; (b) an example of the UIT process on 12.5mm-thick welded joint; (c) the groove after treatment along weld toe.</i>	53
<i>Figure 3.4 The mean S-N curves determined under constant amplitude loading with a forced slope $m = 3$ [178]: (a) under axial loading and (b) under bending loading. The BS 7608 Class F mean curve is included for comparison.</i>	55
<i>Figure 3.5 Pi distribution of the Spectrum I and II adopted in the present study.</i>	56
<i>Figure 3.6 Relative fatigue damage, D_i, distributions of Spectrum I and II adopted in the present study.</i>	58
<i>Figure 3.7 Examples of the two loading sequences: (a) cycling down from a constant maximum stress; (b) cycling up from a constant minimum stress.</i>	59
<i>Figure 3.8 The bending test jig.</i>	60
<i>Figure 3.9 The arrangement of strain gauges on the specimens tested in a) axial loading and b) bending loading (gauge 3 opposite to gauge 2).</i>	61
<i>Figure 3.10 The alternating current potential drop (ACPD) device used for crack depth monitoring.</i>	62
<i>Figure 3.11 Miner's sums, D, obtained from welds subjected to CD loading sequences with different maximum stresses (arrow indicates runout).</i>	67
<i>Figure 3.12 Miner's sum, D, obtained from welds subjected to CU loading sequences with different minimum stresses (arrow indicates runout).</i>	69
<i>Figure 3.13 Macro-sectioning of run-out welds: (a) sectioning positions; (b) example of a macro-sections of the welds of specimen B12.5_1.</i>	71
<i>Figure 3.14 Crack observed in the top weld of specimen B12.5_1 where fatigue failure occurred from the bottom weld.</i>	71
<i>Figure 3.15 Comparison of the experimental fatigue lives with that predicted by Miner's rule. (arrows indicate runout)</i>	74

<i>Figure 3.16 Fatigue crack initiation sites (indicated by red arrows) on the fracture surface: (a) specimen A6_1 and (b) specimen A6_2. The maximum stresses were 300 and 150MPa, respectively.</i>	<i>75</i>
<i>Figure 3.17 UIT specimens failing from the parent material. (a) from the gripping region (UIT_A12.5_1) and (b) from the hole for pin loading (UIT_B12.5_1).</i>	<i>79</i>
<i>Figure 3.18 Comparison of the fracture surfaces between the as-welded and UIT specimens: (a) as-welded specimen (A25_1) and (b) UIT specimen (UIT_A25_1). (arrows indicate the crack initiation site.).....</i>	<i>80</i>
<i>Figure 4.1 Locations where residual stresses were measured in as-welded specimens using the XRD method (in mm).</i>	<i>84</i>
<i>Figure 4.2 X-ray diffraction robot.</i>	<i>84</i>
<i>Figure 4.3 Residual stress distribution along the weld toe: (a) 6mm-thick specimen; (b) 12.5mm- thick specimen; (c) 25mm-thick specimen.</i>	<i>85</i>
<i>Figure 4.4 Residual stress distribution along the transverse centreline: (a) 6mm-thick specimen; (b) 12.5mm- thick specimen; (c) 25mm-thick specimen.....</i>	<i>86</i>
<i>Figure 4.5 Locations where residual stresses were measured on the as-welded specimen: (a) schematic. letters in brackets refer to the measurement locations on the opposite side of the plate; (b) one actual test specimen.</i>	<i>88</i>
<i>Figure 4.6 Centre-hole drilling method for residual stress measurement.....</i>	<i>89</i>
<i>Figure 4.7 Results of residual stress measurements in different plate thicknesses.</i>	<i>90</i>
<i>Figure 4.8 Relaxation of residual stress after fatigue loading: (a) 25mm-thick specimen; (b) 12.5mm-thick specimen.....</i>	<i>91</i>
<i>Figure 4.9 Locations where residual stresses were measured on the UIT treated specimen..</i>	<i>93</i>
<i>Figure 4.10 Residual stress distribution along the weld toe: (a) results obtained at groove; (b) 3mm away from the groove.....</i>	<i>94</i>
<i>Figure 5.1 Nomenclatures used in the mean stress correction models.</i>	<i>102</i>
<i>Figure 5.2 Comparison of fatigue lives between experiments and calculations based on BS 7608 which only considers stress ranges under CD loading sequences (re-plot of Figure 3.14) (arrow indicates run-out).....</i>	<i>111</i>

<i>Figure 5.3 Comparison of fatigue lives between experiments and calculations based on the models developed under CD loading sequences: (a) Goodman (b) Gerber and (c) Morrow. (arrow indicates run-out).</i>	111
<i>Figure 5.4 Comparison of fatigue lives between experiments and calculations based on BS 7608 which only considers stress ranges under CU loading sequences (arrow indicates run-out).</i>	113
<i>Figure 5.5 Comparison of fatigue lives between experiments and calculations based on mean stress correction models developed in the present study under CU loading sequences: (a) Goodman; (b) Gerber and (c) Morrow (arrow indicates run-out).</i>	114
<i>Figure 5.6 Comparison between the fatigue lives of experiments from Study II [34] and calculated based on Morrow mean stress correction model developed under CU loading sequences.</i>	116
<i>Figure 5.7 The relationship between RPi and the average Dm value obtained after mean stress correction under CU loading sequences.</i>	118
<i>Figure 5.8 Comparison between the fatigue lives of experiments and calculated based on analytical models developed under CU loading sequences: (a) Gerber and (b) Morrow. (arrow indicates run-out).</i>	120
<i>Figure 5.9 Comparison between the fatigue lives of experiments and calculated based on BS 7608 which only considers stress ranges under CM loading sequences.</i>	121
<i>Figure 5.10 Comparison of fatigue lives between experiments and calculations based on mean stress correction models developed under CM loading sequences.</i>	121
<i>Figure 5.11 Comparison between the experimental fatigue lives under CM loading sequences with that predicted using models developed in the present study.</i>	122
<i>Figure 6.1 An example of comparison of fatigue crack growth under CD loading between experimental data and calculations based on the FCGR curve give in BS 7910 for steels in air.</i>	130
<i>Figure 6.2 An example of comparison of fatigue crack growth under CU loading between experimental data and calculations based on the FCGR curve give in BS 7910 for steels in air.</i>	131
<i>Figure 6.3 Local stress-strain hysteresis loop ahead of crack tip under various loading sequence: (a) CA sequence, (b) loop under CA sequence, (c) CD sequence, (d) loop under CD sequence, (e) CU sequence, (f) loop under CU sequence.</i>	134

Figure 6.4 Comparison between stress concentration factor M_k estimated using 2D solutions given in BS 7910 and k_p calculated based on 2D FEA model..... 136

Figure 6.5 Comparison between experimental fatigue lives and that predicted using model developed with $L = 0.38$ 137

Figure 6.6 Comparison between measured and predicted fatigue crack propagation with $L = 0.38$ 138

Figure 6.7 Comparison between the measured and predicted crack size under CD loading sequences for steel welded joints tested in the present study: (a) crack depth; (b) crack length. 139

Figure 6.8 Comparison between the measured and predicted crack size under CD loading sequences for steel welded joints tested in Study II. (a) crack depth. (b) crack length. 140

Figure 6.9 Comparison between the measured and predicted crack size under CU loading sequences for welded joints tested in the present study and Study I. (a) crack depth (b) crack length..... 141

Figure 6.10 Comparison of fatigue endurance of welded joints between experimental and calculations based on the model developed under either CD or CU loading sequences..... 142

Chapter 1 Introduction

1.1 Research background

The majority of load-bearing components and structures in service are subjected to variable amplitude (VA) loading. To conduct fatigue assessment on the welded joints in such structures, the fatigue design standards such as BS 7608 [1], in conjunction with Miner's cumulative damage rule, are used to estimate the fatigue damage, D , introduced by the loading cycles of various amplitudes in the VA loading history.

In general, the required fatigue life under CA loading is achieved if $D \geq 1.0$ [1]. However, it has been extensively reported that under certain VA loading sequences, such as those involving fully-tensile cycling stress and each stress cycling down (CD) from an almost constant maximum applied tensile stress, fatigue failure can occur when $D < 1$ [2–5], typically when D is about 0.5 [2,5]. Therefore, the current fatigue design standard advises limiting D to 0.5 if there is any uncertainty about the nature of the service stress spectrum, and no relevant test data is available [1]. However, $D = 0.5$ only corresponds to the CD loading sequences with high tensile maximum stresses [5,6]. It is not clear whether D will still be about 0.5 when the maximum stress is further reduced so some or even all stresses are under compression loading in a CD sequence, as shown in Figure 1.1. In addition, there is also a lack of guidance for choosing a proper D value for other type of VA loading sequences. Therefore, further clarifications and guidance regarding the fatigue damage under VA loading is required.

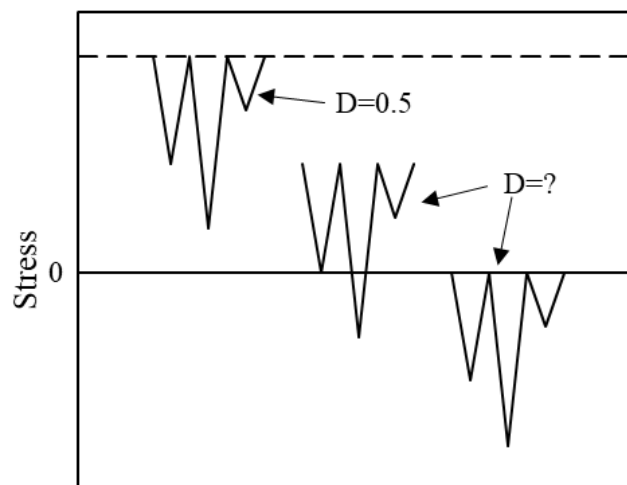


Figure 1.1 Schematic showing three cycling down VA loading sequences with different constant maximum stresses.

Since the fatigue life of welded joints is mainly taken up by fatigue crack growths [7], it can also be estimated using the knowledge of Fracture Mechanics (FM). FM is a mathematical technique to predict fatigue crack growth (FCG) under cyclic loading. Generally, a good agreement can be observed between experiments and FM predictions under CA loading [5]. When welded joints are subjected to VA loading, however, FM predictions can be either conservative or non-conservative due to the stress interactions that can cause either faster or slower crack growth than that obtained under CA loading [8,9].

The effect of stress interactions under VA loading on FCG has been studied intensively [10–13]. Results shows that the crack growth rate could be retreated or even arrested after an overload. On the opposite, the underload may accelerate the FCGR. Moreover, if the VA loading contains stress ranges that are below the fatigue limit, the underload(s) could make them become damaging. In terms of the mechanism accounting for such effects, much of the work focuses on the FCG retardation under the VA sequence containing tensile overloads [10,11]. The study on the mechanism responsible for the FCG acceleration caused by underloads in VA loading is still limited [12,13]. Several alternative mechanisms have been proposed to explain such an acceleration phenomenon, including crack blunting, strain hardening and the tensile mean stress, and they may operate simultaneously [12]. Doré [13] conducted fatigue testing and Finite Element Analysis (FEA) to bridge the gap. The results indicated that the local tensile mean stress ahead of the crack tip was the primary reason for the observed FCG acceleration under VA sequence containing periodic underloads. However, the analytical model corresponding to this mechanism has not been well established.

1.2 Research aim, objective and approach

In view of the situations described above, this research aims to investigate the effect of VA loading sequences on the fatigue life of welded joints, aiming to provide guidance for the future revision of BS 7608 regarding the fatigue damage under VA loading. To this end, the objectives of the study and the approaches adopted include:

- To investigate the effect of the maximum stress level in the CD loading sequence on the fatigue performance of welded joints.

- To evaluate the applicability of $D = 0.5$ when the maximum stress decreases under CD loading sequences.
- To evaluate the effect of plate thickness of the specimen on the fatigue performance of welded joints under VA loading sequences.
- To investigate the effect of mean stress on the fatigue performance of welded joints under VA loading and develop analytical models to improve fatigue damage prediction.
- To study the fatigue performance of life-improved welded joints under VA loading spectra.
- To conduct residual stress measurements before and after fatigue testing in order to study the residual stress and its relaxation under VA loading.
- To investigate the mechanism associated with the effect of VA loading sequence on the FCG and develop an analytical model to improve the prediction of FCG under VA loading.
- To discuss the implication of the results on current fatigue designs and to provide recommendations for future revision of BS 7608 when appropriate.

To achieve these objectives, an extensive experimental programme was carried out in the present study. Two VA loading spectra, Spectrum I and II, were designed, with Spectrum I following the typical Gassner distribution, and the latter produced by adjusting the number of cycles for each stress range in Spectrum I manually. Based on these spectra, CD loading sequences with various constant maximum stresses were produced. Welded joints containing transverse fillet welded attachments were tested under these sequences under either axial or bending loading. The specimens were manufactured from plates with three different thicknesses. A novel test jig was designed to apply a constant tensile axial stress on specimens under bending loading. In addition to testing the as-welded specimens, some life-improved welded joints where the weld toes were peened using Ultrasonic Impact Treatment (UIT) technique were also tested. The crack growth at the weld toe was monitored using the Alternating current potential drop (ACPD) technique, in conjunction with the soap solution method.

Residual stress measurements were conducted using either the centre-hole drilling (CHD) technique at TWI Ltd or the X-ray diffraction (XRD) technique at Coventry University. The residual stress measurements were conducted before fatigue testing to investigate the initial residual stress presented in both as-welded and UIT welded joints. The residual stress was also measured after loading the welded for a few cycles to study the residual stress relaxation.

Based on the residual stress measurements results, the fatigue test data was interpreted using the effective mean stress in order to consider the effect of the applied mean stress on the fatigue life of welded joints. New analytical models were then developed correspondingly on the basis of the conventional mean stress correction models.

The mechanism that leads to FCG acceleration under CD loading sequences was determined by reviewing existing published literature. An analytical model was developed accordingly to improve the prediction of FCG.

Figure 1.2 provides a general description of the research framework employed in the present study.

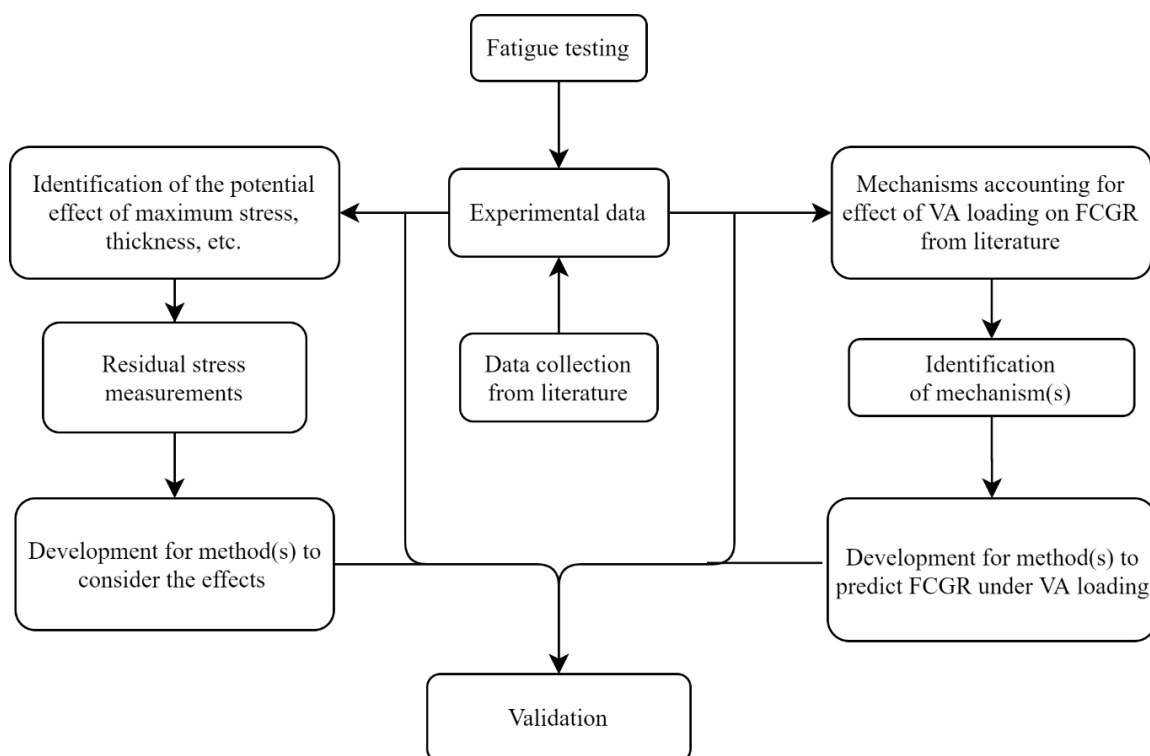


Figure 1.2 The research framework employed to investigate the fatigue performance of welded joints under VA loading spectra.

1.3 Structure of the thesis

The thesis is composed of the following chapters:

Chapter 2 presents a review on the fatigue performance of welded joints under VA loading sequences, especially on the evaluation of the Miner's rule. The influence of residual stress and plate thickness was examined. Additionally, the mechanism associated with the retardation and acceleration of fatigue crack growth under VA loading was also reviewed.

Chapter 3 presents an extensive fatigue testing program to investigate the fatigue performance of welded joints under VA loading sequences with various mean stresses under either axial or bending loading. It describes the effects of loading sequences, the mean stress and the plate thickness on Miner's sum and the fatigue performance of welded plates. This chapter also describes the examination of the fracture surfaces and the production of fatigue crack growth (FCG) data.

Chapter 4 presents the results of residual stress measurements obtained from both CHD and XRD methods. The magnitudes of residual stress in the as-welded condition for each plate thickness of specimen were compared, and the relaxation of residual stress due to fatigue loading was described and discussed.

Chapter 5 discusses the effect of mean stress and presents new models for VA loading based on conventional mean stress correction models. These models can convert each stress range in the given VA loading sequence to an equivalent stress range with a specific maximum stress where the S-N curve was produced. The damage of the applied stress range was then estimated using the equivalent stress range. These models also include a new sequence factor that was developed to consider the sequence effect on the fatigue performance of welded joints.

Chapter 6 presents a new analytical model to predict the FCG under given VA loading sequences. The residual tensile mean stress was considered as the dominant mechanism that accounts for acceleration or retardation in FCGR. The model was validated by the experimental data obtained from the current study and those from the open literature. Moreover, the fatigue lives of welded joints under various VA loading sequences were also estimated using this model.

Chapter 7 concludes this study and provides recommendations for fatigue design and future research.

Chapter 2 Literature review

2.1 Introduction

This chapter provides necessary background information and an indication of the current status of research with respect to the fatigue performance of welded joints under VA loading. A review on published work conducted in this area is presented, including methods of fatigue assessment, the effect of the nature of the loading sequence on the fatigue life, the influence of residual stress. The mechanism associated with the retardation and acceleration in fatigue crack growth under VA loading is examined as well.

2.2 Fatigue damage

It is well known that structures subjected to repeated or fluctuating loads may fail in service, even though the loads applied are well within the material's static strength capacity. The most likely (up to 80% [13]) mechanism behind such failures is material fatigue. Regarding a material's fatigue performance, the magnitude of the range of cyclic stress and the corresponding number of cycles that the structure can endure are termed the fatigue strength and fatigue life of the material, respectively. For metals, fatigue generally involves the initiation and propagation of a crack driven by the application of repeated stresses [14]. One of the dangers of the fatigue failure is that it can occur without any prior indication in the form of visible deformation in the fracture region, even the material is ductile. Similarly, crack initiation and propagation may be undetectable until it reaches a critical size.

The fatigue damage can be measured through three different ways, as proposed by Chaboche [15], which are remaining life, microstructure, and physical parameters.

The remaining life concept is a natural way for an engineer to define fatigue damage as it allows predictions of the lifetime of a structure. The most conventional definition for such a damage parameter is the life ratio which is the ratio of the present number of cycles already applied to the total number of cycles to crack initiation (or failure) [15]. In this case, it corresponds to the linear damage rule, Miner's rule, which has been widely used in the current fatigue design codes, such as, BS7608 [1], IIW [16], to estimate fatigue damage or remaining lifetime of the

welded structure. It should be noted that this remaining life concept does not necessarily lead to the linear rule, a number of non-linear cumulative rules are also available.

The second nature way is through microstructure. It is clear that mechanisms of cyclic microplasticity, based on the glide of dislocations, are responsible for the fatigue damage [17]. One of the most pertinent microstructural parameter used is the cyclic slip irreversibility, which is the ratio of microstructurally irreversible cyclic plastic strain to the total cyclic plastic strain [18,19]. It was reported that an explicit power-law relation exists between the cyclic slip irreversibility and the number of cycles for crack initiation [19,20]. This parameter can be deduced from the surface measurement results using advanced microscopy techniques, e.g., scanning electron microscopy (SEM) [17], transmission electron microscopy (TEM) [18] and atomic force microscopy (AFM) [21,22]. The irreversible and total cyclic plastic strain can be estimated based on the measured grain size, average extrusions height, and inter-band spacing [21,22]. In addition, the number of cycles required for crack initiation could also be correlated with a critical value of the average extrusion height [21,23].

Thirdly, the damage also can be correlated with the changes in material physical parameters. Sun etl. [24] reported the damage evolution in 45C steel could be effectively represented by the electric resistance changes, follow a nonlinear relationship. It was also reported that the ultrasonic velocity in the sample was sensitive to the change of fatigue damage and the inverse function of the logistic equation could be used to describe the evolution curve of fatigue damage [25,26]. The fatigue damage was found to be dependent on the changes in the magnetic properties, especially the variations in coercivity and remanence and impending failure can be well predicted from the rapid decrease in these two parameters [27].

The present research aims to study the fatigue damage in welded joints in line with the fatigue design codes; therefore, the remaining life concept is employed, and more relevant details are given in the following sections.

2.3 Fatigue of welded joints

Welding is the most common joining method to integrate components into a metallic structure. In a structure containing welded joints, fatigue failure is more likely to happen at the weld toe, rather than in the parent metal [6,28]. This can be attributed to three main reasons: firstly, the

welding process introduces large tensile residual stress in welds, so the weld toe experiences a higher stress level than other locations. Secondly, stress concentration may arise at the weld toe due to surface geometry discontinuity and the local notch, which increase the rate of damage by fatigue. Thirdly, and most importantly, welding may introduce crack-like flaws at the weld toe, which can significantly shorten the fatigue life. In view of these, it is essential to assess fatigue performance of welded joints to avoid the premature failure of the structure, typically using fatigue design standards such as BS 7608 [1], DNV-RP-C203 [29], IIW [16] and BS 7910 [30].

To estimate the fatigue life of components, there are two main methods - the stress-life (S-N curve) approach [1,16] and the crack growth analysis [30]. The stress-life method considers the total life to failure as a function of cyclic stress or strain range and ignores the existing flaws. Thus, the fatigue life calculated includes the number of cycles to initiate and propagate the fatigue crack. This method has a particular drawback which is the fatigue lives calculated may show a wide scatter. Such scatter can be attributed to the inconsistent nature of the crack initiation phase in different materials, as the initiation phase depends on the material microstructure and manufacturing process [13]. The crack growth analysis, which is also known as tolerance design, latter, damage tolerant design, is based on the use of fracture mechanics (FM) principles to describe fatigue crack growth from an initial flaw size to a critical crack size [30]. In this case, the crack initiation phase is ignored, leading to a reduction in the scatter of fatigue lives predictions. However, the consistency between the calculated and the actual fatigue life is highly dependent on the accuracy of the initial flaw size measured or assumed [13].

For welded joints, the crack initiation phase occupies a much smaller proportion of life than that for a case such as a plain plate, where most of the fatigue life may spend initiating a crack. Gurney [6] suggested that the initiation stage is very often almost non-existent in the case of welded joints as fatigue cracks in nearly all welded joints start at pre-existing flaws, the presence of which can be taken as the equivalent of an initiated crack. In this case, current standards [1,30] assumes the of fatigue life of welded joints is dominated by crack growth propagation.

It should be noted, the welded joints mentioned here represents the joints in the case of as-welded. For those welded joints which are carefully fabricated or applied to life improvement

techniques, such as post weld heat treatment (PWHT) or ultrasonic impact treatment (UIT), crack initiation life is also should be expected.

2.4 S-N curve

The S-N curve, also known as Wohler curve, was first established by a Germany engineer August Wohler in 1870 [31]. Based on the results obtained from the rotating bending fatigue test on railroad axles, Wohler revealed that the cyclic stress range was more important than the peak stress. S-N curves were then established by plotting the results in terms of the stress range against the number of cycles to failure. Nowadays, the development of technology in fatigue testing allows establishing the S-N curves for a specific component or structure under other loading modes, such as axial and bending loading.

The S-N curve is widely used in current fatigue design codes, such as BS 7608 [1], IIW [32], as the primary method to predict the fatigue life of welded joints under any type of fatigue loading. The S-N curves are primarily based on the fatigue test data obtained from constant amplitude(CA) loading [1]. They are typically plotted in log-log scales, which produces a reverse proportional linear relationship between the stress range and the fatigue life, following:

$$\Delta\sigma^m N = C \quad (2.1)$$

where $\Delta\sigma$ is the stress range applied, N is the number of cycles to fatigue failure, m and C are material constants that can be calculated using a linear regression analysis based on experimental results. Parameter m is the slope of the S-N curve. For steel welded joints, it is usual to consider $m = 3.0$, which is a reasonable average value and generally used in fatigue designs [1]. For safety concerns, an S-N design curve related to the lower bound of the test data is used. Such a design curve is established by setting two standard deviations (2SD) of $\log N$ below the mean curve in order to ascertain 97.7% of survival, see Figure 2.1.

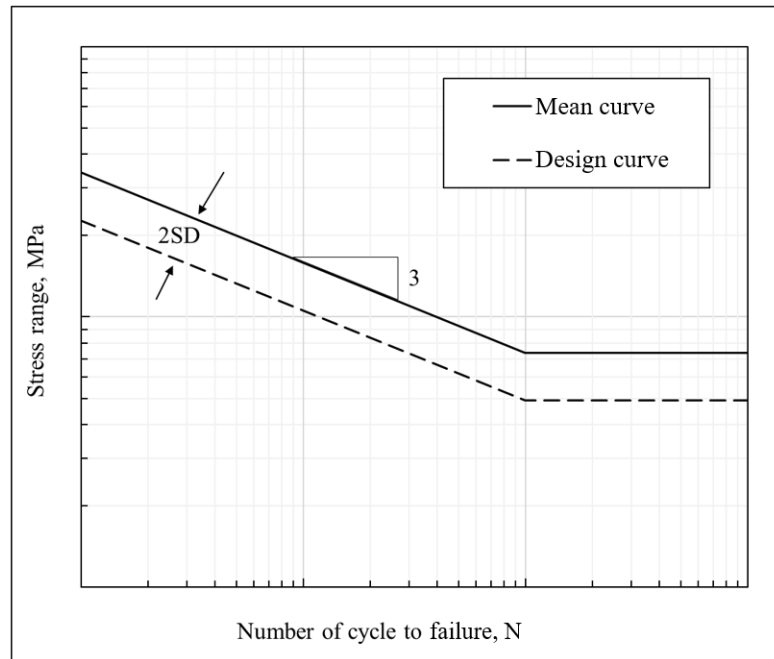


Figure 2.1 Typical mean and design (mean-2SD) S-N curve for steel welded joints.

S-N curve has a knee point below which the S-N curve is turned to horizontal, suggesting the welded joints can sustain the stress range below this point infinitely. Under CA loading, this specific stress range is known as the constant amplitude fatigue limit (CAFL) and is defined as the value corresponding to the fatigue life at 10^7 cycles in standards [1,32]. However, under VA loading, it is found that ignoring the minor stress range that below CAFL can be unsafe [5,6]. Therefore, the S-N curves are advised [33] to extrapolate beyond the knee point with a shallower slope at $m + 2$ (i.e. 5 when $m=3$) at the 5×10^7 cycles [1] or at 10^7 cycles [29]. Some studies also suggest that the damage of the minor stress range can be as much as that estimated with the S-N curve extrapolated with non-slope change [5,13,34].

It should be noted that Figure 2.1 is typical for welded joints where fatigue life is dominated by fatigue crack propagation. For plain materials where crack initiation dominates, the slope of the S-N curve generally has a much shallower gradient with no identifiable knee point [35].

The S-N curves can be established based not only on the nominal stress but also on the hot-spot stress (HSS) or the linear-elastic notch stress. The nominal stress is calculated by conventional engineering methods, which excludes the effects of structural discontinuities (e.g. welds, openings, thickness changes) and the effects of the local shape of the detail [1,36]. This stress is easily calculated in the case of simple axially loaded members or simple beams in

bending. However, for some complicated structures, such as tubular nodal welded joints, HSS is generally used as the reference stress as it includes the stress concentration caused by the structural discontinuities and the presence of attachments [1,36,37]. Another reference stress which is increasingly gaining industrial acceptance is the notch stress, which considers the effect of weld profile and is calculated using finite element modelling with a reference radius [37,38].

In the current standards, various S-N curves are advised depending on the weld class detail. In BS 7608 [1] the classification system uses letters to refer to different weld details. And IIW [32] employs numbers to differ weld details. These numbers are the nominal stress range intersected at the fatigue life of 2×10^6 cycles.

2.5 Variable amplitude loading spectrum

In service, the great majority of structures and components generally experience complex stress loading cycles of variable amplitude (VA) [39,40]. Some representative examples are shown in Figure 2.2. VA loading can arise due to the variation of loads, different loading modes, or as a result of structural discontinuity. Therefore, it is essential to establish the actual VA loading spectrum in service to estimate the fatigue endurance of the welded structure for design purpose. The electrical resistance strain gauge is currently the most common method used to measure the strain at the point of interest, and so the working stress can be calculated accordingly.

A loading history established directly using strain gauges is usually complicated. It needs to be broken down into a corresponded loading stress spectrum before conducting either fatigue testing in the lab or fatigue assessment. The spectrum is a representation of stress range(s) and the corresponding number of cycles, which can be set up using some counting methods, such as the Rainflow or the Range pair methods [6,28]. In BS 7608 [1], the Rainflow method is recommended.

The Rainflow counting method is illustrated in Figure 2.3. First, the loading history is clockwise rotated by 90° (after rotation, the time axis is vertical, while the stress axis is horizontal). Second, imagining a raindrop starts flowing from each successive extremum point of the loading history and stops when a) it falls opposite a larger maximum or minimum point or b) it meets a previous flow falling above or c) it falls below the sequence. A positive or

negative loading cycle can be identified between each pair of start and stop points. Finally, the loading spectrum is determined by pairing up the same counted positive and negative loading cycles.

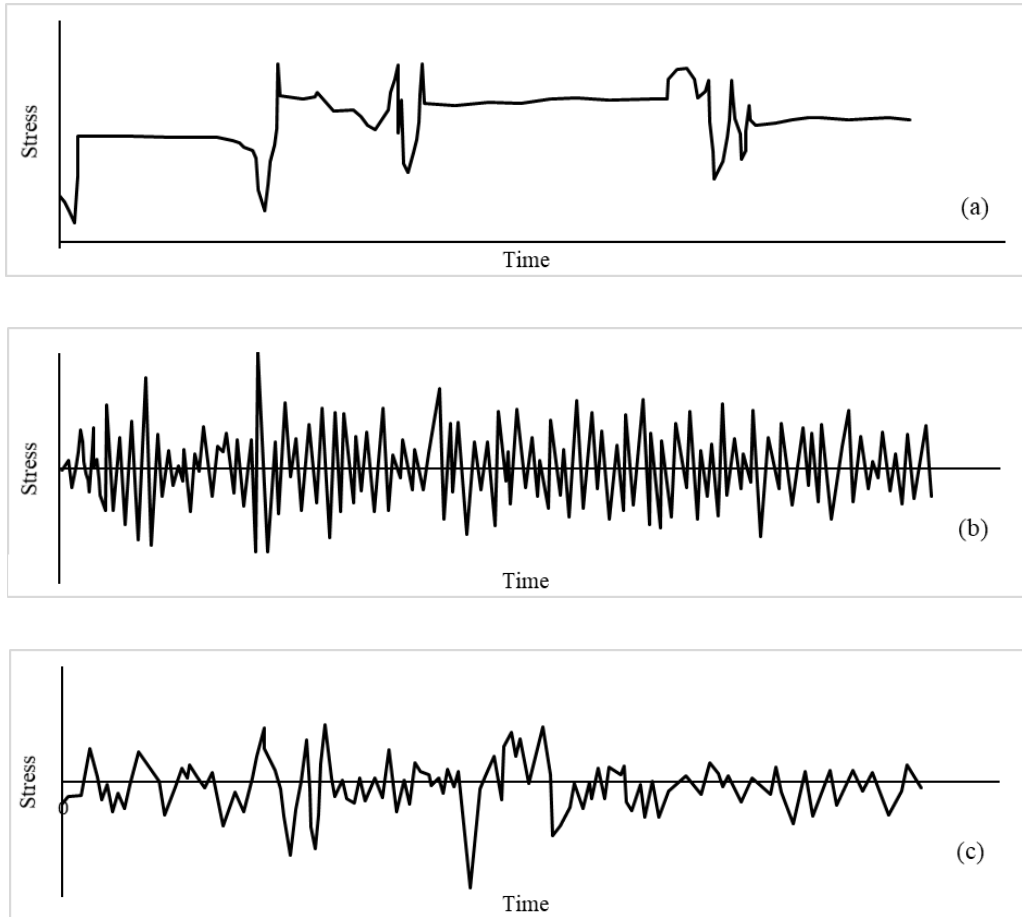


Figure 2.2 Typical variable amplitude loading histories in service [40]:(a) pressure variation in a pipeline; (b) pressure variation in the condensation chamber of a reactor; (c) acceleration in the gravity of a transport plane.

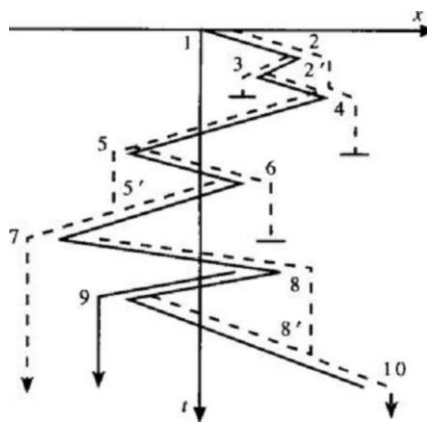


Figure 2.3 Illustration of rain flow counting method.

2.6 Cumulative damage under variable amplitude loading

2.6.1 Cumulative damage rule

2.6.1.1 Overview

A wide range of cumulative damage models for high cycle fatigue of metal were developed in the last four decades and they can generally be categorized as either linear or non-linear damage models [41,42]. The most widely used linear cumulative damage rule is Palmgren–Miner linear damage rule or as simply as Miner’s rule. It has become the industry standard for fatigue design of metal structures due to its intrinsic simplicity and been adopted in leading design standards such as BS 7608 [1], DNVGL-RP-C203:2016 [29], EN 1999-1-3:2007 [43], IIW:2016 [16]. Although its wide usage, however, Miner’s rule is known to give inaccurate prediction under VA loading as it cannot take into account the effect of the loading sequence and interaction [42,44,45]. Hence, in order to overcome this drawback, a wide range of non-linear cumulative damage and life prediction models has also been developed and widely used, which may provide more satisfying results than the linear rule [46]. Nevertheless, these non-linear models have their own drawbacks. Patil et al. [47] and Kris et al. [48] pointed out a significant number of non-linear cumulative fatigue damage models were developed and validated based on relatively small experimental datasets, so their generic performance cannot be judged. Moreover, predictions based on non-linear models sometimes also show a significant deviation from the experimental data [46]. So linear cumulative damage rule still remains the most widely used for fatigue design under variable amplitude loading [48].

As the present study aims to provide guidance for the future revision of BS 7608, it only focuses on Miner’s rule. However, a brief review on the non-linear cumulative models has also been made which is given later in Section 2.15. The review conducted in this section (Section 2.6) is just based on Miner’s rule.

2.6.1.2 Linear cumulative damage rule

Miner’s rule is the most widely used method in the industry to estimate fatigue damage D for metal under a VA loading spectrum:

$$D = \frac{n_1}{N_1} + \frac{n_2}{N_2} + \frac{n_3}{N_3} + \dots = \sum \frac{n_i}{N_i} \quad (2.2)$$

where n_1, n_2 , etc., are the numbers of cycles corresponding to applied stress ranges $\Delta\sigma_1, \Delta\sigma_2$, etc., involved in the VA loading spectrum, and N_1, N_2 , etc., are the numbers of cycles to fatigue failure under constant amplitude (CA) loading at those stress ranges, which can be calculated according to S-N curve (Equation 2.1). i is the number of stress ranges.

Current fatigue design standards, such as BS 7608 [1], EN 1999-1-3:2007 [43], IIW:2016 [16] advise that any structure with Miner's sum $D < 1$ is safe for operation. Otherwise, fatigue failure will occur. An implicit assumption in the Miner's rule is that the fatigue damage introduced by a certain stress range under the VA loading is identical to that due to the same stress range under CA loading. However, there is extensive evidence suggesting the stress range under VA loading could be either more [3–6,40,49] or less [3–5,50–52] damaging than the identical stress range applied under CA loading, depending on the nature of the VA loading sequence; hence, the D value calculated using Equation 2.2 at fatigue failure can be lower (non-conservative) or higher (unduly conservative) than unity, respectively.

2.6.2 The fatigue damage of variable amplitude loading

The nature of a VA loading sequence, such as shape, small stress range and length etc., can strongly influence the D value when fatigue failure occurs. Extensive studies have investigated the fatigue performance of welded joints under VA sequences with three typical shapes, as defined by Zhang and Maddox [5]: Sequence A where all loading cycles are cycling down (CD) from a constant maximum stress; Sequence B where all loading cycles are about a constant mean stress (CM), and Sequence C which involves all loading cycles being cycling up (CU) from a constant minimum stress, see Figure 2.4. These three sequences are also referred to CD, CM and CU sequence, respectively.

It was found that the fatigue life of welded joints could be significantly degraded under the CD loading sequence, with the D value much lower than unity at failure [3–6,13,49,53], typically being about 0.5 [5,6,13] or even lower [49,53]. Although such VA loading sequence was chosen for the purpose of simulating the severe conditions that are expected to exist in welded joints containing high tensile residual stresses, it may actually arise in some engineering structures, such as gas storage vessels, gas turbine blades, railway lines and aircraft wings [12].

Furthermore, a wide band spectrum, where the mean stress of individual cycles included varies widely and generally involves a stress history with irregularity significantly less than 1.0, as shown in Figure 2.5, may also exhibit similar behaviour with the CD sequence, although it does not involve cycling down from a constant maximum stress.

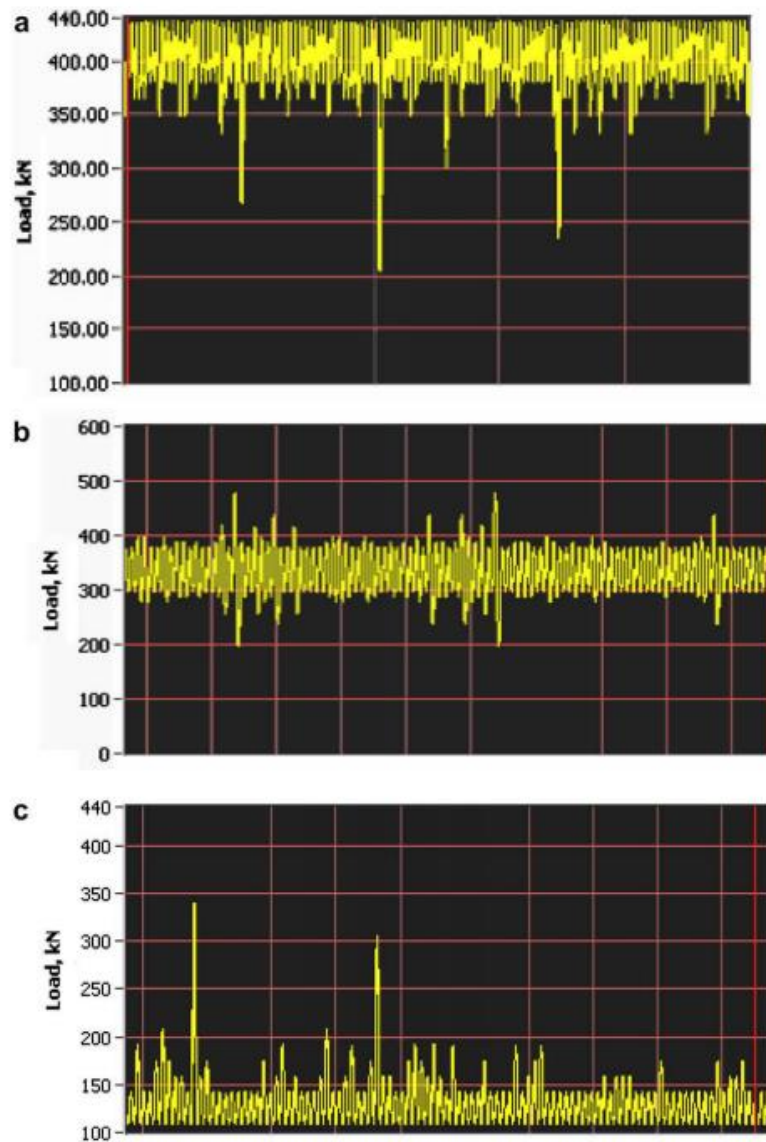


Figure 2.4 Schematic illustration showing the three sequences used in the VA tests [5] : (a) cycling down from a constant maximum stress; (b) cycling at a constant mean stress and (c) cycling up from a constant minimum stress.



Figure 2.5 An example of wideband loading history [6].

For CM loading sequence, which is also known as a narrow band sequence [6], the D value at failure reported in [5] was about 0.8, while fell into the range between 0.25 and 1.6 according to [6]. In terms of CU loading sequences, the D value is generally higher than unity [3,5,52,54]. For example, the D value was reported >1.3 by Zhang and Maddox [5] and even higher to eight [34]. However, some test results implied that the D value depended on the overstress ratio of a CU loading sequence, which is the ratio of the largest stress range to the lowest stress range and could be lower than unity at failure, being about 0.6 [34].

Another problem associated with the application of Miner's rule under VA loading is the method of treating the small stresses that are below the CAFL. The high-stress ranges in the spectrum may lead the fatigue crack to propagate to such an extent that those small stresses below the CAFL become damaging [13]. To deal with this, instead of modifying Miner's rule, it is easier to change the slope of the S-N curve below the fatigue limit [33]. The most widely used assumption is that the slope of an S-N curve obtained under CA loading can be extrapolated beyond the CAFL, at a shallower slope, typically $m = 5$ instead of 3. The number of cycles corresponding to the CAFL is different in design guidelines. For example, in DNVGL-RP-C203:2016 [29] it is $N = 10^7$ cycles, while in BS 7608:2014 it suggests that a slope change from m to $m + 2$ at $N = 5 \times 10^7$ cycles seems to be more suitable. A more extreme recommendation is made by the US AASHTO bridge rules [55] where the S-N curve is suggested to be extrapolated with no slope change.

Gurney [6] further investigated this problem and found that a linear and a bi-linear S-N curve only made little difference for a convex upwards spectrum, but the latter may be unsafe for a concave upwards spectrum. This was further supported by Zhang and Maddox [5], who conducted fatigue testing under a concave up spectrum as well. The results revealed that the

small stress ranges in the spectrum were just as damaging as implied by the CA S-N curve extrapolated beyond the CAFL.

Another factor that affects the value of D under VA loading that involves repeatedly applied blocks of a VA sequence is the block length (i.e. the number of cycles of the repeated VA sequence) [6]. It is proportional to D value at failure. Therefore, a method known as the area rule was derived to describe such relationship, following:

$$\ln\left(\frac{N_B}{N_C}\right) = - (\text{area under curve } p_i \text{ v. } \ln N_{Ei}; \text{ exceedence diagram}) \quad (2.3)$$

where N_B is the number of blocks to failure, N_C is the fatigue life under CA loading corresponding to the top limit stress in the spectrum, P_i the relative stress range in a spectrum and N_{Ei} the number of cycles per block equal to or exceeding P_i times the top limit stress.

2.6.3 Fatigue design under variable amplitude loading

As mentioned, there is extensive evidence [3–6,40,56] suggesting that the stress range under VA loading could be more damaging than the same stress range applied under CA loading in some circumstances. For example, under some stress spectra, including those involving fully-tensile stress cycling about a high tensile mean stress (CD loading sequence) or where there is little variation in the maximum applied tensile stress [3,5,6,13], fatigue tests have shown that fatigue failure can occur when $D < 1$, typically being about 0.5.

Therefore, BS 7608 advises limiting D to 0.5 if there is any uncertainty about the nature of the service stress spectrum, or for particularly critical cases. Alternatively, D can be established for the particular stress spectrum and welded joint type concerned by reference to relevant published data or special testing. The reduction in Miner's rule has also been applied in IIW [16]. It recommends that Miner's rule should be applied, assuming $D = 0.5$ at fatigue failure. The advised D value under VA loading is also related to the mean stress according to Sonsino [40] where D is recommended to be assumed at 0.5 under constant mean stress conditions, whilst even lower at 0.2 for varying mean stress conditions such as under wideband loading [40].

However, $D = 0.5$ is only corresponding to the CD loading sequence with a high maximum stress, at about 80% specified minimum yield stress of the material [5,6]. Although similar results were obtained when the maximum stress was halved from 280 to 147MPa [5], it is still unclear whether $D = 0.5$ is proper under the CD sequence with lower maximum stresses, as shown in Figure 1.2. Moreover, in the current standard there is still no guidance on how to decide a proper D value for either CM or CU loading sequence to not only ascertain safety but also to avoid waste of the remaining fatigue life.

2.7 Residual stress in welded joints

2.7.1 Formation of residual stress in welded joints

Residual stresses are those stresses that remain in a welded joint even in the absence of external loading or thermal gradients. They affect susceptibility to fracture and fatigue performance. Figure 2.6 illustrates the formation of residual stress in welded joints. It is mainly as a consequence of the expansion or contraction in the welding area heated by the welding source being restrained by the adjacent material at low temperature [6,28]. The resulting idealised residual stress distribution, where a uniform through-thickness stress distribution is assumed, are shown in Figure 2.7 in the longitudinal direction (parallel to the weld) and transverse direction (normal to the weld).

Residual stress is independent of external loading, but it is self-balanced or in equilibrium within the material. Residual stress occurs at each welded joints and influences the fatigue behaviour of the joints [28]. Therefore, the actual load applied to the welded joints is the combination of the external load and the residual stress.

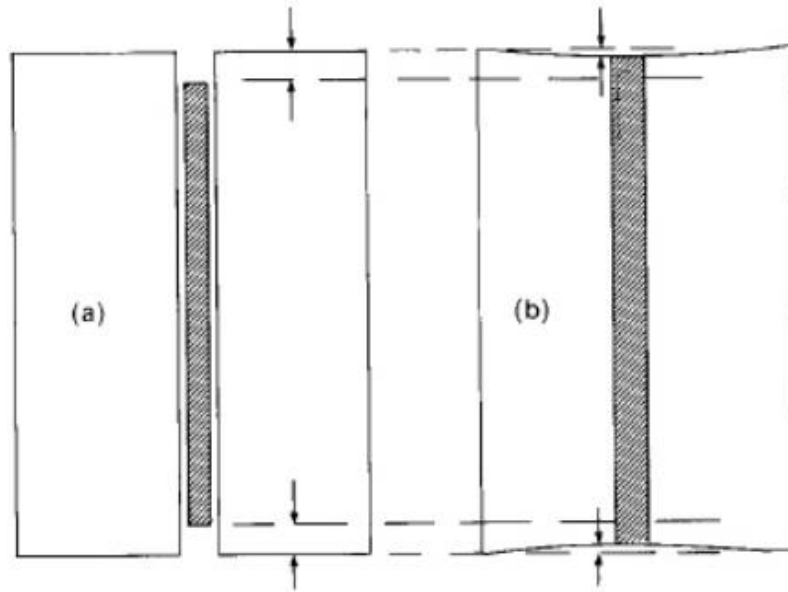


Figure 2.6 Formation of residual stress in welds: (a) before welding and (b) after welding [28].

The magnitude of the tensile residual stress near weld toe depends on the yield tensile strengths of the material, i.e., the weld and parent metal. In steel welded joint, where the two are closely matched, the residual stress may be as high as the yield strength of the parent metal [28].

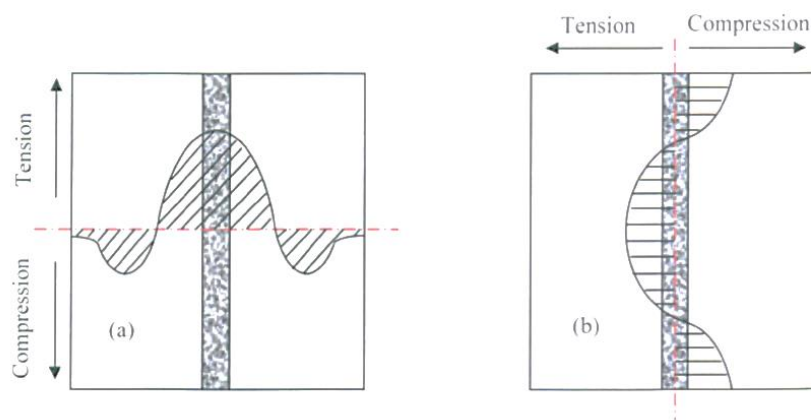


Figure 2.7 Typical residual stress distributions due to a butt weld between two plates: (a) longitudinal and (b) transverse [6].

For the T-butt welds, i.e. plate fillet welded one transverse attachment on one side, as shown in Figure 2.8 (a), standard BS 7910 [30] and R6 [57] provide the residual stress profiles for as-welded joints. The profiles are expressed in terms of the normalized depth through the plate thickness and the normalized residual stress in the longitudinal and transverse directions. The transverse residual stress distribution is illustrated as the solid line in Figure 2.8 (b).

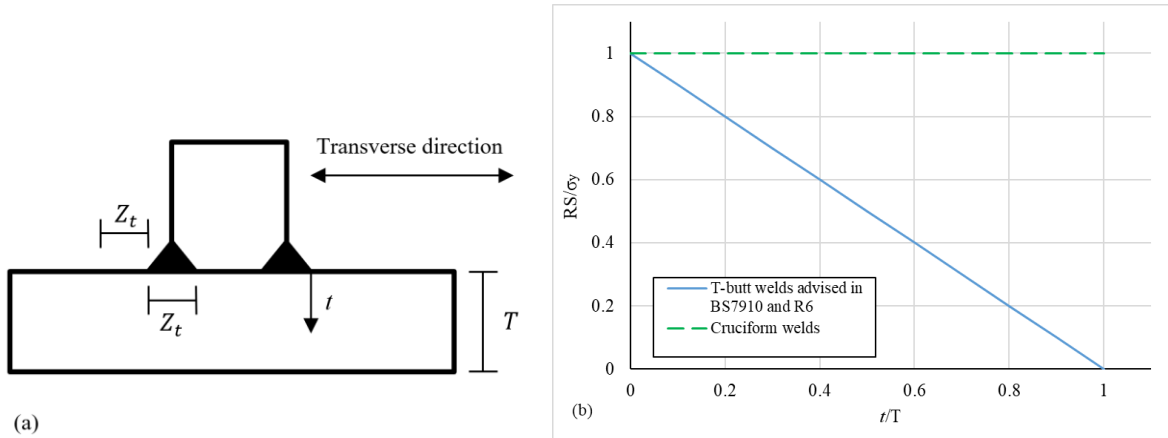


Figure 2.8 Transverse residual distribution in T welded joints: (a) sketch of T welded joints; (b) transfers residual stress profile..

To calculate the transverse residual stress (RS), the follow equation applies [30,57] :

$$\frac{RS}{\sigma_y} = 1 - \frac{t}{T} \quad (2.4)$$

where t is the depth below the plate surface. And this profile is appropriate for assessing flaws that lie within a distance of Z_t from the weld toe, where Z_t is the weld width.

If consider welding another attachment on the other side of the T welded joint, then it becomes a cruciform welded joint, as the one used in the present study. The residual stress profile introduced by the new attachment should be similar as that for the original attachment. So, by superposing these two profiles, the transverse residual stress distribution in the cruciform welded joints should be constant through the plate thickness, as indicated by the dash line in Figure 2.8 (b).

It should be noted that the profiles provided is only suitable for the plate which is thicker than 25mm and corresponding to the upper boundary of the experimental results. For more accurate assessment residual stress distribution may be determined by conducting residual measurement on mock-up weldments [30]. Indeed, the residual stress value was reported to be dependent on the specimen size - smaller dimensions [58] or thinner plates [59,60] yield in lower residual stress. For the cruciform welded joints with a thinner plate thickness, the residual stress was about 60% [61–63] and even 20% [64–66] of the yield strength of the steels investigated.

The type of welded joints also affects the residual stress. The welded joints with longitudinal and edge attachments usually contain tensile residual stress that can reach to the yield stress of the material [6,28].

2.7.2 Effect of residual stresses

Residual stress can influence the fatigue endurance of welded joints significantly. This is because that the externally applied stress is superimposed onto the residual stress, resulting in a higher effective mean stress than that of the applied stress. Typically, welds and the adjacent material may experience the actual stress range cycling down from the yield stress of parent metal [6], as shown in Figure 2.9.

Considering a welded joint, where the residual stress of tensile yield magnitude is presented (line 1), subjected to nominal tensile stress, σ , as the weld metal is already at the yield tensile strength of the material, the further application of σ leads to local plastic straining, and the actual stress in the weld remains at σ_y , while the surrounding stress field changes to accommodate the applied load. The stress distribution on the application of σ is illustrated as line 2. After removing σ , the residual stress in weld reduces to $(\sigma_y - \sigma)$, and the new residual stress system is indicated as line 3. Therefore, if the stress range σ , ranging between zero and σ , is repeatedly applied, the actual stress range in the weld will cycle between a maximum stress of σ_y and a minimum stress of $(\sigma_y - \sigma)$, i.e., a range equal to the stress range applied, but with a mean stress of $\frac{\sigma_y + \sigma}{2}$, rather than that calculated by $\frac{\sigma}{2}$.

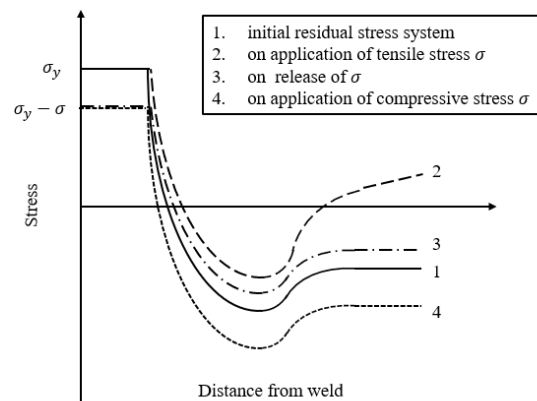


Figure 2.9 Superposition of applied stress and residual stress of tensile yield magnitude.

Similarly, if a compressive stress, $-\sigma$, is repeatedly applied, no local plastic straining occurs, and the actual stress also cycles between $\sigma_y - \sigma$ and σ_y , line 4. Thus, for the same stress range of applied stress, the weld experiences the same stress condition under tensile and compressive loading.

Since it is difficult to predict or measure the residual stress in any particular welded structure, current fatigue design standards, such as BS 7608 [1], BS 7910 [30], IIW [32] and DNV [29], all assume a high tensile residual stress presents in welds with a magnitude of the tensile yield strength of the material to ensure their guidance are conservative. Thus, the fatigue endurance of welded joints depends only on the stress range and is independent of the type of welded joints as well as the mean stress or the stress ratio, R - the ratio of the minimum to the maximum stress of the externally applied load.

Indeed, fatigue tests on the welded joints with longitudinal attachments did not show any significant difference in the fatigue strength when the specimens were loaded with various stress ratios, ranging from -4 to 0.5 [6,28]. Similar results were also reported in [67,68] where the stress ratio ranged between 0.67 and completely compressive load.

However, for the other type or relatively small size welded joints where the residual stress is lower, as mentioned in 2.6.1, the mean stress or the stress ratio matters. For example, butt-welded joints made of different steels were tested with various stress ratios by the National Research Institute For Metals (NRIM) [69,70]. Specimens made of SB42 carbon steel plates with a butt weld in the middle were tested under the stress ratio at -1, 0 and 0.5 [69]. An apparent decrease in the fatigue strength at 10^7 cycles was seen (from 198 to 132MPa) when the stress ratio increases. The same type of specimen was used in [69,70], but the material was changed to SPV50 of which the tensile stress is higher. Familiar results were obtained that the fatigue strength at 10^7 cycles decreased by 30%, from 370 to 265MPa as the stress ratio increase to 0.5.

The transverse fillet welded joints with the plate thickness ranging from 9 to 160 mm were tested under CA loading sequences where either the minimum stress equals to zero ($R=0$) or the maximum stress equals to yield stress of the material [58]. The average residual stress measured in the 9mm-thick specimen was 60MPa, whereas in thicker ones (plate thickness >40 mm) was approximately 180MPa. The result showed that fatigue strength at

2×10^6 were almost the same under these stress ratios, whereas both the strengths at 10^7 and 10^8 were seen a decrease when the stress ratio was increased. This result implied that due to the low residual stress, the mean stress could influence fatigue performance when the applied stress range is small.

Few works have been seen for the effect of the mean stress on the fatigue performance of welded joints under a VA loading spectrum [3,5]. When the maximum stress was reduced from 280 to 147MPa, the Miner's sum D was only increased slightly from 0.53 to 0.60, which probably could be explained by data scatter [5]. Tilly carried out fatigue testing of two types of welded joints: edge attachments and fillet welded longitudinal attachments [3]. The limited data indicated that the fatigue performance of the joints under pulsating compression was only slightly better than that under pulsating tension. This result might not be surprising since these two types of welded joints are expected to contain high tensile residual stress. It is not clear whether a similar result would be observed in other types of welded joints where lower residual stress presents.

In view of this, the mean stress correction is recommended when assessing the fatigue performance of small-size welded joints where the residual stress may be relatively small, or even not exist [58].

2.7.3 Residual stress relaxation

The initial residual stress induced by welding may not sustain during cyclic loading. As the superposition of the high residual stress, plastic deformation may occur even though the applied stress is lower than the material yield, leading to relaxation of the residual stress [71].

There is abundant evidence suggesting that under cyclic loading, significant relaxation of residual stress occurs under the first application of the loading cycle, followed by minimal further relaxation in subsequent cycles [72]. This is supported by the results obtained from notched specimen [73] and smooth butt welds [74] under the application of single loading cycles with stress ratios $R = 0$ and -1 , where residual stress was significantly reduced.

The residual stress relaxation was investigated in welded joints with transverse fillet attachments using the X-ray diffraction method [50]. Results showed that more than 50% of residual stress was relaxed within only 8% of the fatigue life. The residual stress presented in

longitudinal fillet attachments was found to be reduced by 73% in less than one percent of the fatigue life [5], which was in line with the results reported in [71,75]. The extent of residual stress relaxation depends on the magnitude of the cyclic stress range and the yield stress of the material [76].

2.7.4 Residual stress measurement methods

Current residual stress measurement techniques mainly fall into two categories: destructive and non-destructive. The destructive technique includes Centre-hole drilling method and Counter method, etc.. The widely used non-destructive technique are X-ray diffraction, Neutron diffraction and Ultrasonic technique, etc. [77].

X-ray diffraction(XRD) depends on measuring the changes in the spacing of between the lattice planes in a polycrystalline material when a stress is applied [78]. The residual stress is calculated based on the strain measured using $\sin^2\varphi$ method. More details on the principle of XRD the method can be found in [79].

Centre-hole drilling is one of the most widely used methods for measuring surface residual stress in isotropic linearly elastic materials [80,81]. The principle of this method involves drilling a hole into the specimen containing residual stress and measuring the subsequent local surface strains which are caused by the residual stress relief and redistribution in the surrounding material [78]. The strains recorded allows for the back-calculation of the pre-existing residual stress based on the theory of elasticity. More details could be found in [80].

2.8 Mean stress correction

Although the effect of mean stress applied is generally ignored when assessing the fatigue life of welded joints, it can significantly affect the weld-free steel component [82–84]. The fatigue life obtained under a specific constant stress range with zero mean stress was higher than that under the same stress range but with a tensile stress range [82,83] or be lower than that with a compressive mean stress [83]. The mechanism lays behind the trends is that the tensile mean stress can decrease the crack initiation time due to the stress concentration at defects and also impede the happen of crack closure [84].

In this case, some equations have been proposed to consider the effect of applied mean stress on the fatigue limit of materials, such as:

$$\text{Soderberg [85]:} \quad \Delta\sigma_{FL} = \Delta\sigma_{FL,R=-1} \left(1 - \frac{\sigma_m}{\sigma_y}\right) \quad (2.5)$$

$$\text{Goodman [86]:} \quad \Delta\sigma_{FL} = \Delta\sigma_{FL,R=-1} \left(1 - \frac{\sigma_m}{\sigma_{UTS}}\right) \quad (2.6)$$

$$\text{Morrow [87]:} \quad \Delta\sigma_{FL} = \Delta\sigma_{FL,R=-1} \left(1 - \frac{\sigma_m}{\sigma_{tf}}\right) \quad (2.7)$$

$$\text{Gerber [88]:} \quad \Delta\sigma_{FL} = \Delta\sigma_{FL,R=-1} \left(1 - \left(\frac{\sigma_m}{\sigma_{UTS}}\right)^2\right) \quad (2.8)$$

$$\text{Smith-Watson-Topper (SWT) [89]:} \quad \Delta\sigma_{FL,R=-1} = \sqrt{\sigma_{max} \Delta\sigma_{FL}} \quad (2.9)$$

$$\text{Walker equation [90]:} \quad \Delta\sigma_{FL,R=-1} = \sigma_{max}^{1-\gamma} \Delta\sigma_{FL}^\gamma \quad (2.10)$$

where $\Delta\sigma_{FL,R=-1}$ refers to the fatigue limit at fully reversed loading, i.e., $R = -1$. $\Delta\sigma_{FL}$ is the corrected value at a given mean stress, σ_m . σ_y , σ_{UTS} and σ_{tf} are the yield stress, the ultimate tensile stress, and the true fracture stress, respectively. σ_{max} is the maximum stress applied, and γ a material constant, ranging between 0 and 1. The first four methods are illustrated in Figure 2.10.

Comparison of these models has been carried out [88,91,92]. Results showed that most of the predictions by the models usually scatter between the results predicted by Goodman and Gerber model [91]. When the applied mean stress was close to the reference mean stress, the Goodman model could make a better prediction; but as the gap increased, the results predicted by Gerber model were better, and Goodman method became conservative [88]. This trend was further confirmed by the results obtained at a low stress ratio, i.e. $R < 0.1$, that a good agreement was achieved by Goodman method as well [91,92]. SWT model is well-known for its simplicity as only the maximum stress and the stress range are involved, with no material constant required.

However, while providing a proper correction for the high cycle fatigue tests, it becomes conservative in low cycles fatigue tests [92]. Walker model may give a better result, but an additional parameter confirmed by experiments is needed [88].

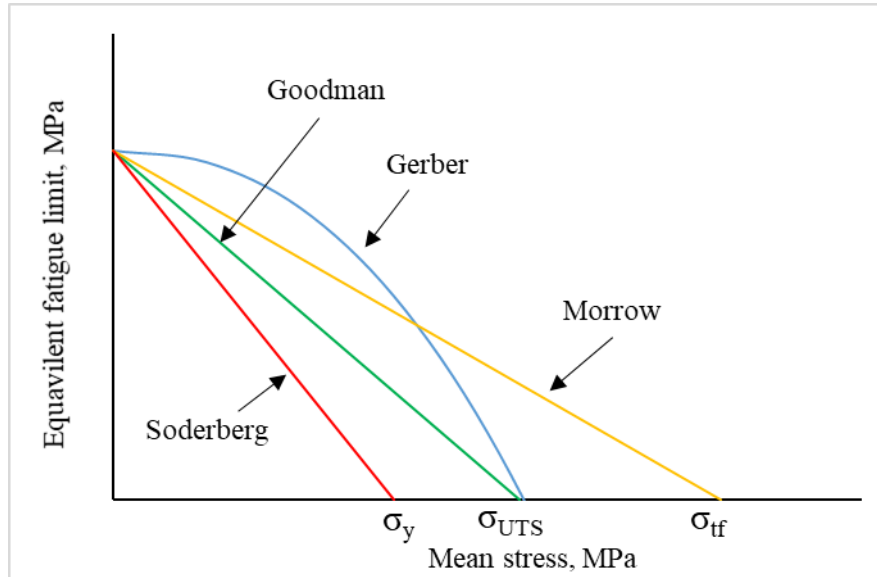


Figure 2.10 Mean stress correction methods.

In addition to the fatigue limit, these equations also can correlate a given stress range, $\Delta\sigma$, with a mean stress, σ_m , to an equivalent fully reversed stress range, $\Delta\sigma_{R=-1}$, that is able to produce the same fatigue damage with the $\Delta\sigma - \sigma_m$ combination [90], which is discussed in Chapter 5.

2.9 Effect of plate thickness on the fatigue life of welded joints

It is well-known that the relevant dimension of a specimen influences the fatigue endurance of welded joints, by decreasing the fatigue strength as the dimensions increase. This phenomenon is well explained by the model established by Berge [93]. By assuming the geometries of the same type of welded joints in various thickness being similar, as long as the depth of the initial flaw is independent of plate thickness, Berge showed that the stress distribution across the plate in the plane are geometrically similar, resulting in a steeper stress gradient in the thinner plate. Therefore, the initial flaw with specific depth in a thinner plate experiences smaller stress than in a thicker plate, leading to a smaller FCGR. Hence, the thinner weld joint has a better fatigue life.

The detrimental effect of larger plate thickness also can be partly attributed to the high residual stress [94]. The magnitude of residual stress may increase as the plate thickness increase, resulting in a higher effective mean stress (the combination of the applied mean stress and the residual stress), especially when the applied mean stress is low.

BS 7608 [1] provides guidance on accounting for such thickness effect. The reference thickness, T_{ref} , for the basic S-N curve in BS 7608 is 25mm for non-nodal welded joints and 16mm for tubular nodal joints. It suggests that the fatigue strength of welded joints also depends on the degree of through-thickness bending. The fatigue strength increases with increasing bending component for a decreasing stress range gradient through the thickness. However, the design S-N curves are established under the conditions that predominantly produce membrane stresses. The potentially detrimental effect of increased thickness but the beneficial effect for bending is combined with the application of the correction factor k_{tb} on stress ranges obtained from the relevant S-N curve, such that:

$$\Delta\sigma_{FL} = k_{tb}\Delta\sigma_{FL,B} \quad (2.11)$$

where $\Delta\sigma_{FL}$ is the fatigue strength including the thickness size correction and $\Delta\sigma_{FL,B}$ the fatigue strength from the basic S-N curve. k_{tb} is estimated as following:

$$\text{For } T > 25\text{mm} \quad k_{tb} = \left(\frac{T_{ref}}{T_{eff}}\right)^{b'} (1 + 0.18\Omega^{1.4}) \quad (2.12)$$

$$\text{For } 4\text{mm} \leq T \leq 25\text{mm} \quad k_{tb} = \left\{1 + \Omega \left[\left(\frac{T_{ref}}{T}\right)^{b'} - 1\right]\right\} (1 + 0.18\Omega^{1.4}) \quad (2.13)$$

where T_{ref} is the thickness related to the basic S-N curve for the weld detail, T_{eff} is the effective plate thickness, T is the actual thickness of the component under consideration. b' is the thickness and bending exponent and depends on joints class. For Class F curve, $b' = 0.25$ [2,93]. Ω is the degree of bending ($\Delta\sigma_b/(\Delta\sigma_m + \Delta\sigma_b)$).

The effect of thickness is also illustrated by calculating the fatigue life as a function of thickness and b' , following [95]:

$$\log N = \log \bar{a} - m \log \left[\Delta \sigma \left(\frac{T}{T_{ref}} \right)^{b'} \right] \quad (2.14)$$

where m is the negative inverse slope of the $S-N$ curve, $\log \bar{a}$ is the intercept of the horizontal axis. The fatigue life is in reverse proportion to T and b' .

Moreover, the plate thickness effect depends on the value of the stress range applied [2]. It was found that under both axial and bending loading, the thickness effect was minor when the stress range is high (in the short life region, about 10^5 cycles) and will become more apparent as the stress range decreases (in the relatively long-life region, $> 2 \times 10^5$ cycles).

2.10 Fatigue life improvement

2.10.1 Overview of fatigue life improvement techniques

In order to overcome fatigue problems and to extend the service life of welded structures, various life improvement techniques have been developed and implemented during the last few decades [96]. These methods can be categorised into either residual stress-based approaches or weld geometry improvement-based approaches [97]. The former introduces compressive stresses near the surface of the weld toe where the crack is likely to initiate and propagate, and the latter removes flaws at the weld toe and reduce stress concentration. In each category, there are various alternative techniques. The most widely used and their benefits are summarised in Table 2.1.

Table 2.1 The primary benefits of the widely used improvement techniques.

Category	Technique	Remove or reduce crack-like flaws	Reduce local stress concentration	Introduce compressive residual stress
Weld geometry improvement-based	Burr grinding	√	√	-
	TIG dressing	√	√	-
Residual stress-based	Shot blasting	-	-	√
	Needle peening	-	√	√
	Hammer peening	-	√	√
	Ultrasonic impact treatment (UIT)	-	√	√

2.10.2 Ultrasonic impact treatment

The residual stress-based method, including conventional peening techniques and high-frequency mechanical impact (HFMI) treatments, are attracting increasing attention and had been significantly developed as a reliable, effective, and user-friendly technique to achieve fatigue strength improvement [96,98].

Compared with the conventional peening method, the HFMI treatment can produce a uniform treatment region with excellent repeatability, and without noises as well as operator fatigue problems [97]. The technique involves applying accelerations of cylindrical indenters at a high frequency (>90 Hz) against the weld toe region. Therefore, the material impacted is highly deformed plastically, causing compressive residual stresses in the area of impact. Also, HFMI can refine the weld profile to reduce local stress concentration.

Ultrasonic impact treatment (UIT) is one of the HFMI techniques. It has been utilized in a wide range of industrial areas, including aerospace, mining, offshore drilling, shipbuilding, etc. The effectiveness of UIT has been verified in numerous laboratory testing and analytical fatigue studies [99–101]. It was reported that UIT could improve the fatigue strength in the order of 50-200% for butt and overlap joints [99], about 120% for joints with filleted longitudinal attachment [100], and 65%-70% for joints with filleted transverse attachment [101].

2.10.3 Fatigue design for life improved welded joints

BS 7608 suggests that UIT may lead to the benefit in increasing the fatigue strength of untreated welds at 10^7 cycles by a factor up to 1.5 and changing the slope of S-N to 3.5 depending on the stress ratio and the maximum stress applied. More details are given in Table 2.2.

It is worth to note that most of the studies and guidance discussed above only demonstrate the improvement in fatigue performance under CA loading, and limited relevant work has been done under VA loading [96,102]. The improvement in fatigue strength of the welded joints containing longitudinal attachments due to UIT was investigated under the CM loading sequence with a stress ratio $R \sim 0.1$ [103]. Results showed that the fatigue strength corresponding to $N = 2 \times 10^6$ cycles was increased by about 80%, with an increase in the fatigue life for about 3 to 17 times.

Table 2.2 Improvement in fatigue strength due to weld toe peening suggested in BS 7608.

Loading conditions	Improvement	Slope before 10^7 cycles
$R \leq 0$, including fully compressive loading	Increase fatigue strength at 10^7 cycles by a factor of 1.5 and the stress range are the sum of the tensile component and 60% of the compressive component	3.5
$0 < R \leq 0.28$ and $\sigma_{max} \leq 0.8\sigma_y$	Increase fatigue strength at 10^7 cycles by a factor of 1.5	
$0.28 < R \leq 0.4$ and $\sigma_{max} \leq 0.8\sigma_y$	Increase fatigue strength at 10^7 cycles by a factor of 1.15	3
$R > 0.4$ or $\sigma_{max} > 0.8\sigma_y$	No benefit unless proved by fatigue testing	

2.11 Linear elastic fracture mechanics

As mentioned previously, fatigue life associated with as-welded joints is almost spent in fatigue crack growth [6]. So it can be estimated by linear elastic fracture mechanics (LEFM) which is an analytical tool that offers a mathematical technique to describe fatigue cracking progress [54,104].

In LEFM theory, the crack growth is determined by the stress state near the tip of a crack caused by a remote load or residual stresses, and the stress state can be characterized using a stress intensity factor (SIF) range, ΔK [105]. In the consideration of a fatigue crack presented at the weld toe, the ΔK is estimated [30]:

$$\Delta K = M_k Y \Delta \sigma \sqrt{\pi a} \quad (2.15)$$

where Y is a dimensionless factor accounting for the geometry of the component and the crack. a is the crack size and M_k a function of the stress concentration effect caused by weld details, which will be discussed in Chapter 6.

Fatigue crack growth can generally be defined in terms of three stages, as shown in Figure 2.11 [30]. Stage I is the transition from no propagation below a threshold value of ΔK_0 to a finite crack growth rate. The threshold is typically below $63N/mm^{3/2}$ for steel (in terms of FCGR at

$da/dN = 10^{-7} \text{ mm/cycle}$) and $21 \text{ N/mm}^{3/2}$ for aluminium alloys at a stress ratio >0.5 in air or other non-aggressive environments [30].

Stage II, referred to as macro-cracking, involves the propagation of a fatigue crack through the majority of the cross-section. Generally, it takes up the majority of the crack growth stage, and a number of empirical laws were proposed to characterise the rate of crack growth in this stage. Paris' Law is the most used method to relate the fatigue crack growth rate (FCGR), da/dN , to ΔK , giving:

$$\frac{da}{dN} = C(\Delta K)^m \quad (2.16)$$

where C and m are material constants which can be estimated experimentally. m is typically about 3.0 for a variety of metals.

Stage III defines the final moments of fatigue crack growth when the remaining cross-section is unable to sustain the applied load, and brittle fracture or ductile collapse occurs.

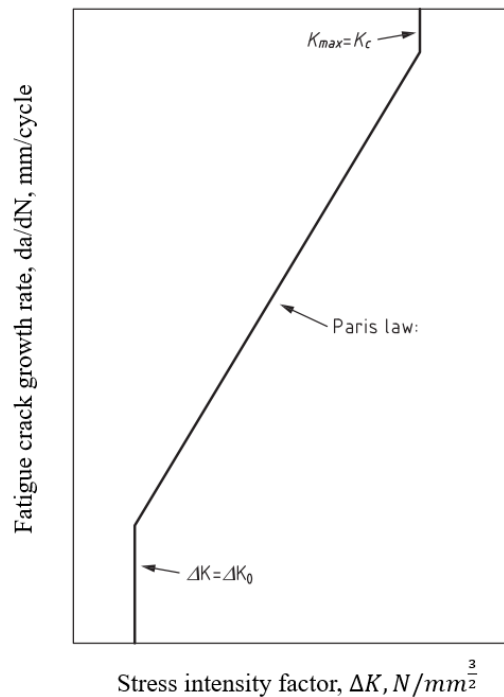


Figure 2.11 Simple Paris law crack growth relationship.

The Paris' Law also can be integrated to estimate the number of cycles for a crack to grow from an initial size, a_i , to the final size, a_c , in accordance with the BS 7910 [30]:

$$\int_{a_i}^{a_c} \frac{da}{(M_k Y \sqrt{\pi \alpha})^m} = C \Delta \sigma^m N \quad (2.17)$$

As mentioned, the fatigue life of welded joints generally involves crack growth due to the initial crack-like flaws at the weld toe. If the geometry and size of flaws are similar in each weld, and the final crack size at fatigue failure is considerably larger than the initial size, the integral component in the equation 2.17 is constant; thus, it can be re-written as:

$$\Delta \sigma^m N = \frac{1}{C} \int_{a_i}^{a_c} \frac{da}{(M_k Y \sqrt{\pi \alpha})^m} = C' \quad (2.18)$$

where C' is a constant.

It is interesting to note that this is the form of the S-N curve obtained from fatigue tests. There is no doubt that the integral component in Equation 2.18 is not constant in reality because the geometry of the initial flaws varies from welds to welds. Such variation is the main reason for the scatter obtained from fatigue tests [28]. Besides, Equation 2.18 also suggests the slope of the S-N curve, m , is identical to that for the crack growth data. As noted above, the value of m is usually about 3, and this the reason for the choice of $m=3$ for the slopes of the design curves provided in BS 7608.

In view of the fatigue crack growth under VA loading sequences, Equation 2.18 can be re-written as:

$$\int_{a_i}^{a_c} \frac{da}{(M_k Y \sqrt{\pi \alpha})^m} = \sum C \Delta \sigma_i^m n_i \quad (2.19)$$

where σ_i and n_i are the stress ranges and the corresponding number of cycles in the loading history. Therefore, fatigue life, $\sum n_i$ can be estimated when the a_i , a_c and $\Delta \sigma_i$ are given.

Although the LEFM is widely used, it has some major limitations. First, it can only take into account single crack growth. However, a stressed welded joints can develop cracks at multiple locations. Fatigue cracks that are present in close vicinity can interact under the load, leading to amplification or reduction in stress levels near the crack-tips [106,107]. Second, it may underestimate the growth of small crack. The crack growth curve near the threshold part is generally produced based on a large crack using a decreasing ΔK approach. However, in many

loading bearing structures, fatigue crack growth from a small initial flaw is a major portion of the fatigue life and it has been found that at low crack growth rate, near the threshold range, the small crack may grow much faster than the large crack at the same ΔK level, even they also grows at ΔK levels below threshold [108]. Thirdly, LEFM is of limited practical use on the crack growth from pre-existing flaws in linear elastic material. One basic assumption for LEFM is small scale-yielding, i.e., the non-linear deformation is small compared to the size of crack [35]. Therefore, it is not suitable for cases of steels which are not perfectly elastic but undergo significant plastic deformation at the tip of a crack [35,105], or when the crack initiate at the stress concentrators, in particular crack-like defects, the plastic zone can be commensurable with the defect size or the typical linear size of the deformed body [109].

Efforts have been made to overcome these limitations. For the multiple cracks, new SIF can be calculated to considering the interaction effect between fatigue cracks using superposition principle [110], weight function method [111] or photoelasticity [107]. In order to predict small crack growth near the threshold range, some non-linear fracture mechanics models have been proposed accordingly [108,109]. When the crack component is in the cases of non-small-yielding, elastic plastic fracture mechanics (EPFM) would be a better choice [112].

2.12 Crack tip plasticity

It is well known that plastic deformation presents at the crack tip as a result of the stress concentration [14]. There are two types of plastic zone ahead of the crack tip under cyclic loading: monotonic plastic zone and reverse or cyclic plastic zone [35,105]. The former is defined as the plastic zone corresponding to the maximum load in a loading cycle, and its dimension is related to the maximum stress intensity factor, K_{max} . The reverse plastic zone, which is a smaller plastic zone within the monotonic zone, is induced by the reserved plastic flow upon unloading in the cycle; its size is determined by the stress intensity factor range, ΔK , the stress state and the material property.

The plastic zone size, r_p^* , was estimated firstly by Irwin in 1958 [113]:

$$r_p^* = \frac{1}{m\pi} \left(\frac{K_{max}}{\sigma_y} \right)^2, \quad m = \begin{cases} 6 & \text{plane strain} \\ 2 & \text{plane stress} \end{cases} \quad (2.20)$$

In subsequent research, it was noticed that Equation 2.20 underestimates the actual size of the plastic zone as the plastic deformation leads to re-distribution of stresses in the vicinity of the crack tip. Therefore, Irwin [114] gave a correction in accordance with von Mises yield criterion to calculate the monotonic plastic zone size:

$$r_p = 2r_p^* \quad (2.21)$$

In terms of the reversed plastic zone, it has been long recognised since the 1960s [115] that as the tensile stress decreases, the monotonic zone is compressed by the surrounding elastic body, and this leads to the redistribution of stresses and the formation of the reversed plastic zone at the crack tip. The reversed plastic zone locates within the monotonic zone, and its size is estimated as:

$$r_c = \frac{1}{\pi} \left(\frac{\Delta K}{2\sigma_y} \right)^2 \quad (2.22)$$

Both monotonic and reversed zone has a significant influence on the fatigue propagation because they can determine the extent of crack opening as well as the effective stress intensity factor, which will be discussed later.

2.13 Fatigue crack growth under variable amplitude loading

2.13.1 Effect of overload on crack growth

2.13.1.1 Single overload

Fatigue crack growth (FCG) under the simplest case of a CU loading sequence which contains only a single overload, as illustrated in Figure 2.12(a), have been studied extensively [8,9,116–120] in various materials, such as stainless steels [116,117], steels [8,118], Aluminium alloys [9,119]. Such a loading sequence can lead to significant fatigue crack growth rate (FCGR) retardation [119]. As shown in Figure 2.12(b) and (c), the FCGR increases instantaneously at the application of the overload, then decreases sharply until a minimum value is reached. Afterwards, it gradually returns to the baseline.

The extent of the retardation effect depends on the overload ratio, which is the overload stress range to the minor stress range [8,118,120]: The higher overload ratio, the more retardation.

When the overstress ratio was increased from 1.3 to 1.9, the FCGR in central cracked specimens manufactured by 18G2A structural steel decreased from the twice time lower than the baseline to five times lower [118]. Additionally, the retardation can be weakened when the plate thickness increases [120].

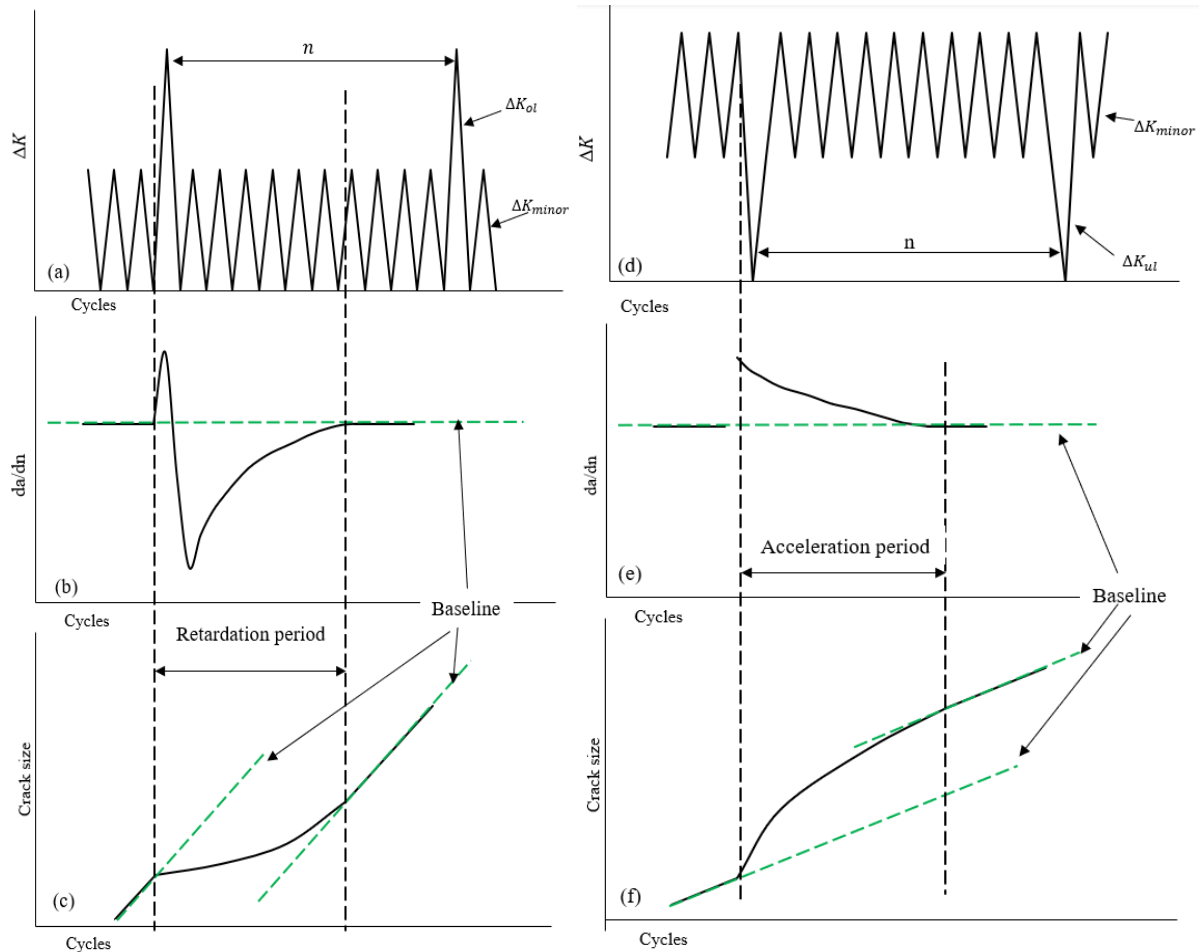


Figure 2.12 Fatigue crack growth under VA loading sequence: (a) CU loading sequence. (b) change in FCGR after an overload. (c) change in crack size after an overload. (d) CD loading sequence. (e) change in FCGR after an underload. (f) change in crack size after an underload.

2.13.1.2 Periodical overloads

Retardation in FCGR was also studied under the loading sequence where the overload was applied periodically [118,120–122]. The extend of retardation can be either enhanced or reduced depending on the interval, referred as n in Figure 2.12 (a), which is the number of minor cycles between neighbouring overloads [121,122], as shown in Figure 2.12 (a). An obvious enhanced retardation was obtained when the number of minor cycles increases from 100 to 10,000 [118]. Similar results were also reported in [120].

Such a retardation effect has been widely observed and applied in actual load-bearing structures in the industry [123]. For instance, an aircraft that occasionally operated through high gusty winds in bad weather has a longer service time than that with a steadier flight weather history. An example of the industry takes advantage of the retardation is that the service life of a bridge can be extended by applying heavy weight vehicles which causes overload. FCGR retardation was also observed under a block loading [5], where a CU loading sequence containing some different stress range levels is applied repeatedly until fatigue failure.

If the interval is further reduced, the retardation phenomenon can be significantly weakened, even resulting in acceleration [12,119]. L.P. Borrego et al. [119] used a centre-crack specimen made of AlMgSi1 (6082) aluminium alloy to study the effect of the interval between multiple overloads on FCGR. Four intervals: 10,100,1000 and 10000 were adopted. Results suggested that the retardation effect was reduced with the decreasing interval. If the interval was 10, the number of cycles for the crack to increase by 10mm was decreased by 20% in comparison of that under a CA loading. Similar results were seen in [12], where compact tensile (CT) specimens made of steel BS4360 50B and BS1510 32A were loaded under CU loading sequences with various intervals ranging from 1 to 1000. Results showed that when the interval was less than 3, FCGR was accelerated and the highest acceleration factor was obtained when the intervals equal to 1, being at 1.11 and 1.24 respectively in these two materials, respectively. The acceleration factor illustrates the extent of acceleration effect and can be expressed as [12]:

$$\gamma = \frac{\text{measured FCGR per block}}{\text{predicted FCGR per block}} \quad (2.23)$$

where the predicted FCGR per block is calculated by a linear summation of the FCGR response under CA condition.

2.13.2 Effect of underload on crack growth

The fatigue crack growth under the CD loading sequences containing either one single underload [8,124] or periodic underloads [12,13,120,125,126], see Figure 2.12 (d), was extensively studied. Results suggested the underload cycle could not only cause crack advancement by itself, but also accelerate the FCGR in the subsequent minor cycles, as shown in Figure 2.12 (e) and (f). The FCGR jumps to a maximum value whereupon the application of the underload, then gradually return to the baseline.

Similar to the retardation effect under a CU loading, the acceleration factor also depends on the interval, n . A peak value of γ could be achieved by taken n at 10 [12,126]. When n is either higher or lower than ten, the value of γ usually reduces [12]. Moreover, the maximum γ can be achieved depends on the material, it ranges between 1.0 and 2.0 [12] for steel and could reach up to 8 for aluminium [126].

The effect of the underload ratio, which is the underload stress range to the minor stress range, was discussed in [12,13,123]. It shows that for both steel and aluminium, when the underload ratio is at about 2, γ is generally at the highest, being at 1.5-2.0.

For welded joints, FCGR acceleration was also observed under CD loading sequence [5,6,13]. The crack length measured was much longer than that calculated by linear summation of the CA crack growth responses [5,13].

2.13.3 Effect of other variable amplitude loading sequences

In addition to CD and CU loading sequence, other types of VA loading sequences, such as the multiple peak overload sequence, the overload-underload sequence, the step-change sequence etc. (Figure 2.13), also can cause either crack acceleration or retardation, but the extent is weaker than that under the purely CD or CU sequences. As fatigue propagation under such loading sequences is beyond the scope of the present study, the relevant information is not included here. Comprehensive reviews on this subject can be found in [12,13,120].

2.14 Mechanisms for load interaction under variable amplitude loading

2.14.1 Fatigue crack growth rate retardation due to overload

Various mechanisms have been established to explain the FCGR retardation due to overloading. Examples of some of them are crack closure [127–129], strain hardening [12,123], crack tip bunting [115,130] or compressive mean stress [12]. These mechanisms are not totally independent of each other, and some of them may active simultaneously [12]. However, crack closure is generally considered as the most important FCGR retardation mechanisms [126].

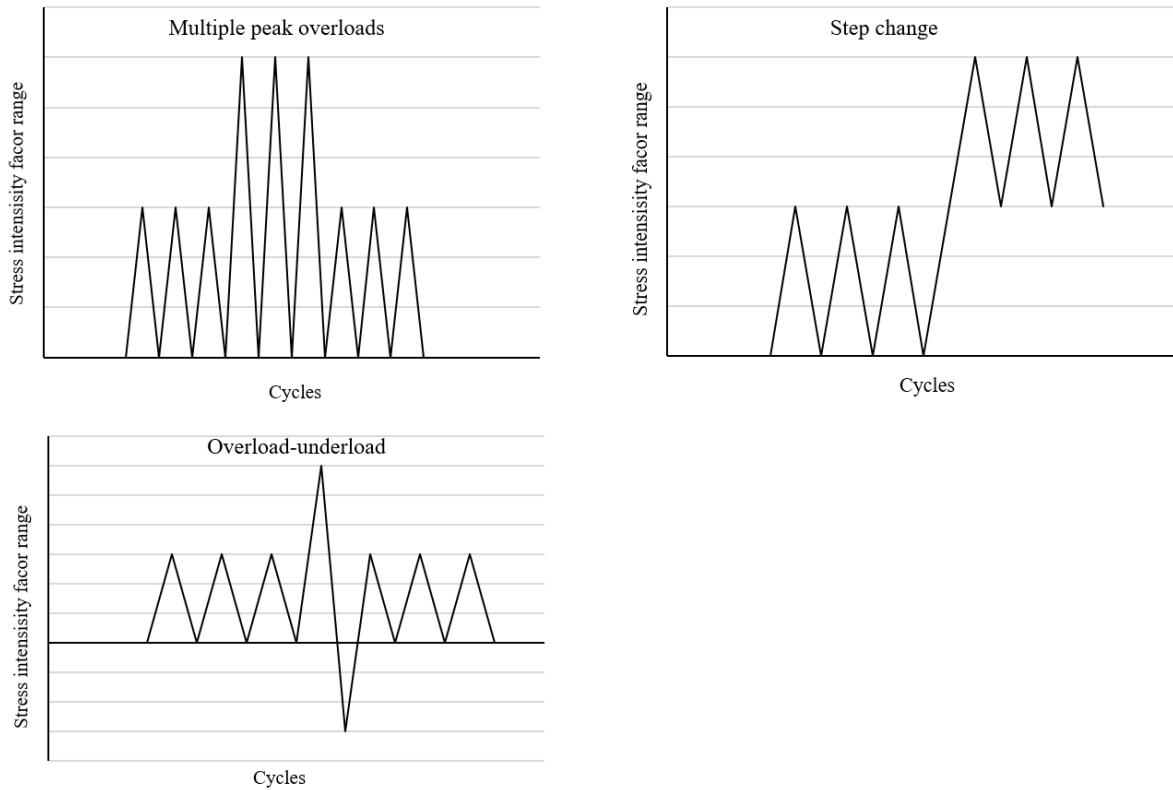


Figure 2.13 Various variable amplitude loading sequences.

Elber [129] first observed that fatigue cracks could close even under tension-tension CA loading. It is a phenomenon that the opposing faces of a crack remain in contact until the driving force, ΔK , has achieved a critical value, ΔK_{op} [129]. So that only a reduced part of ΔK contributes to crack propagation.

Some mechanisms have been proposed for the crack closure phenomenon, such as roughness induced-closure [14], oxide induced-closure [14,131] and plasticity induced-closure [129]. It was argued that the plasticity induced-closure might be the predominant one [13,129]. During cyclic loading, each loading cycle produces monotonic and reverse plastic zones ahead of the crack tip. During loading from the minimum to the maximum far-field load, the crack advances through the residual tensile strains. As a result, a zone of residual tensile deformation is left in the wake of a fatigue crack tip, resulting in that the crack surfaces can still be in contact even if the specimen is loaded under a tensile stress.

Under a VA loading sequence where overloads are involved, overloads may enhance crack closure. This is because overloads can produce a larger plastic zone ahead of a crack tip than

minor cycles do, which produces higher compressive stresses, resulting in an increase of ΔK_{op} . As the fatigue crack grows, ΔK_{op} gradually decreases and finally back to the initial level when the plastic zone caused by subsequent minor cycle reaches to the edge of the larger plastic zone [127].

2.14.2 Effective stress intensity factor

As a fatigue crack only propagates after the crack is fully open, its growth is dominated by an effective stress intensity factor, ΔK_{eff} [129]:

$$\Delta K_{eff} = \Delta K - \Delta K_{op} = U\Delta K \quad (2.24)$$

where U is a parameter in relation to the stress ratio, R .

Under a CA loading sequence, U can be estimated by [129]:

$$U = 0.5 + 0.4R, -1 < R < 0.7 \quad (2.25)$$

Another form of U was developed by Booth G, Maddox S [7]:

$$U = \begin{cases} \frac{1}{1.5 - R} & -2 < R < 0.5 \\ 1 & R > 0.5 \end{cases} \quad (2.26)$$

Under a VA loading sequence where an overload is involved, Wheeler model [127] is one of the least complicated and most commonly used crack growth models, where U was proposed to be a function of the current crack size, a , the size before the overload, a_{OL} , the plastic zone size for minor cycles, r_{CA} , and that for the overload, r_{OL} , giving:

$$U = \begin{cases} \left(\frac{r_{CA}}{a_{OL} + r_{OL} - a} \right)^w ; a + r_p < a_{OL} + r_{pOL} \\ 1 & ; a + r_p \geq a_{OL} + r_{pOL} \end{cases} \quad (2.27)$$

where w is an empirical parameter based on the material and the loading sequence. r_p is the plastic zone size.

2.14.3 Fatigue crack growth rate acceleration due to underload

The mechanism for FCGR acceleration under CD loading sequences has not been well established [5]. One possible mechanism for the acceleration was suggested to be related to strain hardening where the underload is thought to cause reduction of material ductility ahead of the crack tip [12,132]. Crack tip blunting is known to take place after an overload, while sharpening is expected after an underload. However, the opposite trend was also found: cracks were blunted after underloads as well [12], though the magnitude was much less than that under an overload.

In contrast to an overload, it is believed that an underload could cause flattening of asperities in fatigue crack wake, which can weaken the crack closure, resulting in a higher effective intensity factor and an acceleration in FCGR [126,133]. For example, the crack open stress was found to be dropped immediately after the application of an underload, and then gradually return to the initial level with a rate, $\Delta\sigma_{op}$, [134], which follows:

$$\Delta\sigma_{op} = m(\sigma_{cop} - \sigma_{op}) \quad (2.28)$$

where σ_{cop} and σ_{op} are the current and the initial opening stresses, respectively. m is a parameter determined experimentally. In [133], when $m = 0.002$, the crack closure stress could be well calculated.

It should be noted that, when the stress ratio is relatively high (more than 0.5-0.6 in steels [123]), crack closure usually cannot be observed in minor cycles due to the high magnitude of the applied mean stress. However, in such a condition, the acceleration in FCGR was still observed [13,135], implying that crack closure may not be the predominant mechanism for the acceleration.

The strain softening could be a possible mechanism accounting for the FCGR acceleration caused by underload. Although the increase in strain during the minor stress cycle, where $R=0.7$, after an underload with $R=0.1$ was predicted by a finite element analysis in the Ti-17 alloy, experimental validation was not provided [123].

The influence of the local residual mean stress within the reverse plastic zone ahead of the crack tip on the fatigue crack growth under CD loading spectra was discussed in [9]. In the

reverse plastic zone, due to the mean stress relaxation, fully reversed loading takes place even under purely tensile fatigue loading. After an underload, a tensile mean stress could occur in the following small loading cycles, resulting in an acceleration in the crack growth rate. Furthermore, a finite element analysis [13] deduced that the acceleration in FCGR after underloads could be attributed to changes in the local residual mean stress. On the contrary, if a CU loading sequence is applied, a compressive local residual mean stress will be introduced, resulting in lower FCGR. The model according to this mechanism has not been well established yet.

2.15 Non-linear cumulative rule and prediction models for metal under VA loading

2.15.1 Category

As mentioned previously, many non-linear cumulative damage rules and fatigue life prediction models have been developed. Depending on the development method and the fundamental theory, the non-linear damage models can be categorised in different ways [48,136]. Damage models developed before 1970s were generally phenomenological, while those after 1970s have gradually become semi-analytical or analytical [137]. Peng [46] characterised those models into three groups, i.e. phenomenological theories, continuum damage mechanics (CDM) and fracture mechanics (FM). Moreover, more detailed categories were also reported in [44,48,136], including damage curve models, life curve modification model, energy-based models, physical properties degradation of materials, thermodynamic entropy based damage models etc. It should be noted that there is no clear boundary between these categories and other categorizations also exist [48].

A brief review of the non-linear models is given below following the categorization of damage curve models, life curve modification model, CDM and Energy based method. Some typical models in each category were introduced.

2.15.2. Damage curve models

Richart and Newmark [138] first proposed the damage curve concept to correlate damage to the cycle ratio. They speculated that the D -cycle ratio ($= \sum (\frac{n_i}{N_i})$) curve should be dependent on

the stress level. The damage curve concept is illustrated in Figure 2.14. Based on this concept, a nonlinear damage rule was then proposed by Marco and Starkey [139]:

$$D = \sum \left(\frac{n_i}{N_i} \right)^{x(\Delta\sigma_i)} \quad (2.29)$$

where the cumulative damage is expressed as a power function which is load-dependent. $x(\Delta\sigma_i)$ is a function of the stress range, $\Delta\sigma_i$, and this function was not developed in their work. Manson and Halford [140] further developed an analytical formulation for the damage curve based on an empirically formulated effective crack growth model to estimate the cumulative damage under a VA loading sequence containing multiple load levels:

$$\left(\left(\frac{n_1}{N_1} \right)^{a_{1,2}} + \frac{n_2}{N_2} \right)^{a_{2,3}} + \frac{n_3}{N_3} + \dots + \frac{n_{i-1}}{N_{i-1}} \right)^{a_{i-1,i}} + \frac{n_i}{N_i} = 1 \quad (2.30)$$

where $a_{i-1,i}$ is the life ratio characteristic exponent

$$a_{i-1,i} = \left(\frac{N_{i-1}}{N_i} \right)^{0.4} \quad (2.31)$$

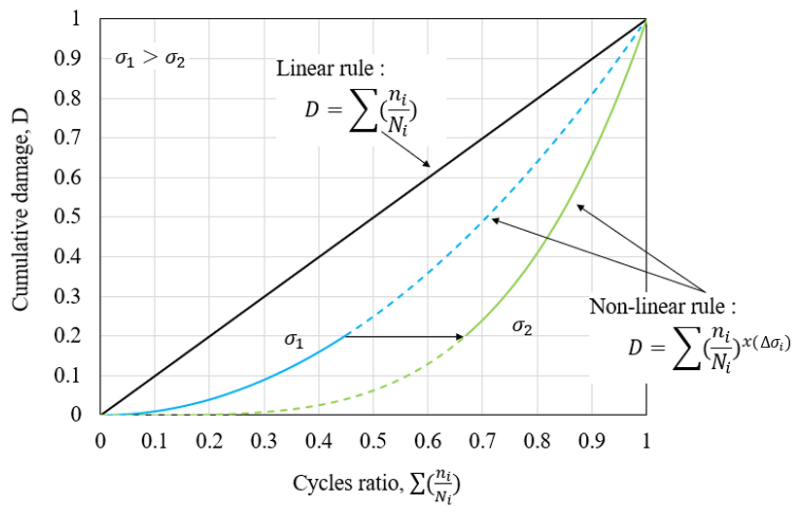


Figure 2.14 Comparison between linear and non-linear cumulative damage rule under a high-low VA loading sequence.

Under VA loading, the load sequences and interaction effects are two important issues in the fatigue damage accumulation [141]. Load interaction effect is the change in fatigue life due to the inclusion or elimination of one or a relatively few cycles of a spectrum, while sequence effect is the changes in fatigue life due to a reordering of a spectrum [142]. Manson and Halford

model can explain the influence of load sequences very well, but the load interactions are ignored. Therefore, some researchers, such as Gao et al. [41,141] and Yuan et al. [143], amended $a_{i-1,i}$ to consider the load interaction effect.

Kwofie and Rahbar [144] proposed a nonlinear damage accumulative concept based on Basquin equation, named fatigue driving stress (FDS), and consider it as the driver of fatigue damage. In conjunction with the conventional S-N curve, FDS can be used to predict the residual fatigue life of a structure under VA loading. The FDS, σ_{D_i} , due to an applied cyclic stress $\Delta\sigma_i$ can be expressed as

$$\sigma_{D_i} = \Delta\sigma_i N_i^{\frac{-\vartheta n_i}{N_i}} \quad (2.32)$$

where ϑ is the fatigue strength exponent, n_i and N_i have their usual meaning. And the damage under the given VA loading is estimated by

$$D = \sum \frac{n_i \ln(N_i)}{N_i \ln(N_1)} \quad (2.33)$$

It should be noted that N_1 represents the fatigue life for the first applied load that initiates fatigue damage, and the load sequence and interaction effects were considered by the ratio $\frac{\ln(N_i)}{\ln(N_1)}$.

2.15.3. Life curve modification models

The life curve modification models were developed by modifying the S-N curve to consider the various under VA loading [48,137]. They were developed based on either Corten-Dolan [145] and Freudenthal-Heller [146] models or the concept of isodamage lines [45,147]. Among these models, the Corten–Dolan’s model has been widely used in industry [136].

Corten-Dolan [145] model is one of the earliest theories to consider the load interaction effects by rotating the S-N curve around a reference point, which is the highest stress level in the VA loading. Thus, fatigue damage D can be estimated according to:

$$D = \frac{n_1}{N_1} + \left(\frac{n_2}{N_1}\right)\left(\frac{\Delta\sigma_2}{\Delta\sigma_1}\right)^d + \dots + \left(\frac{n_i}{N_{i-1}}\right)\left(\frac{\Delta\sigma_i}{\Delta\sigma_1}\right)^d \quad (2.34)$$

where $\Delta\sigma_1$ is assumed to be the maximum stress range in the VA loading and d is a material parameter.

Corten-Dolan model is suitable for a wide range of applications with good precision [53], however, the results are found to be strongly dependent on the d value and it is difficult to determine a consistent value [148]. For steels, the value of d was reported to be ranging from 6.2 to 6.9 with a mean value of 6.57 [136,149]. Peng et al. [150] recommended values of 4.8 for high strength steels and 5.8 for other materials. Some analytical models were also developed to calculate d [136].

2.15.4 Continuum damage mechanics models

Continuum damage mechanics (CDM) deals with the mechanical behaviour of a deteriorating medium at the continuum scale, by assuming that diffuse damage accumulates in a material[151]. This approach was developed based on the research carried out by Kachanov [152] and Rabotnov [153]. Then, Chaboche [154] proposed that fatigue damage accumulation every cycle can be generalized by a function of the load and damage state, and first to apply CDM to predict fatigue damage by introducing a nonlinear continuum damage model:

$$D = 1 - \left[1 - \left(\frac{n}{N} \right)^{\frac{1}{1-\alpha}} \right]^{\frac{1}{1+\beta}} \quad (2.35)$$

where a is a function of the stress state and β is a material constant. This model has four major advantages [48,137]: First, it can account for damage growth due to the stress range below the CAFL if the material is damaged. Second, strain hardening can be considered in order to take into account the load interaction effect. Third, the mean stress effect is also included. Finally, the material parameters can easily be determined from S-N curves. Based on the Chaboche model, some models were developed by introducing different numbers of variables, damage rate equations or boundary conditions [137].

In addition to the Chaboche model, several other type CDM models were also developed based on different concepts, such as thermodynamic mechanical[155], damage stress[156] and material degradation[157], and under each concept, various models also exist [44,48,137].

The CDM models also can be combined with other methods. For example, Peng [46] combined the material degradation concept to model the changes of the residual S-N curve. This model was found to be better than Miner's rule, the FDS [144] and Corten-Dolan model [145].

2.15.5 Energy based method

Generally, a strain energy density parameter is used the energy based models for fatigue analysis [137,158,159]. Golos et al. [160] proposed the fatigue life can be regarded as a function of strain energy density, ΔW_t , which is the combination of damaging plastic strain energy density ΔW_p and the elastic strain energy associated with the tensile mode ΔW_e^+ that facilitates crack growth:

$$\Delta W_t = \Delta W_p + \Delta W_e^+ = \beth N^\alpha + C' \quad (2.36)$$

where \beth , α and C' are material constants. This model was further developed to determine the fatigue life in a multi-block loading [161] and to analysis the fatigue performance of magnesium alloy [162].

Peng [159] proposed a new fatigue driving energy (FDE) method by combing the strain energy density with the FDS concept developed in [144], to predict the residual fatigue life under VA loading:

$$\left(\frac{n_i}{N_i}\right)_{pp} = 1 - \frac{1}{-2\Psi \ln N_i} \ln \left(\frac{(N_i^{-2\Psi} - 1) \left(N_{i-1}^{-2\Psi \left[\frac{n_{i-1}}{N_{i-1}} + 1 - \left(\frac{n_{i-1}}{N_{i-1}}\right)_{pp} \right]} - 1 \right)}{N_{i-1}^{-2\Psi} - 1} + 1 \right) \quad (2.37)$$

where Ψ is a material constant and pp represents the fatigue life predicted by the model. Compared to Miner's rule, the proposed model provided more accurate fatigue life estimations [159].

2.16 Fatigue life under variable amplitude multiaxial loading

The literature review performed so far focuses on fatigue issues under VA uniaxial fatigue loading. With the advent of multiaxial fatigue testing facilities in the last four decades,

extensive research also has been carried out to investigate the issues of multiaxial fatigue, and how to estimate fatigue life under VA multiaxial loading is one of the most critical issues. However, the present study only focuses on fatigue problems under VA uniaxial loading, hence just a brief introduction on the fatigue under VA multiaxial loading is given here.

Similar to uniaxial loading, to assess fatigue life under VA multiaxial loading, there are three essential factors – the selection of a suitable multiaxial fatigue damage model that can estimate damage of each loading cycle identified, a cumulative damage rule to sum damage for the VA loading spectrum, and a proper cycle counting method to identify the VA loading spectrum in the given loading history [163].

Currently, critical plane approaches are the most reliable and robust approaches to conducting multiaxial fatigue life estimations [163,164]. They were developed on the basis of on either maximum shear failure plane or the maximum principal strain or stress failure plane and can be categorized as stress-based, strain-based, and stress-strain based models. The stress-strain models are the most appropriate one as they are applicable for both low and high cycle fatigue and can capture the material constitutive response [165]. Under such a category, a widely used model is Fatemi-Socie (FS) model [166], where the maximum shear strain amplitude is a function of the maximum normal stress acting on the maximum shear strain plane over the cycle.

In addition to the multiaxial fatigue damage model, proper cumulative damage rule that can estimate damage of the given loading cycles is another critical factor. Although some nonlinear cumulative damage rules have been proposed, linear cumulative damage rule is still the simplest and most often used one [137]. The accuracy of the damage predicted based on linear cumulative rule also heavily relies on the selection of the damage model [163].

In terms of the cycle counting method, only a few counting methods have been proposed based on the critical plane concept [163]. In these methods, the VA loading spectrum can be determined by performing the Rainflow counting on a specific strain loading history, such as the shear strain history in the shear failure mode, the normal strain history in the tensile failure mode or an equivalent strain history. Despite relative success, it is still a challenging issue to develop reliable counting methods for VA multiaxial loading due to the lack of understanding

of the possible interaction between the components involved in the damage model selected [163].

Under biaxial loading, the crack growth becomes more complicated to be characterised as it depends on some additional factors such as phases differences, biaxiality stress ratio which is the ratio of horizontal stress to the vertical one (when it equals to zero, it is the case of uniaxial loading, while equals to 1, it is equiaxial loading) [167]. The variation in these factors can lead to changes in both crack growth path and rate [167–170]. In addition, widely conflicting trends of the effect of load biaxiality on growth rate have been reported that is increasing load biaxiality caused increased [171], decreased [172] or negligible [173] effects on the fatigue crack growth rates.

However, the model I stress intensity factor, ΔK , was reported to be independent of the load biaxiality [170,172] and it is identical to that under uniaxial loading, provided the two stresses applied in the two orthogonal directions [174]. In this case, the LFM (Equation 2.16) cannot take into capture the effect of biaxial loading on crack growth, leading to an over- or under-estimation of fatigue life.

2.17 Summary of the background and literature review

The literature review discussed in this Chapter has clearly identified the need for better understanding of the fatigue performance of welded joints under VA loading spectra and the guidance on how to estimate fatigue damage of a given VA loading history.

The combination of S-N curve with Miner's rule is the most widely used method to estimate the fatigue life of welded joints under a given loading history. However, the problem is that while $D = 1$ is an appropriate fatigue failure criterion under CA loading spectra, there is a lack of guidance on how to set a proper D value for the fatigue assessment when welded joints subjected to VA loading spectra. As discussed in 2.5.3, current design codes suggest limiting Miner's sum D to 0.5 when the effect of the nature of the given VA stress spectrum is uncertain or for particularly critical cases. However, 0.5 is only corresponding to the welded joints containing high residual stress under the CD loading sequence with a high maximum stress which is about 80% SMYS. It is still unclear whether $D = 0.5$ is proper for the welded joints with low residual stress under the CD sequence with reduced maximum stresses. In addition,

Miner's sum D estimated under CU loading sequence could exhibit a large scatter, ranging from 0.5 to 8 [52], and there is still no guidance on how to determine a proper D value for welded joints under such sequences to not only ascertain safety but also to avoid waste of the remaining fatigue life.

Fracture Mechanics is another widely used technique to predict the fatigue life of welded joints, by which the FCG process under a given loading history can be estimated. The FCGR at an indicated stress range can be calculated according to the FCGR curves given in the design code BS 7910 [30]. However, these curves are established based on the experimental data produced under CA loading sequences, and it has been discussed (Section 2.13) that under VA loading sequences, the prediction of the FCGR based on BS 7910 could be either under- or over-estimate depending on the nature of sequences, resulting in an unsafe and unduly conservative prediction of the fatigue life, respectively. Therefore, this method needs to be improved in order to capture the interaction effect between stress ranges in VA loading sequences. Some mechanisms for the FCGR transit effect has been proposed, and the local residual mean stress may be the predominant one [12,13] in some circumstance, but the relevant analytical model has not been well established yet.

It is these problems that form the basis of the present study, which aims to provide a better understanding of the fatigue performance of welded joints under VA loading spectra and improve the prediction of fatigue endurance for fatigue design.

Chapter 3 Fatigue testing under variable amplitude loading spectra

3.1 Introduction

Fatigue tests were performed in the present study to investigate the effect of VA loading on the fatigue life of fillet welded plate specimens. The tests aim to address the identified gap in the existing data and to improve understanding of the fatigue performance of welded joints under VA loading.

This chapter provides detailed information on the fatigue tests carried out under VA loading. In total of two VA loading spectra were designed and CD loading sequences with four different maximum stresses were produced accordingly. Welded joints with non-load-carrying transverse fillet-welded attachments, fabricated using steel plates with three thicknesses, were tested under both axial and bending loading mode. A novel fatigue testing jig was developed allowing the application of a constant axial stress during the bending test. In addition to the as-welded joints, four life-improved welded joints, which were treated by ultrasonic impact treatment (UIT), were fabricated, and tested. The fatigue crack growth (FCG) data was collected for the subsequent fracture mechanics analysis.

The results are expressed in terms of Miner's cumulative damage summation and the maximum (minimum) stress of the CD (CU) loading sequences. Based on the test results, the effects of the mean stress, loading mode, plate thickness and post-weld treatment on the fatigue endurance of the welded joints under VA loading are discussed.

3.2 Test specimens

3.2.1 As-welded specimens

The specimens tested in the present study were steel plate specimens containing two transverse non-load-carrying fillet welded attachments, as shown in Figure 3.1. The attachments were in the longitudinal centre and one on each surface of a plate, opposite to each other, as shown in Figure 3.1 (a). The thickness of the attachment was identical to the plate thickness. After welding, the specimens were cut off from the plates in the direction perpendicular to the welds with a specimen width of 100mm, as shown in Figure 3.1 (b).

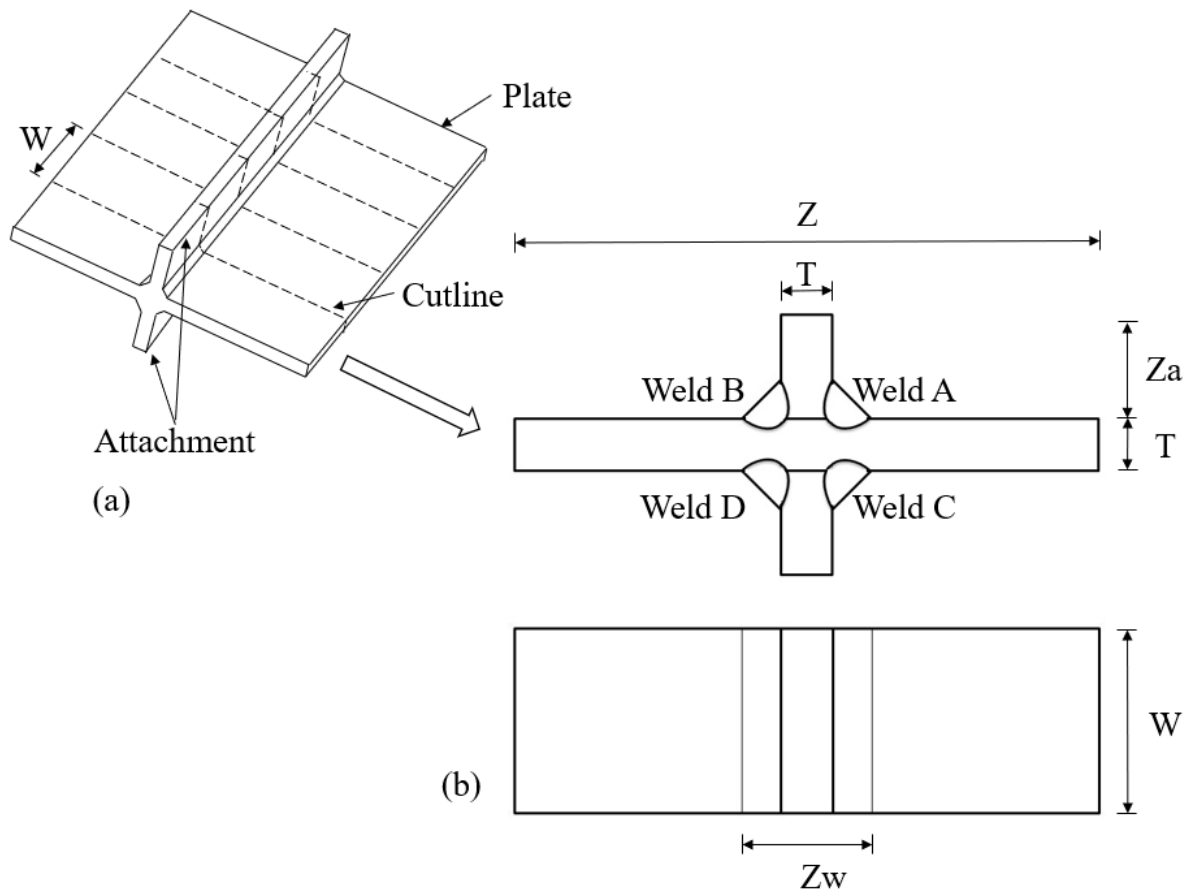


Figure 3.1 Fatigue test specimens: (a) the fabrication process and (b) sketch of the welded specimen (not to scale).

The material of the plate and attachment was S355 which is a structural steel with a good combination of strength and weldability. The monotonic engineering stress-strain data was extracted from [175] and re-plotted in Figure 3.2. In addition, the true stress-strain were also calculated and plotted for comparison. The mechanical properties of S355 are given in Table 3.1.

Table 3.1 Material properties of S355 structure steel.

Young's modulus, E	Minimum specified yield stress, σ_y	Tensile strength σ_{UTS}	Fracture stress σ_f	Reduction rate	True fracture stress, σ_{tf}^1	Cyclic strain hardening exponent, n'^2
207GPa	355MPa	550MPa [175]	350MPa [175]	51%-59% [13]	900MPa	0.16

Note: ¹: σ_{tf} was estimated using $\sigma_{tf} = \sigma_{UTS} + 345MPa$ [8].

²: n' was calculated based on $n' = z/c$, where $z = -0.1667 \log(2.1 + 917/\sigma_{UTS})$ and $v = -0.6$ [176].

To investigate the effect of plate thickness on fatigue performance of welded joints, three different thickness plates were selected: 6, 12.5 and 25mm. The relevant dimensions of the specimens are given in Table 3.2.

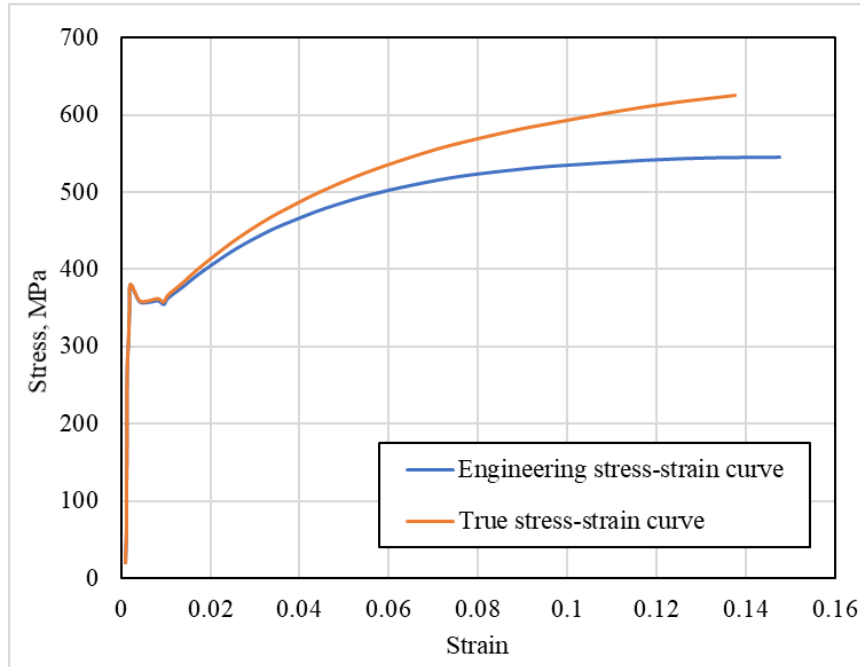


Figure 3.2 Typical engineering and true stress-strain curve for S355 structural steel [175].

The geometry of the fillet welds was characterised using Wiki_Scan welding inspection system manufactured by Servo-Robot. Three specimens, one from each thickness, were randomly selected and inspected. In each specimen, two measurements were carried out on two welds at the mid-width. The results show that the parameters of the two welds in each specimen are almost identical, and the depth of under-cut ranges between 0.1 and 0.3mm in all three plate thicknesses. More details of the inspection system and measurement outcomes are given in Appendix A.

Table 3.2 Dimensions of the test specimens (in mm).

Thickness, T	Length, Z	Width, W	Attachment height, Z_a	Width of attachment and welds, Z_w
6	800	100	40	14.0
12.5				28.5
25				51.0

3.2.2 Ultrasonic impact treated specimens

In order to investigate the effect of VA loading on fatigue performance of the life-improved specimens, four as-welded specimens, of which three were 12.5mm-thick and one 25mm-thick, were randomly selected and treated using the widely used ultrasonic impact treatment (UIT) technique. The equipment used was Stressonic[®] NOMAD portable ultrasonic peening equipment (reference NO. 2017-9101) manufactured by SONATS Europe Technologies group as shown in Figure 3.3. All treatments were conducted manually along the weld toe using multiple passes with a 3 mm diameter impactor. The number of passes of treatment depended on the condition of the weld details to ensure a smooth uniform profile of the weld toe. The impact frequency and air pressure were respectively at around 20,000Hz and 0.5 MPa (70Psi).

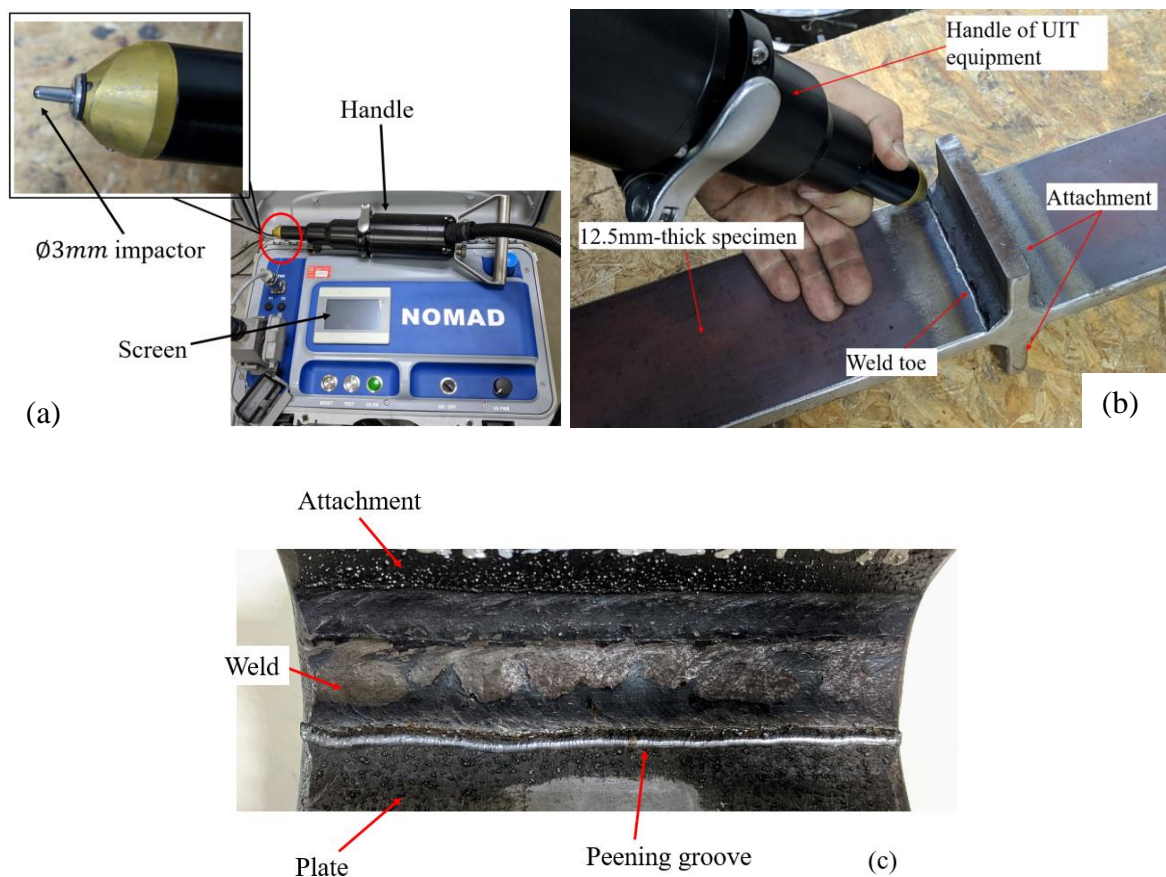


Figure 3.3 Ultrasonic Impact Treatment (UIT) on welded joints: (a) the Stressonic[®] NOMAD portable Ultrasonic Peening Equipment; (b) an example of the UIT process on 12.5mm-thick welded joint; (c) the groove after treatment along weld toe.

The quality of the treatment was evaluated by visual inspection in accordance with the guidance [177]. The groove radius created by the impact was about 3mm. The resulting grooves were smooth and continuous along the weld toe without any visible interruption. The welds were thus regarded as appropriately treated.

3.3 Fatigue tests

3.3.1 Constant amplitude S-N curves for the as-welded specimens

Fatigue tests on the as-welded specimens, manufactured from the same batch, had been carried out under constant amplitude (CA) loading in a previous study and the mean S-N curve for each plate thickness was determined and reported [178]. These S-N curves were adopted in the present study as benchmarks to estimate the cumulative fatigue damage, D , under VA loading. The CA tests were conducted under either axial or bending loading, at a constant maximum stress of 300MPa for axial loading and 330MPa for bending loading, with the stress ratio ranging between 0.03-0.7 (ratio of minimum to maximum stress in a cycle). In each loading mode, seven specimens were tested. Based on the test results, the mean S-N curves established with a forced slope of 3 ($m = 3$, the slope for Class F curve in BS 7608) [178] are re-plotted in Figure 3.4.

BS 7608 [1] specifies Class F curve for this type of weld detail. However, it can be seen from Figure 3.4 that the Class F can be either conservative or non-conservative, depending on the plate thickness and loading mode. Except for the curve for the 25mm-thick plates tested under axial loading, the S-N curves for the other five data sets are above the BS 7608 Class F mean curve. The test results suggest the beneficial effects of thinner specimens under bending loading on fatigue strength which are in line with expectation based on the fatigue design guidance given in BS 7608. In addition, for each thickness specimen, the S-N curve obtained under bending is above that for tensile. This is because fatigue strength depends on the degree of through-thickness bending. The fatigue strength increases with increasing bending component for a decreasing stress range gradient through the plate thickness [1].

It should be noted that the S-N curves mentioned here, including the Class F curve and the curves for the current welded joints, are all for as-welded condition. However, when estimating

fatigue lives for those specimens treated by UIT, those S-N curves were modified according to the guidance provided in standard BS7608 (Table 2.2).

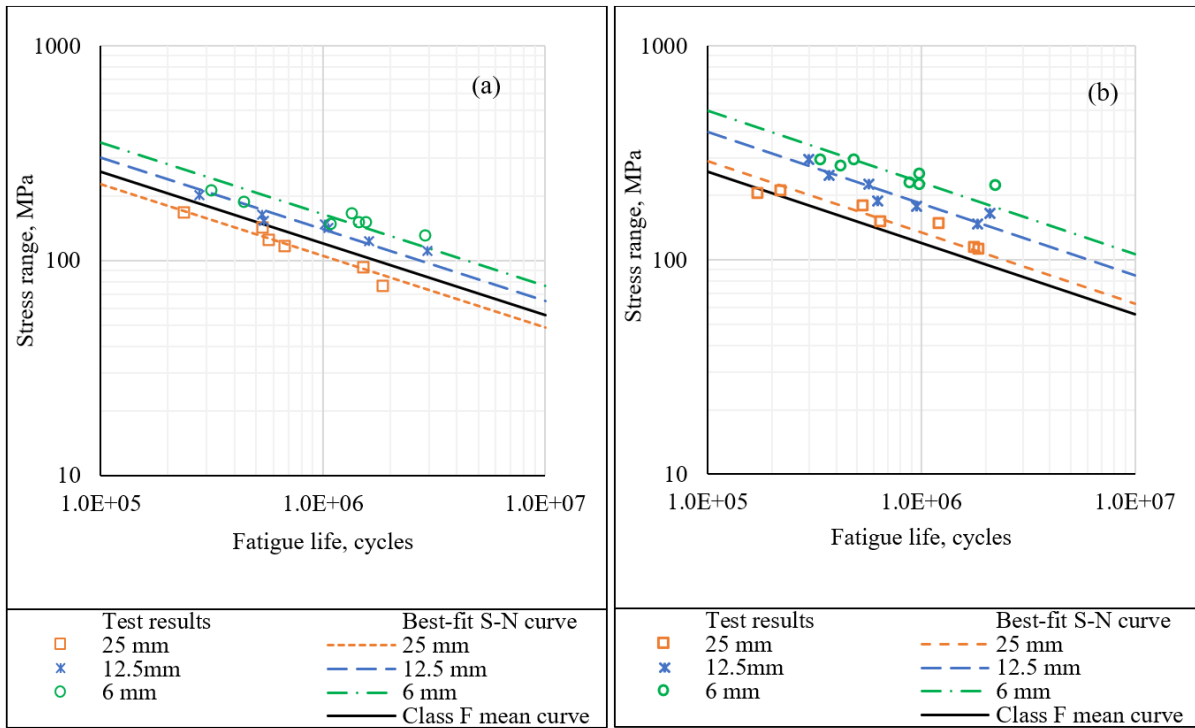


Figure 3.4 The mean S-N curves determined under constant amplitude loading with a forced slope $m = 3$ [178]: (a) under axial loading and (b) under bending loading. The BS 7608 Class F mean curve is included for comparison.

3.3.2 Variable amplitude loading spectra

3.3.2.1 Spectrum I

The VA loading spectrum used in the present study was designed following the typical Gassner distribution [179]:

$$P_i = \left(1 - \frac{\log(N_E)}{\log(N_{max})} \right)^{\frac{1}{b}} \quad (3.2)$$

where P_i is the relative stress range ratio which is defined as the ratio of each stress range, $\Delta\sigma_i$, to the maximum stress range, $\Delta\sigma_{max}$, following:

$$P_i = \frac{\Delta\sigma_i}{\Delta\sigma_{max}} \quad (3.3)$$

N_E is the exceedence corresponding to a specific P_i . N_{max} is the maximum exceedence, i.e., for $P_i = 0$. b is the shape exponent.

The $\Delta\sigma_{max}$ was set at 250MPa that is approximately 70% of the minimum specified yield stress (SMYS) of the material, and the shape factor b in Equation 3.2 was set as 1.0 (linear distribution). To ensure all stress ranges can lead to fatigue damages, the minimum P_i was taken as 0.35 which corresponded to a minimum stress range of 87.5MPa. This value is higher than the constant amplitude fatigue limit (CAFL) defined in BS 7608 for Class F mean curve which is 55MPa at 10^7 cycles. The N_{max} was taken as 1.5×10^5 cycles, and the exceedence for $P_i = 0.35$ was calculated to be 2,316 cycles which was the block length, N_L . The P_i distribution is shown in Figure 3.5, and the stress histogram of the VA spectrum is given in Table 3.3.

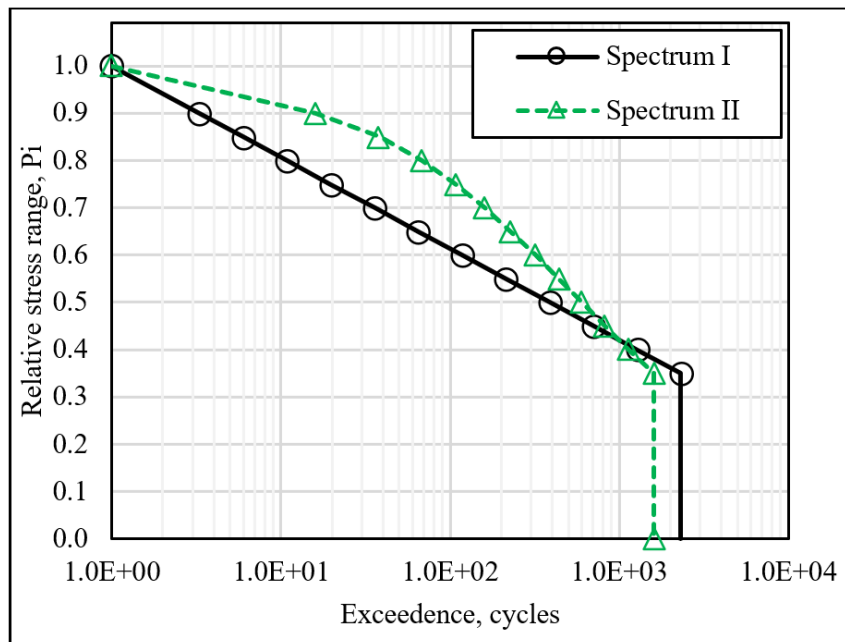


Figure 3.5 P_i distribution of the Spectrum I and II adopted in the present study.

The damage caused by the VA loading spectrum was evaluated using an equivalent CA stress range, $\Delta\sigma_{CA,equ}$. This is the CA stress range which, according to Miner's rule, is equivalent in terms of fatigue damage to the VA stress spectrum:

$$\Delta\sigma_{CA,equ} = \left(\frac{\sum \Delta\sigma_i^m n_i}{N_L} \right)^{\frac{1}{m}} \quad (3.4)$$

The $\Delta\sigma_{CA, equ}$ for the above loading spectrum was calculated to be 107MPa.

Table 3.3 Stress histograms of VA Spectrum I and II.

Relative stress range, P_i	Stress range, $\Delta\sigma_i$ (MPa)	Spectrum I		Spectrum II	
		Cycles	Exceedence, n_E	Cycles	Exceedence, n_E
1	250	1	1	1	1
0.9	225	2	3	15	16
0.85	212.5	3	6	22	38
0.8	200	5	11	30	68
0.75	187.5	9	20	40	108
0.7	175	16	36	52	160
0.65	162.5	29	65	68	228
0.6	150	53	118	90	318
0.55	137.5	96	214	120	438
0.5	125	174	388	161	599
0.45	112.5	316	704	221	820
0.4	100	573	1,277	315	1,135
0.35	87.5	1,039	2,316	470	1,605

To evaluate the fatigue damage level at each stress range, the relative fatigue damage, D_{ri} , defined as the ratio of the fatigue damage at a particular stress level $\Delta\sigma_i$ against that at the maximum stress range $\Delta\sigma_{max}$, is calculated:

$$D_{ri} = \frac{P_i^m n_i}{P_{max}^m n_1} \quad (3.5)$$

where n_1 is the number of cycles at the maximum relative stress range ratio P_{max} . The result is plotted in Figure 3.6. It can be seen that fatigue damage increases with decreasing P_i and most fatigue damage occurs at stress ranges $P_i < 0.6$. This can result in an unpractical test duration for the UIT welded joints. Therefore, a different spectrum, Spectrum II, was developed based on Spectrum I.

3.3.2.2 Spectrum II

In this spectrum, the number of cycles for each stress range in Spectrum I were manually adjusted to increase the number of cycles at higher stress ranges but decrease the number of cycles at lower stress ranges. The distribution of P_i , relative fatigue damage and stress histogram for Spectrum II is shown in Figure 3.5, Figure 3.6 and Table 3.3, respectively. In this case, the fatigue damage at each relative stress level after $P_i \leq 0.6$ is almost constant and

the total fatigue damage at relative stress ranges $P_i < 0.6$ is reduced to about 47% of the total damage (compared to 80% in Spectrum I). The block length for Spectrum II is 1,605 cycles.

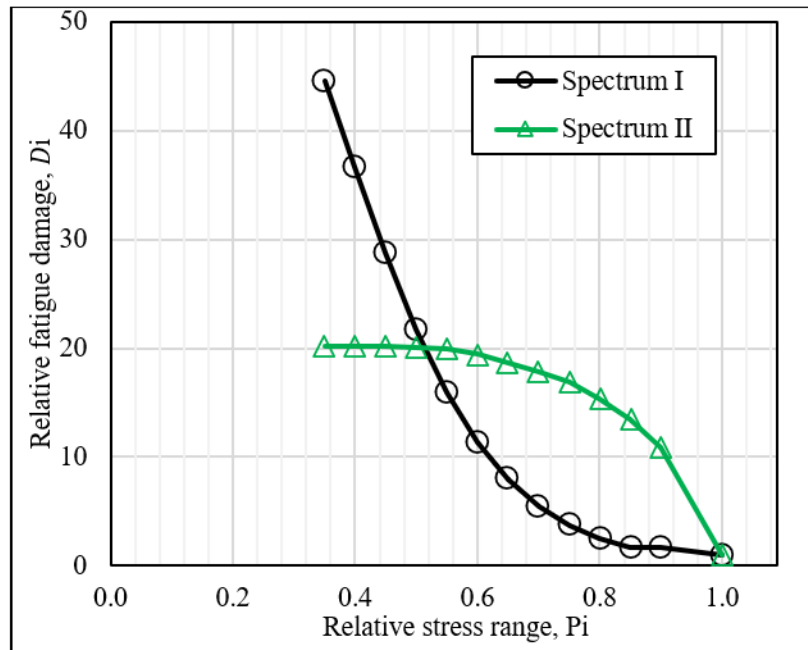


Figure 3.6 Relative fatigue damage, D_i , distributions of Spectrum I and II adopted in the present study.

3.3.3 Loading sequences

Based on these two VA spectra, various CD loading sequences with different maximum stresses were produced to investigate the effect of applied maximum stresses on Miner's sum. There were four maximum stresses: 0, 87.5, 150 and 300MPa. The cyclic stresses in a loading block were arranged in a random order. When the whole of the first block had been applied, the process was repeated, and subsequent blocks were applied in the same random order. This process was continued until the specimen failed. A typical CD loading sequence (part of a loading block) is shown in Figure 3.7 (a).

3.3.4 Loading modes

In the present study, fatigue tests were carried out under either an axial or a bending loading mode, depending on the maximum stresses applied. When the maximum stress in the CD loading sequence was reduced in steps from 300MPa to 0, high compressive loading was introduced, which may cause specimen buckling if the tests were performed under an axial

loading mode, especially for the thin plates. Therefore, some tests involving the maximum stresses less than 150MPa were conducted under bending loading.

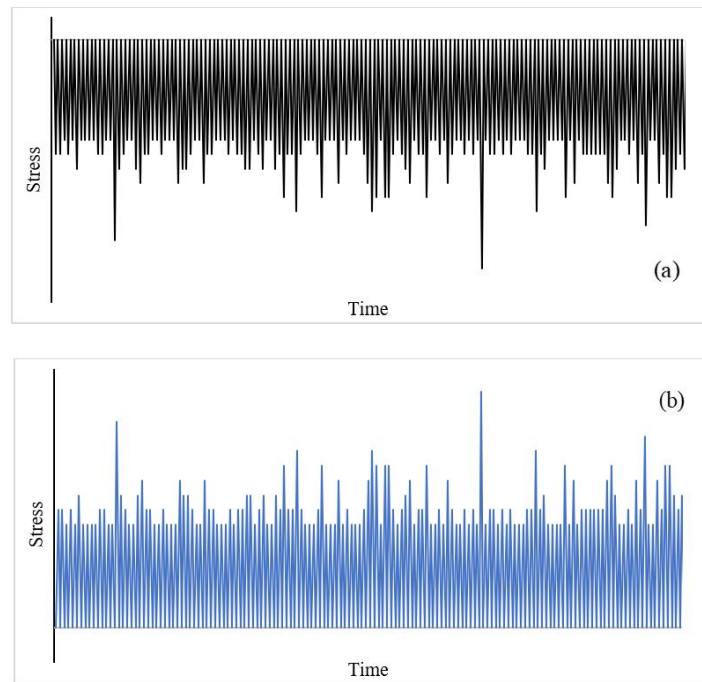


Figure 3.7 Examples of the two loading sequences: (a) cycling down from a constant maximum stress; (b) cycling up from a constant minimum stress.

A novel test jig was designed and manufactured in the present study to apply a constant axial stress for fatigue testing under a bending mode, as shown in Figure 3.8. The specimen was fixed in the frame in a horizontal position by pins, and the specimen was applied with a static axial stress through two parallel jacks connected to the frame. Each specimen was installed with strain gauges to check the stress level achieved. The arrangement of strain gauges is given in the following section. The VA loading was applied by the actuator in a three-point bending set-up. The load was applied through the attachment on the top surface of the plate, in the direction perpendicular to the specimen. A sketch of the jig design is given in Appendix B.

When the maximum stress was zero, tests were conducted under four-point bending mode with an inner span of 200mm while the outer was 400mm.

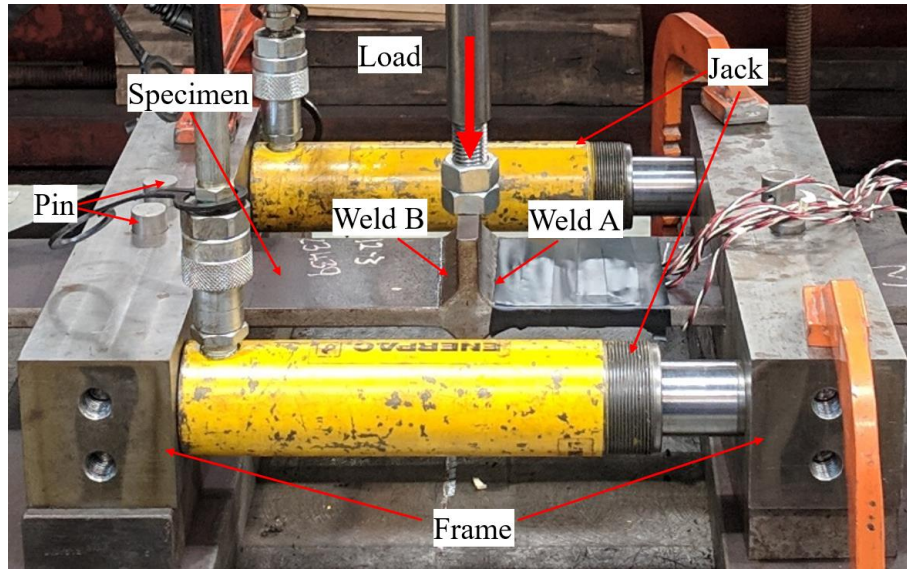


Figure 3.8 The bending test jig.

It is interesting to note that, in the bending mode, when the top welds (e.g., welds A and B in Figure 3.8) are subjected to a CD loading sequence, the bottom welds (e.g., welds C and D) are tested under a cycling up (CU) loading sequence where all cycles have the same minimum stress, Figure 3.7 (b). When the top welds are subject to cyclic loading from a constant zero stress to various levels of compression stresses (CD), the bottom welds are subject to cyclic loading from a constant zero stress to different levels of tension stresses (CU). Therefore, the fatigue damages of these two different loading sequences can be studied in a single specimen. It should also be noted that as the stress histograms (number of cycles at each stress range level) for the two loading sequences are identical, the welds on both the top and bottom sides of each specimen are expected to have the same fatigue life according to BS 7608.

3.3.5 Arrangement of strain gauges

Three strain gauges were used for the tests under axial loading mode. As shown in Fatigue 3.8 (a), a pair of strain gauges, gauge 1 and 2, were mounted in the centreline of specimen width, at distances of $0.4T$ and T to the weld toe, respectively, aiming to determine the hot-spot stress in accordance with BS 7608. The third strain gauge was installed on the other side of the specimen, directly opposite to the gauge 2 to estimate the secondary bending stress due to angular misalignment following:

$$\sigma_b = E \times \left(\frac{\varepsilon_2 - \varepsilon_3}{2} \right) \quad (3.6)$$

where σ_b is the bending stress, ε_2 and ε_3 are the readings recorded from the strain gauges and E is the Young's module of the material.

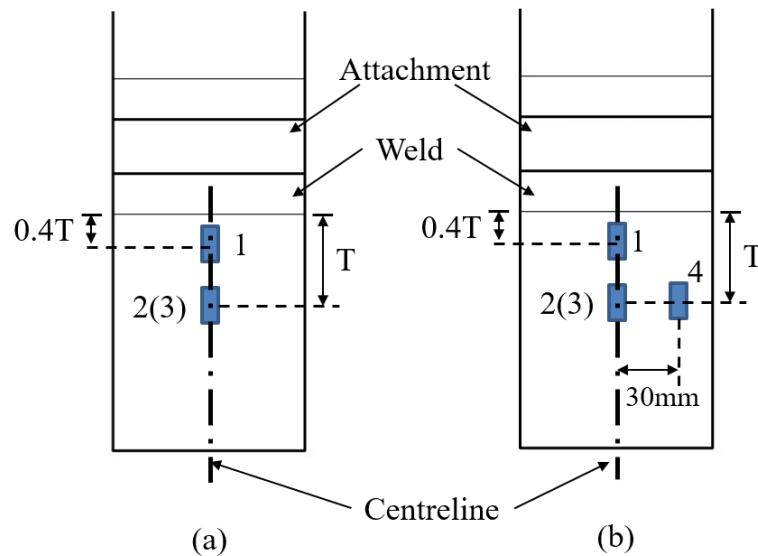


Figure 3.9 The arrangement of strain gauges on the specimens tested in a) axial loading and b) bending loading (gauge 3 opposite to gauge 2).

In the tests in bending mode, one more strain gauge, gauge 4, was applied beside gauge 2, 30mm apart, to check whether the stresses across the specimen width were uniform, as illustrated in Figure 3.9 (b).

The type of strain gauges used in the fatigue tests is FLA-1-11, produced by Tokyo Sokki Kenkyujo Co., Ltd, with the gauge factor ranging from 2.11 to 2.14 and the resistance at 120Ω . Gauges were bonded to the polished surface at the specified locations and connected using a three-wire quarter bridge configuration to a computer-controlled data logger.

3.3.6 Fatigue crack growth monitoring

For the subsequent fracture mechanics analyses, the crack initiation and propagation from the weld toes were monitored in all fatigue tests. The crack depth, a , and the surface crack length, $2c$, were measured using a combination of visual inspection and the alternating current potential drop (ACPD) method.

Visual inspections of the weld toe were performed regularly during a fatigue test, aided by a magnifier and soap solution. This technique can detect a crack of about 2mm in length. When

a crack has initiated, small bubbles can be observed as the crack open and close under cyclic loading. Another benefit of this method is to produce beach marks on the fracture surface. Therefore, the crack depth at a known endurance can be estimated from the measured crack depth after a fatigue test is completed, and the fracture surface is revealed.

Once a crack had been found, a crack depth meter (reference NO. RMG 4015) produced by Karl Deutsch, as shown in Figure 3.10, was used to monitor the crack growth in the depth direction. The crack depth was measured by placing the four spring-loaded pin probes directly across the crack. A constant alternating current is passed through two of the four pins into the specimen, while the other two pins detect the voltage drop across the crack, where the crack depth is estimated from. The ACPD check was performed regularly, at the equal intervals as the application of the soap solution.

3.3.7 Fatigue testing

3.3.7.1 As-welded specimens

A total of twelve as-welded specimens were tested. The specimen numbering system comprises three parts: 'A or B + thickness_ series number'. Letter A or B represents axial or bending loading, respectively, and the series number is the sequential number for a particular specimen thickness. For instance, specimen B12.5_2 means the second test for the 12.5mm-thick specimen tested in bending mode.



Figure 3.10 The alternating current potential drop (ACPD) device used for crack depth monitoring.

Of the twelve as-welded specimens tested, eleven were tested under spectrum I and one 12.5mm-thick specimen was tested under spectrum II. For convenience, the following CD or CU loading sequences refer to those produced from Spectrum I, except as otherwise specified.

Eight specimens were tested under axial loading and four specimens under bending loading. When the maximum stresses in the CD loading sequences were set at 300 and 150MPa, one specimen from each plate thickness were tested under axial loading, making a total of six tests. When the maximum stress was reduced to 87.5MPa, two specimens, one 25mm- and the other 12.5mm-thick, were tested under axial loading mode and two other specimens, one 12.5mm- and 6mm-thick, were tested under bending mode. When the maximum stress was reduced to zero, two specimens were tested under bending mode: one 25mm-thick specimen tested under Spectrum I while another 12.5mm-thick specimen was tested under Spectrum II. The specimen identification numbers (ID), and the corresponded loading conditions are summarised in Table 3.4 for axial loading and Table 3.5 for bending loading.

All fatigue tests were carried out under load control, using four calibrated servo-hydraulic testing machines with load capacities of 25kN, 350kN, 500kN and 1000kN, respectively. The VA loading sequences were applied using an in-house software programmed using LabVIEW. All tests were performed in air at ambient temperature, with a loading frequency ranging between 3 and 6Hz.

Table 3.4 Specimen ID for the tests performed under axial loading.

Maximum stress (MPa) / Plate thickness (mm)	300	150	87.5
6	A6_1	A6_2	-
12.5	A12.5_1	A12.5_2	A12.5_3
25	A25_1	A25_2	A25_3

Table 3.5 Specimen ID for the tests performed under bending loading.

Axial static stress (MPa)	87.5	0
Plate thickness (mm)		
6	B6_1	-
12.5	B12.5_1	B12.5_2*
25	-	B25_1

Note: * the VA loading sequence was produced from Spectrum II.

3.3.7.2 Ultrasonic impact treated specimens

The numbering system for the UIT specimens is similar to that for the as-welded specimens except that they are prefixed with ‘UIT’. For example, specimen UIT_B12.5_2 means the second UIT 12.5mm-thick specimen tested in bending mode.

A total of four UIT welded specimens were tested, of which three were 12.5mm-thick, and one was 25mm-thick. While two 12.5mm-thick specimens were tested in bending mode, the other one and the 25mm-thick specimen were tested under axial loading.

Under the axial loading, the maximum stress of 12.5mm thick specimen tested under the CD loading sequence was 150MPa. In this case, the maximum applied load ratio (corresponding to the minimum stress range in the spectrum) was about 0.4, which is the upper limit advised in the standard [1] to claim the benefit from UIT. The magnitude of fatigue life improvement for UIT depends on the stress ratio applied. To investigate this, two other specimens, with the same plate thickness (12.5mm), were tested at lower maximum stresses, 87.5MPa and 0, respectively. These two specimens were tested under bending loading.

The axial fatigue test for the 25mm-thick specimen was performed with the maximum stress at 300MPa. At such a maximum stress level, the load ratios for most of the stress cycles were higher than 0.4. This test was aimed to study whether there is any life improvement when the stress ratios are greater than the maximum limit set in BS 7608. Details of the fatigue tests under axial and bending modes are given in Tables 3.6 and 3.7, respectively.

The testing machines, loading frequency and test temperature are the same as those used in the tests on the as-welded specimens.

Table 3.6 Specimen ID for the tests performed under axial loading.

Maximum stress (MPa)	300	150
Plate Thickness (mm)		
12.5	-	UIT_A12.5_1
25	UIT_A25_1*	-

Table 3.7 Specimen ID for the tests performed under bending loading.

Axial static stress (MPa)	87.5	0
Plate Thickness (mm)		
12.5	UIT_B12.5_1	UIT_B12.5_2*

Note (for both Table 3.6 and 3.7): * the VA loading sequence was produced from Spectrum II.

3.4 Results for as-welded specimens and discussion

3.4.1 Fatigue lives and Miner's sum

Of the twelve specimens tested, eleven specimens failed and one specimen, B6_1, was declared run-out after it ran 1.4×10^7 cycles without any indication of fatigue cracking at the weld toes. All failures occurred at the weld toes. For the three failed specimens tested in the bending mode, fatigue failures took place at the bottom welds that were subjected to CU loading sequence.

In all specimens, the readings from strain gauges 1, 2 and 3 are almost identical, suggesting that the secondary bending stress due to angular misalignment is negligible and the hot-spot stress is the same as the nominal stress. Thus, the subsequent stress analyses are based on the nominal stress only. Under the bending mode, the reading of gauge 4 is close to gauge 2, indicating that the stresses across the plate thickness are almost uniform.

The predicted fatigue life and Miner's sum, D , for each VA test were calculated based on the CA S-N curves derived in [178] and presented in Table 3.8 for axial loading and Table 3.9 for bending loading.

Table 3.8 Results of the specimens tested under axial loading.

Plate thickness (mm)	Specimen ID	Maximum stress (MPa)	Predicted fatigue life (Blocks)	Experimental fatigue life (Blocks)	Miner's Sum, D
6	A6_1	300	1,550	851	0.54
	A6_2	150		778	0.51
12.5	A12.5_1	300	958	409	0.43
	A12.5_2	150		1,128	1.18
	A12.5_3	87.5		1,863	1.94
25	A25_1	300	413	253	0.61
	A25_2	150		315	0.76
	A25_3	87.5		416	1.00

Table 3.9 Results of the specimens tested under bending loading (cycling down for the top welds and cycling up for the bottom welds).

Plate thickness (mm)	Specimen ID	Predicted fatigue life (Blocks)	Bottom welds			Top welds		
			Minimum stress (MPa)	Experimental fatigue life (Blocks)	Miner's Sum, D	Maximum stress (MPa)	Experimental fatigue life (Blocks)	Miner's Sum, D
6	B6_1	4,270	87.5	12,996 ^a	>3.04	87.5	runout	>3.04 ^b
12.5	B12.5_1	2,170	87.5	1,903	0.88	87.5		>0.88 ^b
	B12.5_2	1,850	0	3,376	1.82	0		>1.82 ^b
25	B25_1	859	0	1,787	2.08	0		>2.08 ^b

Notes: a: There was no indication of cracking after running 2,326 blocks (30 days, $D = 0.55$). To speed up the test, the loading spectrum was modified to exclude all the stress ranges less than 125MPa. The test was resumed using the modified loading spectrum for another 23,738 blocks (equivalent to 10,670 blocks in the original spectrum in terms of fatigue damage). b: These welds ran out. There was no indication of cracking found in the top welds experiencing the CD loading sequence. The 12.5mm- and 25mm-thick specimens failed from the bottom welds experiencing the CU loading sequence.

The implications of the test results and the effects of several variables on fatigue lives of the welds are discussed in the following several sections.

3.4.2 Effect of the maximum stress in cycling down loading sequence

Figure 3.11 shows the results of all the welds tested under CD loading sequences. Some results reported in [5] were also included for comparison. The welded joints tested were also in Class

F, but with longitudinal attachments, rather than transverse ones. As discussed in Section 2.7, this type joints generally have a higher residual stress (281MPa [5]) than those tested in the present study (128 MPa and more details are given in Chapter 4). The maximum stresses of the CD sequences applied in [5] were of 280 and 147MPa.

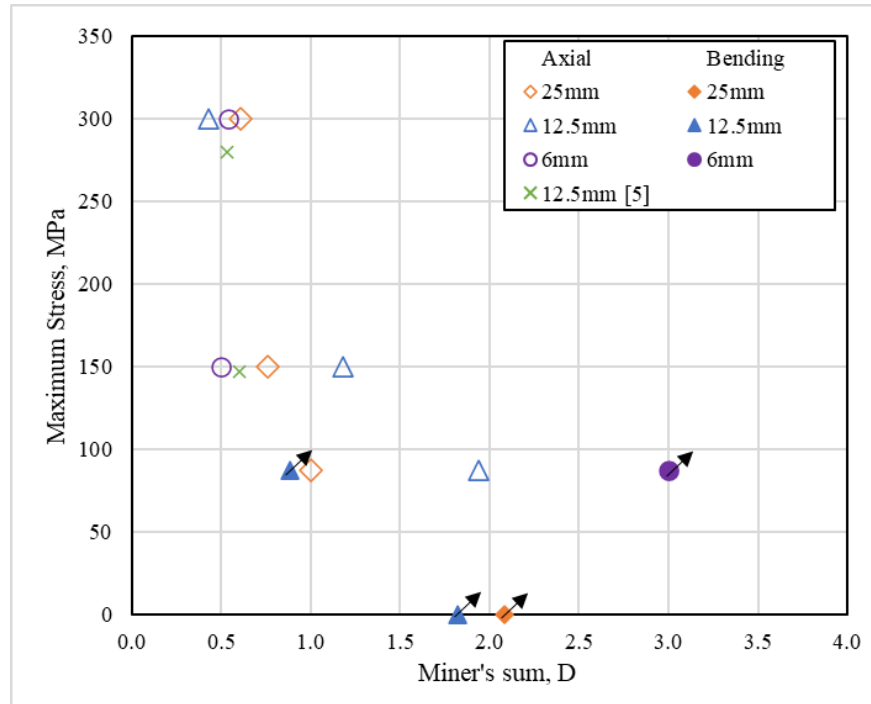


Figure 3.11 Miner's sums, D , obtained from welds subjected to CD loading sequences with different maximum stresses (arrow indicates runout).

It can be seen from Figure 3.11:

- When the maximum stress is 300MPa, about 80% SMYS of the material, the D values for all three specimens are about 0.5, similar to the results reported by other researchers [3,5,6,13].
- The Miner's sums increase with decreasing maximum stress. When the maximum stress is reduced to 150MPa, the results of both 25mm- and 12.5mm-thick specimens show an increase in fatigue life - the D increases from 0.61 to 0.76 for the former and from 0.43 to 1.18 (more than doubled) for the latter.
- The results reported in [5] also shows an increase with decreasing maximum stress, but much smaller - from 0.53 at 280MPa to 0.60 at 147 MPa.

- For the 6mm-thick specimen, there is no significant change in D , although an increase would be expected based on the trend suggested by the results of the thicker specimens. However, the result appears to be in agreement with that reported in [5].
- However, when the maximum stress is further reduced, a significant increase in D values is obtained for the specimens of all three thicknesses. For the four welds tested at a maximum stress of 87.5MPa and subjected to CD loading sequence, two specimen tested in axial loading failed with $D = 1.00$ and $D = 1.94$, respectively. The other two welds tested under bending loading ran out respectively at $D > 0.88$ and $D > 3.08$: the former is a 12.5mm thick specimen which failed from the bottom weld subjected to CU loading sequence and the latter is a 6mm thick specimen which does not fail from either the top or bottom welds.
- One of each 12.5mm and 25mm-thick specimen were tested at a maximum stress of 0. These specimens both failed from the bottom weld with $D = 2.08$ for the 25mm-thick specimen and $D = 1.82$ for the 12.5mm-thick specimen. The top weld subjected to the CD loading sequence ran out at $D > 2.08$ and $D > 1.82$ for the 25mm- and 12.5mm-thick specimen, respectively.

The present test results suggest that, although a CD loading sequence can result in low D values [3,5,6,13], limiting D to 0.5 would be unduly conservative when the maximum stress in a CD loading sequence is below a certain value. The over-conservatism increases with decreasing plate thickness – D is higher than 3.08 for the 6mm-thick specimen subjected to a constant maximum stress of 87.5MPa. This phenomenon can properly be attributed to the residual stress presented in the specimens not high enough to maintain a high local stress level at the weld toe; therefore, the fatigue life of welded joints is seen to increase as the applied mean stress is reduced. Based on this, residual stress measurements were carried out in the present study and presented in Chapter 4.

3.4.3 Effect of the minimum stress in cycling up loading sequence

Figure 3.12 shows the Miner's sums of the welds tested under CU loading (i.e., the bottom welds of the specimens tested under bending loading). The results reported in [5] for

longitudinal fillet welds under two CU loading sequences with a minimum stress of 70MPa are included for comparison.

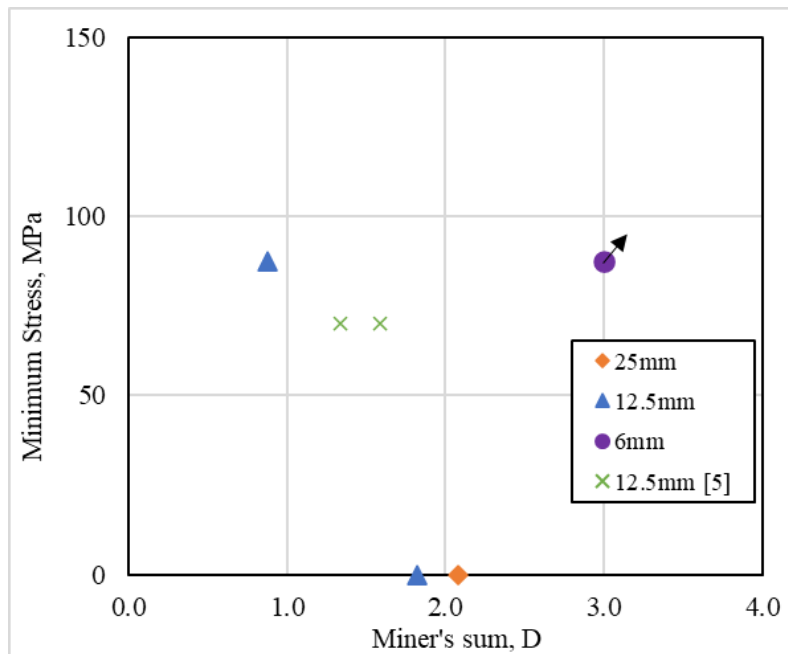


Figure 3.12 Miner's sum, D , obtained from welds subjected to CU loading sequences with different minimum stresses (arrow indicates runout).

The following can be seen from Figure 3.12:

- When the minimum stress is 87.5MPa, the welds in the 6mm-thick specimen run out at $D = 3.08$, whereas for the 12.5mm-thick specimen, the Miner's sum is only 0.88 at fatigue failure.
- When the minimum stress is reduced to 0, the D values of the two specimens are significantly greater than unity. The D value for the 12.5mm-thick specimen is more than doubled to 1.82, while the D value for the 25mm-thick specimen is 2.08.

The test results suggest that the fatigue damage parameter D for the CU loading sequence depends on the minimum stress applied – it increases with decreasing minimum stress level. This is in agreement with the results obtained under the CD loading sequences where the test results suggest a dependence of D on the magnitude of the maximum stress applied. Therefore, it would be inappropriate to use a constant upper limit D value to assess the fatigue life of

welded joints under CU loading, which would be unduly-conservative for sequences with low minimum stresses. More relevant tests would be required to verify this observation.

3.4.4 Effect of type of loading sequence

The damage sum D values for the welds experiencing the CD and CU loading sequences are compared in Table 3.9. Generally, the CD loading sequence is more damaging: $D < 1$ was reported for CD loading sequence while $D > 1$ for CU loading sequence [3–5,50,51]. Therefore, the top welds had been expected to have shorter fatigue lives than the bottom ones for the specimens tested under bending loading. However, the test results showed the opposite: all fatigue failure took place from the bottom welds experiencing CU loading sequence, and not from the top welds experiencing the CD loading sequence. The results from both the CD and CU loading sequences suggest a strong dependence of fatigue damage on the static axial stress level. When the mean stress is reduced through the decrease of either the maximum stress in the CD sequence or the minimum stress in the CU sequence beyond a certain level, a significant increase in D values are obtained. These results would not be expected according to the current fatigue design guidance (e.g., BS 7608, IIW) where the calculation of fatigue damage only considers stress range, not mean stress.

To investigate whether a fatigue crack had initiated in the welds which ran out under bending loading, macro-sectioning of three welds was performed: B12_1, B12_2 and B25_1. Each weld was sectioned at two different positions, as shown in Figure 3.13(a): one at the mid-width of the plate (position A) and another one 25mm apart (position B). The samples were mounted, ground and polished to $1\mu m$ using lapping paste. After etching, the area of interest was observed using an optical microscope. An example of a macro-section sample is shown in Figure 3.13 (b).

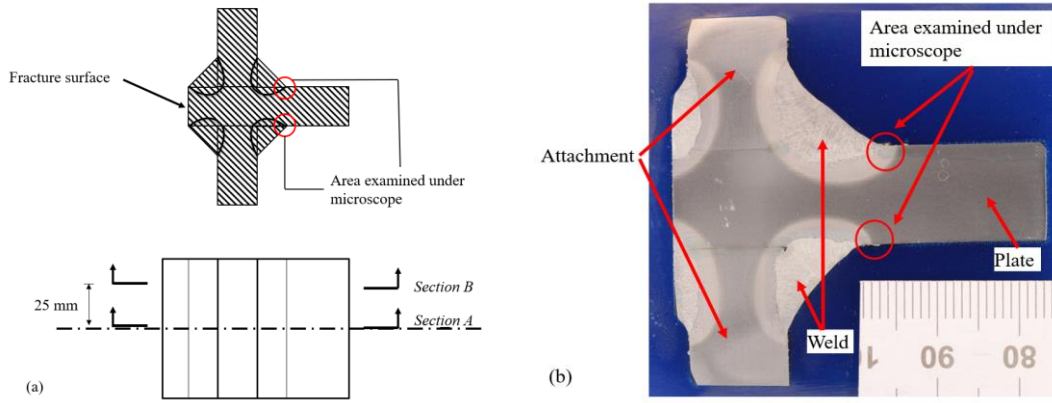


Figure 3.13 Macro-sectioning of run-out welds: (a) sectioning positions; (b) example of a macro-sections of the welds of specimen B12.5_1.

Among these macro-sections, only one small crack of 0.2mm in depth was observed in the top weld of specimen B12.5_1, Figure 3.14. The specimen was loaded with a static axial stress of 87.5MPa. No indication of fatigue cracking was observed in the top welds of specimens B12.5_2 and B25_1 where the static axial stress was 0. Hence, the D values can be significantly greater for the top welds under CD loading sequence than that for the bottom welds under CU loading sequence when the static axial stress is low.

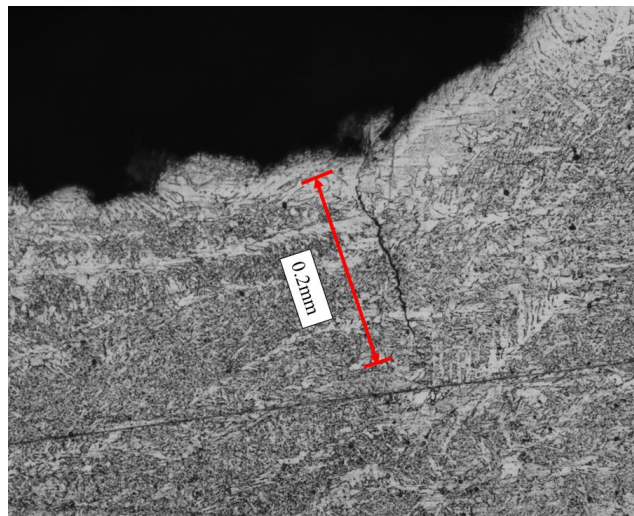


Figure 3.14 Crack observed in the top weld of specimen B12.5_1 where fatigue failure occurred from the bottom weld.

3.4.5 Effect of plate thickness

By comparing the test results shown in Figure 3.11 and 3.12, it can be seen that, although not conclusive, there is a general trend that thinner specimens' fatigue performance is better than that of thicker ones under both CD and CU loading sequences.

Under the CD loading sequence with a maximum stress of 300MPa, plate thickness does not significantly affect Miner's sum which is ~ 0.5 for the specimens of three different plate thicknesses.

However, when the maximum stress is reduced to 150MPa, the D value for the 12.5mm-thick specimen is about 1.5 times higher than that for the 25mm-thick specimen, suggesting that a thinner plate has a better fatigue life. For the 6mm-thick specimen, however, the D value does not change, still at about 0.5. The possible reason for this unexpected is discussed in section 3.4.8.

When the maximum stress is further reduced to 87.5MPa, the D value for the 12.5mm-thick is about two times higher than that for the 25mm-thick specimen, and the D value for the 6mm-thick is the highest, at least 50% higher than that for the 12.5mm-thick specimen. It should be noted that, according to BS 7608, the beneficial effect of thinner specimens (less than 25mm) can only be claimed in bending mode. However, the present results show that the plate thickness effect is also significant under axial loading mode. This effect agrees with the results obtained under CA loading [178] where tests were conducted under axial loading.

These results suggest that D value depends on plate thickness and D increases with decreasing plate thickness when the maximum stress in a CD sequence below a certain level.

Based on the limited data obtained under CU sequences, it can be seen from Figure 3.12 that when the minimum stress in the CU sequence is 87.5MPa, the D value for the 6mm-thick specimen is more than three times higher than that for the 12.5mm-thick specimen. This again suggests a better fatigue performance from thinner specimens. However, the two experimental results from the 12.5mm- and 25mm-thick specimens tested with a minimum stress of zero are similar. This suggests that, in addition to thickness effect, there might be other factors, such as weld profile and variations of welding-induced residual stresses, which also affect fatigue performance and cause data scatter.

3.4.6 Effect of type of welds

Fatigue performance of longitudinal fillet welds under VA loading were studied in [5], while in the present study transverse fillet welds were tested. In Figure 3.11 it can be seen that the fatigue lives of the transverse fillet welds increase significantly when the maximum stress is reduced from 300 to 150MPa. However, no apparent change in fatigue life is observed for the longitudinal fillet welds when almost the same amount of the maximum stress is reduced. As the thickness of these two types of welded joints are identical, being at 12.5mm, this difference may be only related to the difference in welding-induced residual stresses. It is well known that higher tensile residual stresses are present in the welds ahead of longitudinal attachment than that in transverse fillet welds. The residual stress ahead of a longitudinal attachment is about the magnitude of the yield strength of material [5,28], while the residual stress for a transverse fillet welds is much smaller as will be presented in Chapter 4. When the maximum stress is reduced to about 150MPa, the weld toe would still be subject to tension-tension loading for specimens with a longitudinal attachment while partly compressive loading for specimens with a transverse attachment. The test results suggest that the fatigue results of transverse fillet welds are more sensitive to the maximum stress applied in the CD loading sequence than the longitudinal fillet welds does.

3.4.7 Comparison of fatigue lives between experiments and predictions based on BS 7608

To demonstrate the effect of VA loading sequence on the fatigue life, experimental fatigue lives obtained under both CD and CU sequences with different mean stresses, as well as the results predicted using the experimentally determined mean S-N curves [178], in conjunction with the fatigue failure criteria $D = 1.0$, are presented in Figure 3.15. Experimental results for the longitudinal fillet welds under CD, CU and constant mean (CM) sequences [5] are also included for comparison. To indicate the data scatter, two lines with $D = 0.5$ and 2.0 are also included in the plot.

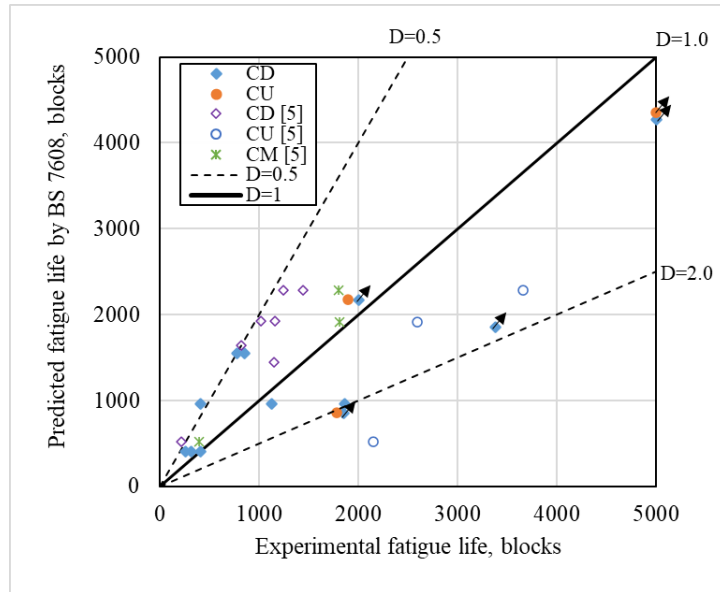


Figure 3.15 Comparison of the experimental fatigue lives with that predicted by Miner's rule. (arrows indicate runout)

It can be seen from Figure 3.15 that, although some data fall along the line with $D = 1.0$ according to BS 7608, the test data exhibit a large scatter, with most data falling between $D = 0.5 - 2.0$. The test results suggest a strong dependence of fatigue damage on loading sequences. BS 7608 recommends using $D \leq 1.0$ in fatigue design in general application. In recognition of the non-conservatism of this method for some VA loading spectra, including those involving little variation in the maximum applied tensile stress, it also advises to set the upper limit of D to 0.5 if the effect of the VA loading spectrum is uncertain. However, the present test results suggest that it can be unduly conservative to set $D = 0.5$ for CD loading sequences since some results obtained under this loading sequence are even greater than 2.0.

Based on the test results, it appears that the fatigue life of welded joints depends on the mean stress in a VA loading spectrum. Therefore, an analytical model has been developed to predict the fatigue life of weld joints under VA loading spectra by incorporating mean stress, which will be introduced in Chapter 5.

3.4.8 Post-test examination

The fracture surfaces of the two 6mm-thick specimens were examined in an optical microscope to explain why the D value was lower than expected when the maximum stress was reduced to 150MPa. Figure 3.16 shows the fracture surfaces of the two 6mm specimens: specimen A6_1

was tested at a maximum stress of 300MPa while specimen A6_2 at 150MPa. Both specimens exhibit multiple crack initiations. There is no indication of welding defects on the fracture surfaces of these two specimens. The reason for the lower D value is unclear. The scatter of the D values at maximum stresses ~ 150 MPa for these specimens might indicate that, when the maximum stress is reduced to this magnitude, the D value begin to depend on the maximum stress level under the CD loading sequence – the influence is clearly seen when the maximum stress is reduced further. Typical scatter of fatigue data can be another factor for the low D value seen in specimen A6_2.

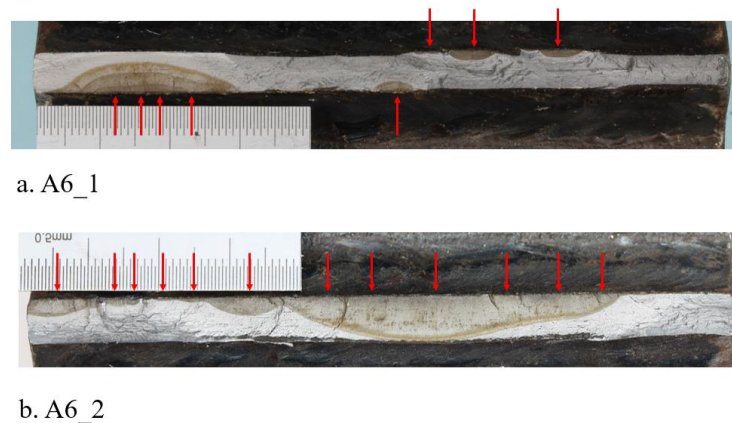


Figure 3.16 Fatigue crack initiation sites (indicated by red arrows) on the fracture surface: (a) specimen A6_1 and (b) specimen A6_2. The maximum stresses were 300 and 150MPa, respectively.

3.5 Results for ultrasonic impact treated specimens and discussion

3.5.1 Fatigue lives and Miner's sum

A total of four UIT specimens were tested under either Spectrum I or II. Specimen UIT_A12.5_1 was tested under axial loading. It was initially tested under Spectrum I with a constant maximum stress of 150MPa. After application of 10,567 blocks, there was still no indication of fatigue cracking. To speed up the test, the loading spectrum was changed to Spectrum II with the same maximum stress of 150MPa. However, after further 7,172 blocks, there was still no indication of fatigue cracking. Afterwards, the maximum stress of Spectrum II was increased to 276MPa. After another 2,731 blocks, the specimen failed from the gripping area. The post-test examination did not find any indication of cracking at the weld toes.

While specimen UIT_B12.5_1 was tested under bending loading under Spectrum I with an axial static stress 87.5MPa, specimen UIT_B12.5_2 was tested under Spectrum II, and the axial static stress was 0. The former failed from the edge of the hole for pin loading after 5,641 blocks and the latter was declared run-out after 2×10^7 cycles (90 days) without any indication of fatigue cracking at the weld toes. Specimen UIT_A25_1 was tested under Spectrum II under axial loading, with a constant maximum stress of 300MPa. The ratio of the maximum stress to yield strength of the material was 85%. According to BS 7608, no benefit of UIT can be claimed at such high stress. This specimen failed at the weld toe after 3,645 blocks.

The improvement of UIT depends on maximum stress, σ_{max} , and stress ratio, R , and the benefit decreases with increase in either. Therefore, the R for each stress range in the VA loading sequences involved in the fatigue tests were calculated. Afterwards, the fatigue strength for UIT treated specimen at each stress level was calculated by modifying the S-N curve for untreated welds, in accordance with the guidance given in BS 7608 (Table 2.2).

After doing this, both the predicted fatigue lives and the Miner's sums for the UIT specimens under the VA loading sequences were estimated, as shown in Tables 3.10 for axial loading and 3.11 for bending loading.

Table 3.10 Results of UIT specimens tested under axial loading.

Plate thickness (mm)	Specimen ID	Maximum stress (MPa)	Experimental results (blocks)		Predicted fatigue life (Blocks)	Miner's sum		Failure location
			CD sequence from Spectrum I	CD sequence from Spectrum II				
12.5	UIT_A12.5_1*	150	10,567	-	1,711	6.18	>12.58	Gripping region
		150	-	7,179	1,956	3.61		
		276	-	2,731	978	2.79		
25	UIT_A25_1	300	-	3,645	392	9.29		Weld toe

Note: *: The specimen ran out and the loading condition was changed twice, and the Miner's sum was calculated for all three loading conditions, respectively.

For UIT specimens tested under axial loading, it can be seen from Table 3.10 that:

For specimen UIT_A12.5_1 tested at the maximum stress 150MPa, the D values calculated under these two CD loading sequences are much greater than unity, being at 6.18 and 3.61, respectively. When the maximum stress is increased to 276MPa, which is about 78% of the SMYS of the material (355MPa), the D is about 2.8. This test resulted in a total of Miner's sum 12.58.

For specimen UIT_A25_1, the maximum stress in the CD sequence is 300MPa, which is about 85% of the SMYS. According to BS 7608, it exceeds the upper limit of the maximum stress, which is $0.8\sigma_y$ (284MPa), to claim the benefit of UIT. Thus, the Miner's sum for this UIT specimen would be expected to be similar to that of the as-welded specimen tested under the CD sequence with the identical maximum stress, i.e., about 0.6 (Specimen A25_1). However, the Miner's sum of this specimen is significantly greater, about 9.3. This result indicates that the maximum stress limit specified, and the associated guidance given in BS 7608 are conservative.

Table 3.11 Results of UIT specimens tested under bending mode.

Plate thickness (mm)	Specimen ID	Axial static stress (MPa)	Experimental fatigue life (Blocks)	Bottom welds		Top welds		Failure location
				Predicted fatigue life (Blocks)	Miner's Sum, D	Predicted fatigue life (Blocks)	Miner's Sum, D	
12.5	UIT_B12.5_1	87.5	5,641	2,402	>2.35	10,635	>0.53	Gripping region
	UIT_B12.5_2	0	13,064	5,825	>2.24	34,761	>0.38	Runout

Table 3.11 summarises the results for the two tests under bending loading. It should be noted that under bending loading, the predicted fatigue life for the top weld experiencing CD sequence would be expected to be higher than that for the bottom weld experiencing CU sequence because the stress ratio for each stress level is lower. Both specimens did not fail from the welds. The Miner's sums for the bottom welds in these two specimens are both greater than 2 when the specimens failed either from the parent material (Specimen UIT_B12.5_1) or ran-out (Specimen UIT_B12.5_2).

Table 3.12 compares the Miner's sums between UIT treated and un-treated specimens which were tested under the same loading conditions (similar for specimen UIT12.5_1) in terms of

loading sequence, loading mode and maximum stress. It can be seen clearly that, in all four cases, the calculated Miner's sums for the UIT specimens are greater than their counterparts, especially for the two axial tests and the bending test at a higher minimum stress. The limited

Table 3.12 Comparison between the fatigue life of as-welded and UIT specimen

Loading mode	Maximum/Minimum stress ^b (MPa)	Specimen ID	UIT	Miner sum D
Axial	150	A12.5_2	no	1.18
	150 & 276 ^c	UIT12.5_1	yes	>12.58
	300	A25_1	no	0.61
		UIT A25_1	yes	9.25
Bending (only for the bottom welds) ^a	87.5	B12.5_1	no	0.88
		UIT B12.5_1	yes	>2.35
	0	B12.5_2	no	1.82
		UIT B12.5_2	yes	>2.24

Note: ^a: Top welds in the bending tests are not shown in the table for comparison since they all ran out. ^b: Maximum stress for axial loading (CD sequence) and minimum stress for bending (CU sequence). ^c: the maximum stress was increased from 150 to 276MPa during the test.

test results obtained under the specific loading spectra suggest that the recommendation given in BS 7608 on fatigue life improvement by UIT is on the conservative side.

No particular conclusion can be drawn from the results obtained from the top welds because the specimens failed at other locations.

3.5.2 Failure locations of the ultrasonic impact treated specimens

Of the three failed UIT specimens, specimen UIT_A25_1 failed at the weld toe, and specimens UIT_A12.5_1 and UIT_B12.5_1 failed from the parent metal, either at the gripping region or at the edge of the hole for pin loading, as shown in Figure 3.17. It should be noted that no fatigue failure occurred in these regions for the untreated specimens - they all occurred at the weld toe. This suggests that due to the UIT, the fatigue strength of the weld toe has been improved to such an extent that the fatigue life of the welded joints may no longer be governed by the welded toe but by other locations with stress concentration.

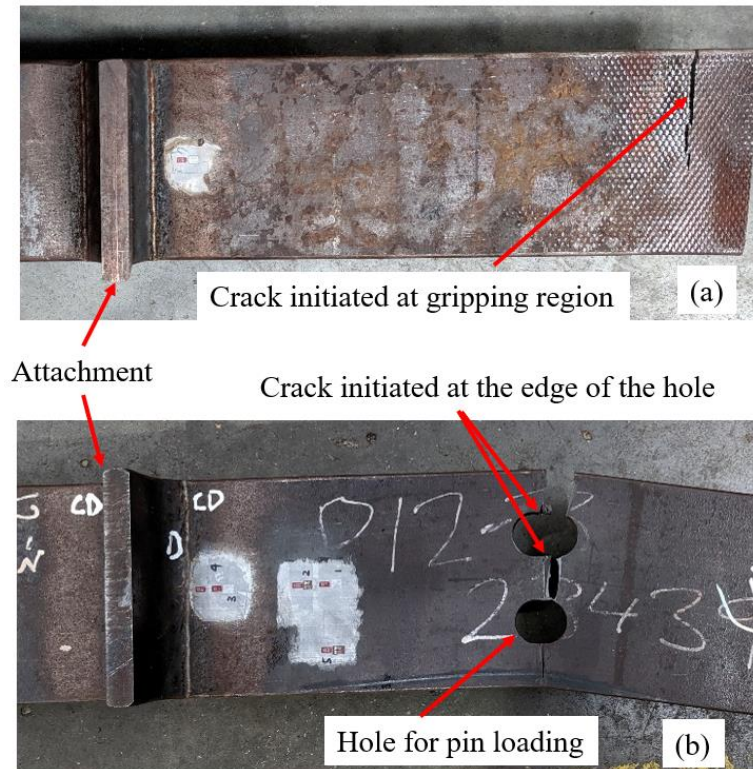


Figure 3.17 UIT specimens failing from the parent material. (a) from the gripping region (UIT_A12.5_1) and (b) from the hole for pin loading (UIT_B12.5_1).

3.5.3 Comparison of fracture surfaces between as-welded and ultrasonic impact treated specimens

The fracture surface of the specimen UIT_A25_1 was examined, as shown in Figure 3.18. The fracture surface of the as-welded specimen A25_1, which was tested under the same CD sequence, is included for comparison. It can be seen that the as-welded specimen exhibits multiple crack initiations (Figure 3.18 a) and a shallow crack shape. On the other hand, for the UIT specimen, fatigue cracking initiated at only two discrete locations (Figure 3.18 b) and exhibit almost a circle shape. This suggests that the UIT significantly reduces the number of crack initiation sites, and the fatigue life is dominated by crack initiation and growth of a single crack, rather than crack coalescence as seen in the as-welded joint.

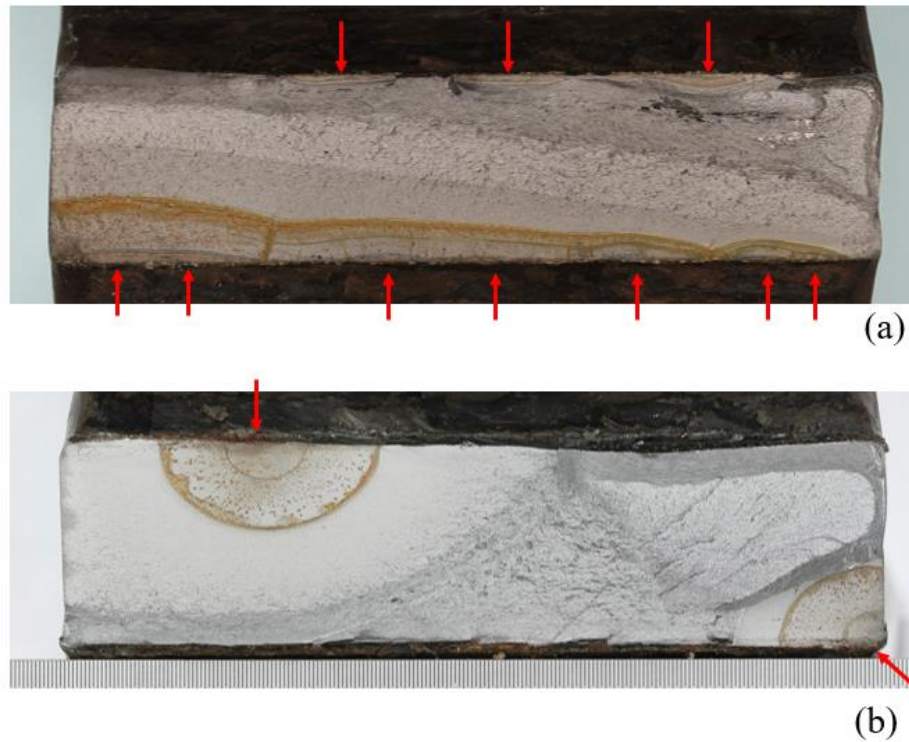


Figure 3.18 Comparison of the fracture surfaces between the as-welded and UIT specimens: (a) as-welded specimen (A25_1) and (b) UIT specimen (UIT_A25_1). (arrows indicate the crack initiation site.)

3.6 Conclusions

VA fatigue tests were carried out on three plate thickness specimens containing transverse non-load-carrying fillet welded attachments. The tests were performed under two VA loading spectra with various sequences, under either axial or bending loading mode. In addition to as-welded joints, those improved using UIT technique were also tested. Based on the test results, the effects of mean stress and the type of the VA loading sequence on the fatigue performance of welded joints were investigated. Also, the effects of plate thickness and UIT treatment were discussed. The following conclusions can be drawn:

- Similar to the results reported for the longitudinal fillet welds, the fatigue life of the transverse fillet welds is significantly degraded under a CD loading sequence with a high constant maximum stress, with the Miner's sum D being around 0.5.
- However, D value is found to depend on the maximum stress applied in the CD loading sequence. When it is reduced below a certain level, between 87.5-150MPa, the D value increases with decreasing maximum stress. When the maximum stress is reduced to

zero, the welds either run-out or the D values are significantly greater than 1.0. Therefore, it would be unduly conservative to limit D to 0.5, as advised in BS 7608 for a loading spectrum with an almost constant maximum tensile stress level.

- The D value at fatigue failure under CU loading sequences maybe also less than unity, and it depends on the minimum stress applied – it increases significantly when decreasing the minimum stress level.
- A CU sequence can produce more damage than a CD sequence when the applied static stress is either zero (the minimum stress in the former equal to the maximum stress in the latter) or low in tension. Similar to the CD loading sequence, the fatigue life of a specimen tested under CU loading sequence also depends on the mean stress applied – longer under lower mean stress.
- Although not conclusive, the test results appear to indicate a general trend that the fatigue performance of thinner specimens is better than that of thicker ones under VA loading sequences, even under an axial loading, which is similar to the results reported for CA loading. And the change of maximum stress applied in the CD loading sequence has a greater impact on the fatigue lives of the thinner specimens.
- The welded joints with transverse fillet welded attachments are more sensitive to the maximum stress applied in the CD loading sequence than those with the longitudinal attachments.
- UIT significantly improves the fatigue life of the welded plates under VA loading. The extent of the improvement depends on the maximum stress applied under CD loading sequence. UIT can improve the fatigue performance even when the maximum stress in the CD sequence exceeded 80% of the SMYS of the material.
- The number of crack initiation sites are reduced after UIT, and the fatigue life of welded joints is dominated by both crack initiation and growth of a single crack, rather than crack coalescence as seen in the as-welded joints.

Chapter 4 Residual stress measurements

4.1 Introduction

As reported in the last chapter, the possible reason for the increase of D with a decreasing maximum stress in the CD loading sequence could be related to the low level of residual stress in the specimen tested in the present study. To be certain, and to investigate any residual stress relaxation during fatigue loading, residual stress in the direction perpendicular to the weld toe were measured in both as-welded and UIT specimens using either the X-ray diffraction (XRD) or Centre-hole drilling (CHD) method.

In total, three sets of residual stress measurement were carried out, as summarised in Table 4.1. For Set 1, only the initial residual stress in the as-welded specimens were measured using the XRD method. Sets 2 and 3 were measured both before and after fatigue loading using the CHD and XRD methods.

This chapter gives details of the residual stress measurements, including measurement locations and the corresponding results. Based on the outcome, the effect of residual stress on the fatigue life of the specimens is discussed to better understand the fatigue behaviour of welded joints under VA loading.

Table 4.1 Details on residual stress measurements.

Set ID	Specimen	Measurement method	Conditions where residual stress was measured	
			Initial residual stress	Residual stress after fatigue loading
1	As-welded	XRD	√	-
2		CHD	√	√
3	UIT	XRD	√	√

4.2 Residual stress measurements on the as-welded specimens using the X-ray diffraction method

4.2.1 Specimen

A total of eight as-welded specimens were measured using the XRD method, of which one was 6mm-thick, four were 12.5mm-thick and three 25mm-thick. The numbering system composes of four parts: 'XRD _ AW _ thickness _ series number'. AW represents as-welded, and the 'series number' is the same as that defined in the last chapter.

4.2.2 Locations of measurement

Locations of residual stress measurement were mapped in a 'T-shape' at each weld, as shown in Figure 4.1. A total of seven points, 15mm apart, were arranged along the y-direction (parallel to the weld), at a distance (X_0) between 1 to 4mm to the weld toe. The value of X_0 was increased with decreasing plate thickness because of the shorter leg length of the fillet weld in thin specimens. This is to prevent the probe being too close to the weld toe as the attachment interferes with the probe. The value of X_0 was also slightly adjusted at each weld in order to avoid the welding spatter on the plate surface. The point located on the transverse centreline was referred to P_0 .

A total of six points were arranged along the transverse centreline (mid-width of the plates). The distance between two adjacent points increased from 2 to 15mm in steps as the points being further away from the weld toe. Additional points were measured at some welds in the 12.5mm-thick specimens. On the other hand, measurements were carried out only at the locations along the weld toe (y-direction) at some welds in order to manage the total measurements. A summary of the locations of measurement in each weld is given in Appendix D Table D.1.

4.2.3 Measurement facilities

Residual stress measurements by the XRD were performed using an Xstress Robot facility (Stresstech, version 1.7.0) at Coventry University, shown in Figure 4.2. The collimator diameter and the radius of the arc are 0.5mm and 50mm, respectively.

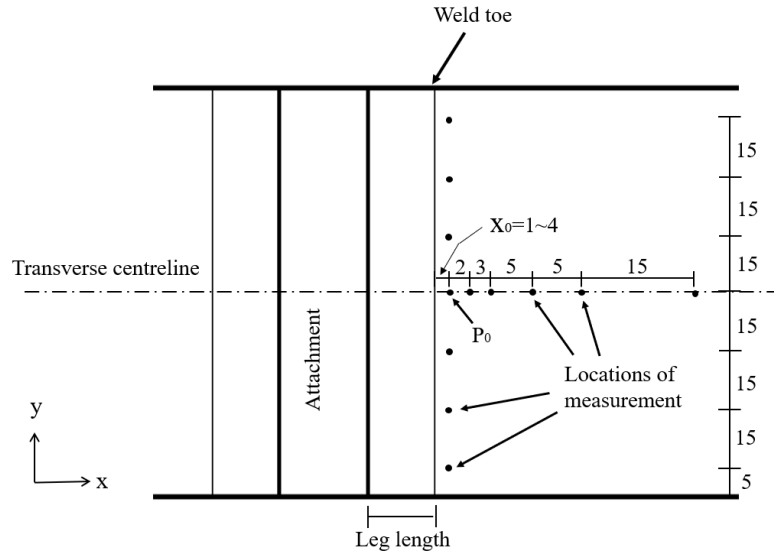


Figure 4.1 Locations where residual stresses were measured in as-welded specimens using the XRD method (in mm).

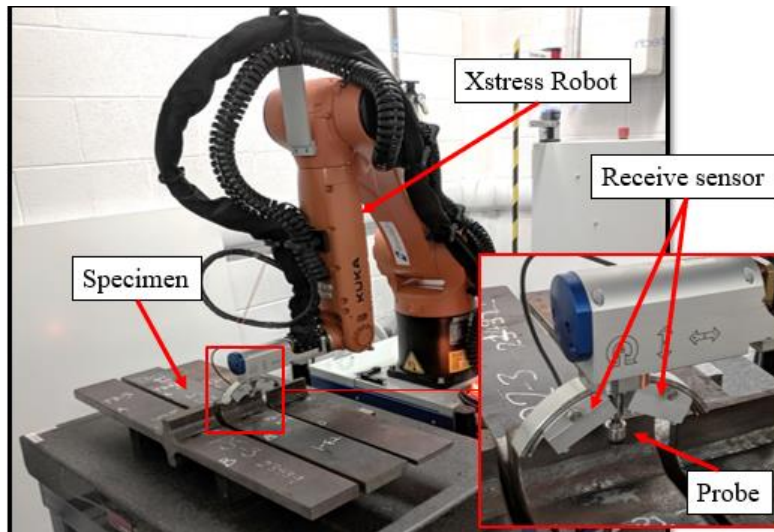


Figure 4.2 X-ray diffraction robot.

4.2.4 Measurement results

Results of the residual stress measurement along the weld toe for all three thicknesses specimen are plotted in Figure 4.3. Since the highest tensile residual stresses are expected near the transverse centreline of fillet transverse welds [28], the results from point P_0 are of the most concerns. However, the large scatter of the measured data shows residual stress varying between -80 and -20 MPa in 6mm-thick specimens, -350 and 110MPa in 12.5mm-thick

specimens and -450 and 150MPa in 25mm-thick specimens, with most of the results being compressive.

Results obtained at other positions are similar – large scatters and compressive. It is concluded that the results obtained by XRD cannot determine reasonably the initial residual stress for samples of all thicknesses. Similar inconclusive outcomes by XRD are also reported in [66].

Therefore, these results suggest that the residual stress distribution exhibits a large scatter in all samples, and no general trend can be concluded.

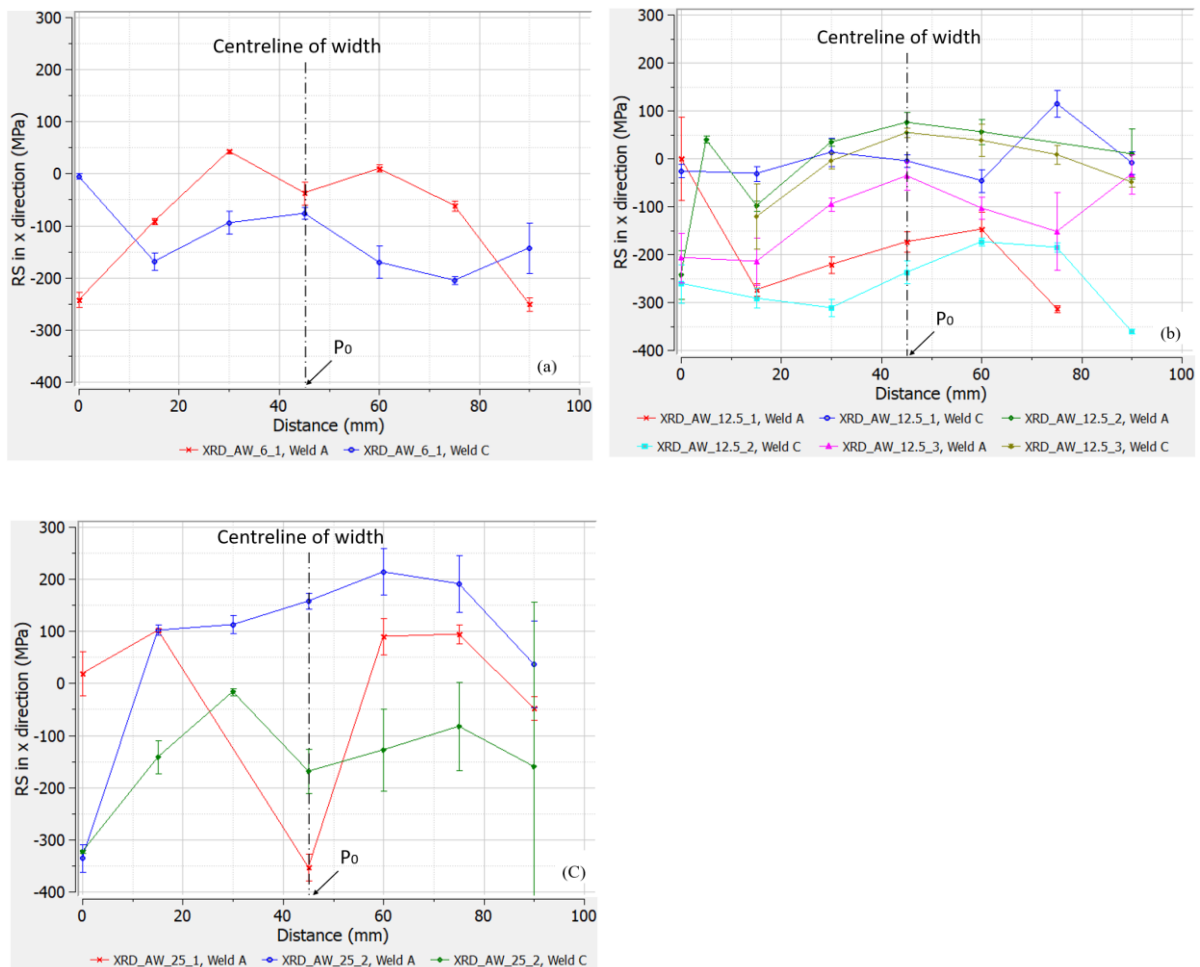


Figure 4.3 Residual stress distribution along the weld toe: (a) 6mm-thick specimen; (b) 12.5mm-thick specimen; (c) 25mm-thick specimen.

Residual stress distributions along the transverse centreline are plotted in Fatigue 4.4. It can be seen that the residual stress distributions in the x-direction at different weld toes also exhibit a

large scatter, and a general trend cannot be identified. No conclusion can be drawn from these results.

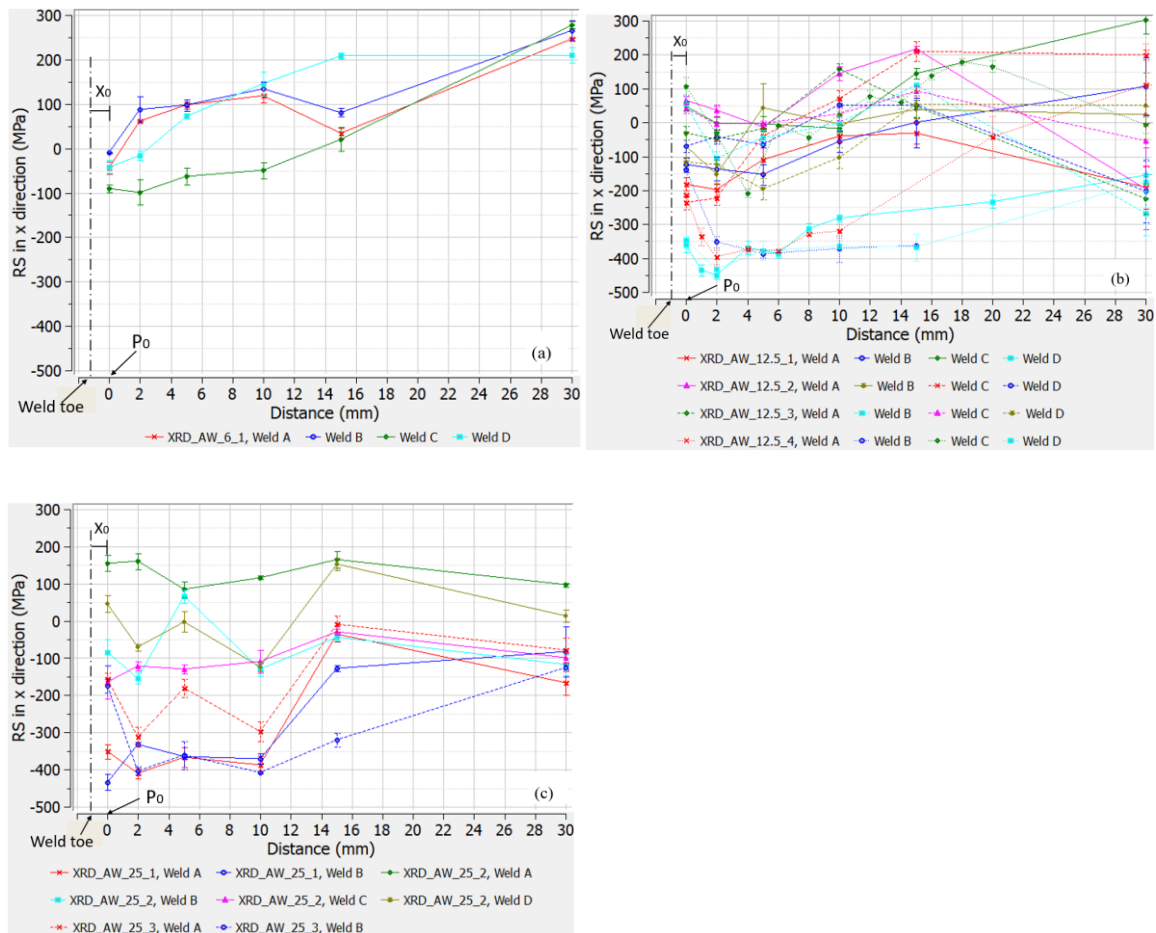


Figure 4.4 Residual stress distribution along the transverse centreline: (a) 6mm-thick specimen; (b) 12.5mm-thick specimen; (c) 25mm-thick specimen.

As mentioned in the literature, for this kind of welded joint the residual stress presented at the weld was reported to be ranged between 20% to 60% [61,62,64–66] of the yield stress of the material. However, only the results measured from few points can achieve such level. In addition, the measurement results obtained from 25mm-thick specimen are much lower than the value advised in standard BS7910 [30] and R6 [57] where the residual stress is assumed to be equal to the yield stress of the material, i.e. 355MPa.

The large scatter of results may be attributed to the poor condition of the plate surfaces as the penetration depth of the X-ray beam is just a few microns [180,181]. In this case, the residual stress obtained using XRD cannot be regarded as being reliable. Further measurements were thus performed using the CHD method.

4.3 Residual stress measurements on the as-welded specimens using the Centre-hole drilling method

4.3.1 Specimen

A total of three specimens, one from each plate thickness, were randomly selected from those having been measured using the XRD method. The numbering system is composed of two parts: ‘CHD_ thickness’, as presented in Table 4.2. The specimen number used in the previous XRD measurement is also included.

Table 4.2 Specimen ID for the residual stress measurements using the CHD method.

Plate thickness (mm)	Specimen ID	Specimen ID used in the previous XRD measurement
6	CHD_6	XRD_6_1
12.5	CHD_12.5	XRD_12.5_2
25	CHD_25	XRD_25_2

4.3.2 Measurement conditions

Residual stress measurement was conducted on each specimen in the as-welded conditions initially. Afterwards, in order to study the residual stress relaxation under the VA loading, the 25mm- and 12.5mm-thick specimens were put into the fatigue testing machine and fatigue loaded under CA loading. The CA loading stress range was identical to the maximum stress range in the VA loading spectrum used, being at 250MPa.

The fatigue tests were also performed under both axial and bending loading. For the tests under axial loading, the specimen was cyclically loaded between stresses from -100 to +150MPa, representing the maximum stress range in the CD loading sequence with a maximum stress of 150MPa. The axial static stress was zero for the specimens under bending loading, so the top welds experienced cyclic compression while the bottom welds experienced cyclic tension.

For the 25mm-thick specimen, three residual stress measurements were carried out: one in the as-welded condition, one after two cycles, and the third one after 100 cycles, both under bending loading. Three residual stress measurements were performed for the 12.5 mm-thick specimen: as-welded condition, after two cycles under axial loading (from 150MPa to -

100MPa), additional two cycles under bending loading. For 6mm-thick specimen, residual stress was measured in the as-welded condition only.

4.3.3 Locations of measurement

All residual stress measurements were made at the locations 10mm from the transverse centreline and 3mm to the weld toe, shown in Figure 4.5. It is assumed that, for each specimen and under the same loading conditions, the residual stress distributions near each weld are similar; therefore, the magnitude of residual stress at the specified locations (a total of eight locations) should be similar. In this case, to determine the residual stress corresponding to as-welded and after any other loading conditions, two residual stress measurements were made at the two opposite locations, e.g. A1 and C1. The average value was used in further analysis.

4.3.4 Measurement facilities

Measurements were performed in TWI's Fatigue Laboratory, in accordance with ASTM E837 [80]. One Vishay CEA-06-062UM-120 type Centre-hole rosette strain gauge was used in each measurement. A hole of 1.9mm diameter was drilled to approximately 2mm in depth each time using the abrasive technique. Figure 4.6 shows the set-up of the CHD measurement used.

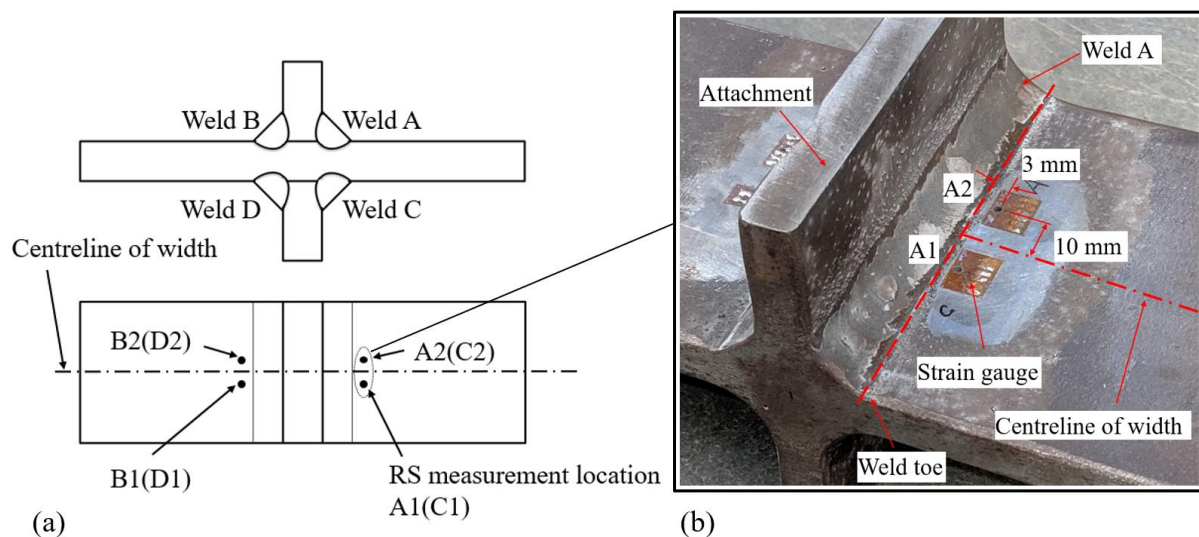


Figure 4.5 Locations where residual stresses were measured on the as-welded specimen: (a) schematic. letters in brackets refer to the measurement locations on the opposite side of the plate; (b) one actual test specimen.

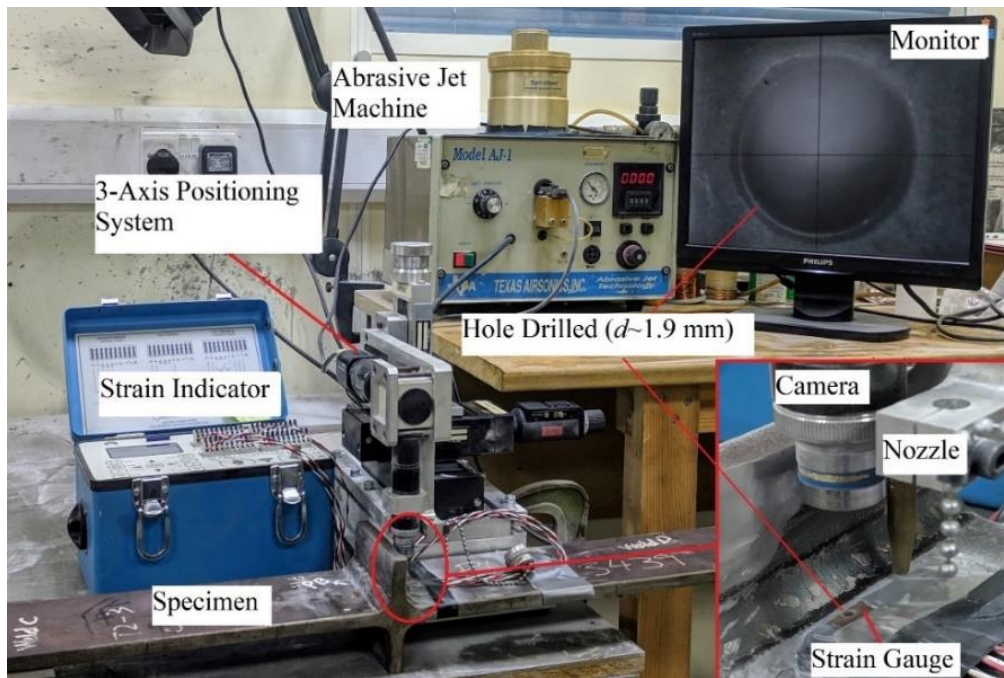


Figure 4.6 Centre-hole drilling method for residual stress measurement.

4.3.5 Measurement results

The residual stress values measured in the x-direction (normal to the welds) are given in Table 4.3. The results confirm the presence of high tensile residual stress near the weld toe where fatigue cracking occurred. The implications of the measurement results and plate thickness effects are discussed in the following two sub-sections.

Table 4.3 Residual stress (RS) measurement results.

Specimen ID	As welded		Axial loading (-100MPa~+150MPa)		Bending loading (top weld: 0 ~ -250MPa, bottom weld: 0 ~ +250MPa)			
			2 CA cycles		2 CA cycles		100 CA cycles	
	Location	RS (MPa)	Location	RS (MPa)	Location	RS (MPa)	Location	RS (MPa)
CHD_25	A1	252	-	-	B1 (top)	183	B2 (top)	161
	C1	213	-	-	D1 (bottom)	166	D2 (bottom)	150
CHD_12.5	A1	128	A2	108	B1 (top)	97	-	-
	C1	116	C2	87	D1 (bottom)	85	-	-
CHD_6	A1	82	-					
	C1	7						
	A2	84						

4.3.5.1 Initial residual stress

The measurement results of the initial residual stress in each plate thickness are plotted in Figure 4.7. The averages of two measurements in the 25mm- and 12.5mm-thick specimen are 230 and 122MPa, respectively. For the 6mm-thick specimen, a significant difference is observed in the two measurements (82MPa from location A1 and 7MPa from location C1). Therefore, one more measurement was carried out at location A2 (Figure 4.5b), and the result is 84MPa, which agrees well with that obtained at location A1. Therefore, the average residual stress in the 6mm-thick specimen is taken as 83MPa. The measurement of 7MPa is regarded as scatter, and the reason is unclear.

Measured results indicate that the average residual stress in specimens of the present study are only about 2/3, 1/3 and a quarter of the SMYS of the material for the 25mm-, 12.5mm- and 6mm-thick specimens, respectively. Additionally, it can be seen from Figure 4.7 that the initial residual stress relates to the plate thickness in a proportional relationship approximately.

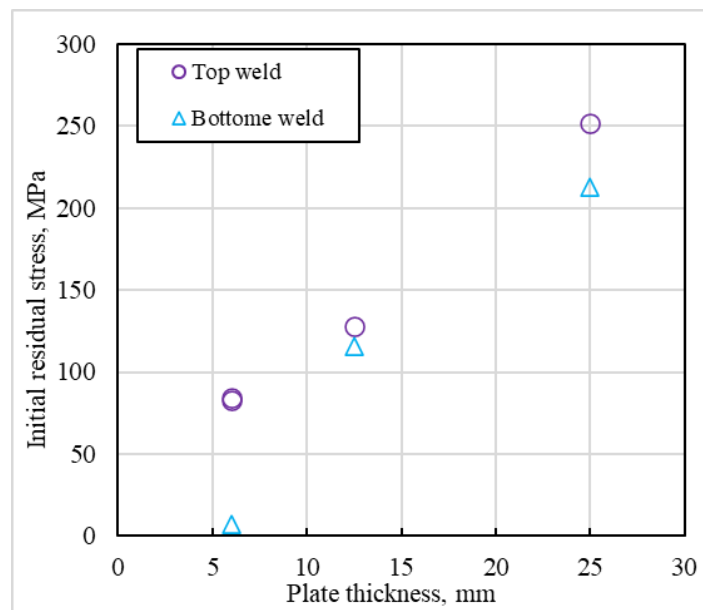


Figure 4.7 Results of residual stress measurements in different plate thicknesses.

4.3.5.2 Residual stress relaxation

The measurement results after fatigue loading are plotted in Figure 4.8, where relaxation of residual stress is observed in both 25mm- and 12.5mm-thick specimens.

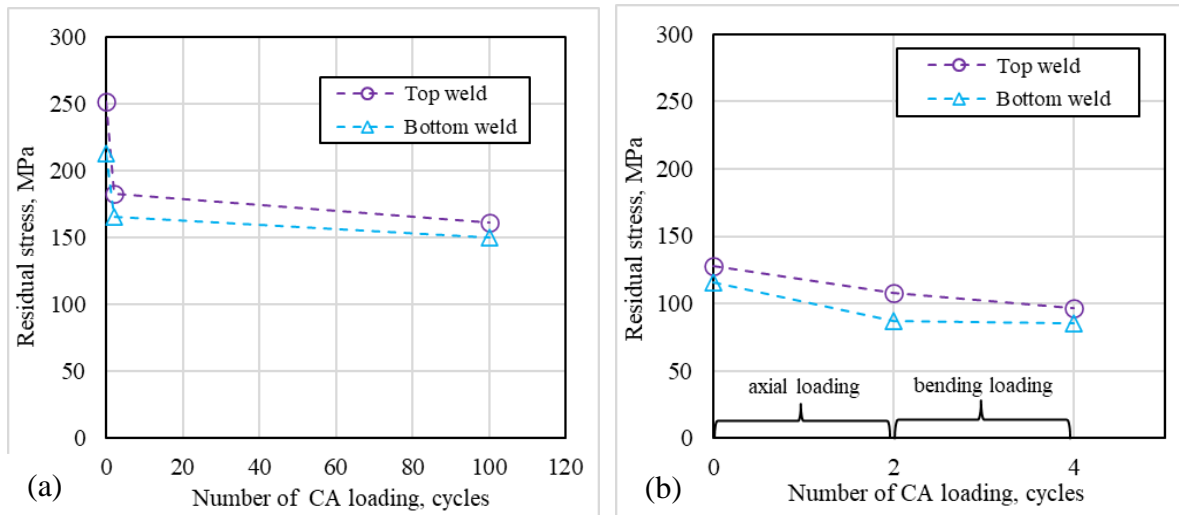


Figure 4.8 Relaxation of residual stress after fatigue loading: (a) 25mm-thick specimen; (b) 12.5mm-thick specimen.

It can be seen the relaxation of residual stress occurred during cyclic loading in the 25mm-thick specimen. The residual stress in both top and bottom welds is reduced significantly after two CA loading cycles of bending loading, with the average residual stress decreased from the original 233MPa to 175MPa (about 25% reduction). However, after another 100 CA loading cycles, the average residual stress relaxed only modestly to 156MPa (about a further 10%). For the 12.5mm-thick specimen, about 80% of the initial residual stress remained after two CA axial loading cycles. Under two further bending loading cycles, the residual stress in both the top and bottom welds is only reduced slightly.

These results indicate that residual stress relaxation mainly takes place in the first two cycles. Further cyclic loading only results in moderate reduction. Additionally, compressive loading can produce similar residual stress relaxation to tensile loading does. However, this is based on limited test data, and further work is required to confirm this observation.

4.4 Residual stress measurements on the ultrasonic impact treated specimens using the X-ray diffraction method

4.4.1 Specimen

A total of three 12.5mm-thick UIT specimens were measured using the XRD method. The numbering system is composed of three parts 'XRD UIT_ series number'.

The specimen XRD UIT_1 was measured before fatigue testing to study the initial residual stress after UIT. The residual stress presented at weld B and D were measured.

Specimen XRD UIT_2 and XRD UIT_3 had been tested under VA loading and failed in the parent metal region. The specimen numbers used in the fatigue testing were UIT_B12.5_1 and UIT_A12.5_1, respectively. Specimen XRD UIT_2 was tested under bending loading with an axial static stress of 87.5MPa. In this specimen, two welds were measured: weld A, the top weld experiencing CD loading, and weld C, the bottom weld experiencing CU loading. Since the maximum stress range in the VA loading was 250MPa, the minimum stress applied on the weld A was -162.5MPa (=87.5-250) and the maximum stress applied on the weld C was 337.5MPa (=87.5+250).

Specimen XRD UIT_3 had been tested under axial loading fatigue with the minimum and maximum stresses applied were -100 and 276MPa (see Table 3.10), respectively. The residual stress presented at weld A was measured.

Detailed information on the measurements is summarised in Table 4.4.

Table 4.4 Residual stress measurements on UIT specimens using the XRD method.

Specimen number	The number used in the previous fatigue test	Welds ID	Condition of the weld (loading mode and min/max stress had been applied)
XRD UIT_1	-	Weld B	Untested
		Weld D	
XRD UIT_2	UIT_B12.5_1	Weld A (top weld)	Bending, +87.5 ~ +337.5MPa
		Weld C (Bottom weld)	Bending, -162.5 ~ +87.5MPa
XRD UIT_3	UIT_A12.5_1	Weld A	Axial, -100 ~ +276MPa

4.4.2 Locations of measurement

Residual stress were measured at six points for each weld, as shown in Figure 4.9. Points P1 to P3, 10mm apart, were at the bottom of the groove introduced by UIT, while points P4 to P6 are 3mm further away from P1 to P3, respectively.

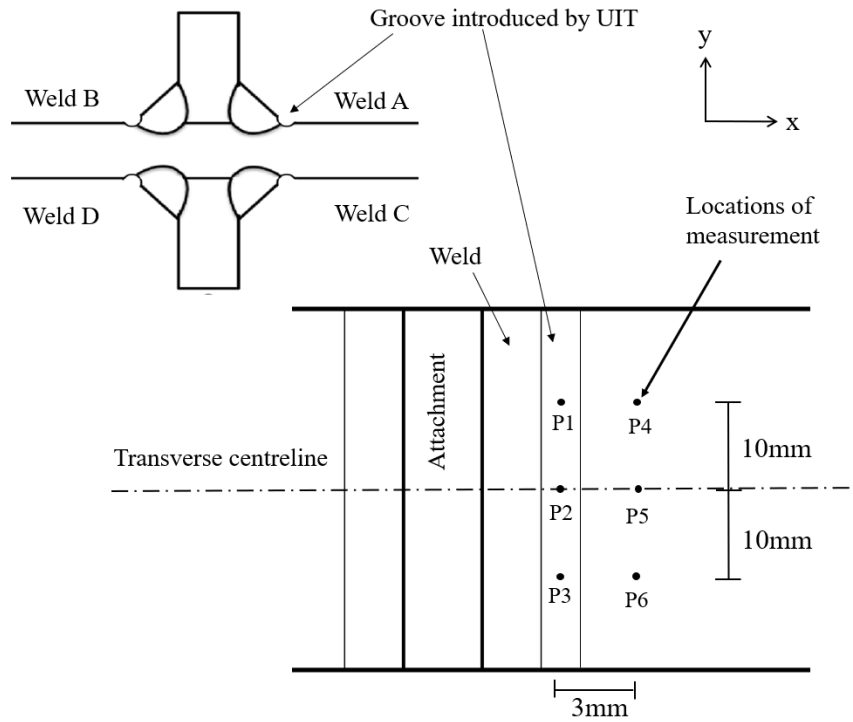


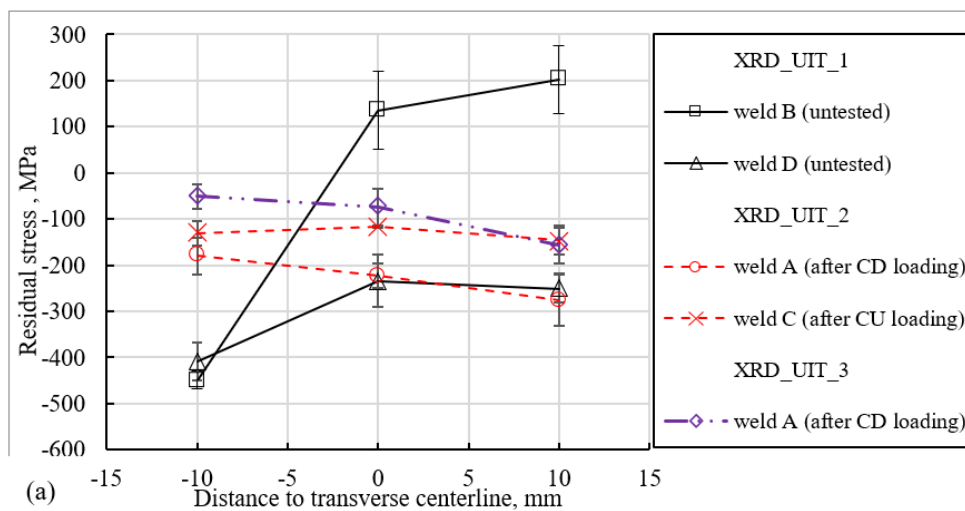
Figure 4.9 Locations where residual stresses were measured on the UIT treated specimen.

4.4.3 Measurement facilities

The measurements were also conducted at Coventry University using the XRD facility, as described in Section 4.2.3.

4.4.4 Measurement results

The residual stress measurements results are plotted in Figure 4.10, and detailed data is given in Appendix D Table D.2.



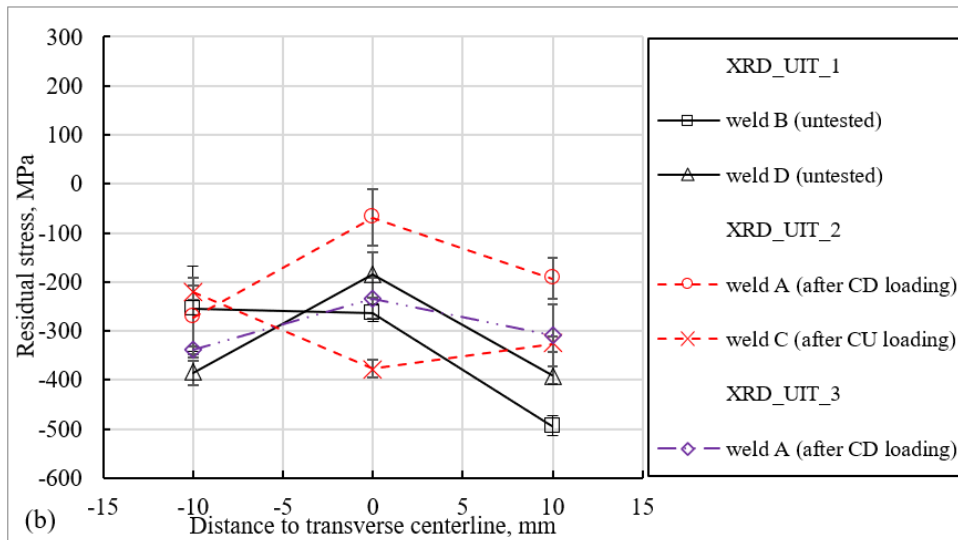


Figure 4.10 Residual stress distribution along the weld toe: (a) results obtained at groove; (b) 3mm away from the groove.

Based on the results obtained at P1 to P3 in all three specimens, as shown in Figure 4.10 (a), the following can be seen:

- For the untested specimen, XRD_UIT_1, results at welds B and D exhibit a large scatter with the data obtained from P2 ranging between -220 and 120MPa. Thus, a reasonable initial residual stress after UIT cannot be determined. A similar large scatter is also reported in [96] where the residual stress measured from different points located at the bottom of the groove ranges between -509 and -44 MPa.
- Some of the compressive measured is higher than the yield stress of the material. This is because UIT can plastically deforming the material, leading to an increase in the number of dislocations. In this case, the material is strengthened; therefore, the compressive can be higher than the yield stress of the material.
- In specimen XRD_UIT_2 subjected to bending loading, measured residual stress at either weld A or weld C are all compressive. And for either weld A or C, all residual stress at P1 to P3 are almost constant, with an average value about -210 and -120MPa, respectively.
- In specimen XRD_UIT_3 subjected to axial loading, results obtained from the three points are similar, being all compressive with an average value at about -100MPa.

From Figure 4.10 (b) for the results from points P4 to P6, it can be seen that:

- In specimen XRD_UIT_1, results exhibit less scatter than that from points P1 to P3. While the average residual stress at P5 is about -220MPa, the average values at P4 and P6 are about 100-200MPa lower (more compressive).
- In specimen XRD_UIT_2, measured residual stress at P4 and P6 do not vary significantly compared with the results obtained in untested specimens. However, result from point P5 increases to -90MPa in weld A, and reduces to about -400MPa at weld C.
- In specimen XRD_UIT_3, residual stress at each point is almost identical to that obtained in XRD_UIT_1, suggesting there is no residual stress relaxation during the fatigue loading.

Based on the measured results, it is difficult to determine a reasonable estimation of residual stress after the UIT. However, a certain amount of compressive residual stress can be confirmed to be remained at the weld toe after fatigue loading, suggesting that not all the compressive residual stresses was relaxed after fatigue testing. In this case, it is not surprising that the fatigue lives of these treated welds were enhanced significantly, as reported in Chapter 3.

In addition, except the measurement results obtained at groove of weld B, all the other residual stress profiles were all compressive. This may be because these profiles measured were only for the residual stress presented on the surface of the area at or close to the weld toe. There must be balancing stresses which are in tensile at other region near the area measured.

4.5 Discussion

4.5.1 The magnitude of residual stress in as-welded welds

The initial residual stress in the welded specimens of each plate thickness was measured using both the XRD and CHD methods. In comparison with the results obtained by the XRD method, CHD measurements are of much less scatter and show tensile stresses, which is in line with the expectation that high tensile residual stresses near the transverse centreline [54]. CHD measured residual stress of 122MPa in 12.5mm-thick specimens is in better agreement with another study

[61], compared with neutron diffraction measurement of 150MPa. Therefore, residual stress obtained using the CHD method is adopted in further analysis.

4.5.2 Effect of residual stress on the fatigue life of welded joints under variable amplitude loading

In Chapter 3, it is concluded that low residual stress may be the main reason for the increase of D when the maximum stress in the CD sequences decreases. Based on the measured residual stress described in this chapter, the effect of residual stress on fatigue life can be discussed quantitatively. For example, in the 12.5mm-thick specimen, the residual stress after cyclic loading is about 97MPa. When the maximum stress in the CD sequences is 150MPa (specimen A12.5_2) and 87.5MP (specimen A12.5_3), the actual maximum stress or the combination of the maximum applied stress and the residual stress, is about 247 and 185MPa, respectively. Therefore, the CD sequence with a low maximum stress would lead to a better fatigue life due to the low value of the actual maximum stress. It is thus not surprising to find the Miner's sum D value is increased.

Chapter 3 also reported that the D values obtained under some CD sequences with low maximum stresses are higher than unity when fatigue failure occurs. The D value estimated under these CD sequences may be overestimated. For instance, D was calculated using the S-N curves produced based on CA tests with a constant maximum stress at 300MPa in axial loading and 330MPa in bending loading [178]. Since the actual maximum stress cannot exceed the SMYS of the material [6,28] which is 355MPa, it is reasonable to assume the actual maximum stresses in all the CA tests were equal to 355MPa after taking residual stress into consideration. However, when the maximum stress in the CD sequences is below a certain level, the actual stress may be less than 355MPa, the fatigue damage will be smaller than that caused by the same stress range with an actual maximum stress of 355MPa. In this case, the fatigue life could be underestimated accordingly using the prementioned S-N curves, resulting in a higher D value.

It is also reported that in the bending mode, all fatigue failures took place in bottom welds experiencing CU loading sequences, instead of top welds experiencing CD loading sequences. This result conflicts with the expectation that a CD sequence causes more damages. Based on the residual stress measurement result, it can be explained by the low residual stress. For

example, in specimen B12.5_2 where the static axial stress is 0 and the residual stress is about 97MPa. The actual minimum stress for both CU and CD sequences are equal to 97MPa. Thus, the actual mean stress for a particular stress range in the CD sequence is lower than that for the same stress range in the CU sequence, resulting in better fatigue life.

Unlike in a CD sequence, the actual maximum stress of each stress rang in a CU sequence is not constant. For a particular stress range, the actual maximum stress is determined by three parts: the stress range itself, the minimum stress in the CU sequence and the residual stress. As the last two are constant, the actual maximum stress depends on the stress range – the higher the stress range, the larger the actual maximum stress.

Another character of a CU sequence is that only the actual maximum stress of the largest stress range in the spectrum can reach the SMYS of the material. Those of small stress ranges are always lower than the SMYS because of the relaxation of the residual stress under the peak stress. In this case, in addition to the retardation effect of a CU loading sequence, the overestimation of the mean stress for small stress ranges should be another reason accounting for $D > 1$ at failure.

Based on the discussion, it suggests that under either CD or CU loading sequences, the mean stress can significantly influence the fatigue endurance of the fillet welds tested in the present study because of the low residual stress. In this case, the accuracy of the fatigue life assessment may be improved by considering the effect of the mean stress.

4.5.3 Stress ratio correction advised in IIW

Fatigue standards/codes assume a high constant effective stress ratio, R_{eff} conservatively, based on consideration of both applied stress and residual stress. However, if $R_{eff} < 0.5$, a fatigue enhancement factor $f(R_{eff})$ may be considered by multiplying the fatigue class of classified details by $f(R_{eff})$. This factor depends on the level of residual stress. IIW [32] advises the following to estimate the enhancement factor $f(R_{eff})$:

$$f(R_{eff}) = \begin{cases} 1.3 & R_{eff} < -1 \text{ or fully compressive} \\ -0.4R_{eff} + 0.9 & -1 \leq R_{eff} \leq -0.25 \\ 1 & R_{eff} > -0.25 \end{cases} \quad (4.1)$$

R_{eff} was calculated for each stress range in a CD loading sequence with low maximum stresses. And the corresponding test results were corrected based on this criterion.

After fatigue loading, the magnitude of residual stress is around 80 to 100MPa in the 6mm- and 12.5mm-thick specimens, and about 150MPa in the 25mm-thick specimen. When the applied maximum stress was decreased from 300 to 150MPa, the minimum R_{eff} in the CD sequence (i.e., R_{eff} corresponding to the maximum stress range of 250MPa) is about -0.08 for the 6mm- and 12.5mm-thick specimens, and 0.17 for the 25mm-thick specimen, all bigger than -0.25. Therefore, there should be no enhancement in fatigue life according to the criteria. However, as observed in tests, although the fatigue lives of the 6mm- and 25mm-thick specimens are not improved, that for the 12.5mm-thick specimen is more than doubled.

When the applied maximum stress in the CD sequence was reduced to 87.5MPa, R_{eff} is less than -0.25 for those stress ranges which are greater than 212.5MPa. It should be noted that these stress ranges only contribute up to 1.5% of the total fatigue damage caused by the sequence (Figure 3.5). Hence, the enhancement in the total fatigue life is still negligible. However, test results show the opposite: a significant improvement in the fatigue life is observed. The circumstance is similar when the maximum stress was reduced to 0.

Therefore, the results obtained in the present study could not be well corrected using the R_{eff} correction method provided in IIW. A new mean stress correction model has been developed and will be introduced in the next Chapter.

4.6 Conclusions

Residual stress measurements were carried out on specimens of all three plate thicknesses using either the CHD or XRD method. The residual stress presented in both as-welded and UIT specimen were measured either before or after fatigue loading. Based on the measurement results, the following conclusions can be drawn:

- For both as-welded and UIT specimens, the magnitude of residual stress before or after cyclic loading cannot be appropriately determined using the XRD method, as the measurement results exhibit a large scatter.

- Residual stress measurement obtained using the CHD method are more reliable than those by the XRD method, thus are used in further analysis.
- In each plate thickness tested, the initial residual stress is lower than the SMYS of the material and is related to the plate thickness in an approximately proportional relationship, with the average value in 6mm-, 12.5mm- and 25mm-thick specimens being at 83, 122 and 233MPa, respectively.
- Residual stress can be reduced by cyclic loading even when the maximum tensile stress is as low as 150MPa (less than half of the SMYS). The relaxation mainly occurs in the first two cycles, and further cyclic loading only leads to limited residual stress reduction.
- Compressive loading appears to produce similar residual stress relaxation as by tensile loading. However, this is based on limited test data. Further work is required to confirm this conclusion.

Chapter 5 Development of analytical models to predict the fatigue life of welded joints under variable amplitude loading spectra

5.1 Introduction

In fatigue design standards, fatigue performance of welded joints is assumed to be independent of the applied mean stress due to the high tensile residual stress in weld toes. However, fatigue test results obtained from the present study shows that the fatigue life increased significantly when the mean stress is below a certain value. This phenomenon can be well explained according to the residual measurements results. It is found that the initial average residual stress in specimens tested is no more than the 2/3 of the SMYS of the material (only a quarter for the 6mm-thick specimens); moreover, residual stress can be further decreased by 40% after only two loading cycles. Therefore, when the applied mean stress is reduced below a certain level, the actual mean stress decreases as well, leading to a better fatigue performance.

In order to improve the accuracy of fatigue assessment for the welded joints under VA loading sequences, the present study developed new analytical models based on the conventional mean stress corrections to consider the effect of the applied mean stress on the fatigue life of welded joints under VA loading spectra. In addition, the VA loading sequence effects are also included in the models by a new sequence factor. Fatigue lives of welded joints under VA loading sequences were estimated using the new models developed, showing a better prediction than that given by the existing models.

This chapter provides detailed information on the development of the new analytical models, including improvement to the conventional mean stress corrections and the procedure to produce new sequence factors for various types of VA loading sequences.

5.2 Development of analytical models

5.2.1 Conventional mean stress correction models

The new models were developed based on three conventional methods: Goodman [86], Gerber [87] and Morrow [88], due to the reason that most actual test data tends to fall between the Goodman and Gerber curves [182]. Although Goodman equation is widely used in the

industrial area, its accuracy appeared to be lower than that of the Morrow equation, which has a similar expression but uses a different material parameter in the equation [90].

As mentioned in the literature review, apart from the fatigue limit, these three equations also can correlate a given stress range, $\Delta\sigma$, with the mean stress, σ_m , to an equivalent fully reversed (i.e. $R = -1$) stress range, $\Delta\sigma_{R=-1}$, that can produce the same fatigue damage with the combination of $\Delta\sigma - \sigma_m$ [90], following:

$$\text{Goodman and Morrow:} \quad \frac{\Delta\sigma}{\Delta\sigma_{R=-1}} + \frac{\sigma_m}{\sigma_p} = 1 \quad (5.1)$$

$$\text{Gerber:} \quad \frac{\Delta\sigma}{\Delta\sigma_{R=-1}} + \left(\frac{\sigma_m}{\sigma_{UTS}}\right)^2 = 1 \quad (5.2)$$

where σ_p is the material parameter. For Goodman and Morrow equations, σ_{UTS} is the ultimate tensile strength, and σ_{tf} is the true fracture stress, respectively. σ_{tf} was estimated to be $(\sigma_{UTS} + 345\text{MPa})$ as its experimental value is unavailable [90].

Fatigue damages of the equivalent $\Delta\sigma_{R=-1}$ can be estimated using the S-N curve that is produced at $R = -1$, in conjunction with the Miner's rule. If the available S-N curve is produced with a non-zero mean stress ($R \neq -1$), Equation 5.1-5.2 can be further modified, as proposed in [183], to convert the given stress range to an equivalent stress range with the known mean stress where the S-N curve is produced, following:

$$\text{Goodman and Morrow:} \quad \Delta\sigma_R = \frac{1 - \left(\frac{\sigma_{R,m}}{\sigma_p}\right)}{1 - \left(\frac{\sigma_m}{\sigma_p}\right)} \Delta\sigma \quad (5.3)$$

$$\text{Gerber:} \quad \Delta\sigma_R = \frac{1 - \left(\frac{\sigma_{R,m}}{\sigma_{UTS}}\right)^2}{1 - \left(\frac{\sigma_m}{\sigma_{UTS}}\right)^2} \Delta\sigma \quad (5.4)$$

where $\Delta\sigma_R$ is the equivalent stress range at a stress ratio R where the S-N curve is produced, and $\sigma_{R,m}$ is its mean stress. The nomenclatures used herein are illustrated in Figure 5.1.

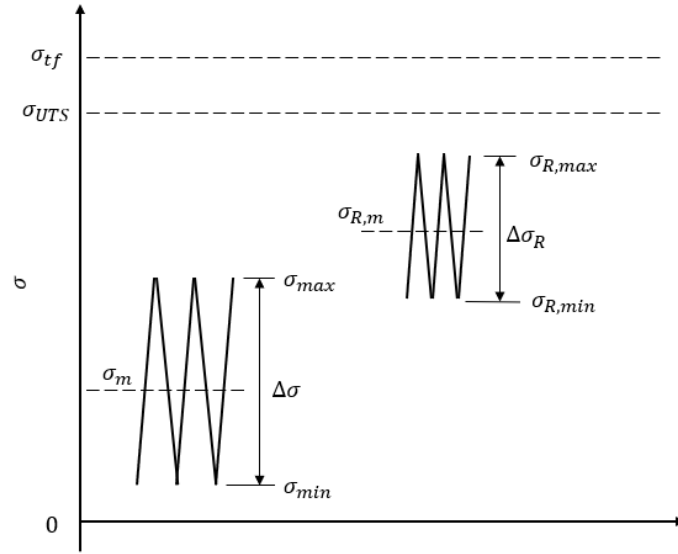


Figure 5.1 Nomenclatures used in the mean stress correction models.

5.2.2 Development on the conventional mean stress correction models

In all Goodman, Morrow and Gerber equations, the mean stress is used as the independent variable. In the present study, since all CA or VA data were obtained at constant maximum stresses, the reference maximum stress, $\sigma_{R,max}$, was proposed to replace $\sigma_{R,m}$. Therefore, Equation 5.3 and 5.4 was modified to use the maximum stress as an independent variable. Considering:

$$\sigma_m = \sigma_{max} - \frac{1}{2} \Delta\sigma$$

$$\sigma_{R,m} = \sigma_{R,max} - \frac{1}{2} \Delta\sigma_R \quad (5.5)$$

Inserting Equation 5.5 into 5.3 and 5.4, respectively, leads to new forms as:

Modified Goodman and Morrow:
$$\Delta\sigma_R = \frac{1 - \left(\frac{\sigma_{R,max} - \frac{1}{2} \Delta\sigma_R}{\sigma_p} \right)}{1 - \left(\frac{\sigma_{max} - \frac{1}{2} \Delta\sigma}{\sigma_p} \right)} \Delta\sigma \quad (5.6)$$

$$\text{Modified Gerber: } \Delta\sigma_R = \frac{1 - \left(\frac{\sigma_{R,max} - \frac{1}{2}\Delta\sigma_R}{\sigma_{UTS}}\right)^2}{1 - \left(\frac{\sigma_{max} - \frac{1}{2}\Delta\sigma}{\sigma_{UTS}}\right)^2} \Delta\sigma \quad (5.7)$$

It should be noted that modified models having been developed so far were for residual stress-free components. In welded joints, residual stress is generally present. Thus, the effective maximum stress, which is the combination of the applied maximum stress and the residual stress, is used to correlate the results obtained in the present study.

When each stress range in a certain VA loading sequence was correlated with the actual maximum stress, a new constant equivalent stress range, $\Delta\sigma'_{CA,equ}$, can be estimated according to Equation 3.4, whereby the fatigue life, N , was predicted using those known S-N curves:

$$N = \frac{C}{(\Delta\sigma'_{CA,equ})^m} \quad (5.8)$$

where C and m are material constants.

5.2.3 Variable amplitude loading sequence factor

In addition to the mean stress, the fatigue life of welded joints also depends on the type of VA loading sequence because fatigue crack propagation rate (FCGR) can be accelerated under the CD loading sequences, or retarded under the CU loading sequences [5,6,13]. Therefore, a new sequence factor, M , was proposed in the present study to take the sequence effect of the VA loading sequence into account, and Equation 5.8 is further developed to:

$$N = M \frac{C}{(\Delta\sigma'_{CA,equ})^m} \quad (5.9)$$

The magnitude of the sequence factor for the CD loading sequence can be determined by the corresponding experimental results straightforwardly. For example, in the present study, fatigue tests were conducted under the CD loading sequences with a constant maximum stress of 300MPa. S-N curves used to estimate the fatigue life under such CD loading sequences were produced based on the CA loading sequences where the maximum stress was 300MPa as well. As the maximum stress in the CD loading sequence and in the CA sequences are identical, the

actual mean stress of each stress range in the CD loading sequence is identical with that in the CA loading sequence. In this case, the reason for the Miner's sum D being less than unity ($D \sim 0.5$) at fatigue failure is due to the sequence effect only, and not the mean stress.

It is worth noting that when welded joints are subjected to a CD sequence where the maximum stress is identical to that in the CA loading sequence used to produce S-N curve, the D value at fatigue failure is typically at about 0.5 [5,13]. Therefore, the sequence factor for the CD loading sequence, M_{CD} , can be assumed to be 0.5.

Compared with the CD loading sequence, the magnitude of the sequence factor for the CU or CM loading sequence cannot be determined from experimental data directly. This is because the effect of the mean stress and the effect of the sequence factor is always active at the same time under these two VA loading sequences. Hence, the sequence factor can only be determined after the effect of the mean stress is eliminated. The procedure to determine the sequence factor for the CU and CM sequences will be discussed later.

5.3 Data collection and input parameters

In addition to the results obtained in the present study, data from Studies I [5], II [34] and III [184] were selected to verify the models developed.

Study I investigated the fatigue performance of two types of welded joints under various VA loading sequences, i.e., CD, CU and CM sequence. The identical types of welded joints were also tested in Study II, but only under CU loading sequences produced from three different VA loading spectra. Study III studied the fatigue lives of transverse fillet welds under CU sequences where the maximum stress range varied between sequence to sequence. The input parameters are detailed below, and more details on the specimen geometry and loading spectrum are given in Appendix E.

5.3.1 Input parameters for the present study

5.3.1.1 S-N curve

S-N curves produced under the axial loading mode were adopted to predict the fatigue life. Therefore, for the tests conducted in the bending mode, stress ranges in the sequence were

converted to an equivalent stress range in the tensile loading mode that would lead to the same damage, using a bending factor, K_b , following:

$$\Delta\sigma_{tensile} = \frac{\Delta\sigma_{bending}}{K_b} \quad (5.10)$$

The K_b was previously investigated by Sun [178] and the magnitudes were 1.46, 1.32 and 1.27 for 6mm-, 12.5mm- and 25mm-thick specimen, respectively.

A forced slope $m = 3$ was adopted, and the corresponded C were 4.42×10^{12} , 2.74×10^{12} and 1.18×10^{12} for 6mm-, 12.5mm- and 25mm-thick specimen, respectively [178].

5.3.1.2 Residual stress

Residual stress values obtained from measurements were adopted to calculate the actual applied maximum stress, σ_{max} , for each stress range in VA loading sequences. For the 6mm-thick specimen, the residual stress is 83MPa, while for the 12.5mm- and 25mm thick specimens, the relaxed residual stress after two CA loading cycles were used, being 97 and 183MPa, respectively.

σ_{max} is assumed not to exceed the SMYS of the material. When this is violated, the residual stress was re-calculated. For example, the bottom welds of specimen B25_1 were tested under a CU loading sequence with the minimum stress of zero under bending mode. The maximum stress range in the loading sequence was 250MPa, and its corresponding equivalent tensile stress estimated using Equation 5.10 was 196MPa ($=250\text{MPa}/1.27$). The measured residual stress was 166MPa (Table 4.3). Thus, the σ_{max} for the largest stress range in this CU loading sequence was 362MPa ($=0+196+166\text{MPa}$), which was higher than 355MPa, the SMYS of the material. Therefore, the residual stress (RS) was re-calculated as:

$$\text{RS} = \text{SMYS} - (\text{constant minimum stress} + \text{maximum stress range}/K_b) \quad (5.11)$$

resulting residual stress is 159MPa. This value was used to calculate the σ_{max} for the rest of the stress ranges in this CU loading sequence.

Based on the principle described above ($\sigma_{max} \leq SYMS$), residual stress values used for each specimen under the CD loading sequence are given in Table 5.1, and under CU loading sequence in Table 5.2.

Table 5.1 Residual stress for CD loading sequences.

Plate thickness (mm)	Specimen ID	Maximum stress (MPa)	Residual stress (MPa)
6	A6_1	300	55*
	A6_2	150	83
	B6_1 (top weld)	87.5	83
12.5	A12.5_1	300	55*
	A12.5_2	150	97
	A12.5_3	87.5	97
	B12.5_1(top weld)	87.5	97
	B12.5_2(top weld)	0	97
25	A25_1	300	55*
	A25_2	150	183
	A25_3	87.5	183
	B25_1(top weld)	0	183

Note: * means calculated based on Equation 5.11.

Table 5.2 Residual stress for CU loading sequences.

Plate thickness (mm)	Bending factor, K_b	Specimen ID	Minimum stress (MPa)	Residual stress (MPa)	Equivalent maximum tensile stress range (MPa)
6	1.46	B6_1 (bottom weld)	87.5	83	171
12.5	1.32	B12.5_1 (bottom weld)	87.5	78*	189
		B12.5_2 (bottom weld)	0	85	
25	1.27	B25_1 (bottom weld)	0	159*	196

Note: * means calculated based on Equation 5.11.

5.3.1.3 Reference maximum stress

The reference maximum stress, $\sigma_{R,max}$, is the actual maximum stress of the stress ranges used to produce S-N curves. It is the sum of the applied maximum stress and the residual stress. The former was constant, being at 300MPa [178]. The initial measured residual stress, as described in Chapter 4, was 83, 122 and 233MPa for the 6mm-, 12.5mm- and 25mm-thick specimen, respectively. Therefore, by assuming that the actual maximum stress does not exceed the SMYS of the material, the reference maximum stress was assumed to be constant and equal to the SMYS at 355MPa.

5.3.2 Input parameters for Study I

5.3.2.1 S-N curve

Two types of welded joints manufactured from BS 4360 Grade 50D and Grade 50B steels were tested which were designated G and F, respectively. The G type specimen consisted of a 12mm-thick plate with attachments fillet welded to each edge, while the type F specimen involved a 12.5mm-thick plate with longitudinal attachments fillet welded on each surface.

Best-fit S-N curves of the two types of welded joints were established under CA loading sequences with a constant maximum stress at 280MPa.

For F type:

$$\Delta\sigma^{3.072}N = 1.312 \times 10^{12} \quad (5.12)$$

For G type:

$$\Delta\sigma^{2.728}N = 1.183 \times 10^{11} \quad (5.13)$$

5.3.2.2 Loading sequence

Based on a basic concave-up shaped spectrum with P_i ranging from 0.04 to 1, various VA loading spectra with different minimum P_i values were produced. Upon these loading spectra and a maximum stress range of 210MPa, three types of loading sequences were generated, i.e., the CD loading sequence, with the constant maximum stress being 280MPa, the CM loading sequence where the constant mean stress 175MPa and the CU loading sequence with the

constant minimum stress 70MPa. The maximum and minimum stress in these three sequences were the same at 280 and 70MPa, respectively, both tensile.

5.3.2.3 Residual stress

The initial residual stress in the F and G type specimens were measured using the Centre-hole drilling method as 281 and 370MPa, respectively. After the F type specimen had been tested under CD sequences for ten blocks, the residual stress relaxed by 73%, reducing to 76MPa. The relaxed residual stress value for G type was not measured; however, by assuming the same percentage of reduction, it was taken as 100MPa.

5.3.2.4 Reference maximum stress

As the maximum stress achieved in the VA loading sequences (280MPa) was identical to that used in the CA loading sequences to produce the S-N curves, the magnitude of the relaxed residual stress under the CA loading was assumed to be the same as measured in the specimen tested under VA loading. Therefore, the reference maximum stress was 356MPa (=280+76MPa) for the F type specimen and 380MPa (=280+100MPa) for the G type.

5.3.3 Input parameters for Study II

5.3.3.1 S-N curve

In Study II, the welded joints tested were identical to those tested in Study I, named as F and G types. They were all made from 12.5mm-thick steel to BS 4360 Grade 50B. The S-N curves for these two types were established under CA loading sequences with a constant stress ratio $R = 0$:

For F type:

$$\Delta\sigma^{2.59}N = 1.59 \times 10^{12} \quad (5.14)$$

For G type:

$$\Delta\sigma^3N = 6.39 \times 10^{11} \quad (5.15)$$

5.3.3.2 Loading sequence

A basic VA loading spectrum referred to Spectrum A, was developed from a standard load spectrum for fighter aircraft wings, with P_i ranging between 0.063 and 1. Based on Spectrum A, two more spectra, Spectrum B and C, were produced by omitting P_i which is higher than 0.667 and 0.377, respectively, i.e., with P_i ranged from 0.063 to 0.667 in Spectrum B and from 0.063 to 0.377 in Spectrum C.

Based on Spectrum A, four CU loading sequences were produced by using four different maximum stress ranges, i.e., 300, 250, 200 and 150MPa. Similarly, three loading sequences were produced on the basis of spectrum B and C with the maximum stresses 300, 200 and 150MPa. All stress ranges in each loading sequence were arranged in a random order, with a constant stress ratio $R = 0$.

5.3.3.3 Residual stress and reference maximum stress

The residual stress was not measured in Study II. However, in consideration of the type of welded joints tested, the residual stress was expected to be as high as 70% of the SYMS of the material according to measurement results in Study I. In this case, the reference maximum stress was assumed to be identical to the SYMS at 355MPa.

5.3.4 Input parameters for Study III

5.3.4.1 S-N curve

The specimens tested in this study were dog-bone shaped joints containing transverse fillet welded attachments in the middle of the length. They were manufactured using 9.5mm-thick steel plates. CA tests were carried out at a constant stress ratio $R = 0.1$. Based on the test results, the fatigue endurance was found to comply with class FAT 80 design curve provided in standard IIW [16], following:

$$\Delta\sigma^3 N = 1.024 \times 10^{12} \quad (5.16)$$

5.3.4.2 Loading sequence

The VA loading spectrum was produced based on an in-service loading history for the mid-span moment in a 40m long, simply-supported girder [184]. P_i values were between 0.06 and 1. Afterwards, four CU sequences were generated from this spectrum with four different maximum stress ranges at 367, 239, 217, 171MPa, and the corresponding constant minimum stresses were 9, 12, 13 and 20 MPa, respectively.

5.3.4.3 Residual stress and reference maximum stress

The residual stress in the tested specimen was measured using the XRD method. It showed an approximately uniformly distributed tensile residual stress in the top 2 to 3 mm below the surfaces with a magnitude 20% of the SMYS. Therefore, a uniform tensile residual stress of 20% of the yield stress was assumed [66]. As tests were performed at a constant stress ratio, the maximum stress applied was not constant in each test under different stress ranges. The reference maximum stress was estimated by combining the maximum stress applied (160MPa) with the residual stress to 240MPa (=160+80MPa).

5.4 Comparison of fatigue lives between experiments and predictions under cycling down loading sequences

Figure 3.15 in Chapter 3 provides a comparison of fatigue lives of experiments and calculations based on BS 7608 where only stress ranges are considered. It is re-plotted in logarithmic scales in Figure 5.2, to compare with Figure 5.3, where experimental results are plotted against predicted results using the models developed in the present study. The Miner's sum calculated based on the fatigue life predicted by the models is referred to as D_{ms} .

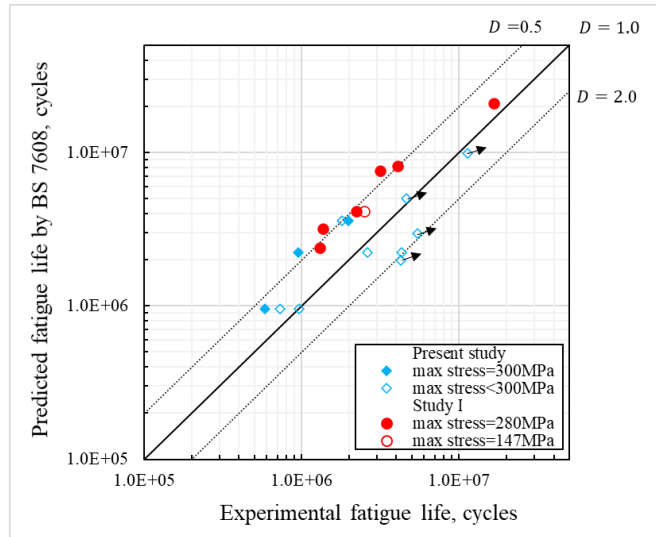


Figure 5.2 Comparison of fatigue lives between experiments and calculations based on BS 7608 which only considers stress ranges under CD loading sequences (re-plot of Figure 3.14) (arrow indicates run-out).

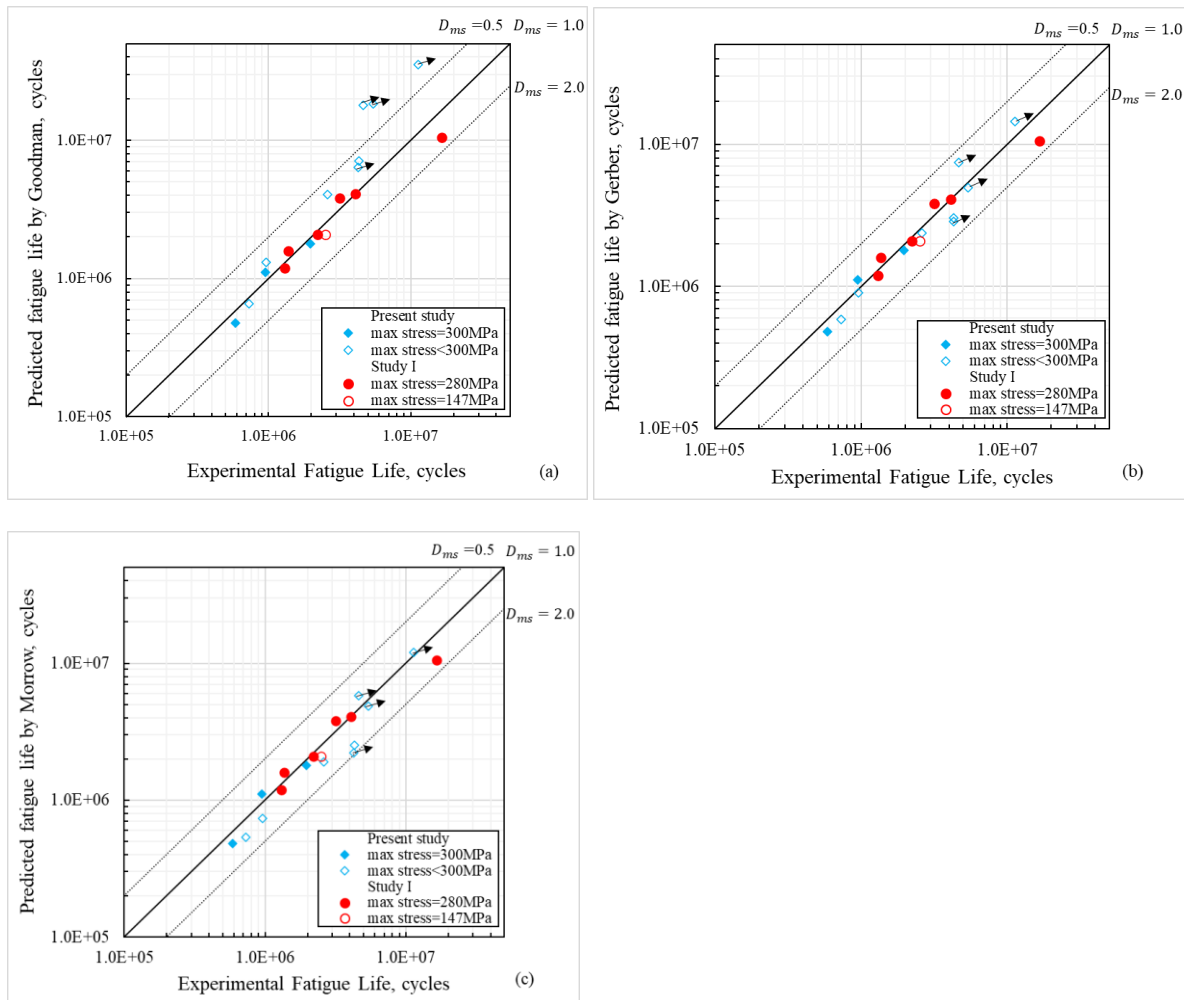


Figure 5.3 Comparison of fatigue lives between experiments and calculations based on the models developed under CD loading sequences: (a) Goodman (b) Gerber and (c) Morrow. (arrow indicates run-out).

As discussed in Section 3.4.7, the main conclusion derived from Figure 5.2 is that a large scatter is seen when only stress ranges are considered to calculate the fatigue life as advised in the standard. The D value ranges from 0.5 to 2, depending on the maximum stress in the CD loading sequence.

The following can be seen from Figure 5.3:

- When the maximum stress in the CD sequence is identical to that used to produce the S-N curves, i.e., 300MPa for the present study and 280MPa for Study I, the predicted fatigue lives obtained using the three models developed in the present study all agree well with experimental results, with D_{ms} being about 1.
- When the maximum stress in the CD sequence is decreased (<300MPa), predicted results are close to experimental results. D_{ms} obtained using the Goodman method scatters between 0.5 and 1.5, and 1 and 1.5 using the Gerber or Morrow method.
- For tests which ran-out, D_{ms} predicted using the Goodman method are all less than 1.0 - three out of four results are less than 0.5 and the remaining one is about 0.7 (Figure 5.3 (a)), implying a large remaining fatigue life in the specimen. These predictions agree well with experimental results. There is no indication of fatigue crack initiation and propagation at the weld toe when tests were stopped, which also means the actual fatigue life should be much higher. The predictions made using the Gerber or Morrow method may be conservative (Figure 5.3 (b) and (c)) as two of these D_{ms} values exceed unity.

Based on the predicted results, it shows that when the mean stress correction is considered, scatter becomes smaller, and the predicted lives agree better with experimental data.

5.5 Comparison of fatigue lives between experiments and predictions under cycling up loading sequences

5.5.1 Fatigue lives predicted based on BS 7608

Figure 5.4 shows the comparison between experimental fatigue lives obtained under CU loading sequences with those predicted by BS 7608 where neither the mean stress nor the

sequence effect is considered. It can be seen that the results clearly exhibited a large scatter, with D value ranging from 0.5 to 8. Therefore, the fatigue life under CU loading sequence cannot be well predicted using the method as advised in BS 7608.

In the following sections, fatigue lives are re-estimated using the model developed in the present study, with both the mean stress and the loading sequence considered, in addition to the stress range.

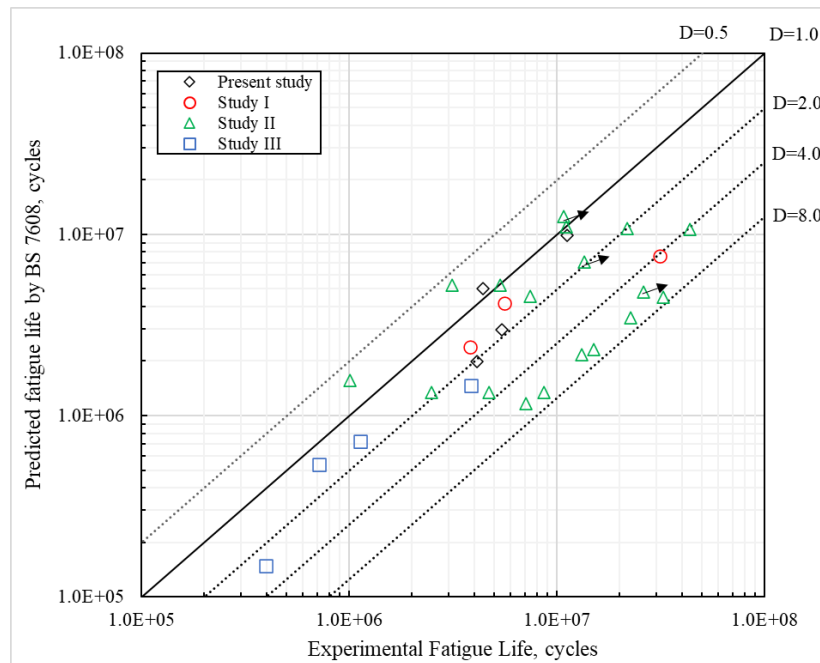


Figure 5.4 Comparison of fatigue lives between experiments and calculations based on BS 7608 which only considers stress ranges under CU loading sequences (arrow indicates run-out).

5.5.2 Sequence factor for cycling up loading sequence

As discussed in Section 5.2.3, the magnitude of the sequence factor for a CU loading sequence cannot be determined directly from experimental results because of the combined effects of the mean stress and the sequence factor. Hence, in order to eliminate the mean stress effect, experimental results were first correlated with the mean stress. Then the sequence effect of CU was determined accordingly based on the results obtained after the mean stress correction.

For the mean stress correction, equivalent stress ranges were calculated by correlating the original stress ranges in a CU loading sequence with the reference maximum stress of 355MP using the models developed in the present study (Equation 5.6-5.8). Fatigue lives were then

estimated based on the equivalent stress ranges and plotted against the experimental results in Figure 5.5. The Miner's sum, estimated based only on the means stress correction and excluding the sequence effect, is named as D_m .

It can be seen that predictions based only on the mean stress correction do not agree well with the experimental results, and still exhibit a large scatter, with D_m ranging between 0.5 and 2 using the Goodman method (Figure 5.5 (a)), and 0.5 and 4 using the Gerber or Morrow method (Figure 5.5 (b) and (c)).

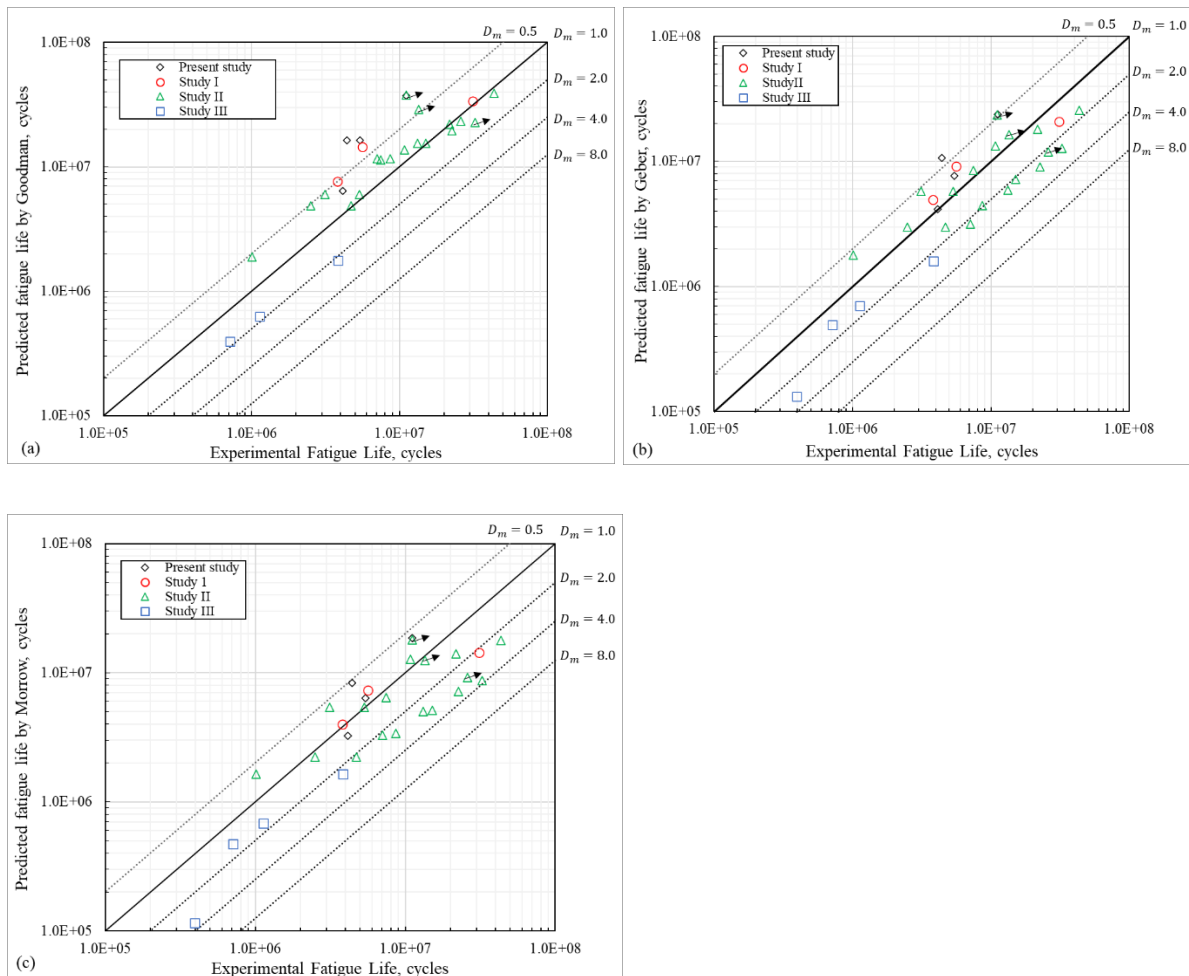


Figure 5.5 Comparison of fatigue lives between experiments and calculations based on mean stress correction models developed in the present study under CU loading sequences: (a) Goodman; (b) Gerber and (c) Morrow (arrow indicates run-out).

As the effect of the mean stress was eliminated after the mean stress correction, the deviation between the predicted and experimental results was considered to be only relating to the sequence effect. However, at the current stage, the sequence effect still cannot be concluded

because of the wide range of the value of D_m . Hence, unlike the case under a CD loading sequence, it is inappropriate to simply set the sequence factor at a constant value for CU loading sequences.

In order to determine the sequence factor, further investigation was carried out based on the data presented in Figure 5.5 from four different studies where fatigue tests were performed using different welded joints under various CU loading sequences. The scatter might be related to the type of specimen or certain feature(s) of a CU loading sequence. Investigations were performed on the results obtained using the Gerber and the Morrow methods (Figure 5.5 (b) and (c)), as the Goodman method was reported to be more suitable for brittle materials [182], rather than for ductile steels like S355.

Investigations were carried out first on data from Study II [34], in which a basic VA spectrum, Spectrum A, was produced first, with the P_i value ranging from 0.063 to 1. Afterwards, two more VA spectra, spectrum B and C, were derived from Spectrum A, with the P_i value ranging from 0.063 to 0.667 and 0.063 to 0.377, respectively. The ratio of the maximum P_i to the minimum P_i , for A, B and C were 15.8, 10.5 and 5.8, respectively. This ratio was defined as the overload ratio, R_{P_i} . Based on each spectrum, various CU loading sequences were generated with different maximum stress ranges. Two welded joints, F and G types, were tested under those loading sequences.

The data for Study II were extracted from Figure 5.5 (c) and re-plotted in Figure 5.6.

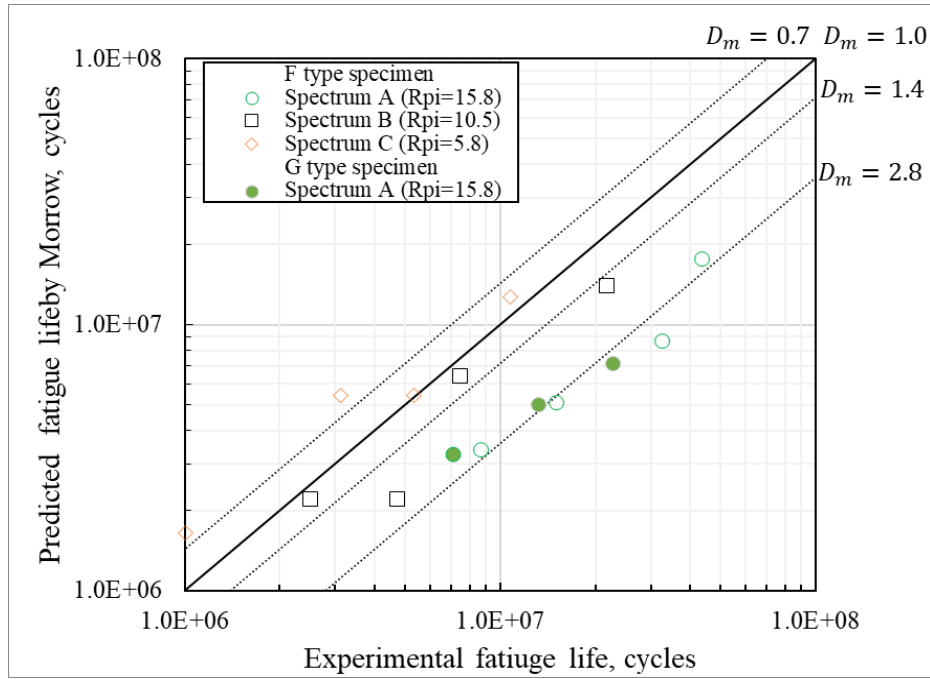


Figure 5.6 Comparison between the fatigue lives of experiments from Study II [34] and calculated based on Morrow mean stress correction model developed under CU loading sequences.

According to Figure 5.6, the potential relationship between the overload ratio, maximum stress ranges, the specimen type related to the sequence factor can be discussed, as follows:

- The effect of specimen types can be investigated based on the results of F and G type specimens obtained under spectrum A. It can be seen that D_m for both F and G specimens are almost identical, at about 2.8, regardless of the loading sequence. Hence, the type of welded joint appears to have no significant influence on the fatigue endurance.
- Similar to results obtained under spectrum A, D is of similar value at fatigue failure under spectrum B or C, regardless of the loading sequences where the maximum stress ranges are different. These results suggest that the fatigue life is not affected by the maximum stress range in the sequence.
- In terms of the effect of overload ratio, there is a clear trend that D_m reduces in value with a decreasing overload ratio, as the retardation effect of the CU loading sequence on the crack propagation being dependent on the overload ratio [8,118,120].

It can be summarised that in comparison with the specimen type and the maximum stress range, the overload ratio is the driven factor that affects the sequence factor of a CU loading sequence. The same conclusion is also obtained from the results corrected using the Gerber method. Therefore, further analysis was carried out to investigate the effect of overload ratio on the fatigue lives of welded joints.

To examine the relationship between the overload ratio R_{Pi} and D_m , R_{Pi} for all the CU sequences involved in the four studies, i.e., the present study, Study I, II and III, were calculated. And the corresponding average D_m obtained using the Morrow and the Gerber methods were estimated as well. Results are given in Table 5.3 and plotted in Figure 5.7.

The following can be seen from Figure 5.7:

- For the 12.5mm-thick specimen, the average D_m is proportional to the overload ratio. i.e., the higher R_{Pi} , the larger D_m .
- D also appears to depend on the plate thickness. For $P_i = 2.8$, D_m value for the 25mm specimen is about two times the value for the 12.5mm specimen, suggesting the thicker the plate, the higher D_m . Identical trends also can be seen by comparing the results obtained from 9.5 or 6mm-thick specimens with that of the 12.5mm-thick specimen. However, as there are limited results, and more results are required.

Table 5.3 The overload ratio and the corresponding average D_m value after mean stress correction.

Specimen Thickness (mm)	overload ratio, R_{Pi}	Average D_m		Data source
		using Gerber	using Morrow	
25	2.8	0.99	1.27	P
12.5	2.8	0.41	0.53	P
	4.0	0.77	0.95	I
	5.0	0.61	0.77	I
	5.9	0.71	0.76	II
	10.0	1.49	2.16	I
	10.5	1.12	1.49	II
	15.8	2.33	2.94	II
	15.8	2.07	2.66	II
9.5	16.6	2.11	2.23	III
6	2.8	0.47	0.60	P

Note: P indicates the present study.

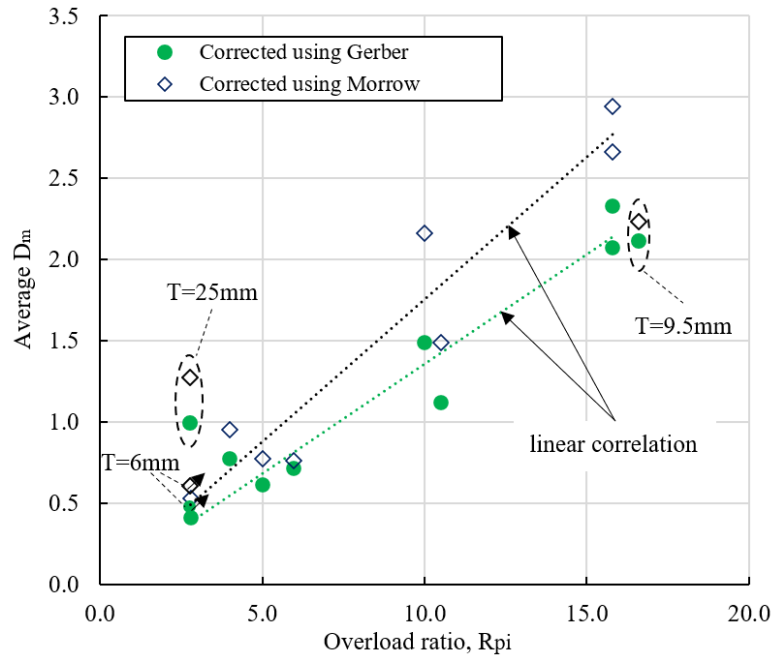


Figure 5.7 The relationship between R_{pi} and the average D_m value obtained after mean stress correction under CU loading sequences.

To estimate the relationship between R_{pi} and D_m , a regression analysis was conducted to produce a linear correlation, as shown in Figure 5.7, following:

$$D_m = kR_{pi} + q \quad (5.17)$$

where k and q are constants, as shown in Table 5.4. This linear correlation provides a fair fitting to the data, with R^2 at about 0.92. As q is small, it is omitted by setting the linear correlation intercepted at the origin. Thus, Equation 5.1 was developed to:

$$D_m = k'R_{pi} \quad (5.18)$$

where k' is the new constant, and its value is given in Table 5.4. The correlation also agrees well with the data, with R^2 at 0.92.

Table 5.4 Parameters in the correlation between R_{pi} and the average D_m value obtained after mean stress correction.

Mean stress correction method	Original fitting			Interception at origin	
	k	q	R^2	k'	R^2
Gerber	0.13	0.0176	0.93	0.13	0.93
Morrow	0.17	-0.0037	0.92	0.17	0.92

It can be seen that the two values of k' are similar. Therefore, the average value of 0.15 was adopted in subsequent analyses.

The sequence factor for CU loading sequences can be estimated by:

$$M_{CU} = D_m \quad (5.19)$$

It should be noted that the relationship between the sequence factor and the CU loading sequence (Equation 5.2) was established based on the results obtained under those CU sequences where various stress ranges were applied in a random order, with R_{Pi} ranging between 3 and 17. Whether this relationship is proper for other CU sequences with different features, such as R_{Pi} out of this range, or stress ranges applied in a particular order, is unknown, and further studies are needed.

5.5.3 Fatigue life prediction based on analytical models developed in the present study

After integrating the sequence factor developed with the mean stress corrections, the predicted fatigue lives are plotted against the experimental results in Figure 5.8. The Miner's sum estimated based on the means stress correction and the sequence effect is referred to D_{ms} . Figure 5.8 (a) suggests that:

- After the application of the Gerber mean stress correlation and the sequence factors developed, predicted fatigue lives agree well with the experimental ones, with D_{ms} ranging mainly between 0.5 and 1.5.
- The predicted fatigue life of the 25mm-thick specimen is relatively conservative compared with those of other thicknesses, probably due to the sequence factor being conservative for the latter, as discussed in section 5.5.2.

Similar results also can be summarised from Figure 5.8 (b) where the data is obtained based on the Morrow method.

The prediction results show that when the mean stress correction is considered, the scatter becomes smaller, and the predicted lives agree better with the experimental data.

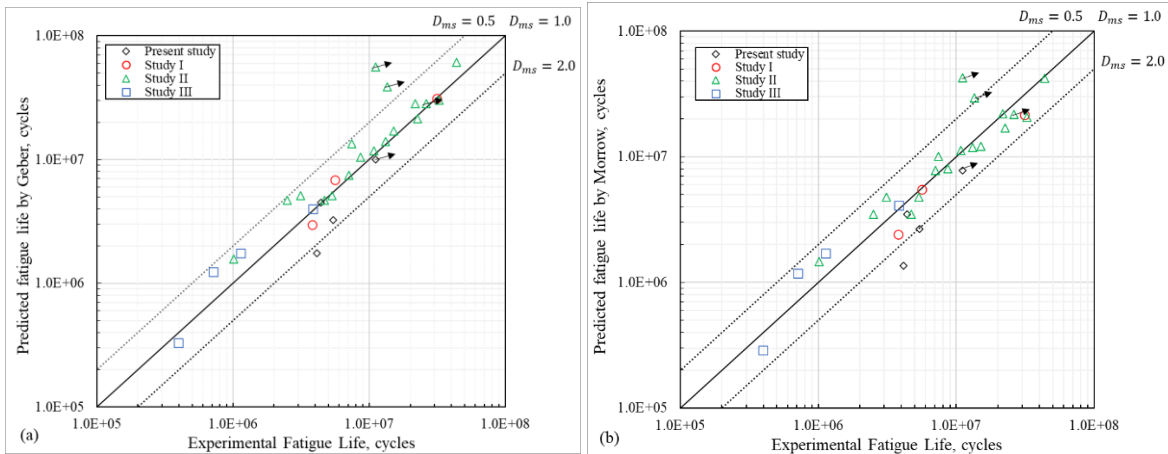


Figure 5.8 Comparison between the fatigue lives of experiments and calculated based on analytical models developed under CU loading sequences: (a) Gerber and (b) Morrow. (arrow indicates run-out).

5.6 Comparison of fatigue lives between experiments and predictions under constant mean stress sequences

5.6.1 Fatigue life predicted based on BS 7608

Results under three CM loading sequences were collected in Study I. Figure 5.9 shows the comparison between the experimental fatigue lives with those predicted based on BS 7608 where the fatigue lives are calculated only based on stress range. It can be seen that the predictions range between 0.7 to 1.0. Although these results are only slightly lower than 1.0, it should be mentioned that neither the mean stress effect nor the sequence effect is included in the calculation.

5.6.2 Sequence factor for constant mean loading sequence

Similar to a CU loading sequence, results obtained under a CM loading sequence were corrected using the mean stress first, and the sequence factor for such loading sequence was developed accordingly. For the mean stress correction, stress ranges in CM loading sequences were correlated with the reference maximum stress of 355MPa using the mean stress correction models developed in the present study. Fatigue lives were then estimated based on the equivalent stress ranges and plotted against experimental results in Figure 5.10. It can be seen that after the mean stress correction, D_m obtained using the Gerber and the Morrow method are all about 0.5.

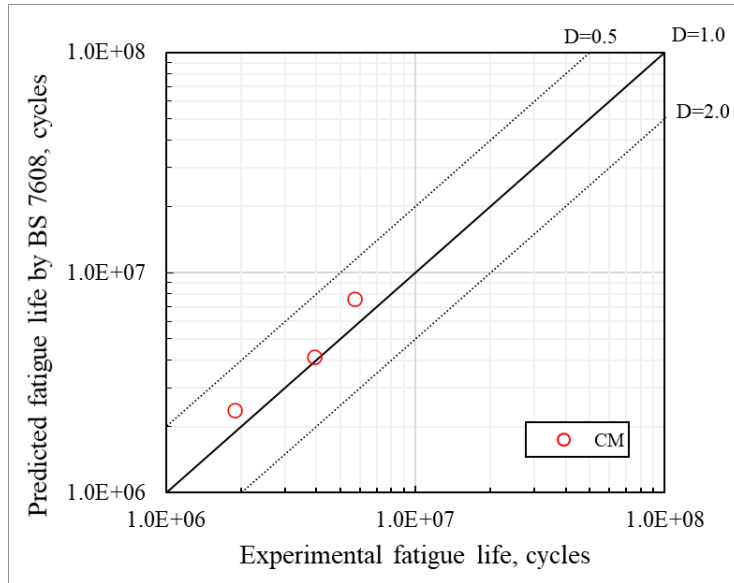


Figure 5.9 Comparison between the fatigue lives of experiments and calculated based on BS 7608 which only considers stress ranges under CM loading sequences.

In this case, the sequence factor for a CM loading sequence, M_{CM} , was assumed to be 0.5. It is interesting to note that sequence factors for CM and CD loading sequences were identical, suggesting that a CM loading sequence can reduce the fatigue endurance of welded joints as a CD sequence does.

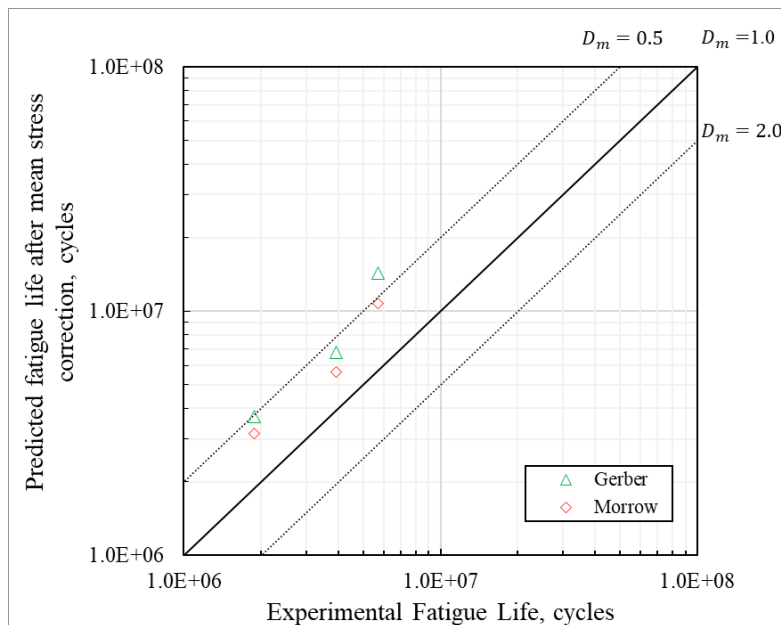


Figure 5.10 Comparison of fatigue lives between experiments and calculations based on mean stress correction models developed under CM loading sequences.

5.6.3 Fatigue life predicted based on analytical models developed

After the value of the sequence factor was determined, predicted fatigue lives were calculated using the three models developed in the present study, as shown in Figure 5.11. It can be seen that fatigue lives predicted by the developed models agree well with experimental results, with D_{ms} in the range between 0.5 and 1.5.

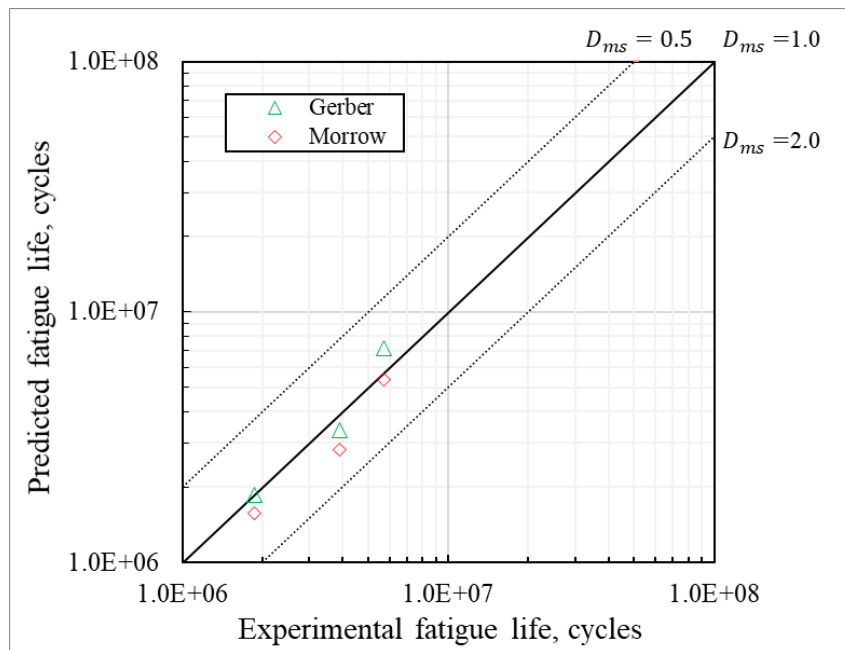


Figure 5.11 Comparison between the experimental fatigue lives under CM loading sequences with that predicted using models developed in the present study.

5.7 Conclusions

Analytical models were developed to predict the fatigue life of welded joints under VA loading sequences. Effects of both the mean stress and the sequence can be considered. To establish the new models, the conventional Goodman, Gerber and Morrow equations, were re-written into the form where a reference maximum stress is used as the independent alternative. In addition, a new sequence factor that indicates the effect of the VA loading sequence on the fatigue performance of welded joints was estimated for CD, CM and CU loading sequences, respectively. Fatigue lives were re-calculated using the analytical models developed in the present study.

Conclusions drawn from the results are as follows:

- Under both CD and CM loading, the sequence factor can be determined according to the experimental results, being constant at 0.5, while the sequence factor for CU sequence is a function of the overload ratio, R_{pi} and may relate to the plate thickness.
- In comparison with the method provided in BS 7608, the model developed can take into account both the mean stress and sequence effect and provide a fair prediction for fatigue endurance of welded joints under CD loading sequence, with D_{ms} ranging between 0.5 to 1.5.
- Similarly, this model can also significantly improve the prediction for the fatigue life of welded joints under a CU loading sequence, with D_{ms} mostly in the range of 0.5 to 1.5, rather than ranging from 0.5 to 8 which were obtained using the method given in BS 7608.
- When welded joints are subjected to CM sequences, the fatigue life can be closely predicted using the models developed as well, with D_{ms} ranging between 1 and 1.5.

Chapter 6 Fracture Mechanics Analysis

6.1 Introduction

In addition to the S-N curve method, Fracture Mechanics is another widely used method to conduct fatigue assessment on welded joints in the industry area. The fatigue crack growth rate (FCGR) at an indicated stress range can be calculated based on the FCGR curves given in design codes, such as BS 7910 [30], so the fatigue endurance of the welded joints is estimated by calculating the number of cycles for the fatigue crack growing from an initial size to a critical size. However, these curves are established based on the experimental data produced under CA loading sequences.

The fatigue crack growth (FCG) data, which is the crack size (i.e., length and depth) and the corresponding number of loading cycles, under VA loading sequences has been generated in the present study, and they were compared with the result predicted based on BS 7910 under CA loading sequences. The results suggest that the predictions of the FCGR based on BS 7910 could be either under- or over-estimate depending on the type of the VA loading sequence. Therefore, in order to improve the accuracy of FCGR prediction, new factors were proposed in the present study to modify the model given in BS 7910. These factors were developed on the basis of the effective stress ratio, and the local residual mean stress mechanism, aiming to consider both mean stress and VA loading sequences effect on the FCGR.

The new model was validated by comparing the calculated FCGR and fatigue endurance to the experimental data obtained in the present study and those from open literature. It shows the new model can improve the accuracy of FCGR and provide guidance to determine the fatigue endurance of welded joints under VA loading sequences.

This Chapter introduces detailed information on the development of the new model and the validation process.

6.2 Fatigue crack growth data under variable amplitude loading sequences

As mentioned in Chapter 3, the FCG in welded joints under VA loading sequences was monitored by a combination of visual inspection with the alternating current potential drop (ACPD) method during fatigue testing. When tests stopped, welded joints tested under axial

loading were remained in the test machine and completely split by static tensile loading in displacement control, while those tested under bending were removed from the test machine and soak in liquid Nitrogen for one hour before breaking. The fracture surface of each specimen was examined and photographed under a microscope. The crack size was then measured according to the ACPD measurement results and the crack beach marks introduced by the soap solution on the fracture surface.

The fracture surface of each specimen is presented in Appendix C. It can be seen that multiple cracks with a semi-elliptical shape were initiated at the weld toe and coalescence happened when they grew to a certain size. From some fracture surfaces, the FCG data of individual cracks can be extracted based on the clear beach marks before coalescence, such as A12.5_1 and A25_3, where the FCG data for the crack with the greatest number of beach marks were selected for further analysis. For those fracture surfaces where the beach marks of individual cracks are blurry, the FCG data was only extracted for the largest crack after coalescence, e.g., B12.5_2 and B25_1. For other mixed surfaces, such as A6_2, B6_1 and A12.5_3, no data was generated. In addition, an assumption was made here that is the growth of an individual crack was independent of other cracks. Therefore, FM can be used to describe the crack growth of the crack selected before it coalesced with others. The FCG data extracted from test specimens are presented in Table 6.1.

6.3 Fracture Mechanics approach

FM was used to describe the crack growth of the crack selected. The principle of fracture mechanics has been introduced in Chapter 2, so only a brief introduction is given here. Along the lines detailed in BS 7910 [30], the relationship between the FCGR (da/dN) and the stress intensity factor, ΔK , is assumed to adopt the normal form of Paris' Law:

$$\frac{da}{dN} = A(\Delta K)^m \quad (6.1)$$

where A and m are material constants. ΔK is the stress intensity factor (SIF). For a semi-elliptical fatigue crack at the toe of a fillet weld, ΔK can be estimated using:

$$\Delta K = Y M_k \Delta \sigma \sqrt{\pi a} \quad (6.2)$$

where Y is a function of the crack depth to the plate thickness ratio, a/T , and the crack aspect ratio $a/2c$, where c is half of the surface crack length. $\Delta\sigma$ is the nominal stress range applied.

Table 6.1 Fatigue crack growth data extracted for the welded joints tested under VA loading sequences.

Specimen ID	Number of Blocks	Crack Size (mm)		Specimen ID	Number of Blocks	Crack Size (mm)	
		Depth, a	Length, 2c			Depth, a	Length, 2c
A6_1	598	0.8	13.0	A25_1	99	0.5	3.0
	777	2.8	20.2		122	0.8	4.1
	827	4.1	26.1		135	1.0	5.8
A6_2	-		198		1.8	16.0	
B6_1	-		A25_2	221	21.9	1.8	
A12.5_1	76	0.2		2.1	251	33.8	2.7
	215	1.0	5.5	A25_3	216	1.0	6.0
	254	1.4	7.3		246	1.5	10.0
	297	1.8	9.5		326	3.0	19.0
A12.5_2	615	1.2	5.5		358	4.2	23.0
	747	2.1	9.0	B25_1	1431	3.2	40.5
	867	3.1	12.8		1514	4.4	43.1
	960	4.2	16.0		1578	5.0	47.2
A12.5_3	-		1658		5.6	50.9	
B12.5_1	1664	6.3	51.0		1724	6.3	58.5
	1903	8.5	70.0		1801	6.9	63.4
B12.5_2	1679	0.5	2.0		1886	8.8	73.3
	2053	0.9	3.5		2040	11.2	81.3
	2166	1.0	4.5				
	2368	1.3	5.1				
	2417	1.6	5.6				
	2529	2.0	6.5				

M_k is a stress magnification factor due to the stress concentration effect of the joint geometry. It is defined as [28]:

$$M_k = \frac{\Delta K_{in\ the\ plate\ with\ welds}}{\Delta K_{in\ the\ plate\ without\ welds}} \quad (6.3)$$

M_k can quantify the change in the stress intensity factor because of the surface discontinuity at the weld toe. The relationship between the magnitude of M_k and the ratio of a/T was established using Finite Element Analysis (FEA) based on either a 2D or 3D model, and the corresponding solutions are given in BS 7910.

Therefore, the number of cycles for a fatigue crack to grow from an initial size, a_i , to the final size, a_c under an indicated stress range can be calculated on the basis of the Paris' Law:

$$\int_{a_i}^{a_c} \frac{da}{A(\Delta K)^m} = N \quad (6.4)$$

And FM was only used to

6.4 Input parameters

In addition to the FCG data collected from the present study, relevant data were also collected from Study I [5] and Study IV [13], which are also referred in Chapter 5. The parameters used in the Paris' Law for each study are detailed below.

6.4.1 Parameters for the present study

In the present study, the crack propagation was assumed to follow the simplified one-stage mean curve given in BS 7910 for stress ratio $R > 0.5$. The corresponding A and m are 2.31×10^{-13} and 3, respectively. The threshold ΔK_{th} is the lower bound value in BS 7910, at $63 \text{ N/mm}^{3/2}$.

The solution of Y for the semi-elliptical surface in BS 7910 was employed. The specific value of the crack aspect ratio $a/2c$ was determined by examining the fracture surface of the tested specimens. From the fracture surface, it can be seen that cracks are very shallow in the early stage with the aspect ratio being about 0.1. As the cracks grow, the ratio gradually increases to about 0.2. Finally, coalescence between adjacent cracks occurs, and the aspect ratio decreases sharply to a lower value, and failure occurs shortly.

In terms of M_k , the 3D solution of finite element analysis was adopted as advised in BS 7910 [30]. M_k is a function of the crack depth, a , the attachment length from weld toe to weld toe, L , and the attachment length to plate thickness ratio, L/T . The value of M_k in the thickness direction, M_{ka} , normally decreases sharply as the fatigue crack grows deeper, and reaches to unity when the crack depth achieves 30% of the plate thickness.

6.4.2 Parameters for Study I

In this study, the FCG data was collected from welded joints containing longitudinal fillet welded attachments under CA loading sequences, using a combination of visual inspection and ACPD technique, and a best-fit FCGR curve was produced by regression analysis, following:

$$\frac{da}{dN} = \begin{cases} 0 & , \Delta K \leq 63N/mm^{\frac{3}{2}} \\ 2.1 \times 10^{-13} \Delta K^3 & , \Delta K > 63N/mm^{\frac{3}{2}} \end{cases} \quad (6.5)$$

The parameter M_{ka} solutions adopted are:

$$M_{ka} = 0.845 \left(\frac{a}{T}\right)^{-0.316} \quad \text{for } \frac{a}{T} \leq 0.1$$

$$M_{ka} = 0.853 \left(\frac{a}{T}\right)^{-0.312} \quad \text{for } \frac{a}{T} > 0.1 \quad (6.6)$$

The value of M_k at crack tips, M_{kc} , was assumed to be equal to 3.9, the value of M_{ka} at the crack depth of 0.15mm. As the fatigue crack grows away from the region where the stress concentration presents, M_{kc} decreases gradually to 1.0 when the length of the crack was just beyond the end of the longitudinal weld.

6.4.3 Parameters for Study IV

The FCG data was collected from the welded joints that are identical to that used in Study I [5], but the plate thickness is thinner, being at 8mm. The FCGR curve produced follows:

$$\frac{da}{dN} = \begin{cases} 0 & , \Delta K \leq 63N/mm^{\frac{3}{2}} \\ 2.78 \times 10^{-13} \Delta K^3 & , \Delta K > 63N/mm^{\frac{3}{2}} \end{cases} \quad (6.7)$$

M_k was calculated using Equation 6.6. The initial value of M_{kc} was also assumed to be equal to 3.4, the value of M_{ka} at a depth of 0.15mm, and gradually decreased to 1.0 when the crack length achieved to about 30mm.

6.5 Matlab code for the calculation

Tools have been developed to calculate FCG in welded joints in accordance with BS 7910, e.g., Crackwise, which is a widely used commercial software produced by TWI. However, these tools are not open source, so they cannot be further modified to consider the VA loading sequence effect on FCG. Therefore, a new code was first programmed in the present study using Matlab 2016 Ra according to BS 7910, to implement the calculation.

In order to validate this code, three pairs of the initial crack depth and the length were selected, one from each study mentioned in section 6.4. The FCG corresponding to these three pairs data were calculated using the new code programmed and Crackwise 5.0, respectively, and the calculation results were compared. It is found that the calculation results obtained using the code agree well with those produced based on Crackwise, verifying the new code. Detailed information about the code and the validation are given in Appendix F.

6.6 Predictions based on BS 7910

The FCG under VA loading sequences were calculated using the Matlab code, and the results of the calculation were compared with the experimental data, as introduced below.

6.6.1 Fatigue crack growth predictions under cycling down loading sequences

The FCG in welded joints tested under CD loading sequences in these three studies were calculated, and the predictions were compared with the experimental data. From each study, one example of comparison result was selected, being for specimens A12.5_1, F15 and ST04, and they are plotted in Figure 6.1. As can be seen in Figure 6.1:

- The FCG under CD loading sequences cannot be well predicted using the FCGR curve given in BS 7910. It is significantly under-estimated, which can result in non-conservative predictions on fatigue lives.
- For all three cases studied, the number of cycles predicted according to BS 7910, where the fatigue crack grew from the initial to the final size, are about two times as high as that obtained from tests. This agrees well with Miner's rule for each test result, which is 0.43 for A12.5_1, 0.63 for F15 [5] and 0.66 for ST04 [13]. This implies that factors

responsible for the underestimation of the fatigue lives under CD loading sequence is mainly related to crack propagation rather than initiation.

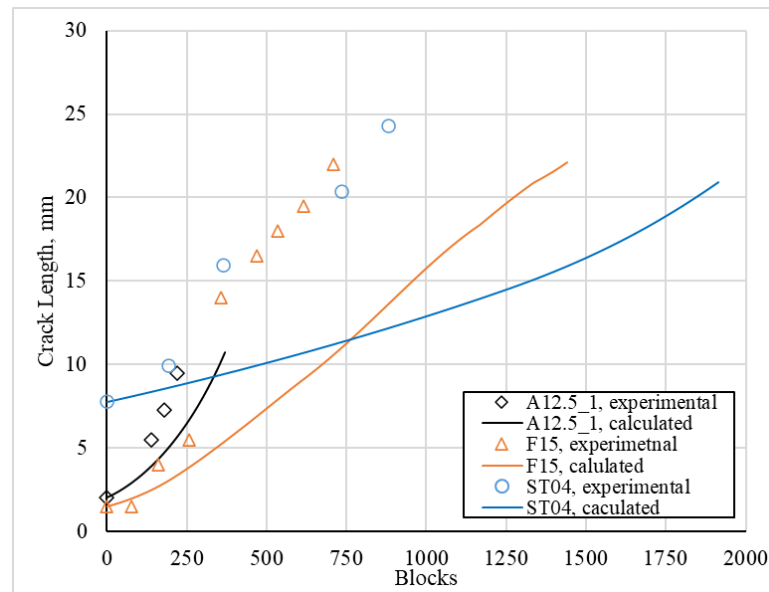


Figure 6.1 An example of comparison of fatigue crack growth under CD loading between experimental data and calculations based on the FCGR curve give in BS 7910 for steels in air.

6.6.2 Fatigue crack growth predictions under cycling up loading sequences

FCG under CU loading sequences were also calculated according to BS 7910 and compared with the experimental data. Two typical comparison results, one for specimen B25_1 in the present study and another for F09 in Study I [5], are presented in Figure 6.2. It can be seen that the FCG predicted are overestimated, which can result in a conservative prediction.

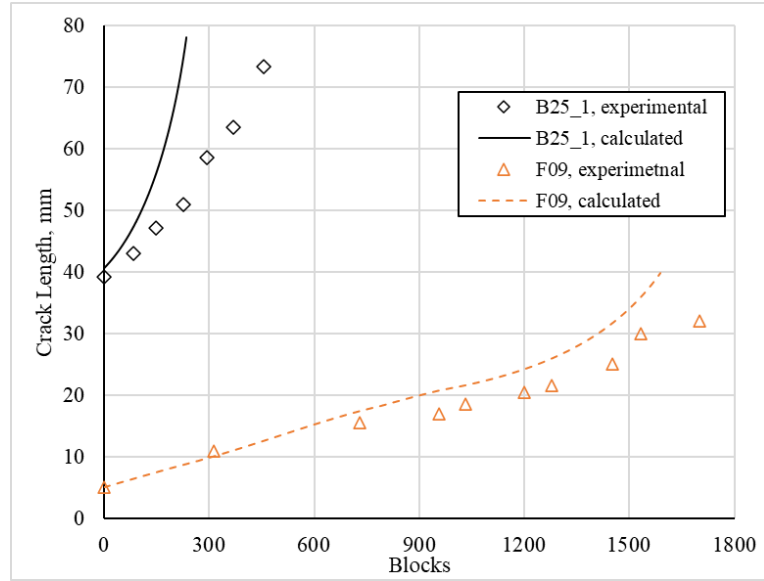


Figure 6.2 An example of comparison of fatigue crack growth under CU loading between experimental data and calculations based on the FCGR curve give in BS 7910 for steels in air.

Based on these comparison results, it can be concluded that the FCG in welded joints under VA loading sequences cannot be well predicted using the FCGR curve given in BS 7910. It can be either under- or over-estimated depending on the nature of the VA loading sequences. Therefore, in the following sections, new analytical model is developed in order to improve the accuracy of prediction of FCG under VA loading sequences.

6.7 Development of the analytical model

Based on the FCGR curve given in BS 7910 (Equation 6.1), an effective stress intensity factor, ΔK_{eff} , was developed in the present study to take into account both effects of mean stress and VA loading sequence. Hence, the analytical model developed is following:

$$\frac{da}{dN} = A(\Delta K_{eff})^m \quad (6.5)$$

where A and m are constants as referred previously.

6.7.1 Effective stress intensity factor

For welded joints, the FCGR is assumed to be independent of the stress ratio because of the high tensile residual stress at the weld toe [30]. However, as reported in Chapters 3 and 4, the residual stress measured in the three plate thicknesses specimens tested in the present study are

only about 70%, 30% and 22% of the specified minimum yield stress (SMYS) of the material, resulting in fatigue lives being increased significantly when the mean stress is below a certain level. Therefore, the mean stress effect on the FCGR should be considered to improve the accuracy of predictions. To consider such an effect, an effective stress intensity factor, ΔK_{eff} , is generally used in the Paris' law [7], following

$$\Delta K_{eff} = U\Delta K \quad (6.6)$$

where U is a function of the stress ratio, R .

In addition, as the FCGR can be either accelerated or retarded under VA loading sequences, a new parameter, H , was also proposed correspondingly in the present study to consider the effect of the VA loading sequence. Therefore, Equation 6.6 was further developed to:

$$\Delta K_{eff} = UH\Delta K \quad (6.7)$$

The value of parameter U and H are determined in the following sections.

6.7.2 Estimation of parameter U

For the parameter U , the solution developed by Booth and Maddox [7] is widely used, given:

$$U = \begin{cases} \frac{1}{1.5 - R} & -2 < R < 0.5 \\ 1 & R > 0.5 \end{cases} \quad (6.8)$$

R is the stress ratio of the applied stress range:

$$R = \frac{\sigma_{min}}{\sigma_{max}} \quad (6.9)$$

where σ_{min} and σ_{max} is the applied minimum and maximum stress, respectively, in the stress cycle.

Equation 6.9, however, was established based on residual stress-free specimens. In the presence of residual stress, the effective stress ratio R_{eff} due to the applied stress and the residual stress can be calculated by:

$$R_{eff} = \frac{\sigma_{min} + RS}{\sigma_{max} + RS} \quad (6.10)$$

6.7.3 Estimation of sequence factor

Sequence factor, H , was developed based on the local residual mean stress presented in the reverse plastic zone ahead of the crack tip, which is considered as the predominant mechanism accounting for the transit in FCGR under VA loading sequences [12,13].

6.7.3.1 Local residual mean stress mechanism

It is well known that under a CA loading sequence (Figure 6.3 (a)), there is a reverse plastic zone ahead of the crack tip, where the local stress-strain hysteresis loop is fully reversed (i.e. local mean stress equals to zero) even the applied load is entirely tension-tension [35], as shown in Figure 6.3 (b).

However, when a specimen is subjected to VA loading sequences, it is likely that the local residual mean stress of the major cycles relaxes to zero, but not the mean stress of the small cycles [12]. When a CD loading sequence (Figure 6.3 (c)) is applied to the specimen, the local hysteresis loop of the underload (UL), $\Delta\sigma_{UL}$, is fully reserved, while the loop of the small cycles, $\Delta\sigma$, associates with a tensile local residual mean stress, $\sigma_{m,L}$, Figure 6.3 (d). This local residual mean stress is considered as the predominant reason for the FCGR corresponding to $\Delta\sigma$ in a CD loading sequence being higher when compared with that corresponding to the identical stress range in a CA loading sequence.

On the contrary, under a CU loading sequence (Figure 6.3 (e)), the loop of small cycles has a compressive local residual mean stress, $\sigma_{m,L}$ (Figure 6.3 (f)), resulting in FCGR retardation.

6.7.3.2 Estimation of parameter H

Due to the local residual mean stress, the local stress ratio corresponding to a specific stress range, $\Delta\sigma$, under a VA sequence is different from that of the identical stress range under a CA sequence. Under a CA loading sequence, the local stress ratio, $R_L(=\sigma_{min,L}/\sigma_{max,L})$, is constant,

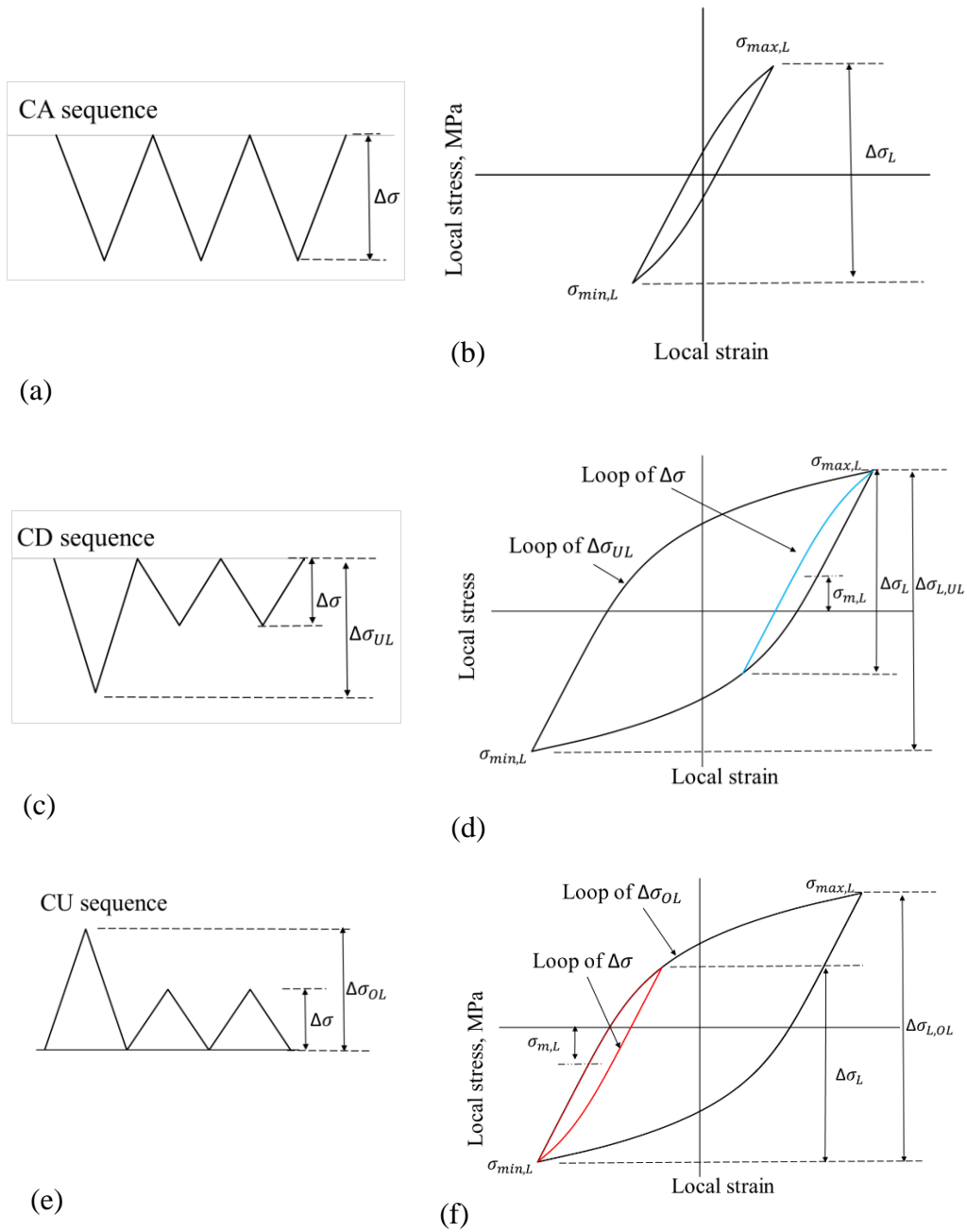


Figure 6.3 Local stress-strain hysteresis loop ahead of crack tip under various loading sequence: (a) CA sequence, (b) loop under CA sequence, (c) CD sequence, (d) loop under CD sequence, (e) CU sequence, (f) loop under CU sequence.

being at -1 for the fully reversed loop, as seen in Figure 6.3(b). $\sigma_{min,L}$ and $\sigma_{max,L}$ are the minimum and maximum local stress, respectively. However, the local stress ratio corresponding to $\Delta\sigma$ under a VA loading sequence, R'_L , is either increased or decreased after considering the local residual mean stress, $\sigma_{m,L}$, and can be estimated by:

$$R'_L = \frac{\sigma_{min,L} + \sigma_{m,L}}{\sigma_{max,L} + \sigma_{m,L}} \quad (6.11)$$

In this case, the sequence factor, H , was developed by considering the changes in the local stress ratio:

$$H = \left[\frac{U(R'_L)}{U(R_L)} \right]^L \quad (6.12)$$

where $U(R)$ is the function that considers the effect of the stress ratio (Equation 6.8). L is a best-fit parameter, which can be determined by experimental results, to be discussed later.

6.7.3.3 Calculation of local stress

The local stress ahead of the crack tip at each loading cycle was calculated using the model developed by Ghahremani and Walbridge [65]. In this model, a cyclic Ramberg-Osgood material model is used to determine the stresses and strains for each load cycle:

$$\Delta\varepsilon_L = \frac{\Delta\sigma_L}{E} + 2\left(\frac{\Delta\sigma_L}{2K'}\right)^{1/n'} \quad (6.13)$$

where $\Delta\varepsilon_L$ and $\Delta\sigma_L$ are the changes in the local strain and stress, respectively, and $K' = 960$ and $n' = 0.16$ are material constants, which are estimated using the following equations [176]:

$$\begin{aligned} K' &= \sigma_y(0.002)^{-n'} \\ n' &= z/v \\ z &= -0.1667 \log\left(2.1 + \frac{917}{\sigma_{UTS}}\right) \\ v &= -0.6 \end{aligned} \quad (6.14)$$

Neuber's rule is used to calculate strain histories at various crack depths below the surface of the weld toe.

$$\Delta\sigma_L \Delta\varepsilon_L = \frac{(k_p \Delta\sigma)^2}{E} \quad (6.15)$$

where $\Delta\sigma$ is the nominal applied stress range and k_p is the stress concentration factor that considers the presence of the crack in the weld toe. The relationship between k_p and the ratio of crack depth to the plate thickness (a/T) was established based on an FEA analysis where a 2D model was used [65], as shown in Figure 6.4. The 2D solution for M_k given in BS 7910 is also plotted in this figure for comparison and a good agreement can be observed. In this case, an assumption was made herein that if k_p is estimated based on a 3D model, the result will be also comparable with M_k using 3D solutions given in BS 7910. In the present study, therefore, k_p was simply assumed to be equal to the value of M_k used in the model.

6.7.3.4 Estimation of parameter L

The five sets of experimental FCG data reported in Study I [5], regarding the fatigue crack length at the indicated number of cycles, were selected as the reference data to determine the value of parameter L in Equation 6.10. For each set of data, the fatigue life, i.e., the number of cycles for the crack grows from the initial to the final size, was calculated using the model developed, and a best-fit L was determined by repeating the calculations multiple times with various L values until the calculated fatigue life is comparable with the experimental result.

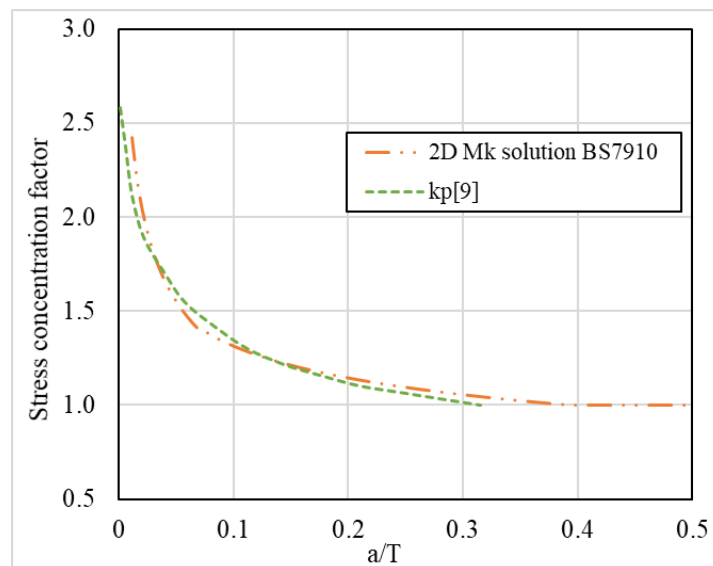


Figure 6.4 Comparison between stress concentration factor M_k estimated using 2D solutions given in BS 7910 and k_p calculated based on 2D FEA model.

Details of these five sets data in Study I [5] and the calculated results are given in Table 6.2, from which it can be seen that except the value for the data obtained from specimen F05 (i.e.

$L=0.67$), the best-fit L for the rest of the four sets of data are similar, ranging between 0.32 and 0.41. The sudden rise in the value of parameter L for specimen F05 may be due to the relatively large initial crack size in the specimen, resulting in the remained fatigue life involves a large percentage of number of cycles where the FCG is in stage III. As the model developed is only applicable in stage II, the value of 0.67 is not proper. Hence, in this case, the value of parameter L was alternated to the average of these four similar values, being at 0.38.

Table 6.2 Comparison of the experimental fatigue lives and those predicted using either best-fitted or average value of parameter L

Specimen ID	Initial length (mm)	Final length (mm)	Experimental fatigue life (Blocks)	Best-fit L	Calculated fatigue life with best-fit L (Blocks)	Calculated fatigue life with average $L = 0.38$ (Blocks)
F04	14.0	23	258	0.32	264	238
F05	25.0	40	86	0.67	86	185
F08	12.0	40	319	0.41	325	359
F13	4.0	29	554	0.39	557	581
F15	1.5	22	716	0.39	719	746

The fatigue lives and fatigue crack growths for these five specimens were re-calculated and are plotted against experimental results in Figures 6.5 and 6.6, respectively. It can be seen that except for specimen F05, all predictions for other specimens agree well with the experimental results. Therefore, the value of parameter L is assumed to be constant at 0.38 in further calculations of FCG under VA loading sequences.

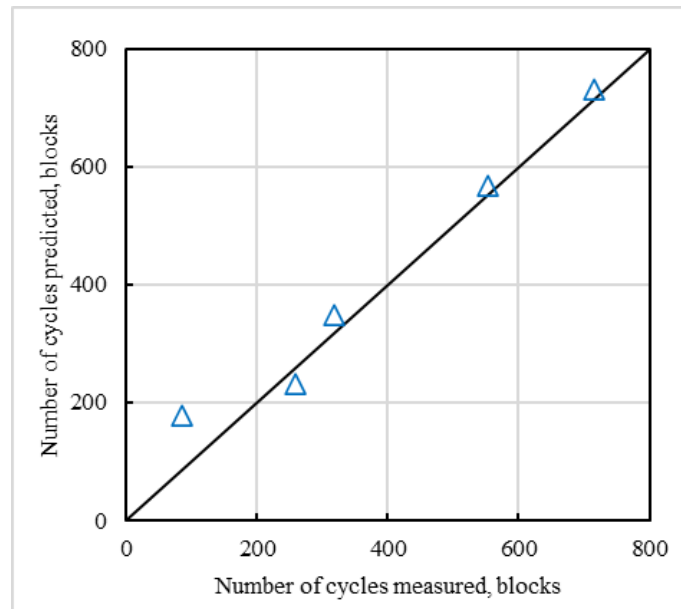


Figure 6.5 Comparison between experimental fatigue lives and that predicted using model developed with $L = 0.38$.

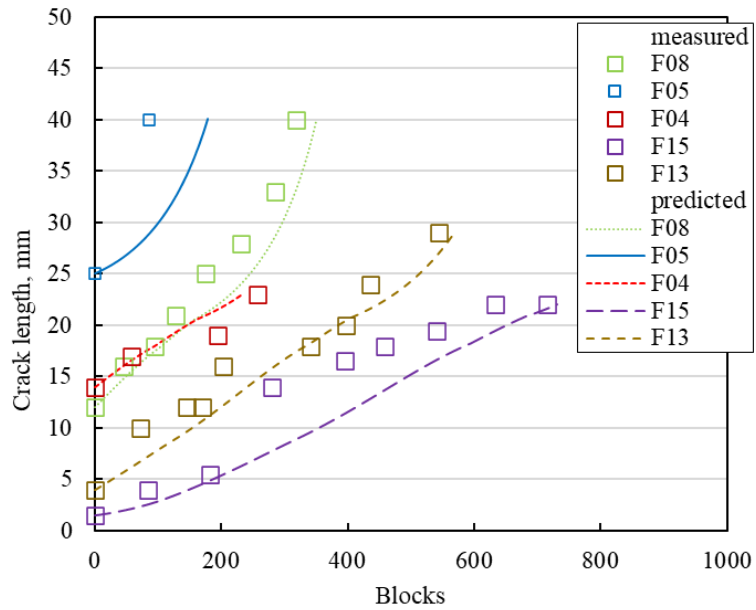


Figure 6.6 Comparison between measured and predicted fatigue crack propagation with $L = 0.38$.

6.8 Model validation

To validate the model developed, experimental FCG data was collected from the present study, Study I [5] and IV [13]. There were eleven sets of FCG data under CD loading sequences, where six sets from the present study and five sets from Study IV. Under CU loading sequences, six sets of FCG data were selected from the present study and Study I with three sets from each. The validation results are presented below.

6.8.1 Validation under cycling down loading sequences

The comparison between the experimental FCG measured in the present study and that predicted using the model developed is shown in Figure 6.7, where it can be seen that:

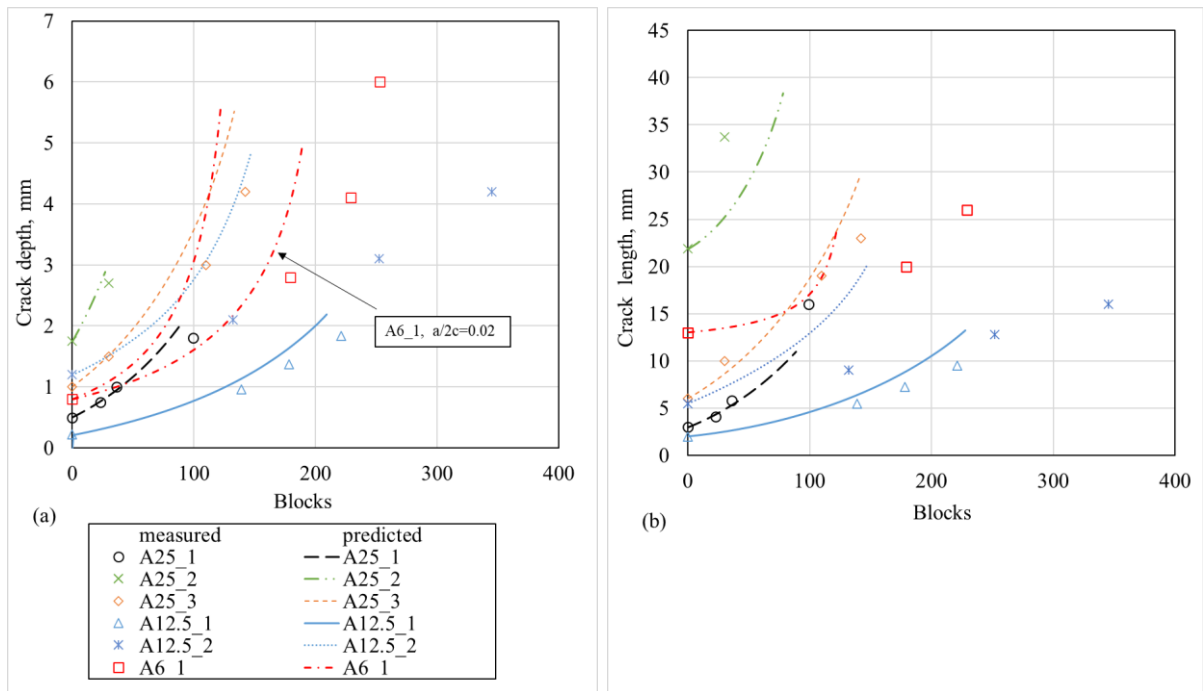


Figure 6.7 Comparison between the measured and predicted crack size under CD loading sequences for steel welded joints tested in the present study: (a) crack depth; (b) crack length.

- For 25mm-thick specimens, all predictions for the crack depth agree well with the experimental data, although they are slightly higher. In terms of the crack length, the predictions for A25_1 and A25_3 are still slightly conservative, which is in line with the calculations for the crack depth. However, predictions for A25_2 are lower than the experimental results.
- For 12.5mm-thick specimens, the predictions of both the crack depth and length for specimen A12.5_1 are comparable with the experimental data. However, those for specimen A12.5_2 are unduly conservative.
- For specimen A6_1, both the crack depth and length are over-estimated. This may be because the aspect ratio of the fatigue crack changed significantly during growth, increasing from an initial value of 0.06 to 0.2. However, the prediction was made only based on the initial value. Thus, the crack size was over predicted. In this case, another calculation was performed with the aspect ratio being 0.2, as shown in Figure 6.6 (a), with the new predicted result in line with the experimental one.

Figure 6.8 presents the comparison between experimental and predicted results of the FCG in the welded joints tested in Study IV [13]. It can be concluded that:

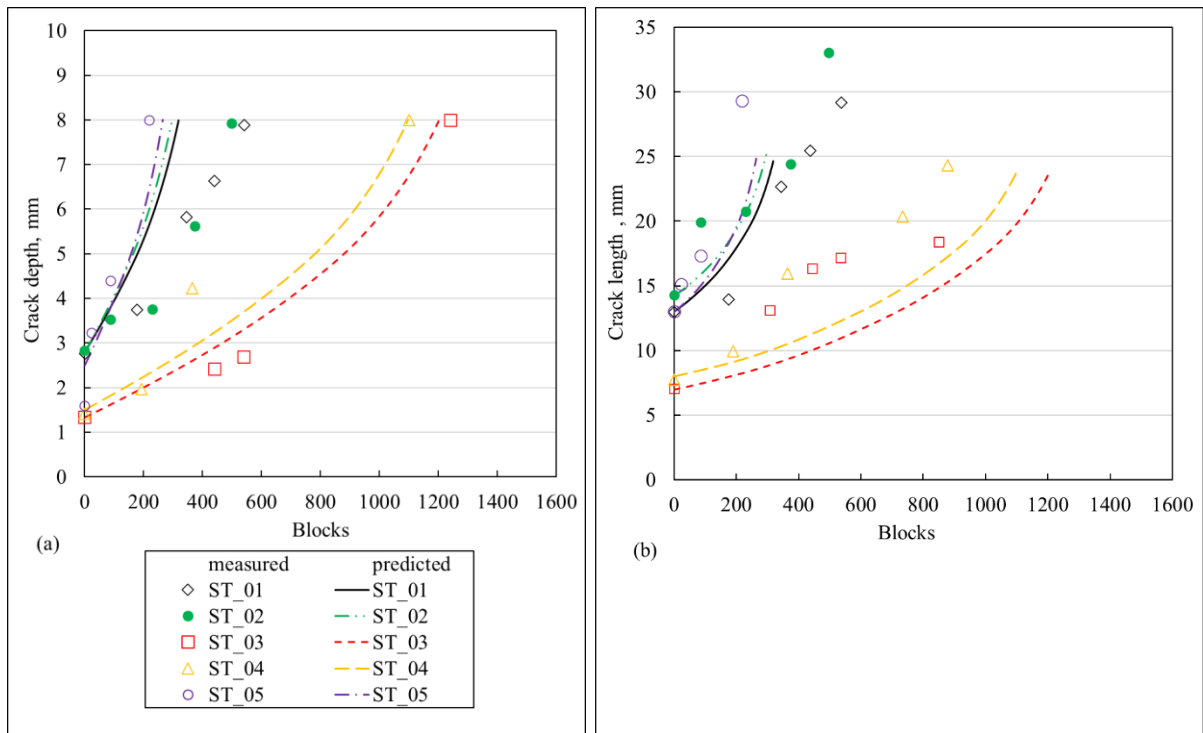


Figure 6.8 Comparison between the measured and predicted crack size under CD loading sequences for steel welded joints tested in Study II. (a) crack depth. (b) crack length.

- The FCG in specimens ST_03, ST_04 and ST_05 can be well predicted by the new model developed.
- For specimens ST_01 and ST_02, the FCGR in the crack depth is overestimated, as shown in Figure 6.7 (a). No typical FCGR acceleration is found in these two sets of data, and they can be satisfactorily predicted using the crack growth rate relationship that had been suitable for CA loading [13]. Surprisingly, however, the Miner's sums for these two specimens are still around 0.6, suggesting an apparent acceleration. The reason for this conflicting result is unclear by the current study and required for further research.

6.8.2 Validation under cycling up loading sequences

The FCG measured under CU sequences is plotted in Figure 6.9, against the results predicted using the new model developed. The following can be seen:

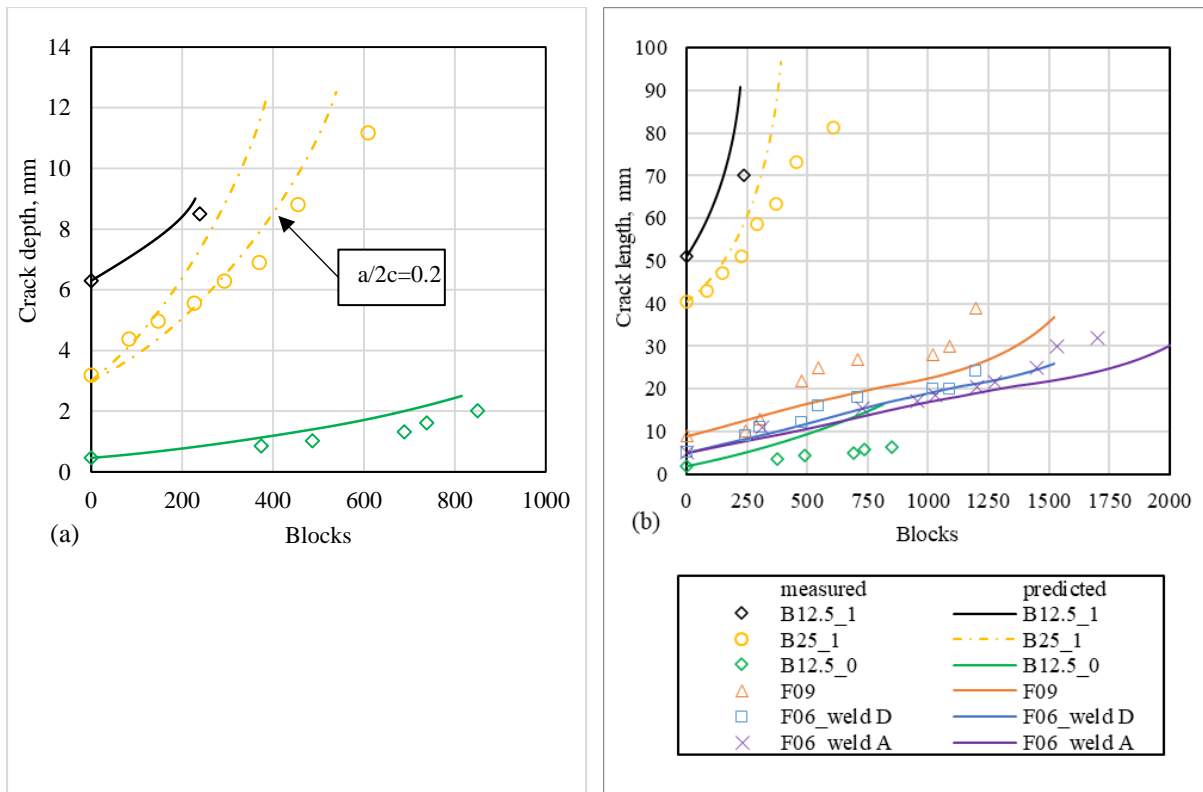


Figure 6.9 Comparison between the measured and predicted crack size under CU loading sequences for welded joints tested in the present study and Study I. (a) crack depth (b) crack length.

- Most of the predicted crack propagation under various CU loading sequences agree with the measurement. While predictions are slightly conservative for the specimens in the present study, and unconservative for the specimens in Study I [5].
- For Specimen B25_1, the crack growth is over-estimated, similar to that of Specimen A6_1. The aspect ratio of the fatigue crack in this specimen was 0.08 initially and increased to 0.2 as the crack grew. Therefore, one more calculation was carried out with an initial aspect ratio of 0.2, and the result predicted with this aspect ratio is close to the measured results, as illustrated in Figure 6.9 (a).

It is worth noting that when comparing Figures 6.2 to 6.9, similar deviations are obtained between the experimental and the predicted results using either the FCGR curve given in BS 7910 or the model developed in the present study. However, the predictions obtained using the latter would be better as both the mean stress effect and the sequence effect are considered.

6.9 Prediction of the fatigue endurance

The fatigue endurance of welded joints in the present study, study I [5], III [184] and IV [13], under either CD or CU loading sequences, were also estimated using the new model developed. The average initial flaw depth is assumed to be 0.15mm [5,7] for all welded joints. For the joints with longitudinal fillet welded attachments, the final crack depth and the aspect ratio of fatigue crack are the plate thickness and 0.25, respectively, while for welded joints containing transverse attachments, they are half-plate thickness and 0.2, respectively.

The calculated fatigue endurances are given in Table 6.3 and plotted in Figure 6.10, along with experimental results. It can be seen that the model can reasonably predict the fatigue life of welded joints under either CD or CU loading sequences with the Miner's sum mainly ranging between 1 to 2, which is similar to the predictions based on the mean stress correction model developed in Chapter 5.

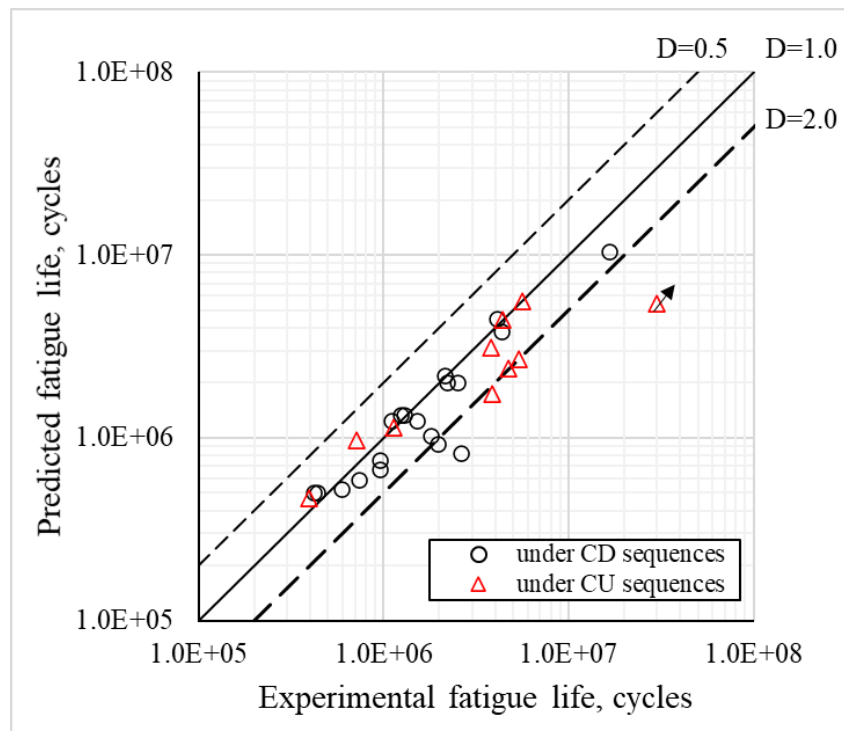


Figure 6.10 Comparison of fatigue endurance of welded joints between experimental and calculations based on the model developed under either CD or CU loading sequences.

Table 6.3 Comparison of fatigue endurance between experimental data and prediction based on the fracture mechanics model developed in the present study.

VA loading sequence	Data source	Specimen ID	Experimental fatigue life		Predicted fatigue life	
			Blocks	Cycles	Blocks	Cycles
CD	Present study	A12.5_1	409	9.47E+05	328	7.60E+05
		A12.5_2	1128	2.61E+06	358	8.29E+05
		A12.5_3	1863	4.31E+06	1660	3.84E+06
		A25_1	254	5.88E+05	225	5.21E+05
		A25_2	315	7.30E+05	256	5.93E+05
		A25_3	413	9.57E+05	290	6.72E+05
		A6_1	851	1.97E+06	403	9.33E+05
		A6_2	778	1.80E+06	444	1.03E+06
	Study I	F03	1053	1.10E+06	1094	1.25E+06
		F15	1441	1.50E+06	1094	1.25E+06
		F04	1021	2.21E+06	876	2.02E+06
		F13	1158	2.51E+06	876	2.02E+06
		F05	822	4.10E+06	835	4.47E+06
		F08	1147	1.66E+07	685	1.05E+07
	Study IV	ST_01	1182	1.23E+06	1206	1.34E+06
		ST_02	1242	1.29E+06	1206	1.34E+06
		ST_03	2163	4.37E+05	2376	5.04E+05
		ST_04	2069	4.18E+05	2376	5.04E+05
		ST_05	983	2.13E+06	939	2.19E+06
	CU	Present study	B12.5_1	1903	4.41E+06	1913
B12.5_2			3328	5.34E+06	1687	2.71E+06
B25_1			2040	4.72E+06	1028	2.38E+06
B6_1			12996	3.01E+07	2351	5.44E+06
Study I		F-06	2592	5.62E+06	2643	5.57E+06
		F-09	3661	3.81E+06	3056	3.10E+06
Study III		XAV-1	376	3.82 E+06	170	1.73E+06
		XAV-2	111	1.13E+06	112	1.14E+06
		XAV-3	70	7.13E+05	95	9.67E+05
		XAV-4	39	3.97E+05	46	4.68E+05

6.10 Conclusions

A new analytical model was developed based on fracture mechanics to predict the fatigue crack growth rate (FCGR) in welded joints under VA loading sequences. The mean stress effect on FCGR was considered based on the effective stress ratio. In addition, this model is also able to consider the effect of VA loading sequence. By considering that the acceleration or retardation in FCGR under VA loading sequences is mainly attributed to the local residual mean stress that

generated in the reverse plastic zone ahead of the crack tip, the local residual mean stress was estimated, and a new parameter was proposed accordingly to quantify its influence on FCGR.

The model was validated by comparing the experimental results for two types of welded joints under various VA loading sequences. It is found that this model can well improve the prediction of FCGR under either CD or CU loading sequences. For welded joints with transverse fillet welded joints, taking the aspect ratio as 0.2 can ensure prediction accuracy, although its actual value varies during the crack growth. A good agreement was also observed between the fatigue endurance from experiments and model predictions, with D value ranging between 1 to 2. These predictions agree well to those obtained based on the mean stress correction model developed in Chapter 5.

Chapter 7 Conclusions, recommendations, and future works

The summary and conclusions presented in this chapter are divided into to four main areas according to the research works involved in the present study, including (I) the fatigue behaviour of both ultrasonic impact treated and as-welded specimens under variable amplitude loading spectra, (II) residual stress measurements on both types welded joints, (III) development of mean stress correction models to predict fatigue life under VA loading sequences, and (IV) fracture mechanics analysis.

7.1 Conclusions of the research

7.1.1 Fatigue behaviour of both ultrasonic impact treated and as-welded specimens under variable amplitude loading spectra

An extensive fatigue testing program and analysis were performed to address the knowledge gap regarding the effect of the mean stress under VA loading spectra. Two VA loading spectra were designed and based on which various CD loading sequences with different maximum stresses were produced. Both as-welded and UIT specimens containing transverse non-load-carrying fillet welded attachments were tested under either axial or bending loading. The results were compared with the current fatigue design recommendations. The following conclusions are drawn based on the results of these tests and the related analysis:

- The fatigue life of the specimen with transverse fillet welded attachments is significantly degraded under a CD loading sequence with a high constant maximum stress, with the Miner's sum D much lower than unity, at only around 0.5. This result is similar to that obtained from the joints with either longitudinal fillet welded attachments or non-load carrying attachments on the edge of a plate.
- The value of Miner's sum D is found to depend on the maximum stress in a CD loading sequence. When the maximum stress is below a certain level, it increases with decreasing maximum stress further and the level depends on the plate thickness. When the maximum stress is reduced to zero, the welds are either run-out or D becomes significantly greater than unity.

- Limiting D to 0.5, as advised in BS 7608 for a loading sequence with an almost constant maximum tensile stress level, would be unduly conservative in some circumstances.
- Although a CD sequence is usually expected to be more damaging, a CU sequence could cause more damages than a CD sequence does when the applied static axial stress is either zero or low in tension under a bending mode.
- Similar to the CD loading sequence, the minimum stress in a CU loading sequence can influence the fatigue life of a specimen – the lower the minimum stress, the longer the fatigue life.
- Although not conclusive, the test results seem to follow a general trend that the fatigue performance is inversely proportional to the plate thickness under VA loading sequences, even under axial loading, which agrees with the results reported for CA loading.
- The fatigue life of welded joints can be significantly improved using the UIT technique. The magnitude of the improvement depends on the maximum stress applied under the CD loading sequence.
- The improvement in fatigue performance of UIT specimens is observed even when the maximum stress in the CD sequence exceeded 80% of the SMYS of the material.

7.1.2 Residual stress measurements

Residual stress measurements were conducted on both as-welded and UIT specimens using either a destructive technique centre-hole drilling (CHD) or a non-destructive method X-ray diffraction (XRD), respectively. The initial residual stress in specimens of three plate thicknesses under the untested condition and the residual stress relaxation after certain loading cycles were investigated. Based on the measurement results, a discussion was made mainly on the effect of residual stresses on the fatigue performance of welded joints under different VA loading sequences. In addition, the suitability of the measurement method and the relationship between the magnitude of residual stress and the plate thickness was discussed. On the basis of these measurements and analysis, the following conclusions can be drawn:

- The measurement results obtained using the XRD method exhibit large scatters comparing with those from the CHD method, and no general conclusions can be deduced from the former. In contrast, results obtained using the CHD technique are more reliable based on which the subsequent analysis is conducted.
- The initial residual stress in all specimens is much lower than SMYS of the material and generally proportional to the plate thickness, with the average value in 6mm-, 12.5mm- and 25mm-thick specimens being 83, 122 and 233MPa, respectively.
- Residual stress can be reduced after cyclic loading, even the maximum tensile is only 150MPa (less than half of the SMYS). The relaxation mainly takes place in the first two cycles, and further loading cycles only lead to a small residual stress reduction.
- Compressive loading produces similar residual stress relaxation as tensile loading does. However, this is based on limited test data. Further work is required to confirm this observation.
- When the maximum stress in a CD sequence below a certain level, the remaining residual stress in the welds after relaxation cannot maintain the actual mean stress at a high level. In a CU or CM loading sequence, the actual maximum stress for the small loading cycles is lower than that for the largest loading cycle due to residual stress relation. Therefore, it recommends considering the effective mean stress in the fatigue life assessment under VA loading sequences.

7.1.3 Development of the mean stress correction model to predict the fatigue life under variable amplitude loading spectra

Mean stress correction models were established based on three conventional models, i.e., Goodman, Gerber and Morrow, in order to predict the fatigue life of welded joints under VA loading sequences. In contrast to the conventional models, a reference maximum stress was adopted as the independent variable. In addition to the mean stress effect, a novel factor, which could take the effect of different VA loading sequences into consideration on the fatigue life, was included in the new models based on the fatigue testing results. The models were validated by the data obtained from the present study, and those from the literature. The conclusion drawn from the results are as follows:

- The sequence factor for either CD or CM sequence is constant, being at 0.5, which means the fatigue crack growth rate caused by the minor loading cycles in these two types of VA loading sequences could be accelerated when compared with that caused by the same loading cycles in a CA loading sequence.
- For a CU loading sequence, the sequence factor is a linear function of the overload ratio (maximum stress range/minimum stress range). When the overload ratio is higher than five, the sequence factor is larger than unity, suggesting the FCGR is retarded. When the overload ratio is lower than five, the factor is lower than unity, leading to an accelerated FCGR.
- Under CD sequences, a good agreement is observed between the experimental results and predictions given by the models developed, with the Miner's sum D mostly ranging between 0.5 to 1.5.
- Under a CU loading sequence, the model developed based on Gerber and Morrow equation give a reasonable conservative prediction for the fatigue life, with the most of the D values falling within the range of 0.5 to 1.5.
- Under a CM loading sequence, results predicted using Gerber and Morrow methods agree well with the experimental results, with the D ranging between 1 and 1.5.

7.1.4 Fracture Mechanics analysis

An analytical model was developed based on Fracture Mechanics to investigate the influence of different VA loading sequences on the fatigue crack growth. The stress intensity factor, ΔK , in the original Paris' Law was replaced by an effective stress intensity factor, ΔK_{eff} , to take into account the effect of both the mean stress and the VA sequence. ΔK_{eff} was developed according to the local residual mean stress mechanism. This model was validated by the experimental results from the present study and those published in the open literature. The following conclusions can be drawn:

- The model predictions are in reasonable agreement with the fatigue crack growth measured in steel welded joints with either transverse and longitudinal fillet welded attachments under either CD or CU sequence.

- Although the crack aspect ratio may increase significantly in the welded joints with transverse attachments during fatigue testing, the prediction agrees with the experimental results when an initial aspect ratio of 0.2 is assumed.
- By assuming an initial crack-like flaw of 0.15mm deep and the final critical crack depth either equal to the plate thickness for specimens with longitudinal attachments or to the half-plate thickness with transverse attachments, the fatigue life predicted by the model is in a reasonable agreement with the experimental results of the two types of welded joints under either CD or CU loading sequences, with the D value ranging between 1 and 2.

7.2 Fatigue design recommendations for welded joints under variable amplitude loading spectra

- Test results obtained in the present study supports limiting the Miner's sum to 0.5 for Class F detail under the VA loading sequences, as advised in the BS 7608, provided that the sequence contains a constant maximum tensile stress (CD sequence) or fully-tensile stress cycling about a high tensile mean stress (CM sequence).
- However, the results also suggest caution is needed when the maximum stress in the CD sequence is at a low level, since the Miner's sum D , at fatigue failure, could be significantly higher than 0.5. It would strongly recommend to estimating the actual mean stress for the loading cycles involved in the given VA loading sequence; thus, in addition to the sequence effect, the effect of mean stress should be considered accordingly in the fatigue assessment.
- In the case of the CU loading sequence, $D = 1$ may not be conservative. A proper D should be determined by considering the combined effect of the mean stress and the particular loading sequence on the fatigue performance of welded joints. The mean stress effect trends to yield $D > 1$ because the actual mean stresses for minor cycles are expected to be lower than those under the CA loading due to the relaxation of residual stresses under the major cycles. For the sequence effect, although it is generally found to cause retardation in the fatigue crack growth, which results in $D > 1$, experimental results obtained in the present research and from the literature show that the CD

sequence appears to be able to cause the fatigue crack growth to accelerate in some circumstances, leading to $D < 1$ at failure.

7.3 Recommendations for future works

- The above conclusions are all based on the experimental results produced in the laboratory with small scale specimens, which can be further validated by data collected from full-scale load-bearing structures experienced in-service VA loading spectra such as gas storage vessels, gas turbine blades, railway lines and bridges.
- The effect of mean stress on the fatigue life of UIT welded joints should be further investigated using a VA loading spectrum where the equivalent CA stress range is fairly high, leading to reasonable test times.
- Further investigation on the residual stress and its relaxation under VA loading for UIT specimens is recommended. Data on the fatigue life and the crack propagation can thus be used to validate the new methods developed in the present research. The crack initiation life of a UIT specimen can also be investigated.
- In order to obtain more accurate justification for the life improved welded joints, S-N curves for UIT specimen should be produced based on testing the UIT specimens as the fatigue life predicted basing on the improvement guidance may be unduly conservative.
- The equations/models proposed to predict the fatigue crack growth have been validated by experimental data produced only from surface cracks. Other types of cracks, such as through-thickness and edge cracks, etc., should be tested to confirm the suitability of the models.
- In addition to the Miner's rule and LEFM approach advised in the fatigue design codes, there are a wide range of nonlinear cumulative damage and life prediction models which may provide a more satisfying results in some circumstances. Therefore, it worth to consider using them to analysis the test results. Especially those can take into account both load sequence and interaction effects.

- The proposed relationship between the sequence factor and the CU loading sequence is for those CU sequences where various stress ranges are applied in a random order, with R_{Pi} ranging between 3 and 17. Whether this relationship is appropriate for other CU sequences with different features, such as R_{Pi} out of this range, or stress ranges applied in a particular order, is unknown, and further studies are recommended.

Reference

- [1] BS 7608:2014+A1:2015. Guide to fatigue design and assessment of steel products. London: British Standards Institution; 2014.
- [2] Gurney TR. Thickness effect in relatively thin welded joints. Offshore Technology Report. Health and Safety Executive; 1995.
- [3] Tilly GP. Fatigue of land-based structures. *Int J Fatigue* 1985;7:67–78. doi:10.1016/0142-1123(85)90036-2.
- [4] Dahle T. Spectrum fatigue life of welded specimens in relation to the linear damage rule. *Fatigue under Spectr Load Corros Environ* 1993:133–147.
- [5] Zhang Y-H, Maddox SJ. Investigation of fatigue damage to welded joints under variable amplitude loading spectra. *Int J Fatigue* 2009;31:138–52. doi:10.1016/J.IJFATIGUE.2008.04.006.
- [6] Gurney TR. Cumulative damage of welded jointse. Woodhead Publishing; 2006.
- [7] Booth G, Maddox S. Correlation of fatigue crack growth data obtained at different stress ratios. *Mech. Fatigue Crack Clos.*, 100 Barr Harbor Drive, PO Box C700, West Conshohocken, PA 19428-2959: ASTM International; 2009, p. 516-516–12. doi:10.1520/stp27229s.
- [8] Ding Z, Wang X, Gao Z, Bao S. An experimental investigation and prediction of fatigue crack growth under overload/underload in Q345R steel. *Int J Fatigue* 2017;98:155–66. doi:10.1016/j.ijfatigue.2017.01.024.
- [9] Schijve J, Skorupa M, Skorupa A, Machniewicz T, Gruszczynski P. Fatigue crack growth in the aluminium alloy D16 under constant and variable amplitude loading. *Int J Fatigue* 2004;26:1–15. doi:10.1016/S0142-1123(03)00067-7.
- [10] Borrego LP, Ferreira JM, Pinho da Cruz JM, Costa JM. Evaluation of overload effects on fatigue crack growth and closure. *Eng Fract Mech* 2003;70:1379–97. doi:10.1016/S0013-7944(02)00119-4.
- [11] Silva FS. Fatigue crack propagation after overloading and underloading at negative stress ratios. *Int J Fatigue* 2007;29:1757–71. doi:10.1016/j.ijfatigue.2007.03.012.
- [12] Fleck NA. Fatigue crack growth due to periodic underloads and overloads. *Acta Metall* 1985;33:1339–54. doi:10.1016/0001-6160(85)90244-5.
- [13] Doré MJ. An investigation of fatigue crack growth acceleration. PhD thesis. Open

- University, 2016.
- [14] Suresh S. Fatigue of materials. Cambridge Univ Press 1991.
 - [15] Chaboche JL. Continuum Damage Mechanics: Part I - General Concepts. J Appl Mech Trans ASME 1988;55:59–64.
 - [16] Hobbacher A. Recommendations for fatigue design of welded joints and components. 2008.
 - [17] Mughrabi H. Cyclic slip irreversibilities and the evolution of fatigue damage. Metall Mater Trans B Process Metall Mater Process Sci 2009;40:431–53. doi:10.1007/s11663-009-9240-4.
 - [18] Mughrabi H. Fatigue, an everlasting materials problem - still en vogue 2010. doi:10.1016/j.proeng.2010.03.003.
 - [19] Mughrabi H. Cyclic slip irreversibility and fatigue life: A microstructure-based analysis. Acta Mater 2013;61:1197–203. doi:10.1016/J.ACTAMAT.2012.10.029.
 - [20] Shen Ho H, Risbet M, Feaugas X. A cyclic slip irreversibility based model for fatigue crack initiation of nickel base alloys n.d. doi:10.1051/mateconf/201816504002.
 - [21] Risbet M, Feaugas X, Guillemer-Neel C, Clavel M. Use of atomic force microscopy to quantify slip irreversibility in a nickel-base superalloy. Scr Mater 2003;49:533–8. doi:10.1016/S1359-6462(03)00357-9.
 - [22] Risbet M, Feaugas X. Some comments about fatigue crack initiation in relation to cyclic slip irreversibility. Eng Fract Mech 2008;75:3511–9. doi:10.1016/J.ENGFRACTMECH.2007.04.014.
 - [23] Cretegnny L, Saxena A. AFM characterization of the evolution of surface deformation during fatigue in polycrystalline copper. Acta Mater 2001;49:3755–65. doi:10.1016/S1359-6454(01)00271-3.
 - [24] Sun B, Guo Y. High-cycle fatigue damage measurement based on electrical resistance change considering variable electrical resistivity and uneven damage. Int J Fatigue 2004;26:457–62. doi:10.1016/J.IJFATIGUE.2003.10.004.
 - [25] Li R, Wang Y, Fu F. Research on Fatigue Damage and Affecting Factors of Defected Rock Mass Based on Ultrasonic Wave Velocity 1848;3651:1061–7.
 - [26] Sang G, Liu S, Elsworth D. Quantifying fatigue-damage and failure-precursors using ultrasonic coda wave interferometry. Int J Rock Mech Min Sci 2020;131:104366. doi:10.1016/J.IJRMMS.2020.104366.

- [27] Rao Govindaraju M, Strom A, Jiles DC, Biner SB. EVALUATION OF LOW-CYCLE FATIGUE DAMAGE IN STEEL STRUCTURAL COMPONENTS BY A MAGNETIC MEASUREMENT TECHNIQUE n.d.
- [28] Maddox SJ. Fatigue Strength of Welded Structures. 2nd ed. Elsevier; 1991. doi:10.1016/C2013-0-17455-7.
- [29] Der Norske Veritas. DNVGL-RP-C203. Fatigue Design of Offshore Steel Structures. Recomm Pract 2016:176.
- [30] BS7910. Guide to methods for assessing the acceptability of flaws in metallic structures. BSI; 2015. doi:10.1007/s13398-014-0173-7.2.
- [31] Schütz W. A history of fatigue. Eng Fract Mech 1996;54:263–300. doi:10.1016/0013-7944(95)00178-6.
- [32] Hobbacher AF. Recommendations for Fatigue Design of Welded Joints and Components. Int Inst Welding, Doc XIII-2151r4-07/XV-1254r4-07 2008. doi:10.1007/978-3-319-23757-2_8.
- [33] Lotsberg I. Fatigue design of marine structures. Cambridge University Press; 2016.
- [34] Maddox SJ. Variable amplitude fatigue tests on welded joints (TWI Report No. 3561/3/79). Cambridge: 1979.
- [35] Suresh. Fatigue of materials. Cambridge university press; 1998.
- [36] Lee J-M, Seo J-K, Kim M-H, Shin S-B, Han M-S, Park J-S, et al. Comparison of hot spot stress evaluation methods for welded structures. Int J Nav Archit Ocean Eng 2010;2:200–10. doi:10.2478/ijnaoe-2013-0037.
- [37] Al Zamzami I, Susmel L. On the use of hot-spot stresses, effective notch stresses and the Point Method to estimate lifetime of inclined welds subjected to uniaxial fatigue loading. Int J Fatigue 2018;117:432–49. doi:10.1016/j.ijfatigue.2018.08.032.
- [38] Sonsino CM, Fricke W, De Bruyne F, Hoppe A, Ahmadi A, Zhang G. Notch stress concepts for the fatigue assessment of welded joints - Background and applications. Int J Fatigue 2012;34:2–16. doi:10.1016/j.ijfatigue.2010.04.011.
- [39] Marquis GB. Fatigue assessment methods for variable amplitude loading of welded structures. Fract. Fatigue Welded Joints Struct., Elsevier; 2011, p. 208–38. doi:10.1533/9780857092502.2.208.
- [40] Sonsino CM. Fatigue testing under variable amplitude loading. Int J Fatigue 2007;29:1080–9. doi:10.1016/j.ijfatigue.2006.10.011.

- [41] Gao K, Liu G, Tang W. An improved manson-halford model for multi-level nonlinear fatigue life prediction. *Int J Fatigue* 2021;151:106393. doi:10.1016/J.IJFATIGUE.2021.106393.
- [42] Lv Z, Huang H-Z, Zhu S-P, Gao H, Zuo F. A modified nonlinear fatigue damage accumulation model n.d. doi:10.1177/1056789514524075.
- [43] EN 1999-1-3: Eurocode 9: Design of aluminium structures - Part 1-3: Structures susceptible to fatigue 2007 n.d.
- [44] Yang XH, Yao WX, Duan CM. The review of ascertainable fatigue cumulative damage rule. *Eng Sci* 2003;5:82–7.
- [45] Zhu SP, Liao D, Liu Q, Correia JAFO, De Jesus AMP. Nonlinear fatigue damage accumulation: Isodamage curve-based model and life prediction aspects. *Int J Fatigue* 2019;128:105185. doi:10.1016/j.ijfatigue.2019.105185.
- [46] Peng Z, Huang HZ, Wang HK, Zhu SP, Lv Z. A new approach to the investigation of load interaction effects and its application in residual fatigue life prediction. *Int J Damage Mech* 2016;25:672–90. doi:10.1177/1056789515620910.
- [47] Patil N, Mahadevan P, Chatterjee A. A constructive empirical theory for metal fatigue under block cyclic loading. *Proc R Soc A Math Phys Eng Sci* 2008;464:1161–79. doi:10.1098/RSPA.2007.0109.
- [48] Hectors K, De Waele W. Cumulative damage and life prediction models for high-cycle fatigue of metals: A review. vol. 11. 2021. doi:10.3390/met11020204.
- [49] Berger C, Eulitz K-G, Heuler P, Kotte K-L, Naundorf H, Schuetz W, et al. Betriebsfestigkeit in Germany — an overview. *Int J Fatigue* 2002;24:603–25. doi:10.1016/S0142-1123(01)00180-3.
- [50] Bogren J, Lopez Martinez L. Spectrum fatigue testing and residual stress measurements on non-load carrying fillet welded test specimens. In: Blom AF, editor. *Proc. Nord. Conf. Fatigue Under Spectr. Load. an Corros. Environ., EMAS*; 1993, p. 77–90.
- [51] Tai M, Miki C. Improvement effects of fatigue strength by Burr Grinding and Hammer Peening under variable amplitude loading. *Weld World* 2012;56:109–17. doi:10.1007/BF03321370.
- [52] Maddox S. Variable amplitude fatigue tests on welded joints. (TWI Report 3561/3/79). 1979.
- [53] Sonsino C M, Guminor P HA. Cumulative damage behaviour of magnesium welded

- joints under service loadings. *Mater. Compon. performance under Var. amplitude Load.*, 2009, p. 1013–20.
- [54] Maddox SJ. Fatigue design rules for welded structures. *Prog Struct Eng Mater* 2000;2:102–9. doi:10.1002/(SICI)1528-2716(200001/03)2:1<102::AID-PSE12>3.0.CO;2-A.
- [55] Pérez F. AASHTO LRFD 2010 Bridge Design Specifications 5th Ed. fifth. American Association of State Highway and Transportation Officials; n.d.
- [56] Berger C, Eulitz KG, Heuler P, Kotte KL, Naundorf H, Schuetz W, et al. Betriebsfestigkeit in Germany - An overview. *Int J Fatigue* 2002;24:603–25. doi:10.1016/S0142-1123(01)00180-3.
- [57] R6 Assessment of the integrity of structures containing defects, Revision 4 2001. doi:10.1016/0308-0161(88)90071-3.
- [58] Kihl DP, Sarkani S. Mean stress effects in fatigue of welded steel joints. *Probabilistic Eng Mech* 1999;14:97–104. doi:10.1016/S0266-8920(98)00019-8.
- [59] Qiang B, Li Y, Yao C, Wang X, Gu Y. Through-thickness distribution of residual stresses in Q345qD butt-welded steel plates. *J Mater Process Technol* 2018;251:54–64. doi:10.1016/j.jmatprotec.2017.08.001.
- [60] Andreassen MJ, Yu Z, Liu S, Nielsen JH. 02.08: The influence of plate thickness on the welding residual stresses from submerged arc welding in offshore steel structures. *Ce/Papers* 2017;1:499–504. doi:10.1002/cepa.86.
- [61] Chukkan JR, Wu G, Fitzpatrick ME, Zhang X, Kelleher J. Residual Stress Redistribution During Elastic Shakedown in Fillet Welded Plate. *Residual Stress*. 2018, vol. 6, Materials Research Forum LLC; 2018, p. 233–8. doi:10.21741/9781945291890-37.
- [62] NIMS. Data sheet on fatigue property of non-load-carrying cruciform welded joints of SM490B rolled steel for welded structure. Tokyo, Japan: 2011.
- [63] Suzuki T, Okawa T, Shimanuki H, Nose T, Ohta N, Suzuki H, et al. Effect of ultrasonic impact treatment (UIT) on fatigue strength of welded joints 2014. doi:10.4028/www.scientific.net/AMR.996.736.
- [64] Tehrani Yekta R, Ghahremani K, Walbridge S. Effect of quality control parameter variations on the fatigue performance of ultrasonic impact treated welds. *Int J Fatigue* 2013;55:245–56. doi:10.1016/j.ijfatigue.2013.06.023.
- [65] Ghahremani K, Walbridge S. Fatigue testing and analysis of peened highway bridge

- welds under in-service variable amplitude loading conditions. *Int J Fatigue* 2011;33:300–12. doi:10.1016/j.ijfatigue.2010.09.004.
- [66] Ghahremani K, Walbridge S, Topper T. A methodology for variable amplitude fatigue analysis of HFMI treated welds based on fracture mechanics and small-scale experiments. *Eng Fract Mech* 2016;163:348–65. doi:10.1016/j.engfracmech.2016.06.004.
- [67] Maddox S. Influence of tensile residual stresses on the fatigue behavior of welded joints in steel. *Residual Stress Eff. Fatigue*, 100 Barr Harbor Drive, PO Box C700, West Conshohocken, PA 19428-2959: ASTM International; 1982, p. 63-63–34. doi:10.1520/STP30099S.
- [68] Booth G. Constant amplitude fatigue tests on welded steel joints performed in air. *European Offshore Steels Research Seminar*; 1978.
- [69] NIMS. Data Sheets on fatigue crack propagation properties for butt welded joints of SB42 carbon steel plate for boilers and other pressure vessels: Effect of stress ratio. Tokyo, Japan: 1984.
- [70] NIMS. Data sheets on fatigue properties for butt welded joints of SPV50 steel plate for pressure vessels: Effect of stress ratio. Tokyo, Japan: 1985.
- [71] Sanger CL, McDonald RJ, Kurath P. Prediction of welding residual stresses and redistribution/relaxation due to cyclic loading. *SAE Tech Pap* 2005;2005:641–64. doi:10.4271/2005-01-1322.
- [72] McClung RC. A literature survey on the stability and significance of residual stresses during fatigue. *Fatigue Fract Eng Mater Struct* 2007;30:173–205. doi:10.1111/j.1460-2695.2007.01102.x.
- [73] Iida K, Yamamoto S, Takanashi M. Residual stress relaxation by reversed loading. *Weld Res Abroad* 1998;44:39–X.
- [74] Takanashi M, Kamata K, Lida K. Relaxation behavior of welding residual stresses by fatigue loading in smooth longitudinal butt welded joints. *Weld World* 2000;44:28–34.
- [75] Kim WS, Lotsberg I. Fatigue test data for welded connections in ship-shaped structures. *J Offshore Mech Arct Eng* 2005;127:359–65. doi:10.1115/1.2087507.
- [76] N. E. Frost KJM and LPP. *Metal Fatigue*. Clarendon Press, Oxford. 1974. n.d.
- [77] Rossini NS, Dassisti M, Benyounis KY, Olabi AG. Methods of measuring residual stresses in components. *Mater Des* 2012;35:572–88. doi:10.1016/j.matdes.2011.08.022.

- [78] Kandil F a, Lord JD, Fry a T, Grant P V. A review of residual stress measurement methods - A guide to technical selection. NPL Mater Cent 2001:1–42.
- [79] Pintschovius L. Determination of residual stresses by neutron diffraction. Mem Etudes Sci La Rev Metall 1989;86:723–8. doi:10.1016/s0026-0657(96)93572-9.
- [80] ASTM. Standard Test Method for Determining Residual Stresses by the Hole-Drilling Strain-Gage Method. ASTM Sandard. 2013. doi:10.1520/E0837-13A.
- [81] Stefanescu D, Truman CE, Smith DJ, Whitehead PS. Improvements in residual stress measurement by the incremental centre hole drilling technique. Exp Mech 2006;46:417–27. doi:10.1007/s11340-006-7686-8.
- [82] Xia Z, Kujawski D, Ellyin F. Effect of mean stress and ratcheting strain on fatigue life of steel. Int J Fatigue 1996;18:335–41. doi:10.1016/0142-1123(96)00088-6.
- [83] Kumbhar S V., Tayade RM. A Case Study on Effect of Mean Stress on Fatigue Life. Int J Eng Dev Res 2014;2:304–8.
- [84] Gaur V, Enoki M, Okada T, Yomogida S. A study on fatigue behavior of MIG-welded Al-Mg alloy with different filler-wire materials under mean stress. Int J Fatigue 2018;107:119–29. doi:10.1016/j.ijfatigue.2017.11.001.
- [85] Melters M. fatiguetoobox 2017. <http://fatiguetoobox.org/>.
- [86] Goodman J. Mechanics applied to engineering. vol. 5885. n.d.
- [87] Morrow J. Fatigue Design Handbook. 1968.
- [88] Dowling NE. Mean stress effects in stress-life and strain-Life fatigue. SAE Tech Pap Ser 2010;1. doi:10.4271/2004-01-2227.
- [89] Smith, K.N., Topper, T.H., Watson P. A stress–strain function for the fatigue of metals. J Mater 1970;5:767–78. doi:10.1179/1752270612Y.0000000008.
- [90] Dowling NE, Calhoun CA, Arcari A. Mean stress effects in stress-life fatigue and the Walker equation. Fatigue Fract Eng Mater Struct 2009;32:163–79. doi:10.1111/j.1460-2695.2008.01322.x.
- [91] Kovacs S, Beck T, Singheiser L. Influence of mean stresses on fatigue life and damage of a turbine blade steel in the VHCF-regime. Int J Fatigue 2013;49:90–9. doi:10.1016/j.ijfatigue.2012.12.012.
- [92] Lu S, Su Y, Yang M, Li Y. A modified walker model dealing with mean stress effect in fatigue life prediction for seroengine disks. Math Probl Eng 2018;2018:1–12. doi:10.1155/2018/5148278.

- [93] Berge S. On the effect of plate thickness in fatigue of welds. *Eng Fract Mech* 1985;21:423–35. doi:10.1016/0013-7944(85)90030-X.
- [94] Gurney TR. The influence of thickness on the fatigue strength of welded joints. *Proc 2nd Int. Conf. Behav. Offshore Struct.*, Imperial College, London, UK: 1979, p. 523–34.
- [95] Lotsberg I. Assessment of the size effect for use in design standards for fatigue analysis. *Int J Fatigue* 2014;66:86–100. doi:10.1016/j.ijfatigue.2014.03.012.
- [96] Ghahremani K. Fatigue assessment of repaired highway bridge welds using local approaches. PhD Thesis. Waterloo University. 2015.
- [97] Kirkhope KJ, Bell R, Caron L, Basu RI, Ma KT. Weld detail fatigue life improvement techniques. Part 1: Review. *Mar Struct* 1999;12:447–74. doi:10.1016/S0951-8339(99)00013-1.
- [98] Yildirim HC, Marquis GB. A round robin study of high-frequency mechanical impact (HFMI)-treated welded joints subjected to variable amplitude loading. *Weld World* 2013;57:437–47. doi:10.1007/s40194-013-0045-3.
- [99] Tryfyakov VI, Mikheev PP, Kudryavtsev YF, Reznik DN. Ultrasonic impact peening treatment of welds and its effect on fatigue resistance in air and seawater. *Proc. Annu. Offshore Technol. Conf.*, Publ by Offshore Technology Conference; 1993, p. 183–7. doi:10.4043/7280-ms.
- [100] Haagenen PJ, Statnikov ES, Lopez Martinez L, AB SS. Introductory fatigue tests on welded joints in high strength steel and aluminium improved by various methods including ultrasonic impact treatment (UIT). *IIW Doc* 1998;13:1748–98.
- [101] Statnikov ES, Muktepavel VO, Blomqvist A. Comparison of ultrasonic impact treatment (UIT) and other fatigue life improvement methods. *Weld World* 2002;46:20–32. doi:10.1007/BF03266368.
- [102] Mikkola E, Doré M, Marquis G, Khurshid M. Fatigue assessment of high-frequency mechanical impact (HFMI)-treated welded joints subjected to high mean stresses and spectrum loading. *Fatigue Fract Eng Mater Struct* 2015;38:1167–80. doi:10.1111/ffe.12296.
- [103] HUO L. Investigation of the fatigue behaviour of the welded joints treated by TIG dressing and ultrasonic peening under variable-amplitude load. *Int J Fatigue* 2005;27:95–101. doi:10.1016/j.ijfatigue.2004.05.009.
- [104] Hobbacher A. The use of fracture mechanics in the fatigue analysis of welded joints.

- Fract. Fatigue Welded Joints Struct., Elsevier; 2011, p. 91–112. doi:10.1533/9780857092502.1.91.
- [105] Anderson TL. Fracture Mechanics: Fundamentals and Applications, Fourth Edition. 2017.
- [106] Vivekanandan A, Ramesh K. Study of interaction effects of asymmetric cracks under biaxial loading using digital photoelasticity. *Theor Appl Fract Mech* 2019;99:104–17. doi:10.1016/J.TAFMEC.2018.11.011.
- [107] Phang Y, Ruiz C. Photoelastic determination of stress intensity factors for single and interacting cracks and comparison with calculated results. Part I: Two-dimensional problems. *J Strain Anal Eng Des* 1984;19:23–34. doi:10.1243/03093247V19I023.
- [108] Newman JC. A nonlinear fracture mechanics approach to the growth of small cracks. *Behav Short Crack Airframe Components, AGARD Conf Proc* 1983;5:1–26.
- [109] Panasyuk V, Dmytrakh I. Some Actual Problems of Fracture Mechanics of Materials and Structures. *Recent Adv Mech* 2011:413–35. doi:10.1007/978-94-007-0557-9_22.
- [110] Kachanov M. Elastic Solids with Many Cracks and Related Problems. *Adv Appl Mech* 1993;30:259–445. doi:10.1016/S0065-2156(08)70176-5.
- [111] Orynyak I V., Borodii M V., Torop VM. Approximate construction of a weight function for quarter-elliptical, semi-elliptical and elliptical cracks subjected to normal stresses. *Eng Fract Mech* 1994;49:143–51. doi:10.1016/0013-7944(94)90118-X.
- [112] Wang H, Liu X, Wang X, Wang Y. Numerical method for estimating fatigue crack initiation size using elastic–plastic fracture mechanics method. *Appl Math Model* 2019;73:365–77. doi:10.1016/J.APM.2019.04.010.
- [113] Irwin G. Fracture//Handbook of Physics. Berlin 1958;Springer V:551–90.
- [114] Irwin GR. Plastic zone near a crack and fracture toughness. *Sagamore Res Conf Proc* 1961;4:63–78.
- [115] Rice J. Mechanics of crack tip deformation and extension by fatigue. *Fatigue Crack Propag.*, ASTM International; 2009, p. 247-247–65. doi:10.1520/stp47234s.
- [116] Kalnaus S, Fan F, Jiang Y, Vasudevan AK. An experimental investigation of fatigue crack growth of stainless steel 304L. *Int J Fatigue* 31:840–9. doi:10.1016/j.ijfatigue.2008.11.004.
- [117] Kalnaus S, Fan F, Vasudevan AK, Jiang Y. An experimental investigation on fatigue crack growth of AL6XN stainless steel. *Eng Fract Mech* 2008;75:2002–19.

- doi:10.1016/j.engfracmech.2007.11.002.
- [118] Skorupa M, Schijve J, Skorupa A, Machniewicz T. Fatigue crack growth in a structural steel under single and multiple periodic overload cycles. *Fatigue Fract Eng Mater Struct* 1999;22:879–87. doi:10.1046/j.1460-2695.1999.00219.x.
- [119] Borrego LP, Costa JM, Ferreira JM. Fatigue crack growth in thin aluminium alloy sheets under loading sequences with periodic overloads. *Thin-Walled Struct* 2005;43:772–88. doi:10.1016/J.TWS.2004.11.001.
- [120] Skorupa M. Load interaction effects during fatigue crack growth under variable amplitude loading - a literature review. Part II: qualitative interpretation. *Fatigue Fract Eng Mater Struct* 1999;22:905–26. doi:10.1046/j.1460-2695.1999.00158.x.
- [121] Corbly DM, Packman PF. On the influence of single and multiple peak overloads on fatigue crack propagation in 7075-T6511 aluminum. *Eng Fract Mech* 1973;5:479–97. doi:10.1016/0013-7944(73)90034-9.
- [122] Tür YK, Vardar Ö. Periodic tensile overloads in 2024-T3 Al-alloy. *Eng Fract Mech* 1996;53:69–77. doi:10.1016/0013-7944(95)00116-D.
- [123] Yu M. Crack growth behavior of pipeline steels under variable pressure fluctuations in a near-Neutral PH environment. PhD Thesis. Ualberta university. 2015.
- [124] Salvati E, Sui T, Zhang H, Lunt AJG, Fong KS, Song X, et al. Elucidating the mechanism of fatigue crack acceleration following the occurrence of an underload. *Adv Eng Mater* 2016;18:2076–87. doi:10.1002/adem.201600069.
- [125] Zitounis V, Irving PE. Fatigue crack acceleration effects during tensile underloads in 7010 and 8090 aluminium alloys. *Int J Fatigue* 2007;29:108–18. doi:10.1016/j.ijfatigue.2006.02.048.
- [126] Zitounis V. Fatigue crack growth rates under variable amplitude load spectra containing tensile underloads. PhD Thesis. Cranfield University. Cranfield University, 2003.
- [127] Wheeler OE. Spectrum loading and crack growth. *J Fluids Eng Trans ASME* 1972;94:181–6. doi:10.1115/1.3425362.
- [128] Willenborg J, Engle RM, Wood HA. A crack growth retardation model using an effective stress concept. *Tech Memo 71-1-FBR* 1971:1–22.
- [129] Elber W. The significance of fatigue crack closure. *Damage Toler Aircr Struct* 1971:230-230–13. doi:10.1520/STP26680S.
- [130] Tvergaard V. Overload effects in fatigue crack growth by crack-tip blunting. *Int. J.*

- Fatigue, vol. 27, Elsevier; 2005, p. 1389–97. doi:10.1016/j.ijfatigue.2005.06.003.
- [131] Stewart AT. The influence of environment and stress ratio on fatigue crack growth at near threshold stress intensities in low-alloy steels. *Eng Fract Mech* 1980;13:463–78. doi:10.1016/0013-7944(80)90078-8.
- [132] Sharifimehr S, Fatemi A, Cha SC, Bae MK, Hong SH. Fatigue behavior of AHSS lap shear and butt arc welds including the effect of periodic overloads and underloads. *Int J Fatigue* 2016;87:6–14. doi:10.1016/j.ijfatigue.2015.12.009.
- [133] Khalil M, Topper TH. Prediction of crack-opening stress levels for 1045 as-received steel under service loading spectra. *Int J Fatigue* 2003;25:149–57. doi:10.1016/S0142-1123(02)00072-5.
- [134] Dabayeh AA, Topper TH. Changes in crack-opening stress after underloads and overloads in 2024-T351 aluminium alloy. *Int J Fatigue* 1995;17:261–9. doi:10.1016/0142-1123(95)00010-Q.
- [135] Hassanipour M, Verreman Y, Lantaigne J, Chen JQ. Effect of periodic underloads on fatigue crack growth in three steels used in hydraulic turbine runners. *Int J Fatigue* 2016;85:40–8. doi:10.1016/J.IJFATIGUE.2015.11.027.
- [136] Zhu SP, Huang HZ, Liu Y, He LP, Liao Q. A practical method for determining the Corten-Dolan exponent and its application to fatigue life prediction. *Int J Turbo Jet Engines* 2012;29:79–87. doi:10.1515/tjj-2012-0013.
- [137] Fatemi A, Yang L. Cumulative fatigue damage and life prediction theories: A survey of the state of the art for homogeneous materials. *Int J Fatigue* 1998;20:9–34. doi:10.1016/S0142-1123(97)00081-9.
- [138] Richart, FE, Newmark NM. A hypothesis for the determination of cumulative damage in fatigue. *Am Soc Test Mater* 1948;48:767–800.
- [139] S.M.Marco, W.L.Starkey. A concept of fatigue damage. *Trans ASME* 1954:627–32.
- [140] Manson SS, Halford GR. Practical implementation of the double linear damage rule and damage curve approach for treating cumulative fatigue damage. *Int J Fract* 1981;17:169–92. doi:10.1007/BF00053519.
- [141] Gao H, Huang HZ, Zhu SP, Li YF, Yuan R. A modified nonlinear damage accumulation model for fatigue life prediction considering load interaction effects. *Sci World J* 2014;2014. doi:10.1155/2014/164378.
- [142] Behavior—Analysis JP-CS-S, 1971 undefined. The effect of load interaction and

- sequence on the fatigue behavior of notched coupons. AstmOrg n.d.
- [143] Yuan R, Li H, Huang H, ... SZ-IJ of, 2015 undefined. A nonlinear fatigue damage accumulation model considering strength degradation and its applications to fatigue reliability analysis. JournalsSagepubCom 2015;24:646–62. doi:10.1177/1056789514544228.
- [144] Kwofie S, Rahbar N. A fatigue driving stress approach to damage and life prediction under variable amplitude loading. Int J Damage Mech 2013;22:393–404. doi:10.1177/1056789512449638.
- [145] Corten, H. T, and Dolan TJ. Cumulative Fatigue Damage. Proc. Intl. Conf. Fatigue Met. ASME, IME, 1956, p. 235.
- [146] FREUDENTHAL AM, HELLER RA. On Stress Interaction in Fatigue and a Cumulative Damage Rule. J Aerosp Sci 1959;26:431–42. doi:10.2514/8.8131.
- [147] Subramanyan S. A Cumulative Damage Rule Based on the Knee Point of the S-N Curve. J Eng Mater Technol 1976;98:316–21. doi:10.1115/1.3443383.
- [148] Jiao J, Lei H, Chen YF. Numerical simulation and experimental study on constant amplitude fatigue behavior of welded cross plate-hollow sphere joints. J Southeast Univ (English Ed 2018;34:62–70. doi:10.3969/J.ISSN.1003-7985.2018.01.010.
- [149] Rao JS, Pathak A, Chawla A. Blade Life: A Comparison by Cumulative Damage Theories. J Eng Gas Turbines Power 2001;123:886–92. doi:10.1115/1.1384879.
- [150] Peng Z, Huang HZ, Zhou J, Li YF. A new cumulative fatigue damage rule based on dynamic residual S-N curve and material memory concept. Metals (Basel) 2018;8. doi:10.3390/met8060456.
- [151] Schwab TD, Johnston CR, Oxland TR, Thornton GM. Continuum damage mechanics (CDM) modelling demonstrates that ligament fatigue damage accumulates by different mechanisms than creep damage. J Biomech 2007;40:3279–84. doi:10.1016/J.JBIOMECH.2007.04.014.
- [152] Kachanov LM. Rupture Time Under Creep Conditions. Int J Fract 1999 971 1999;97:11–8. doi:10.1023/A:1018671022008.
- [153] Rabotnov YN, Leckie FA, Prager W. Creep Problems in Structural Members. J Appl Mech 1970;37:249–249. doi:10.1115/1.3408479.
- [154] J. L Chaboche, A differential law for nonlinear cumulativ... - Google Scholar n.d. <https://scholar.google.com/scholar?q=J. L Chaboche, A differential law for nonlinear>

- cumulative fatigue damage, In *Materials and Building Research*, Paris Institut Technique Du Batiment Et Des Travaux Publies, Annales de IITBTP, 39 1974:117-124., (accessed September 17, 2021).
- [155] Bhattacharya B, Ellingwood B. A damage mechanics based approach to structural deterioration and reliability 1998. doi:10.2172/573315.
- [156] Mesmacque G, Garcia S, Amrouche A, Rubio-Gonzalez C. Sequential law in multiaxial fatigue, a new damage indicator. *Int J Fatigue* 2005;27:461–7. doi:10.1016/J.IJFATIGUE.2004.08.005.
- [157] Duyi Y, Zhenlin W. A new approach to low-cycle fatigue damage based on exhaustion of static toughness and dissipation of cyclic plastic strain energy during fatigue. *Int J Fatigue* 2001;23:679–87. doi:10.1016/S0142-1123(01)00027-5.
- [158] Santecchia E, Hamouda AMS, Musharavati F, Zalnezhad E, Cabibbo M, El Mehtedi M, et al. A Review on Fatigue Life Prediction Methods for Metals. *Adv Mater Sci Eng* 2016;2016. doi:10.1155/2016/9573524.
- [159] Peng Z, Huang H-Z, Zhu S-P, Gao H, Lv Z. A fatigue driving energy approach to high-cycle fatigue life estimation under variable amplitude loading. *Fatigue Fract Eng Mater Struct* 2016;39:180–93. doi:10.1111/FFE.12347.
- [160] Golos K, Ellyin F. A total strain energy density theory for cumulative fatigue damage 1988.
- [161] Golos K, Ellyin F. Generalization of cumulative damage criterion to multilevel cyclic loading. *Theor Appl Fract Mech* 1987;7:169–76. doi:10.1016/0167-8442(87)90032-2.
- [162] PARK SH, HONG S-G, LEE BH, LEE CS. FATIGUE LIFE PREDICTION OF ROLLED AZ31 MAGNESIUM ALLOY USING AN ENERGY-BASED MODEL. [Http://DxDoiOrg/101142/S0217979208050723](http://DxDoiOrg/101142/S0217979208050723) 2012;22:5503–8. doi:10.1142/S0217979208050723.
- [163] Fatemi A, Shamsaei N. Multiaxial fatigue: An overview and some approximation models for life estimation. *Int J Fatigue* 2011;33:948–58. doi:10.1016/j.ijfatigue.2011.01.003.
- [164] Zhu SP, Yu ZY, Correia J, De Jesus A, Berto F. Evaluation and comparison of critical plane criteria for multiaxial fatigue analysis of ductile and brittle materials. *Int J Fatigue* 2018;112:279–88. doi:10.1016/j.ijfatigue.2018.03.028.
- [165] Lu C, Melendez J, Martínez-Esnaola JM. A universally applicable multiaxial fatigue

- criterion in 2D cyclic loading. *Int J Fatigue* 2018;110:95–104. doi:10.1016/j.ijfatigue.2018.01.013.
- [166] Fatemi A, Socie DF. A Critical plane approach to multiaxial fatigue damage including out-of-phase loading. *Fatigue Fract Eng Mater Struct* 1988. doi:10.1111/j.1460-2695.1988.tb01169.x.
- [167] Neerukatti RK, Datta S, Chattopadhyay A, Iyyer N, Phan N. Fatigue crack propagation under in-phase and out-of-phase biaxial loading. *Fatigue Fract Eng Mater Struct* 2018;41:387–99. doi:10.1111/FFE.12690.
- [168] Misak HE, Perel VY, Sabelkin V, Mall S. Crack growth behavior of 7075-T6 under biaxial tension–tension fatigue. *Int J Fatigue* 2013;55:158–65. doi:10.1016/J.IJFATIGUE.2013.06.003.
- [169] Lee EU, Taylor RE. Fatigue behavior of aluminum alloys under biaxial loading. *Eng Fract Mech* 2011;78:1555–64. doi:10.1016/J.ENGFRACMECH.2010.11.005.
- [170] Jones DL, Poulouse PK, Liebowitz H. The effects of biaxial loading on the fracture characteristics of several engineering materials. *Eng Fract Mech* 1986;24:187–205. doi:10.1016/0013-7944(86)90051-2.
- [171] Yuuki R, Akita K, Kishi N. The effect of biaxial stress state and changes of state on fatigue crack growth behaviour. *Fatigue Fract Eng Mater Struct* 1989;12:93–103.
- [172] Jones DL, Eftis J, Force BA, Ntis B, D71 C, Washington T El. Fracture and fatigue characterization of aircraft structure materials under biaxial loading 1978.
- [173] KITAGAWA H, YUUKI R, TOHGO K. A fracture mechanics approach to high-cycle fatigue crack growth under in-lane biaxial loads.S. *Fatigue Fract Eng Mater Struct* 1979;2:195–206. doi:10.1111/J.1460-2695.1979.TB01355.X.
- [174] MEEK C. The influence of biaxial loading on the assessment of structure with defects. The university of Manchester, 2017.
- [175] Krolo P, Grandić D, Smolčić Ž. Experimental and numerical study of mild steel behaviour under cyclic loading with variable strain ranges. *Adv Mater Sci Eng* 2016;2016. doi:10.1155/2016/7863010.
- [176] Zhang Y-H, Maddox SJ. Fatigue life prediction for toe ground welded joints. *Int J Fatigue* 2009;31:1124–36. doi:10.1016/J.IJFATIGUE.2009.01.003.
- [177] Marquis GB, Barsoum Z. IIW recommendations on high frequency mechanical impact (HFMI) treatment for improving the fatigue strength of welded joints, 2016, p. 1–34.

- doi:10.1007/978-981-10-2504-4_1.
- [178] Sun X. Improved bending correction factor for fatigue assessment of welded joints. Welding Institute Member Report 1118/2019. 2019.
- [179] Heuler P, Klätschke H. Generation and use of standardised load spectra and load–time histories. *Int J Fatigue* 2005;27:974–90. doi:10.1016/J.IJFATIGUE.2004.09.012.
- [180] Fitzpatrick ME, Fry AT, Holdway P, Kandil FA, Shackleton J, Suominen and L. Determination of residual stresses by X-ray diffraction. Practice Guide. 2005.
- [181] Prevey PS. X-Ray diffraction residual stress techniques. *ASM Handb.*, 2018, p. 380–92. doi:10.31399/asm.hb.v10.a0001761.
- [182] Bader Q, Kadum E. Mean stress correction effects on the fatigue life behavior of steel alloys by using stress life approach theories. *Int J Eng Technol IJET-IJENS* 2014;14.
- [183] Zhang YH, Maddox SJ, Manteghi S. Verification of Class B S-N curve for fatigue design of steel forgings. *Int J Fatigue* 2016;92:246–61. doi:10.1016/j.ijfatigue.2016.07.015.
- [184] Ghahremani K, Walbridge S, Topper T. High cycle fatigue behaviour of impact treated welds under variable amplitude loading conditions. *Int J Fatigue* 2015;81:128–42. doi:10.1016/j.ijfatigue.2015.07.022.











Appendix A Geometry measurement on welds

The weld geometry for each plate thickness specimens was investigated using Wiki-scan welding inspection system, as shown in Figure A.1. One specimen from each plated thickness was randomly selected. In each specimen, two welds were measured in the mid-width section. Table A.1 summarises the measurement results.



Figure A.1 Wiki-scan welding inspection system

Table A.1 Wi-Ki scan measurements results (in mm and degree)

Thickness	Measurement Order										
		Leg1	Leg2	Leg1 Size1	Leg1 Size2	Throat	Convexity	Undercut 1	Undercut 2	Toe angle 1	Toe angle 2
6	1	9.6	8	8.1	7	5.4	-1.1	0.2	0	155	143
	2	8.5	7.4	6.2	7.2	4.7	-1.4	0.1	0.1	160	140
12.5	1	12.7	10.1	9.7	9.3	6.7	-1.7	0	0.1	155	137
	2	9.8	10.4	8	9.5	6.2	-1.3	0.3	0.1	152	149
25	1	16.4	16.9	16.1	13.7	10.5	-1.7	0.1	0.1	138	145
	2	18	14.7	16.3	12.1	9.7	-1.9	0.2	0.1	145	144

Appendix B The sketch of the rigs

In order to apply CD loading sequences with low maximum stress, i.e., 87.5MPa, fatigue tests were conducted in bending mode. A new rig was designed and manufactured in-house, allowing the application of the target constant axial loading for the fatigue testing.

The design sketching produced using SOLIDWORKS software at TWI is shown in Figure B.1. The rigs include two parts: top and side frames and they were connected using M16 bolts. The relevant dimensions are given in Figure B.2.

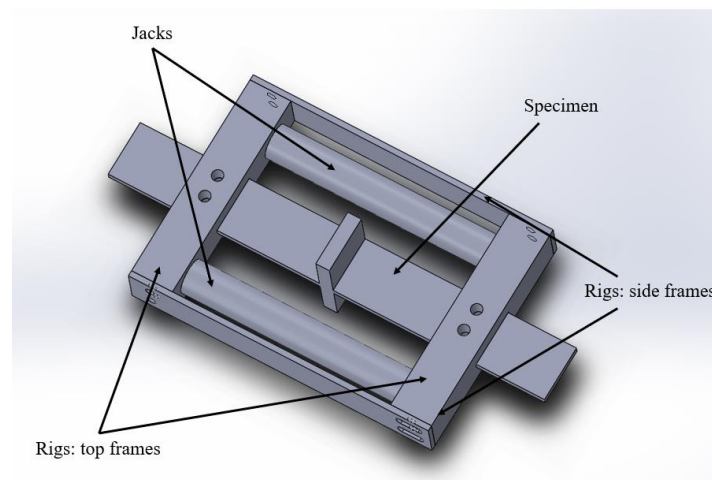


Figure B.1 Design sketching for rigs.

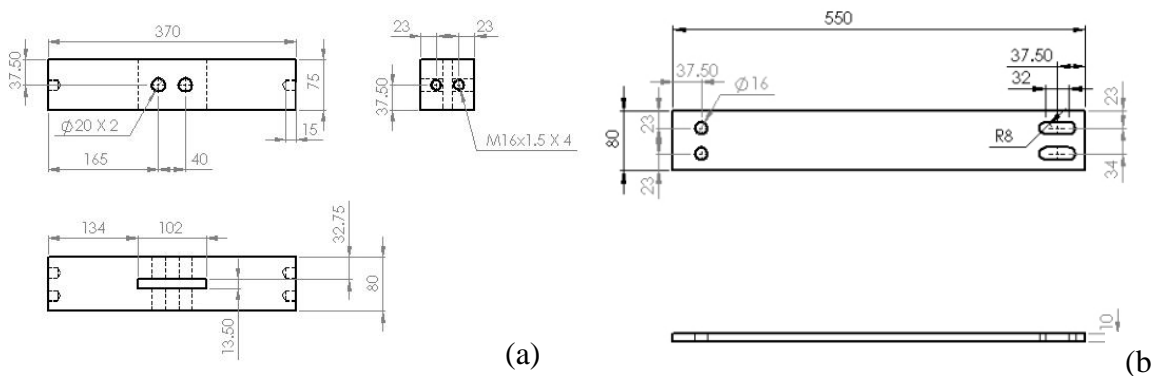


Figure B.2 Relevant dimensions of the rigs designed: (a) for top frames and (b) for side frames.

Appendix C Fracture surface

In order to collect the fatigue crack growth (FCG) data, the fracture surfaces of each welded joint tested were revealed after fatigue testing, then examined and photographed under a microscope at TWI. The photos of the fracture surface are shown below:

1. 6mm-thick specimen

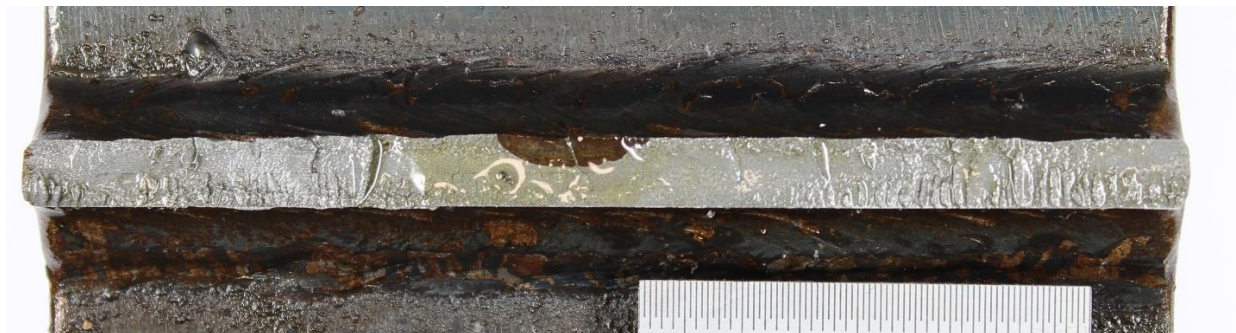
1.1 Specimen: A6_1



1.2 Specimen: A6_2

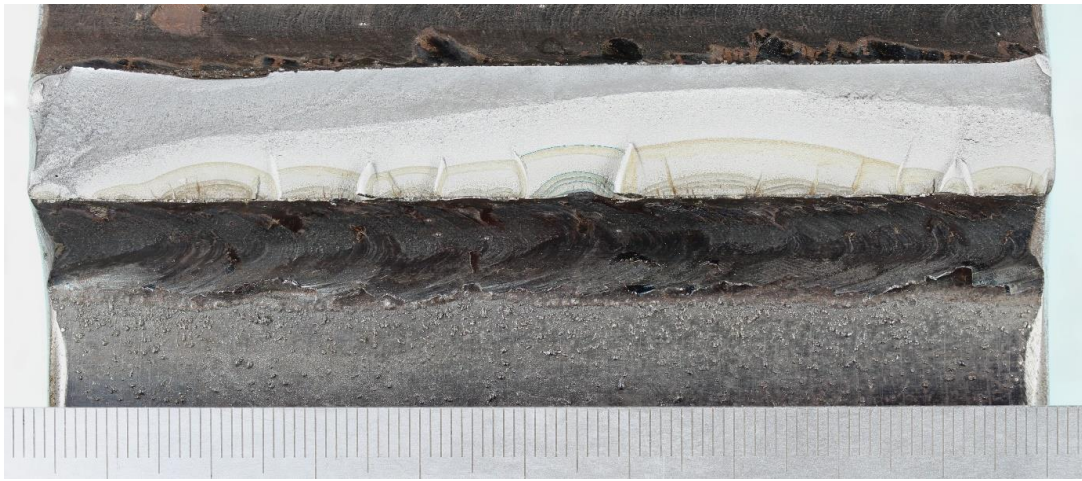


1.3 Specimen: B6_1 (break in liquid Nitrogen)



2. 12.5mm-thick specimen

2.1 Specimen: A12.5_1



2.2 Specimen: A12.5_2



2.3 Specimen: A12.5_3



2.4 Specimen: B12.5 _1 (break in liquid Nitrogen)



2.5 Specimen: B12.5 _2 (new spectrum)



3. 25mm-thick specimen

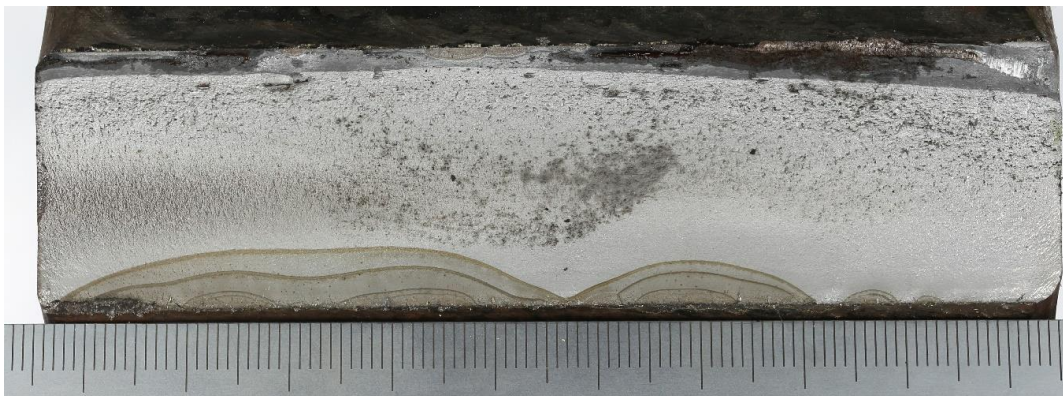
Specimen: A25_1



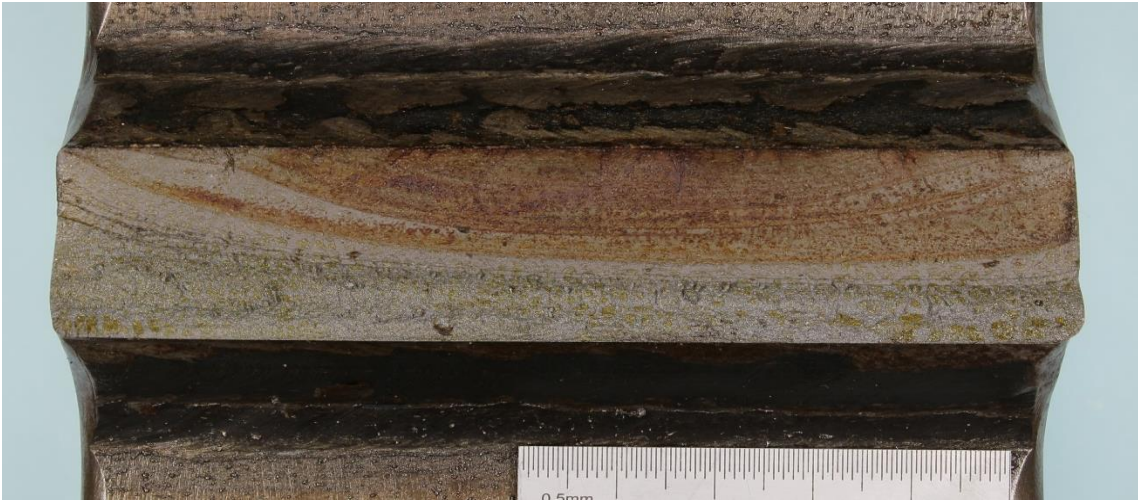
Specimen: A25_2



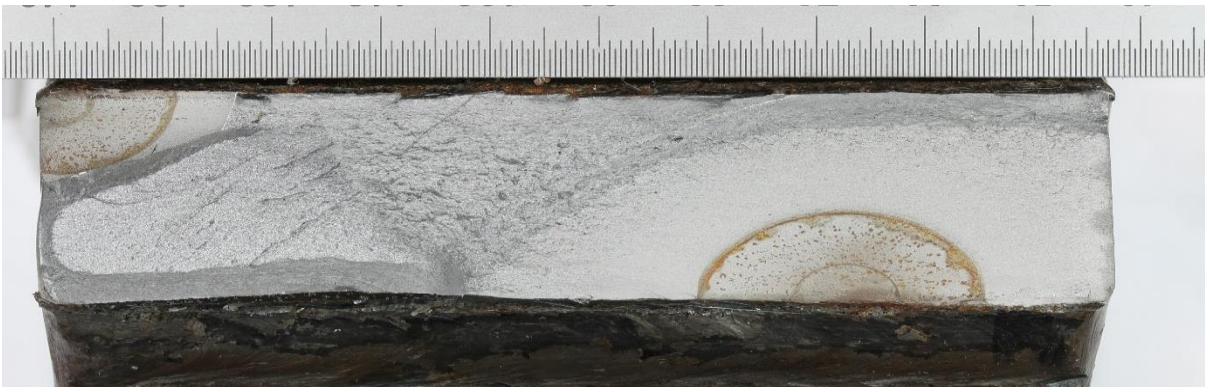
Specimen: A25_3



Specimen: B25_1 (break in liquid Nitrogen)



Specimen: UIT_A25_1



Appendix D Residual stress measurement location and results

Table D.1 summarises the residual stress measurements carried out at each weld in specimens of all three plate thicknesses. The weld ID was defined in Figure 4.5 and the locations of measurement and X_0 are defined in Figure 4.1. At some welds, measurements were only carried out at the locations along the weld toe (y-direction) to reduce measurement effort.

Table D.1 Details on the residual stress measurement on the as-welded specimen using the XRD method.

Plate thickness (mm)	Specimen ID	Weld ID	Locations of measurement (the direction points along with)	X_0 (mm)
6	XRD_AW_6_1	A	x y	4.0
		B	y	3.0
		C	x y	4.0
		D	y	4.0
12.5	XRD_AW_12.5_1	A	x y	1.0
		B	y	2.0
		C	x y	2.0
		D	y	2.0
	XRD_AW_12.5_2	A	x y	2.0
		B	y	2.0
		C	x y	1.5
		D	y	1.5
	XRD_AW_12.5_3	A	x y	1.0
		B	y	2.0
		C	x y	1.5
		D	y	2.5
	XRD_AW_12.5_4	A	y	1.0
		B	y	3.0
		C	y	1.5
		D	y	2.0
25	XRD_AW_25_1	A	x y	1.5
		B	y	1.5
	XRD_AW_25_2	A	x y	1.0
		B	y	1.0
		C	x y	1.0
		D	y	1.0
	XRD_AW_25_3	A	y	1.0
		B	y	1.0

Table D2 gives the residual stress measurement results obtained from different locations in the UIT specimen. The locations are defined in Figure 4.9.

Table D.2 Residual stress (RS) measurement results on UIT specimen using the XRD method.

Specimen ID	Weld ID	Condition	Location	RS (MPa)	Location	RS (MPa)
XRD_UIT_1	B	untested	P1	202 ± 73	P4	-494 ± 20
			P2	135 ± 85	P5	-263 ± 18
			P3	-449 ± 19	P6	-255 ± 88
	D	untested	P1	-251 ± 31	P4	-390 ± 18
			P2	-234 ± 56	P5	-186 ± 46
			P3	-409 ± 41	P6	-385 ± 25
XRD_UIT_2	A	after CD loading	P1	-146 ± 31	P4	-327 ± 15
			P2	-117 ± 3	P5	-377 ± 19
			P3	-131 ± 27	P6	-222 ± 15
	C	after CU loading	P1	-275 ± 57	P4	-193 ± 42
			P2	-223 ± 27	P5	-69 ± 58
			P3	-180 ± 40	P6	-273 ± 82
XRD_UIT_3	A	after axial loading	P1	-157 ± 39	P4	-310 ± 63
			P2	-74 ± 40	P5	-234 ± 42
			P3	-51 ± 26	P6	-339 ± 8

Appendix E Details on welded joints geometries and variable amplitude loading sequences in the literature

In order to verify the models developed in the present study, experimental data on both fatigue endurance and fatigue crack growth (FCG) of welded joints under variable amplitude (VA) loading sequences were collected from open literature. The information regarding the specimen geometry and VA loading sequence used in these studies are summarised below.

E.1. Specimen geometry

E.1.1 Study I [5], II [34] and IV [13]

Types of welded joints tested in Study I [5], II [34] and IV [13] are identical. Two types, one involves filleted longitudinal attachments (i.e. Class F), while another associates with filleted edge attachments (i.e. Class G), were tested in Study I [5] and II [34], as shown in Figure E1, and they are referred to F and G type, respectively. F type was tested in Study IV [13]. The dimensions of the welded joints are summarised in Table E1.

These specimens were manufactured by 12.5mm- and 12mm-thick steel plate, respectively (Figure E.1).

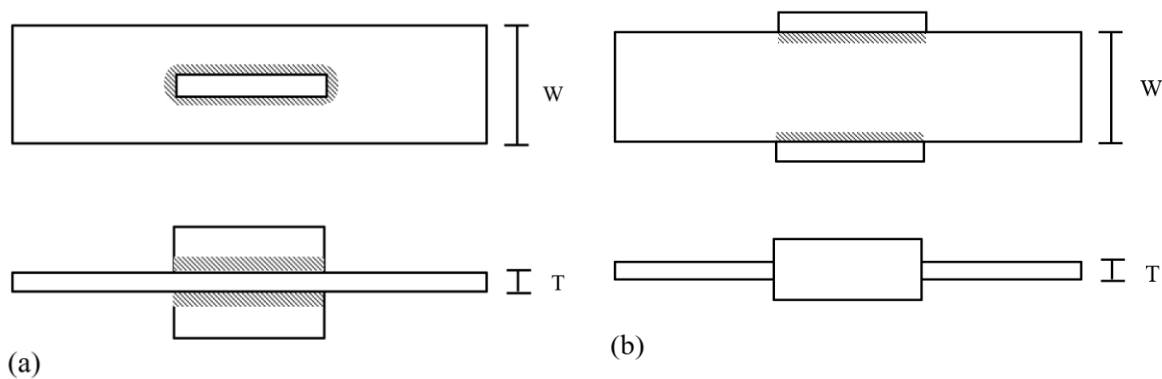


Figure E.1 Details of test specimens: (a) longitudinal non-load-carrying longitudinal fillet welded joints (F type); (b) longitudinal non-load-carrying longitudinal attachments on plate edges (G type).

Table E.2 Dimensions of welded joints

Study	Type of welded joints	Plate thickness, T (mm)	Plate width, W (mm)
I [5]	F	12.5	150
	G	12	125
II [34]	F & G	12.7	125
IV [13]	F	8	150

E.1.2 Study III [96]

The specimens tested in this study were dog-bone shape welded joints containing transverse fillet welded attachments. They were manufactured using 9.5mm-thick steel plate, Figure E2.

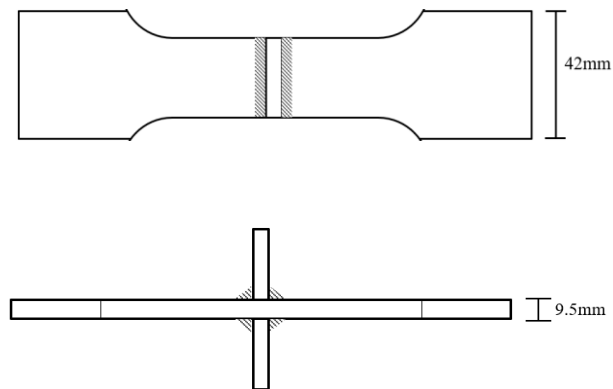


Figure E.2 Transverse non-load-carrying attachments welded joints.

E.2 VA loading spectra and sequences

E.2.1 Study I [5] and IV [13]

The loading spectrum used associated with a concave-up shape in the plot of relative stress range, P_i , against exceedence, N_L , as shown in Figure E3 and Table E2. The block length in a given test depends on the minimum value of P_i , adopted. The length of the basic spectrum, in which the lowest value of P_i was 0.04.

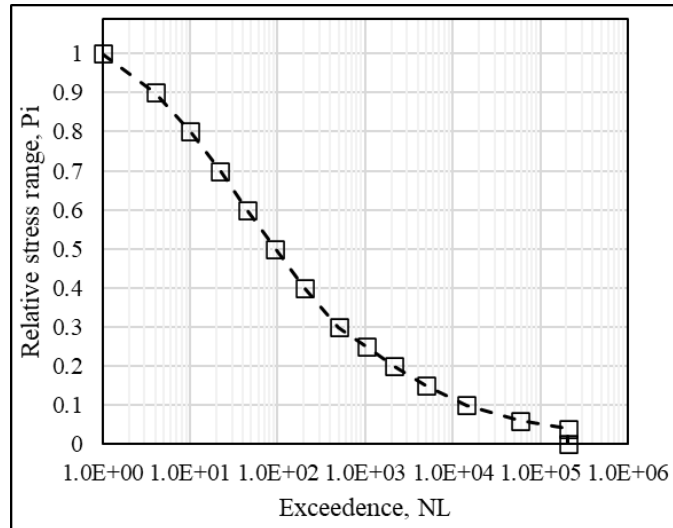


Figure E.3 The concave-up VA loading spectrum used in fatigue testing.

Table E.2 Details of spectrum used in fatigue testing.

P_i	Cycles	Exceedence	P_i	Cycles	Exceedence
1.00	1	1	0.20	1125	2,167
0.90	3	4	0.15	2815	4,982
0.80	6	10	0.10	9500	14,482
0.70	12	22	0.06	43981	58,463
0.60	23	45	0.04	148438	206,901
0.50	48	93			
0.40	109	202			
0.30	296	498			
0.25	544	1,042			

Based on the VA loading spectrum, various VA loading sequences were produced with different minimum P_i values, as summarised in Table E.3.

In Study IV [13], the same loading spectrum was used, and three CD loading sequences were produced where the P_i are 0.2, 0.25 and 0.4, respectively.

E.2.2 Study II [34]

The loading spectrum used in this study involved total 524,287 loading cycles with a minimum P_i value being at 0.063, Figure E.4. The exceedence corresponding to a specific P_i is given in Table E.4.

Table E.3 Details of VA loading sequence used in fatigue testing.

Sequence	Minimum P_i	Maximum stress range (MPa)	Applied maximum stress (MPa)	Applied minimum stress (MPa)
Sequence A (CD)	0.25	210	280	70
	0.20			
	0.15			
	0.10			
Sequence B (CM)	0.25			
	0.20			
	0.10			
Sequence C (CU)	0.25			
	0.20			
	0.10			

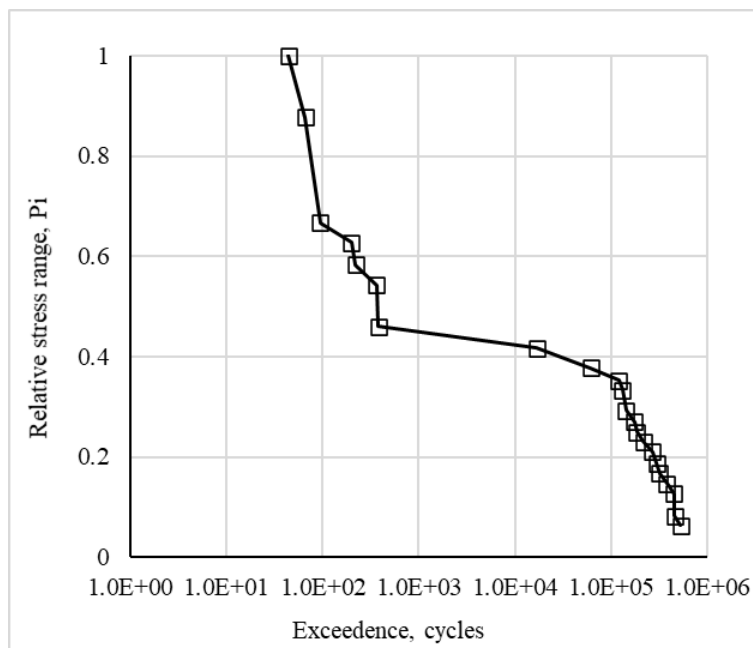


Figure E.4 VA spectrum used in the fatigue testing.

Based on the spectrum, three spectra, where the maximum P_i were 1, 0.667 and 0.377, respectively, were produced. Then, CU loading sequences used in the fatigue testing were generated by combining those spectra with different maximum stress ranges, i.e., 300, 250, 200 and 150MPa, as given in Table E.5. The stress ratio in all sequences was the same, at 0.

Table E.4 Details of spectrum used in fatigue testing.

Pi	Cycles	Exceedence	Pi	Cycles	Exceedence
1	44	44	0.293	11,010	141,558
0.877	22	66	0.270	33,030	174,588
0.667	28	94	0.250	11,010	185,598
0.627	105	199	0.230	30,409	216,007
0.583	21	220	0.210	53,477	269,484
0.543	142	362	0.187	27,263	296,747
0.46	16	378	0.167	22,020	318,767
0.417	16400	16,778	0.147	58,720	377,487
0.377	44040	60,818	0.127	69,730	447,217
0.353	58720	119,538	0.083	11,010	458,227
0.333	11010	130,548	0.063	66,060	524,287

Table E.5 Details of loading sequences produced based on the VA loading spectrum.

Specimen type	VA loading Sequence	Maximum P_i	Minimum P_i	Overload ratio, R_{pi}	Maximum stress range (MPa)	Applied maximum stress range (MPa)	Number of specimens tested
F	A	1	0.063	15.8	300	300	1
					250	250	1
					200	200	1
					150	150	1
	B	0.667		10.5	300	200	1
					200	135	2
					150	101	1
	C	0.377		5.8	300	113	2
					200	75	1
150			56		1		
G	A	1	15.8	380	380	1	
				300	300	1	
				250	250	1	

E.2.3 Study III [96]

The VA histories were generated using traffic data from a survey of axle spacings and loads conducted in Ontario, Canada in 1995, which included a total of 10,198 trucks, Figure E.6.

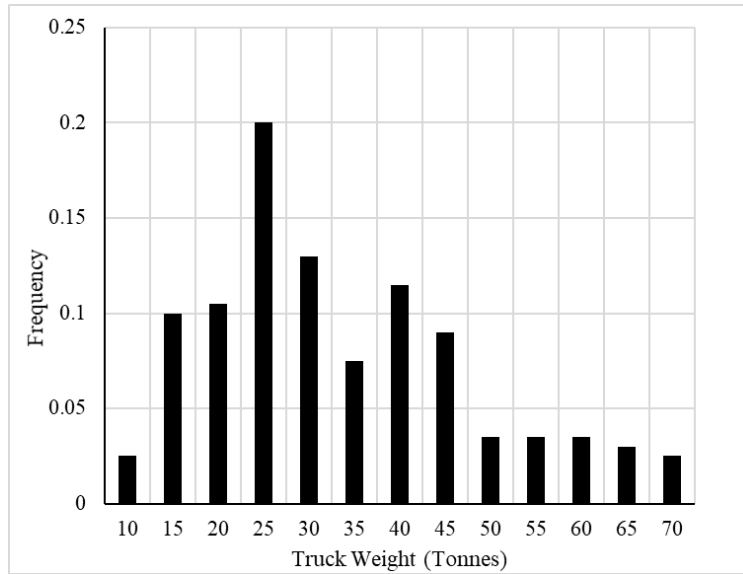


Figure E.6 Truck weight histogram [65].

Based on this histogram, a concave-down shape loading spectrum was produced, Figure E.7. The exceedence corresponding to a specific P_i value is given in Table E.6.

According to this spectrum, four CU loading sequences were generated with the different maximum stress ranges, as summarised in Table E.7.

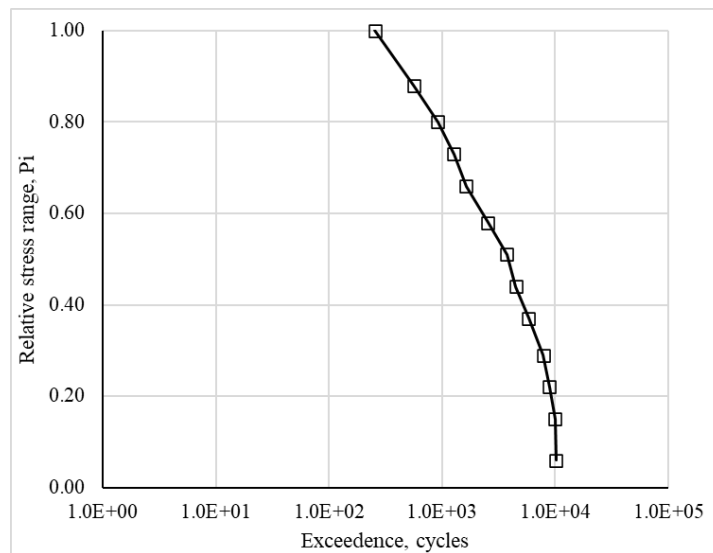


Figure E.7 VA spectrum used in the fatigue test.

Table E.6 Details of spectrum used in fatigue testing.

P_i	Cycles	Exceedence
1.00	255	255
0.88	306	561
0.80	357	918
0.73	357	1,275
0.66	357	1,632
0.58	918	2,550
0.51	1,173	3,722
0.44	765	4,487
0.37	1,326	5,813
0.29	2,040	7,853
0.22	1,071	8,923
0.15	1,020	9,943
0.06	255	10,198

Table E.7 Details of loading sequences produced based on the VA loading spectrum.

VA loading Sequence	Maximum stress range (MPa)	Applied maximum stress range (MPa)	Applied maximum stress range (MPa)
Cycling up	171	180	9
	217	229	12
	239	252	13
	367	387	20

Appendix F Matlab code

In the present study, Matlab (2016a) was used to carry out the complex calculation involved. The codes for Gerber mean stress correction model, and the model developed to predicted fatigue crack propagation under VA loading sequences are given as follows.

F.1 Matlab code for Gerber model

```
Sminapp=9; % minimum stress in the CU sequence
RS=80; % residual stress
Smaxref=240; %reference stress i.e., the maximum stress where the S-N curve obtained
uts=550; % tensile strength
Sapp=[ ]; % spectrum
Sequ=zeros(length(Sapp),1); % equivalent stress range
Smaxapp=zeros(length(Sapp),1); %actual maximum stress of each loading stress range in the VA loading spectrum
for i=1:length(Sapp)
Smaxapp(i,1)=Sminapp+RS+Sapp(i,1);
x=fsolve(@(x)(((uts^2-(Smaxref-0.5*x)^2)/(uts^2-(Smaxapp(i,1)-0.5*Sapp(i,1))^2))*Sapp(i,1)
x),1,optimset('Display','off'));
Sequ(i,1)=x;
end
```

F.2 Matlab code for the model developed to predict fatigue crack growth

Some tools such as Crackwise 5.0 have been well developed based on BS 7910 to predicted crack growth under CA loading spectra. However, they are not able to take into account the interaction between loading cycles under VA loading spectra [5,13], and could not be modified. In this case, a new code was programmed in Matlab 2016Ra in the present study to achieve the model developed. This code was programmed in two steps. In the first step, the code was programmed according to BS 7910 and then validated by the Crackwise software. In the second step, the effect of interaction between each loading cycles in the VA loading sequence was included in the code.

F.2.1 Matlab code for crack wise

Crackwise was developed in accordance with BS 7910; however, it uses an incensement method to calculate the crack size for simplification, rather than calculating the increases of the

crack cycle by cycle. When a welded joint is loaded for N blocks of a given VA loading spectrum, where there are different stress ranges, referring to $\Delta\sigma_i$ and the corresponding number of cycles is n_i , the crack propagation is predicted by j increments (generally 1000). If the initial crack size is a and $2c$, the SIF corresponded to each stress range in the j_{th} increment, $\Delta\sigma_{i,j}$ is:

$$\Delta K_{i,j} = f(a_{j-1}, 2c_{j-1}, \Delta\sigma_{i,j}) \quad (\text{F. 1})$$

If the $\Delta K_{i,1}$ is higher than the threshold, ΔK_{th} , the FCGR is calculated using Paris' Law:

$$\frac{da}{dN_{i,j}} = C(\Delta K_{i,j})^m \quad (\text{F. 2})$$

where C and m are constants. Then the increase of crack depth, Δa_1 , is estimated by:

$$\Delta a_j = \sum_{i=1}^z \frac{n_i \cdot N}{v} \cdot \frac{da}{dN_{i,j}} \quad (\text{F. 3})$$

Therefore, the crack depth after the j_{th} increments is:

$$a_j = a_{j-1} + \Delta a_j \quad (\text{F. 4})$$

The crack length is calculated following the same procedure. The calculation will stop either the a_{j+1} has reached the critical value or the v increments has been calculated. The flow chart is shown in Figure F.1 (a).

F.2.2 Matlab code for the method used in the present study

In Crackwise, a VA loading spectrum is simply regarded as a combination of different loading stress ranges and the effect of interaction between each loading cycles on the FCGR is not considered. However, in view of the above studies [8,12,13,126], the FCGR is affected by the loading sequence significantly. Therefore, in order to consider such effect in the subsequent calculation, the method used in the Crackwise was modified to calculate the fatigue crack block by block, strictly following the loading history, rather than calculating the crack by specific increments. The modified method follows the flowchart given in Figure F.1 (b).

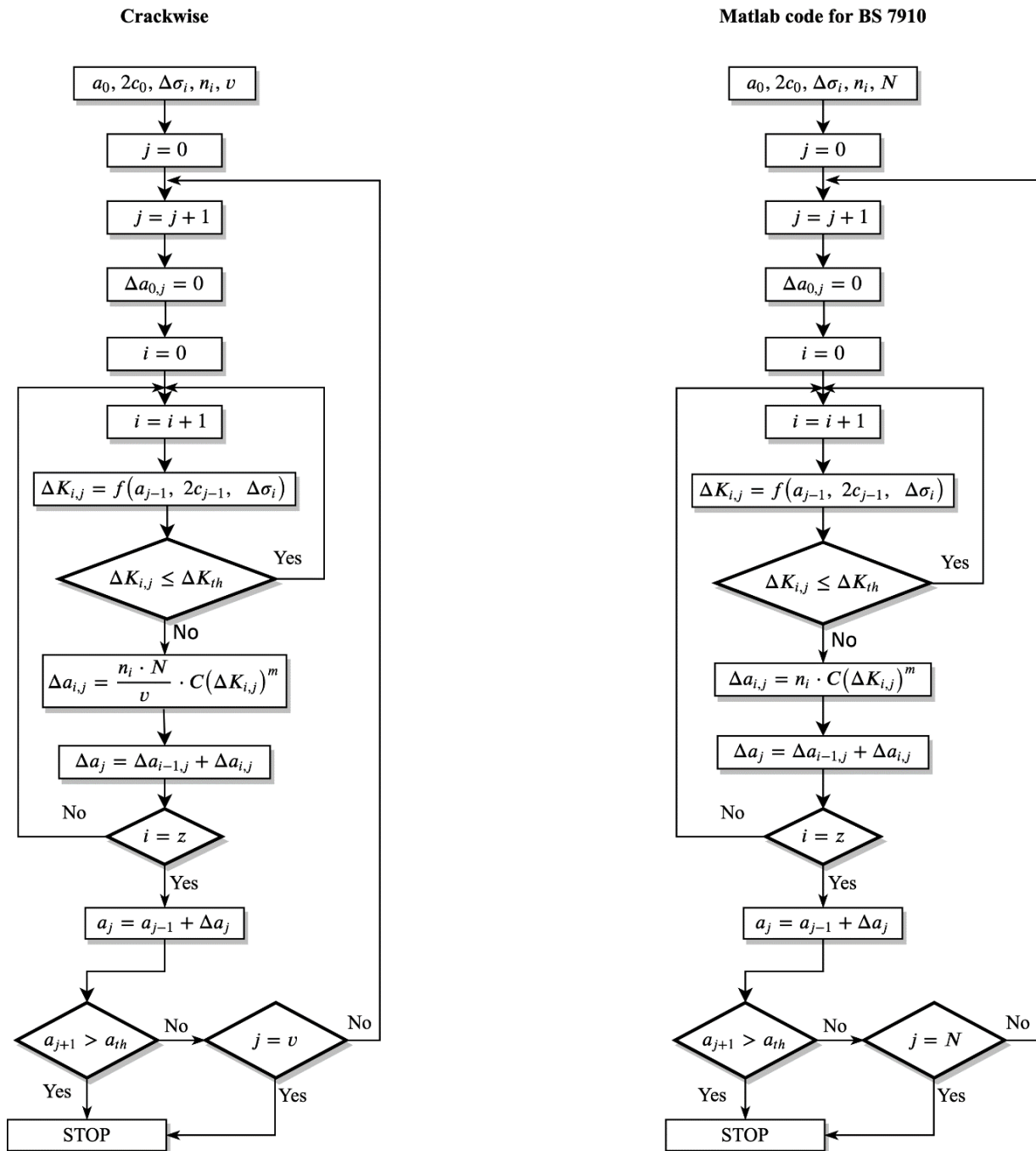


Figure F.1 The flow chart for estimating FCG under VA amplitude loading spectrum: (a) Crackwise 5.0 and (b) method used in the present study.

When a welded joint is loaded for N blocks of a VA loading spectrum contained z different stress ranges, referring $\Delta\sigma_i$ and the number of cycles is n_i , the SIF and the FCGR corresponding to each stress range were calculated. Then the extension in the crack depth, $\Delta a'_j$, due to the j_{th} block can be estimated by:

$$\Delta a'_j = \sum_{i=1}^z (n_i \cdot \frac{da}{dN_i}) \quad (\text{F.5})$$

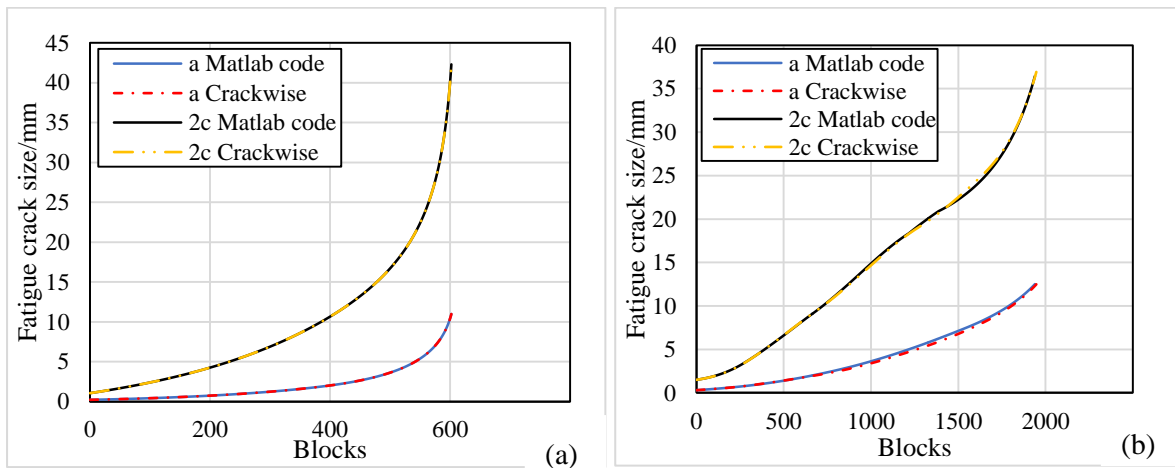
The crack depth after the first block increases to:

$$a'_j = a_{j-1} + \Delta a'_j \quad (\text{F.6})$$

The crack length is calculated following the same procedure. The calculation will stop either the a'_j has reached the critical value after j_{th} block or all N blocks has been calculated.

F.2.3 Verification

In order to verify the method that had been modified, three VA loading sequences were selected, and the corresponding crack propagation under each sequence was calculated using both Crackwise 5.0 and the modified method and compared in Figure F.2. As it will be seen, the all the results calculated by the Matlab code agree well with those obtained from Crackwise 5.0, implying this method modified in the present study is able to predict fatigue crack propagation well as the Crackwise does. Afterwards, this modified method was further developed to take into account the effect of VA loading sequences.



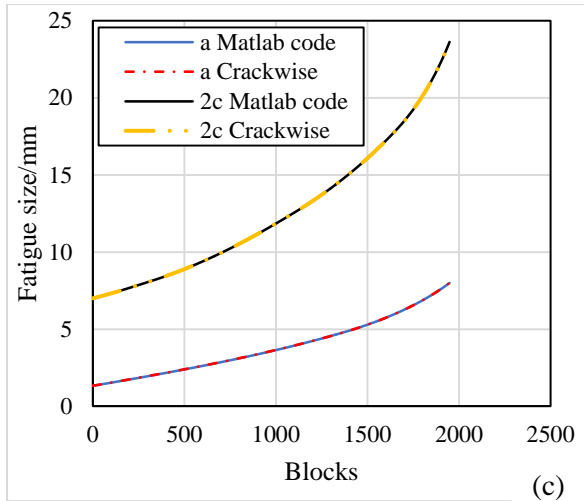


Figure F.2 Comparison between the crack propagation estimated by Crackwise and the modified method under three VA loading sequences: (a) for specimen T125_CD_300 in the present research, (b) for specimen L15 [5], (c) for specimen FIL_VAL_ST04 [13].

F.2.4 Effect of VA loading sequence

According to Equation (6.5) to (6.13), new code was programmed and added into the code had developed and validated. An example of the Matlab code that used to calculate the FCGR in Specimen A12.5_1 is shown as follows:

```

Spec=[250 1
225 2
212.5 3
200 5
187.5 9
175 16
162.5 29
150 53
137.5 96
125 174
112.5 316
100 573
87.5 1039
];

a=zeros(1e7,1); %crack depth
c=zeros(1e7,1); %crack length
deltaKa=zeros(1e7,1); %at the deepest point
deltaKc=zeros(1e7,1); %at crack tips
Deltaa=zeros(1e7,1);
Deltac=zeros(1e7,1);
crack=zeros(10000,3);

E=207000;
K=960;

H=0.16;
Sy=355; %yield stress
Su=550; %ultimate strength
S0=0.5*(Sy+Su);

a(1,1)=0.2174; %initial crack depth
c(1,1)=2; %initial crack length corresponding to 2c
mentioned in the standard

T=12.5; %thickness
W=100; %width

if T<12;
    LL=14;
else if T<25;
    LL=28.5;
else LL=51;
end
end

A=2.31e-13;
m=3; % da/dn=A*deltaK^m

fw=zeros(1e7,1); %correction factor of finite size of
specimen

```

```

Mm=zeros(1e7,2); M1=zeros(1e7,1);
M2=zeros(1e7,1); M3=zeros(1e7,1);
g=zeros(1e7,2);
ftheta=zeros(5e7,2);
phi=zeros(5e7,1);
theta1=pi/2; %deepest point, 0 for surface point
theta2=0; %crack tips

Mka=zeros(1e7,1);
Mkc=zeros(1e7,1);

Mka_b=zeros(1e4,1);%the Mka value of the first
cycle in each block
Mkc_b=zeros(1e4,1); Stmaxa=zeros(1e4,1);
Stmaxc=zeros(1e4,1);
Stvalleya=zeros(1e7,1);
Stvalleyc=zeros(1e7,1);
Ua2=zeros(1e7,1);
Uc2=zeros(1e7,1);
Rta=zeros(1e7,1);
Rtc=zeros(1e7,1);
Ueffa=zeros(1e7,1);
Ueffc=zeros(1e7,1);

ff1=zeros(1e7,1); ff2=zeros(1e7,1);
ff3=zeros(1e7,1); gg1=zeros(1e7,1);
gg2=zeros(1e7,1); gg3=zeros(1e7,1);
gg4=zeros(1e7,1); gg5=zeros(1e7,1);
gg6=zeros(1e7,1); gg7=zeros(1e7,1);
gg8=zeros(1e7,1);
% for 3D Mka

fc1=zeros(1e7,1); fc2=zeros(1e7,1);
fc3=zeros(1e7,1); gc1=zeros(1e7,1);
gc2=zeros(1e7,1); gc3=zeros(1e7,1);
gc4=zeros(1e7,1); gc5=zeros(1e7,1);
gc6=zeros(1e7,1); gc7=zeros(1e7,1);
gc8=zeros(1e7,1); gc9=zeros(1e7,1);
gc10=zeros(1e7,1); gc11=zeros(1e7,1);
gc12=zeros(1e7,1); gc13=zeros(1e7,1);
%for 3D Mkc

block=1;
crack(1,1)=0;
crack(1,2)=a(1,1);
crack(1,3)=c(1,1);

for i=1:10000
    for j=1:length(Spec)
        n=(i-1)*length(Spec)+j;
        r=a(n,1)/c(n,1);
        r1=c(n,1)/a(n,1);
        % fw
    if r==0
        fw(n,1)=1;
    else
        fw(n,1)=sqrt(sec((0.5*pi*c(n,1)/W)*sqrt(a(n,1)/T))
);
        end
        % fw
        if r<=0.5
            M1(n,1)=1.13-0.09*(2*r);
            M2(n,1)=0.89/(0.2+2*r)-0.54;
            M3(n,1)=0.5-1/(0.65+2*r)+14*(1-2*r)^24;
            g(n,1)=1+(0.1+0.35*(a(n,1)/T)^2)*(1-
sin(theta1))^2;
            g(n,2)=1+(0.1+0.35*(a(n,1)/T)^2)*(1-
sin(theta2))^2;

            ftheta(n,1)=(((2*r)^2*cos(theta1)^2)+sin(theta1)^2)
^0.25;

            ftheta(n,2)=(((2*r)^2*cos(theta2)^2)+sin(theta2)^2)
^0.25;
            phi(n,1)=sqrt(1+1.464*(2*r)^1.65);
        else
            M1(n,1)=sqrt(r1/2)*(1+0.04*(r1/2));
            M2(n,1)=0.2*(r1/2)^4;
            M3(n,1)=-0.11*(r1/2)^4;
            g(n,1)=1+(0.1+0.35*(r1/2)*(a(n,1)/T)^2)*(1-
sin(theta1))^2;
            g(n,2)=1+(0.1+0.35*(r1/2)*(a(n,1)/T)^2)*(1-
sin(theta2))^2;

            ftheta(n,1)=(((r1/2)^2*sin(theta1)^2)+cos(theta1)^2)
^0.25;

            ftheta(n,2)=(((r1/2)^2*sin(theta2)^2)+cos(theta2)^2)
^0.25;

            phi(n,1)=sqrt(1+1.464*(r1/2)^1.65);
        end

        Mm(n,1)=(M1(n,1)+M2(n,1)*(a(n,1)/T)^2+M3(n,1)
)*(a(n,1)/T)^4*g(n,1)*ftheta(n,1)/phi(n,1);
        Mm(n,2)=(M1(n,1)+M2(n,1)*(a(n,1)/T)^2+M3(n,1)
)*(a(n,1)/T)^4*g(n,2)*ftheta(n,2)/phi(n,1);

        gg1(n,1)=-1.0343*(2*a(n,1)/c(n,1))^2-
0.15657*(2*a(n,1)/c(n,1))+1.3409;
        gg2(n,1)=1.3218*(2*a(n,1)/c(n,1))^2-0.61153;
        gg3(n,1)=-0.87238*(2*a(n,1)/c(n,1))+1.2788;
        gg4(n,1)=-
0.4619*(2*a(n,1)/c(n,1))^3+0.6709*(2*a(n,1)/c(n,1)
)^2-0.37571*(2*a(n,1)/c(n,1))+4.6511;
        gg5(n,1)=-
0.015647*(LL/T)^3+0.090889*(LL/T)^2-
0.17180*(LL/T)-0.24587;

```

```

gg6(n,1)=-0.20136*(LL/T)^2+0.93311*(LL/T)-
0.41496;
gg7(n,1)=0.20188*(LL/T)^2-
0.97857*(LL/T)+0.068225;
gg8(n,1)=-0.027338*(LL/T)^2+0.12551*(LL/T)-
11.218;

ff1(n,1)=0.43358*(a(n,1)/T)^(gg1(n,1)+(gg2(n,1)*
a(n,1)/T)^gg3(n,1))+0.93163*exp((a(n,1)/T)^-
0.050966)+gg4(n,1);
ff2(n,1)=-0.21521*(1-
(a(n,1)/T)^176.4199+2.8141*((a(n,1)/T))^(-
0.1074*(a(n,1)/T));
ff3(n,1)=0.33994*(a(n,1)/T)^gg5(n,1)+1.9493*(a(n
,1)/T)^0.23003+gg6(n,1)*(a(n,1)/T)^2+gg7(n,1)*(a
(n,1)/T)+gg8(n,1);

Mka(n,1)=ff1(n,1)+ff2(n,1)+ff3(n,1);

if Mka(n,1)<1
    Mka(n,1)=1;
end

%3D Mkc

gc1(n,1)=0.0078157*(0.5*c(n,1)/a(n,1))^2-
0.070664*(0.5*c(n,1)/a(n,1))+1.8508;
gc2(n,1)=-
0.000054546*(LL/T)^2+0.00013651*(LL/T)-
0.00047844;
gc3(n,1)=0.00049192*(LL/T)^2-
0.0013595*(LL/T)+0.0114;
gc4(n,1)=0.0071654*(LL/T)^2-0.033399*(LL/T)-
0.25064;
gc5(n,1)=-
0.01864*(0.5*c(n,1)/a(n,1))^2+0.24311*(0.5*c(n,1
)/a(n,1))-1.7644;
gc6(n,1)=-0.0016713*(LL/T)^2+0.009062*(LL/T)-
0.016479;
gc7(n,1)=-0.0031615*(LL/T)^2-
0.010944*(LL/T)+0.13967;
gc8(n,1)=-0.045206*(LL/T)^3+0.3238*(LL/T)^2-
0.68935*(LL/T)+1.4954;
gc9(n,1)=-
0.25473*(2*a(n,1)/c(n,1))^2+0.40928*(2*a(n,1)/c(
n,1))+0.0021892;
gc10(n,1)=37.423*(2*a(n,1)/c(n,1))^2-
15.741*(2*a(n,1)/c(n,1))+64.903;
gc11(n,1)=-0.10553*(LL/T)^3+0.59894*(LL/T)^2-
1.0942*(LL/T)-1.265;
gc12(n,1)=0.043891*(LL/T)^3-
0.24898*(LL/T)^2+0.44732*(LL/T)+0.60136;
gc13(n,1)=-
0.011411*(2*a(n,1)/c(n,1))^2+0.0043695*(2*a(n,1
)/c(n,1))+0.51732;

fc1(n,1)=gc1(n,1)*(a(n,1)/T)^(gc2(n,1)*(0.5*c(n,1)
/a(n,1))^2+gc3(n,1)*(0.5*c(n,1)/a(n,1))+gc4(n,1))+

```

```

gc5(n,1)*(1-
a(n,1)/T)^(gc6(n,1)*(0.5*c(n,1)/a(n,1))^2+gc7(n,1)
*(0.5*c(n,1)/a(n,1))+gc8(n,1));
fc2(n,1)=(-
0.28639*(2*a(n,1)/c(n,1))^2+0.35411*(2*a(n,1)/c(
n,1))+1.643)*(a(n,1)/T)^gc9(n,1)+0.27449*(1-
a(n,1)/T)^gc10(n,1);
fc3(n,1)=gc11(n,1)*(a(n,1)/T)^0.75429+gc12(n,1)*
exp((a(n,1)/T)^gc13(n,1));

Mkc(n,1)=fc1(n,1)*fc2(n,1)*fc3(n,1);

if Mkc(n,1)<1
    Mkc(n,1)=1;
end

%% %% %% %% %%
if j==1
Mka_b(i,1)=Mka(n,1);
Mkc_b(i,1)=Mkc(n,1);

deltaSt=fsolve(@(deltaSt)(deltaSt^2+2*E*(0.5/K)^
(1/H)*deltaSt^(1+1/H)-
(Mka_b(i,1)*Spec(j,1))^2),1,optimset('Display','off'
)); % local stress at deepest point
Stmaxa(i,1)=0.5*deltaSt; % maximum local stress
in underload

deltaSt=fsolve(@(deltaSt)(deltaSt^2+2*E*(0.5/K)^
(1/H)*deltaSt^(1+1/H)-
(Mkc_b(i,1)*Spec(j,1))^2),1,optimset('Display','off'
)); % local stress at tips
Stmaxc(i,1)=0.5*deltaSt; % maximum local stress
in underload
end

%% %% %% calculation of Ueff
deltaSt=fsolve(@(deltaSt)(deltaSt^2+2*E*(0.5/K)^
(1/H)*deltaSt^(1+1/H)-
(Mka_b(i,1)*Spec(j,1))^2),1,optimset('Display','off'
));
Stvalleya(n,1)=Stmaxa(i,1)-deltaSt;

Ua1=1/(1.5-(-1));

Rta(n,1)=Stvalleya(n,1)/Stmaxa(i,1);

if Rta(n,1)<-2
    Ua2(n,1)=1/(1.5-(-2));
else if Rta(n,1)<=0.5
    Ua2(n,1)=1/(1.5-Rta(n,1));
else
    Ua2(n,1)=1;
end
end

```

```

deltaSt=fsolve(@(deltaSt)(deltaSt^2+2*E*(0.5/K)^
(1/H)*deltaSt^(1+1/H)-
(Mkc_b(i,1)*Spec(j,1))^2),1,optimset('Display','off'
));
Stvalleyc(n,1)=Stmaxc(i,1)-deltaSt;

Uc1=1/(1.5-(-1));

Rtc(n,1)=Stvalleyc(n,1)/Stmaxc(i,1);

if Rtc(n,1)<-2
    Uc2(n,1)=1/(1.5-(-2));
else if Rtc(n,1)<=0.5
    Uc2(n,1)=1/(1.5-Rtc(n,1));
else
    Uc2(n,1)=1;
end
end

l=0.38;
Ueffa(n,1)=(Ua2(n,1)/Ua1)^l;
Ueffc(n,1)=(Uc2(n,1)/Uc1)^l;
%% % % % %
deltaKa(n,1)=Spec(j,1)*fw(n,1)*Mm(n,1)*Mka(n,1
)*sqrt(pi*a(n,1))*Ueffa(n,1);
deltaKc(n,1)=Spec(j,1)*fw(n,1)*Mm(n,2)*Mkc(n,1
)*sqrt(pi*a(n,1))*Ueffc(n,1);

if deltaKa(n,1)<=63
    Deltaa(n,1)=0;
else
    Deltaa(n,1)=A*deltaKa(n,1)^3;
end

if deltaKc(n,1)<=63
    Deltac(n,1)=0;
else
    Deltac(n,1)=A*deltaKc(n,1)^3;
end

a(n+1,1)=a(n,1)+Deltaa(n,1)*Spec(j,2);
c(n+1,1)=c(n,1)+2*Deltac(n,1)*Spec(j,2);
end

crack(i+1,1)=i;
crack(i+1,2)=a(n+1,1);
crack(i+1,3)=c(n+1,1);

if a(n+1,1)>=T

    break
else if c(n+1,1)>100

    break
end

end

```

